Submitted to
the Graduate School of Science of Osaka University
for the degree of Doctor of Physics

Exotic few-baryon systems with a heavy meson

Yasuhiro Yamaguchi*

Research Center for Nuclear Physics (RCNP), Osaka University,
Ibaraki, Osaka, 567-0047, Japan
Department Physics, Graduate School of Science, Osaka University

February 3, 2014

* E-mail: yamaguti@rcnp.osaka-u.ac.jp

Abstract

The recent findings of hadronic molecules, such as $X(3872)$ and Z_b, are a topic of great current interest in the hadron physics. Hadronic molecules are deuteron-like loosely bound states or resonances of hadrons, appearing near the thresholds. Therefore, such states cannot be reached by the standard quark model (for mesons of $q\bar{q}$ and baryons of qqq), and are new evidences of the exotic hadrons.

In the formation of the hadronic molecules, there are two important symmetries, chiral symmetry and heavy quark symmetry. The pion as a Nambu-Goldstone boson, exchanging between constituent hadrons, plays a significant role to generate a strong attraction. Furthermore, the pion exchange interaction is enhanced by the heavy quark symmetry. This symmetry manifests the mass degeneracy of a heavy pseudoscalar meson (P) and a heavy vector meson (P^*). Therefore, for molecules containing the heavy mesons, the one pion exchange potential (OPEP) produced by the $PP^*\pi$ and $P^*P^*\pi$ verticies becomes important when the P and P^* mesons are degenerate.

Thanks to the presence of the attraction provided by the OPEP, we expect formation of new hadronic molecules, being meson-baryon states. The molecules formed by a heavy meson ($\bar{D}$ (B) or D ($\bar{B}$) meson) and a nucleon N are interesting. The $\bar{D}N$ and BN are manifestly exotic states whose minimal quark content is $\bar{Q}qqqq$, where $\bar{Q}$ (q) is a heavy antiquark (light quark). These states have never been found in experiment in the heavy flavor region. On the other hand, the DN ($\bar{B}N$) states have the non-exotic flavor structure, and are coupled to the ordinary heavy hadrons such as Λ_c and Σ_c. They are exotic baryon states in which the molecular component dominates rather than the three-quark one. In addition, the attraction between a heavy meson and a nucleon motivates us to explore not only two-body systems, but also few-body systems as exotic nuclei with heavy quarks, such as $\bar{D}NN$ and BNN. Those systems show us the interesting phenomena which cannot be seen in the normal nuclei.

In this thesis, the possible existence of the hadronic molecules, being $\bar{D}N$ (BN) and DN ($\bar{B}N$) for two-body systems, and $\bar{D}NN$ (BNN) for three-body systems, is discussed. By solving the coupled-channel Schrödinger equations for PN and P^*N, we obtain many bound and resonant states near the thresholds both in the charm and bottom sectors. For these states, the OPEP between the heavy meson and the nucleon plays a crucial role to produce a strong attraction. In particular, the tensor force mixing the PN and P^*N channels with different angular momenta, e.g. L and $L \pm 2$, is dominant not only in the PN states, but also in the PNN states.

We also discuss the PN and PNN states in the heavy quark limit. The suppression of spin-dependent forces between quarks leads to the spin degeneracy of the states with heavy quarks. The degeneracy has been discussed in the normal heavy hadrons. However, it can be generalized to the multi-hadron systems, such as hadronic molecules. We find that the spin degeneracy is also realized in the PN and PNN states as multi-hadron states.

Acknowledgments

First of all, I would like to express my gratitude to Prof. Atsushi Hosaka (Research Center for Nuclear Physics (RCNP), Osaka University) for his fruitful guidance and helpful supports. I am very grateful to Dr. Shigehiro Yasui (Institute of Particle and Nuclear Studies (IPNS), KEK) for stimulating discussions and providing me with instructive advices. They are not only educational supervisors, but also very important collaborators. I would also like to appreciate Mr. Shunsuke Ohkoda (RCNP) for discussing and and collaborating on the research. I would like to thank them again for supporting me in my research life in Osaka.

I'm really grateful to Dr. Yuma Kikuchi (RCNP) for instructing in the numerical method to solve three-body problems and for valuable advices and discussions.

I would like to appreciate Prof. Hiroyuki Noumi (RCNP), Prof. Tetsuo Hyodo (Yukawa Institute for Theoretical Physics (YITP), Kyoto University) and Prof. Kazutaka Sudoh (Nishogakusha University) for fruitful discussions and helpful supports. I also wish to thank Prof. Hiroshi Toki (RCNP), Prof. Veljko Dmitrasinovic (Institute of Physics, Belgrade University), Prof. Bing-song Zou (ITP, CAS), and Prof. Dmitri Diakonov (Petersburg Nuclear Physics Institute) for useful discussions and valuable advices.

I would like to acknowledge RCNP staffs, Prof. Kazuyuki Ogata, Prof. Hiroyuki Kamano, Dr. Raquel Molina, Dr. Kazuhito Mizuyama, and Dr. Yoko Ogawa for their kind hospitality and stimulating discussions on Physics. I am also very grateful to secretaries of RCNP theory group, Ms. Machi Yamakami and Ms. Mika Tambara for kind supports and hospitality. I wish to thank RCNP students, Hiromi Kaneko, Takuya Shibata, Tokuro Fukui, Kim Sang-ho, Katsunori Sadato and Kazuki Yoshida for warm friendship, interesting discussions and a lot of help.

This work is supported in part by Grant-in-Aid for "JSPS Fellows(24-3518)" from Japan Society for the Promotion of Science.

Contents

Chapter 1

Introduction

Many quarkonium-like states called X, Y, Z in the heavy flavor sectors have been observed in several accelerator facilities such as KEK-Belle and SLAC-BaBar [1–4]. They are attracted a great deal of interest in hadron and nuclear physics, because these states have exotic quantum numbers which cannot be explained by the standard quark model describing mesons as a quark-antiquark state ($q\bar{q}$) and baryons as a three-quark state (qqq) [5]. Therefore, they are a new evidence of the exotic hadrons in addition to candidates such as a_0, f_0 and $\Lambda(1405)$ in the strangeness sector [6–8].

As new aspects of structures of these exotic mesons, there have been discussions about the possibility of (i) a hadronic molecule which is a loosely bound state formed by a heavy meson and antimeson such as $D\bar{D}^*$, (ii) a tetraquark which is a tightly bound four quark state, $Q\bar{Q}q\bar{q}$, considering additional constituents, a light quark and antiquark, and (iii) a quarkonium hybrid which has an additional gluonic constituent. Here, Q and q denote a heavy quark (c, b) and a light quark (u, d, s), respectively. The categories (i) and (ii) are classifies as multiquark states. Such states are also expected to be seen in exotic baryon states as a hadronic molecule composed of a meson and a baryon, and pentaquark which is a tightly five quark state. The study of the exotic hadrons beyond the standard quark model provides us with information to understand how the Quantum Chromodynamics (QCD) produces hadrons from quarks and gluons.

1.1 Hadronic molecules

Recently, there have been progresses in the researches of hadronic molecules. In experiment, the candidates of meson-antimeson molecules have been found, such as $X(3872)$ [9–13] and $Z_c(3900)$ [14–16] in the charm sector, and $Z_b(10610)$ and $Z_b(10650)$ [17] in the bottom sector. These quarkonium-like states locate near the threshold, $D\bar{D}^*$ threshold for $X(3872)$ and $Z_{\rm c}(3900)$, and $B\bar{B}^*$ and $B^*\bar{B}^*$ thresholds for $Z_b(10610)$ and $Z_b(10650)$, respectively. Hence, these states are expected to be a $D\bar{D}^*$ bound state for $X(3872)$ and resonance for $Z_{\rm c}(3900)$, and $B\bar{B}^*$ and $B^*\bar{B}^*$ resonances for $Z_b(10610)$ and $Z_b(10650)$, respectively. In particular, charged states $Z_c(3900)$, $Z_b(10610)$ and $Z_b(10650)$ should be multiquark states with non-zero isospin.

For the theoretical researches, meson-antimeson states with heavy quarks were first discussed by M. B. Voloshin and L. B. Okun [18], and A. De Rujula, H. Georgi,

and S. L. Glashow [19] in 1970s. They investigated the charmed meson-antimeson molecules interacting via short-range forces. In 1994, N. A. Törnqvist investigated the "deuson" systems [20], where the deuson is the deuteron-like meson-antimeson bound states. The deuteron is a loosely bound state in which the one pion exchange potential (OPEP) as a long-range force dominates. In the study, the author emphasized the importance of the OPEP in the deuson as an analogue state of the deuteron. The long-range force is easy to construct a loosely bound state with a small binding energy. The state appearing near the threshold is necessary condition that the states can be interpreted as hadronic molecules with keeping their identities as constituent hadrons. The ideas of the hadronic molecules as a bound or resonant state of constituent hadrons have been incorporated in the recent theoretical calculations of the observed X, Y, Z states including $X(3872)$, $Z_c(3900)$ and Z_b's, and other exotic states [21–32].

The hadronic molecular pictures being successfully applied to the meson-antimeson states are also useful in the meson-baryon systems. Recently, a novel structure has been suggested in manifestly exotic baryon states with a single heavy antiquark, namely the $\bar{D}N$ and $\bar{D}^*N$ (BN and B^*N) states, whose minimal quark content is $uudd\bar{c}$ ($uudd\bar{b}$) [33–41]. Therefore, they are genuinely exotic states whose bound states are stable against a strong decay. Such states are analogue of the pentaquark Θ^+ composed of $uudd\bar{s}$ in the strangeness sector [34, 42–47]. Experimentally, the H1 collaboration reported the charmed pentaquark with the mass 3099 MeV at HERA [48], which is about 150 MeV above the $\bar{D}^*N$ threshold, while it has not been confirmed yet. However, the charmed and bottom pentaquark states are expected to be found near the thresholds as a hadronic molecule in analogy with exotic meson sectors.

The hadronic molecules as a bound or resonant states formed a D or D^* meson ($\bar{B}$ or $\bar{B}^*$ meson) and a nucleon for non-exotic channels are also interesting [49–66]. Since the DN and D^*N ($\bar{B}N$ and $\bar{B}^*N$) molecules have ordinary flavor structures of three quarks, they are intimately related to the ordinary heavy baryons [67], Λ_c, Σ_c, Σ_c^* and their excited states for the charm sector, and Λ_b, Σ_b, Σ_b^* and their excited states for the bottom sector, while the $\bar{D}N$ and BN states are genuinely exotic states. The excited states of the ordinary baryons have been studied in the quark model extensively [68, 69]. However, near the DN and D^*N ($\bar{B}N$ and $\bar{B}^*N$) thresholds, it is expected that the properties of such baryon states are strongly affected by DN and D^*N ($\bar{B}N$ and $\bar{B}^*N$) states. There would be even such states that are dominated by the molecular components.

The attraction between a heavy meson ($\bar{D}$ or D (B or $\bar{B}$)) and a nucleon motivates us to explore the few-body problems in exotic nuclei with heavy quarks, because it is naturally expected that the binding energy becomes larger as the baryon number increases. In the light flavor sector, it has been studied that the hadron-nucleon interaction gives us rich phenomena in few-body systems such as the impurity effects. For instance, the modifications of the nuclear properties, such as size, shape, cluster and shell structures, and collective motions, induced by bound hadrons as an impurity can be investigated. The nuclear shrinking for hypernuclei, e.g. ${}^{6}_{\Lambda}\mathrm{He}$, ${}^{7}_{\Lambda}\mathrm{Li}$ and ${}^{9}_{\Lambda}\mathrm{Be}$, has been studied [70–72]. In $\bar{K}$ nuclei, the attractive interaction between a $\bar{K}$ meson and a nucleon causes high density states [73, 74] which have never been realized in normal

nuclei. In the heavy flavor sector, we can also expect such impurity effects caused by heavy mesons. In addition, since $\bar{D}$ and D mesons (B and $\bar{B}$ mesons) contain a light quark, the mass modification of the heavy mesons can be observed as discussed in the systems of vector mesons, ρ, ω and ϕ, in the nuclear matter. This is related to partial restoration of chiral symmetry breaking in the nuclear medium [75]. There have been many works for heavy mesons in nuclear matter with infinite volume [76–87] and in atomic nuclei such as ^{12}C, ^{40}Ca and ^{208}Pb with larger baryon numbers [81, 83, 88–91]. On the other hand, there have been a few studies for few-body systems of heavy mesic nuclei so far in the literature [92, 93]. In particular, the $\bar{D}$ and B nuclei are manifestly exotic states whose bound states have no lower hadronic channel connected by a strong decay. We emphasize that the counterpart of the K nuclei has not been discussed due to the repulsive force between a K meson and a nucleon [94], while the $\bar{K}$ nuclei for the non-exotic channel is a topic of great current interest in the strangeness sector. Therefore, the $\bar{D}$ and B nuclei are unique as exotic meson-nucleus systems.

1.2 Heavy quark spin symmetry and one pion exchange potential

The hadronic molecules are expected to be a loosely bound or resonant states which are spatially extended. Therefore, the one pion exchange potential (OPEP) as a long range force is expected to be important. In particular, the tensor force of the OPEP yields a strong attraction through mixing of L and $L \pm 2$ waves, where L stands for an orbital angular momentum. This mechanism is induced by the pseudoscalar nature of the pion, and can be seen in the deuteron, where the tensor force mixing $^3S_1$ and $^3D_1$ channels generates a strong attraction [95, 96]. In the heavy meson systems, the OPEP is enhanced by a new symmetry which emerges in the heavy quark limit ($m_Q \to \infty$). This is called the heavy quark spin symmetry.

In the heavy flavor sector, the chiral symmetry and the heavy quark spin symmetry are essential to provide the OPEP in systems containing heavy mesons $Q\bar{q}$ ($Q\bar{q}$). The chiral symmetry is a symmetry for the light quarks whose masses are smaller than the scale of a nonperturbative strong dynamics $\Lambda_{\rm QCD}$. The spontaneous breaking of chiral symmetry provides the pion as a Nambu-Goldstone boson [97, 98]. In contrast, the heavy quark spin symmetry appears when a quark mass is an infinite value [99–103]. This is applied approximately to a heavy quark whose mass is much larger than $\Lambda_{\rm QCD}$. In the heavy quark limit ($m_Q \to \infty$), a spin-dependent force between quarks is suppressed because it is proportional to inverse of the quark masses. Therefore, the heavy quark spin s_Q is decoupled from the total angular momentum j of the brown muck. The brown muck is defined as everything other than the heavy quark in the hadrons, e.g. light quarks and gluons. The spin decoupling leads to spin degeneracy of the states. In a system with a single heavy quark, degenerate states with total angular momentum and parity, $(j - 1/2)^P$ and $(j + 1/2)^P$, emerge for $j \neq 0$, while non-degenerate state emerges for $j = 0$ [103, 104]. For the heavy mesons, therefore, a heavy pseudoscalar meson P with $J^P = 0^-$ and a heavy vector meson P^* with $J^P = 1^-$ are degenerate. Indeed, the mass splitting between D (B) and D^* (B^*)

mesons is small, $m_{D^*} - m_D \sim 140$ MeV and $m_{B^*} - m_B \sim 45$ MeV. The small mass splittings in the heavy flavor sectors should be compared with the large mass splittings in the light flavor sectors, about 400 MeV for K and K^* mesons and about 600 MeV for ρ and π mesons.

Because the Yukawa vertices of $PP^*\pi$ and $P^*P^*\pi$ generate the OPEP through the $PN - P^*N$ mixings in the PN molecules, this interaction becomes important especially when P and P^* mesons are degenerate. Here, we note that only P meson cannot generate the OPEP because the $PP\pi$ vertex is forbidden due to the parity conservation. For the light meson systems, the mixing effect is much suppressed because of large mass splittings between π and ρ, and K and K^*. Therefore, the OPEP plays a minor role in πN and KN systems.

1.3 Spin degenerate states in the heavy quark limit

The heavy quark spin symmetry manifests the spin degeneracy of the states with heavy (anti-)quarks as mentioned in the previous section. In the state with a single heavy (anti-)quark, existence of doublet states with $(j - 1/2)^P$ and $(j + 1/2)^P$ for $j \neq 0$ and singlet states for $j = 0$ is expected. The doublet and singlet states have been discussed in the ordinary heavy hadrons, e.g. Λ_c as the singlet state, and D and D^* mesons and Σ_c and Σ_c^* baryons with the small mass splittings as the doublet states [69, 100, 101, 103, 105–108]. The degeneracy can be also generalized to multi-hadron systems such as the PN molecules and exotic nuclei with heavy hadrons [104, 109]. For such systems, the brown muck has a bit more complex structure composed not only of light quarks and gluons in the heavy hadrons, but also of light hadrons, while the brown muck in the normal hadrons contains only the light degrees of freedom in the heavy hadrons. However, both in the normal and exotic heavy hadrons, the brown muck is useful to classify the states with heavy quarks because the total angular momentum j of the brown muck is conserved in the heavy quark limit. This is expected to provide us with information to study the mass spectra, decays and productions of the (non-)degenerate states in experiment.

In the thesis, the possible existences of the PN states, being $\bar{D}N$ (BN) for exotic channels and DN ($\bar{B}N$) for non-exotic channels, and the three-body PNN states, being $\bar{D}NN$ (BNN) for the exotic channels, are investigated. Respecting the heavy quark symmetry and chiral symmetry, the interaction Lagrangians for a heavy meson with a light meson, π, ρ and ω, are constructed as shown in chapter 2. We consider the one boson exchange potential produced by those Lagrangians. The tensor force of the $PN - P^*N$ mixing component is expected to generate a strong attraction between constituent hadrons. By solving the coupled-channel Schödinger equations for PN and P^*N channels, we obtain bound and resonant states numerically. The two-body and three-body states are discussed in chapter 3 and in chapter 4, respectively.

For exotic channels, we emphasize that the $\bar{D}N$ (BN) and $\bar{D}NN$ (BNN) are unique as genuinely exotic meson-baryon systems, because the counterparts of KN and KNN in the strangeness sector do not exist due to the repulsive interaction between a K meson and a nucleon.

For non-exotic channels, the DN and D^*N ($\bar{B}N$ and $\bar{B}^*N$) channels only are considered. In reality, however, such hadronic molecules do not necessarily correspond to the observed states, because there should be couplings not only to three quark states, Λ_c, Σ_c and Σ_c^* (Λ_b, Σ_b and Σ_b^*), but also to other meson-baryon states such as $\pi\Lambda_c$, $\pi\Sigma_c$ and $\pi\Sigma_c^*$ ($\pi\Lambda_b$, $\pi\Sigma_b$ and $\pi\Sigma_b^*$). However, we may expect that such couplings are small for DN and $\bar{B}N$ baryons near the thresholds. The reasons are that the wave functions of hadronic molecules are spatially large as compared to the conventional three quark states, and that the transitions, e.g. from DN ($\bar{B}N$) to $\pi\Sigma_c$ ($\pi\Sigma_b$), are suppressed by a heavy quark exchange. From those points of view, in the present discussion, we focus on the role of the DN and D^*N ($\bar{B}N$ and $\bar{B}^*N$) sectors and study the bound or resonant states generated by $D^{(*)}N$ and $\bar{B}^{(*)}N$.

Furthermore, we discuss the spin degeneracy of the exotic PN and PNN states in the heavy quark limit in chapter 5. The brown muck is utilized to understand the spin structures of the molecules states.

The final chapter is devoted to a summary of the thesis.

Chapter 2

Heavy quark symmetry and Effective Lagrangian for heavy mesons.

2.1 Introduction

The heavy quark symmetry can be used to describe the properties of the hadrons containing the heavy quarks Q [99–103]. The symmetry arises in the effective Lagrangian of QCD in the heavy quark limit ($m_Q \to \infty$), which is called Heavy quark effective theory (HQET) [101–103, 110–112]. In the real world, this is applied to the heavy quarks ($Q = c$, b and t) whose masses are much larger than the scale $\Lambda_{\rm QCD}$, while there are corrections, of order $\Lambda_{\rm QCD}/m_Q$. The heavy quark symmetry implies that (i) the dynamics is independent of the heavy quark flavors, and (ii) the dynamics is independent of the spin-flip of the heavy quarks. Thus, the flavor-spin symmetry gives relations between properties of heavy hadrons, for instance $\bar{D}$ and B mesons which are pseudoscalar mesons with different heavy flavors, and $\bar{D}$ and $\bar{D}^*$ mesons which are charmed mesons with different spins.

The effective Lagrangian for heavy mesons with light mesons is constructed by the chiral perturbation theory as satisfying the heavy quark symmetry and chiral symmetry. The spin symmetry for the heavy quarks leads to remarkable feature that both heave pseudoscalar meson P and heavy vector meson P^* are considered as fundamental degrees of freedom in the dynamics. Since the vertices of $PP^*\pi$ and $P^*P^*\pi$ generate the OPEP, the spin symmetry enhances the OPEP in the heavy meson systems.

In this chapter, we introduce the heavy quark symmetry in the HQET, and the chiral lagrangian which is used in the construction of the meson exchange potentials in the systems of a heavy meson and a nucleon, addressed in the thesis.

2.2 Heavy quark symmetry and heavy quark effective theory

Heavy quark symmetry is manifested by the HQET being good approximation to QCD, when the quark mass is much larger than $\Lambda_{\rm QCD}$. The HQET provides processes where the heavy quark bound in a hadron interacts with light degrees of freedom by exchanging the soft gluons.

Let us consider the heavy quark moving with the hadron at the velocity v, and being almost on-shell. In the hadron, the heavy quark is surrounded by the brown muck. The brown muck is defined as everything other than the heavy quark in the hadron, i.e. light (anti-)quarks and gluons. The momentum of the heavy hadron is given as

$$P_H^\mu = M_Q v^\mu, \tag{2.1}$$

with the heavy hadron mass M_Q. The four-velocity v^μ satisfies $v^2 = 1$. The heavy quark mass m_Q is expected to be nearly equal to the heavy hadron mass, namely $m_Q \sim M_Q$. The heavy quark also carries nearly all of momentum of the heavy hadron, while the brown muck carries a small momentum q^μ. The momentum of the heavy quark can be written as

$$P_Q^\mu = P_H^\mu - q^\mu = m_Q v^\mu + k^\mu \,, \tag{2.2}$$

where k is the residual momentum expressed by

$$k^\mu = (M_Q - m_Q)v^\mu - q^\mu \,, \tag{2.3}$$

which is of order $\Lambda_{\rm QCD}$.

The heavy quark field $Q(x)$ is separated into two components as

$$Q(x) = \exp\left(-im_Q v\cdot x\right)\left[h_v(x) + H_v(x)\right] \,, \tag{2.4}$$

where $h_v(x)$ and $H_v(x)$ are upper and lower components of $Q(x)$ defined as

$$h_v(x) = \exp\left(im_Q v\cdot x\right)P_+ Q(x) \,, \tag{2.5}$$
$$H_v(x) = \exp\left(im_Q v\cdot x\right)P_- Q(x) \,. \tag{2.6}$$

The phase factor is chosen to describe that the space-time dependence of the fields is weak. P_+ and P_- are positive and negative energy projection operators:

$$P_\pm = \frac{1\pm\not{v}}{2} \,. \tag{2.7}$$

The projection operators satisfy

$$P_\pm^2 = P_\pm \,, \quad P_\pm P_\mp = 0 \,. \tag{2.8}$$

h_v annihilates a heavy quark with velocity v, and H_v create a heavy antiquark with velocity v. From Eq. (2.7), the fields h_v and H_v are transformed by

$$\not{v} h_v = h_v \,, \quad \not{v} H_v = -H_v \,. \tag{2.9}$$

As for a hadron containing a heavy antiquark, the field is defined as

$$Q(x) = \exp\left(i m_Q v \cdot x\right) \left[h_v^-(x) + H_v^-(x)\right] \,, \tag{2.10}$$

where

$$h_v^-(x) = \exp\left(-i m_Q v \cdot x\right) P_- Q(x) \,, \tag{2.11}$$

$$H_v^-(x) = \exp\left(-i m_Q v \cdot x\right) P_+ Q(x) \,. \tag{2.12}$$

The QCD Lagrangian for heavy quarks is written as

$$\mathcal{L}_{\rm QCD} = \bar{Q}\left(i\not{D} - m_Q\right) Q \,, \tag{2.13}$$

where the covariant derivative is given by $D_\mu = \partial_\mu + i g A_\mu^a T^a$ with the gluon field A_μ^a and the generators of SU(3), T^a. Inserting the field $Q(x)$ in Eq. (2.4) into the QCD Lagrangian, we obtain

$$\mathcal{L}_{\rm QCD} = \bar{h}_v i v \cdot D h_v - \bar{H}(i v \cdot D + 2 m_Q) H_v + \bar{h}_v i\not{D}_\perp H_v + \bar{H}_v i\not{D}_\perp h_v \,. \tag{2.14}$$

The transverse part of the covariant derivative is written as

$$\not{D}_\perp = \gamma^\mu \left(g_{\mu\nu} - v_\mu v_\nu\right) D^\nu = \not{D} - \not{v}(v \cdot D) \,, \tag{2.15}$$

which is orthogonal to the velocity v, namely $v \cdot \not{D}_\perp = 0$.

As the next step, the field H_v is eliminated by using the equation of motion of QCD as

$$\begin{aligned} &(i\not{D} - m_Q) Q = 0 \\ \rightarrow\, &(i\not{D} - m_Q) \exp\left(-i m_Q v \cdot x\right) \left[h_v(x) + H_v(x)\right] = 0 \\ \rightarrow\, &i\not{D} h_v + (i\not{D} - 2 m_Q) H_v = 0 \,. \end{aligned} \tag{2.16}$$

Premultiplying it by P_-, we obtain

$$i\not{D}_\perp h_v - (i v \cdot D + 2 m_Q) H_v = 0 \,. \tag{2.17}$$

This can be transformed into

$$H_v = (i v \cdot D + 2 m_Q - i\varepsilon)^{-1} i\not{D}_\perp h_v \,. \tag{2.18}$$

Substituting Eq. (2.18) into the QCD Lagrangian in Eq. (2.14) yields the effective Lagrangian

$$\mathcal{L}_{\rm eff} = \bar{h}_v i v \cdot D h_v + \bar{h}_v i\not{D}_\perp (i v \cdot D + 2 m_Q - i\varepsilon)^{-1} i\not{D}_\perp h_v \,. \tag{2.19}$$

The second term can be expanded in iD/m_Q. Using the identity

$$i\not{D}_\perp i\not{D}_\perp = \left[(iD_\perp)^2 + \frac{1}{2}ig\sigma_{\alpha\beta}G^{\mu\nu}\right], \tag{2.20}$$

where $[D^\mu, D^\nu] = igG^{\mu\nu}$ is the gluon field strength tensor, we derive the effective Lagrangian at tree level as

$$\mathcal{L}_{\text{eff}} = \bar{h}_v iv\cdot D h_v + \bar{h}_v \frac{(iD_\perp)^2}{2m_Q} h_v + \bar{h}_v \frac{ig\sigma_{\alpha\beta}G^{\mu\nu}}{2m_Q} h_v + \mathcal{O}(1/m_Q^2)\,. \tag{2.21}$$

The leading term does not contain the dependence of heavy quark mass and spin. Hence, in the heavy quark limit, the Lagrangian manifests spin and flavor symmetries, namely heavy quark flavor and spin symmetries. The heavy flavor symmetry indicates that dynamics is not changed under the exchange of heavy quark flavors. The heavy quark spin symmetry indicates that dynamics is not changed by the spin flip of the heavy quark. The second and third terms which are proportional to the inverse of heavy quark mass m_Q violate the heavy quark symmetry in the finite heavy quark mass. The second term is the heavy quark kinetic energy which breaks the flavor symmetry. The third term describes the spin-dependent interaction between the heavy quark and the gluon field. Hence, this term violates both flavor and spin symmetries.

The heavy quark spin symmetry shows us remarkable feature in the heavy hadron systems. Because the heavy quark spin symmetry emerges due to the suppression of the spin-dependent forces such as the third term in Eq. (2.21), it leads to the separation of the heavy quark spin s_Q and the total angular momentum j of brown muck. Thus, the spin symmetry induces the spin degeneracy of the heavy hadron. For hadrons containing a single heavy quark ($s_Q = 1/2$), the states with total angular momentum and parity $(j-1/2)^P$ and $(j+1/2)^P$ for $j \neq 0$ are degenerate in the heavy quark limit, while the non-degenerate states appear for $j = 0$. The spin degeneracy has been discussed in the normal heavy hadrons as the observation of the small mass splittings between the heavy hadrons with different spins in the charm and bottom sectors. For the heavy mesons, the mass degeneracy of the heavy pseudoscalar and vector mesons are present: the mass splitting of D and D^* mesons for the charm sector are about 140 MeV, and that of B and B^* mesons for the bottom sector are about 45 MeV. They can be compared with the splitting in the light quark sector: $m_\rho - m_\pi \sim 600$ MeV and $m_{K^*} - m_K \sim 400$ MeV. The small mass splittings are also seen in the heavy hadrons with $J^P = 1/2^+$ and $3/2^+$ such as $m_{\Sigma_c^*} - m_{\Sigma_c} \sim 65$ MeV and $m_{\Sigma_b^*} - m_{\Sigma_b} \sim 20$ MeV for the charm and bottom baryons, respectively. The heavy quark spin symmetry also manifests the spin degeneracy in the multi-hadron states with heavy quarks, such as hadronic molecules and exotic nuclei [104,109]. The spin degeneracy for the hadronic molecules will be discussed in Chapter 5.

2.3 Heavy meson effective Lagrangian

In this section, we describe the effective Lagrangian for the heavy meson interacting with the pion and the vector mesons (ρ and ω). For the hadronic molecules addressed

in this study, the effective degrees of freedom are hadrons such as $\bar{D}$ and B mesons, and nucleon. From the effective Lagrangian, the one boson exchange potentials between constituent hadrons are constructed.

First of all, the field operators of the heavy pseudoscalar meson P and the heavy vector meson P^* are introduced in Sec. 2.3.1. Second, the chiral Lagrangian for the heavy mesons with Nambu-Goldstone bosons is constructed in Sec. 2.3.2. Finally, in Sec. 2.3.3, the effective Lagrangian for the heavy mesons with the light vector mesons are obtained.

2.3.1 Heavy meson fields

The heavy mesons composed of $\bar{Q}q$ ($Q\bar{q}$) with negative parity are represented by the 4×4 matrix H_a [113–118] as

$$H_a = \frac{1+\not{v}}{2}\left[P^*_{a\mu}\gamma^\mu - P_a\gamma_5\right] , \tag{2.22}$$

$$\bar{H}_a = \gamma_0 H_a^\dagger \gamma_0 = \left[P^{*\dagger}_{a\mu}\gamma^\mu + P^\dagger_a\gamma_5\right]\frac{1+\not{v}}{2} , \tag{2.23}$$

which are written as a linear combination of the P_a and P^*_a meson fields, where P_a (P^*_a) is annihilation operator which destroys P (P^*) mesons with the velocity v. The pseudoscalar and vector meson fields are normalized as

$$\langle 0 \,|\, P \,|\, P(p_\mu)\rangle = \sqrt{p^0} , \tag{2.24}$$

$$\left\langle 0 \,\middle|\, P^*_\mu \,\middle|\, P^*(p_\mu,\lambda)\right\rangle = \varepsilon(\lambda)_\mu \sqrt{p^0} , \tag{2.25}$$

where $\varepsilon(\lambda)_\mu$ is the polarization vector of P^* with polarization λ. The positive energy projection operator $(1+\not{v})/2$ chooses the upper component of the heavy quark. The subscript a is for light flavors (u, d, s).

Under the Lorenz transformation,

$$H_a \to D(\Lambda) H_a D(\Lambda)^{-1} , \tag{2.26}$$

where $D(\Lambda)$ is the Lorenz transformation matrix for spinors. Under the heavy quark spin transformation,

$$H_a \to S H_a, \tag{2.27}$$

where S belongs to SU(2), and satisfies $[\not{v}, S] = 0$.

2.3.2 Effective Lagrangian with light pseudoscalar mesons

Let us show the effective Lagrangian for the heavy meson with the Nambu-Goldstone (NG) bosons. The Lagrangian is described by the chiral perturbation theory [119–123], where is consistent with the symmetries, namely the heavy quark and chiral symmetries, and expressed as the expansion in terms of powers of Q/Λ_χ, with a small

momentum or pion mass Q, and chiral symmetry breaking scale $\Lambda_\chi \sim 1$ GeV. The NG bosons are expressed by

$$\xi = \sqrt{\Sigma} = \exp\left(i\mathcal{M}/f_\pi\right), \tag{2.28}$$

where $f_\pi = 132$ MeV is the pion decay constant and

$$\mathcal{M} = \begin{pmatrix} \frac{\pi^0}{\sqrt{2}} + \frac{\eta}{\sqrt{6}} & \pi^+ & K^+ \\ \pi^- & -\frac{\pi^0}{\sqrt{2}} + \frac{\eta}{\sqrt{6}} & K^0 \\ K^- & \bar{K}^0 & -\sqrt{\frac{2}{3}}\eta \end{pmatrix}. \tag{2.29}$$

The NG boson Σ builds up the chiral Lagrangian as

$$\mathcal{L}_{\text{chiral}} = \frac{1}{8} f_\pi^2 \text{Tr}\left[\partial^\mu \Sigma \partial_\mu \Sigma^\dagger\right], \tag{2.30}$$

at the lowest order in the derivatives, and in the massless limit. The Lagrangian is invariant under the transformation of $\text{SU}(3)_L \otimes \text{SU}(3)_R$,

$$\Sigma \to g_L \Sigma g_R^\dagger. \tag{2.31}$$

Under this chiral transformations, $\xi(x)$ and H_a are

$$\xi(x) \to g_L \xi(x) U^\dagger(x) = U(x)\xi(x) g_R^\dagger \tag{2.32}$$

$$H_a \to H_b U_{ba}^\dagger. \tag{2.33}$$

The matrix $U(x)$ belongs to the $\text{SU}(3)_v$ subgroup. The NG bosons interact with the heavy mesons through the covariant derivative

$$D_{ab}^\mu = \delta_{ab}\partial^\mu + V_{ab}^\mu, \tag{2.34}$$

with the vector current

$$V^\mu = \frac{1}{2}\left(\xi^\dagger \partial^\mu \xi + \xi \partial^\mu \xi^\dagger\right), \tag{2.35}$$

and through the axial current

$$A^\mu = \frac{1}{2}\left(\xi^\dagger \partial^\mu \xi - \xi \partial^\mu \xi^\dagger\right). \tag{2.36}$$

The V^μ and A^μ are transformed as

$$V^\mu \to U V^\mu U^\dagger + U \partial^\mu U^\dagger, \tag{2.37}$$

$$A^\mu \to U A^\mu U^\dagger. \tag{2.38}$$

At the leading order in the momentum expansion and in the $1/M_Q$ expansion (M_Q is a mass of the heavy meson), the strong interactions of the heavy meson and NG bosons [113–118] are described by

$$\mathcal{L}_{psHH} = i\mathrm{Tr}\left[H_b v_\mu D^\mu_{ba} \bar{H}_a\right] + ig\mathrm{Tr}\left[H_b \gamma_\mu \gamma_5 A^\mu_{ba} \bar{H}_a\right] . \tag{2.39}$$

The vector current in the first term in Eq. (2.39) leads to a coupling of even numbers of the NG bosons with the heavy meson, while the second term with the axial current expresses a coupling of odd numbers of the NG bosons. Hence, the one pion exchange potential is constructed by the second term as shown in Sec. 3.2.

The second term in Eq. (2.39) includes the interactions of heavy mesons (P, P^*) with a light pseudoscalar meson M_{ps} as vertices of PP^*M_{ps} and $P^*P^*M_{ps}$:

$$\mathcal{L}_{psPP^*} = 2\frac{g}{f_\pi}(P^\dagger_a P^*_{b\mu} + P^{*\dagger}_{a\mu} P_b)\partial^\mu \mathcal{M}_{ba} , \tag{2.40}$$

$$\mathcal{L}_{psP^*P^*} = 2i\frac{g}{f_\pi}\varepsilon^{\nu\mu\alpha\beta} v_\mu P^{*\dagger}_{a\beta} P^*_{b\nu} \partial_\alpha \mathcal{M}_{ba} . \tag{2.41}$$

The PPM_{ps} vertex is forbidden due to the parity conservation. The coupling constant g for the pion (expressed by g_π) can be fixed by the observed width of the $D^* \to D\pi$ decay. At the rest frame of the D^* meson, the decay width $\Gamma(D^* \to D\pi)$ is

$$\Gamma(D^* \to D\pi) = \frac{|p_\pi|}{8\pi m_{D^*}} |M|^2 , \tag{2.42}$$

where

$$p_\pi = \sqrt{\left(\frac{m^2_{D^*} - m^2_D + m^2_\pi}{2m_{D^*}}\right)^2 - m^2_\pi} . \tag{2.43}$$

The scattering amplitude $|M|$ is obtained by the Lagrangian in Eq. (2.40), and therefore we obtain the decay widths [103, 118]

$$\Gamma(D^{*+} \to D^0\pi^+) = \frac{g^2_\pi}{6\pi f^2_\pi} |p_\pi|^3 , \tag{2.44}$$

$$\Gamma(D^{*+} \to D^+\pi^0) = \frac{g^2_\pi}{12\pi f^2_\pi} |p_\pi|^3 . \tag{2.45}$$

From the experimental values, the D^{*+} decay width $\Gamma = 96$ KeV, and the fractions $\Gamma(D^{*+} \to D^0\pi^+)/\Gamma = 0.677$ and $\Gamma(D^{*+} \to D^+\pi^0)/\Gamma = 0.307$ [124], we obtain $|g_\pi| = 0.59$. The coupling of the $D^*D\pi$ vertex ($g_{D^*D\pi}$) is also studied by other approaches. The lattice QCD simulation in Ref [125] predicted $g_{D^*D\pi} = 18.8 \pm 2.3^{+1.1}_{-2.0}$ with systematic and statical errors. The definition is related to g_π through $g_{D^*D\pi} = 2\sqrt{m_D m_{D^*}} g_\pi / f_\pi$, and therefore they obtained a large value, $g_\pi = 0.67 \pm 0.08^{+0.04}_{-0.06}$.

In the heavy quark limit, we can use g_π with the same value for Eqs. (2.40) and (2.41) from the heavy quark spin symmetry. For finite heavy quark masses, however, the $1/M_Q$ corrections split the couplings for $PP^*\pi$ and $P^*P^*\pi$ vertices as discussed in Refs. [103, 118, 126–130].

2.3.3 Effective Lagrangian with light vector mesons

The interaction Lagrangian for heavy mesons with light vector mesons is introduced by the hidden gauge symmetry approach [131].

The pseudoscalar meson field Σ is written as

$$\Sigma = LR^\dagger \,. \tag{2.46}$$

The chiral Lagrangian in Eq. (2.30) is invariant under the transformation of $\mathrm{SU}(3)_L \otimes \mathrm{SU}(3)_R \otimes \mathrm{SU}(3)_H$,

$$L \to g_l L h^\dagger \,, \tag{2.47}$$

$$R \to g_R L h^\dagger \,, \tag{2.48}$$

where $h \in \mathrm{SU}(3)_H$ is a local gauge transformation [118, 132]. When we chose the gauge fixing $L = R = \xi$, this is the same as the Lagrangian in the previous section. The vector and axial currents are then expressed as

$$V^\mu = \frac{1}{2}\left(L^\dagger \partial^\mu L + R^\dagger \partial^\mu R\right) \,, \tag{2.49}$$

$$A^\mu = \frac{1}{2}\left(L^\dagger \partial^\mu L - R^\dagger \partial^\mu R\right) \,, \tag{2.50}$$

which are transformed as

$$V^\mu \to h V^\mu h^\dagger + h\partial^\mu h^\dagger \,, \tag{2.51}$$

$$A^\mu \to h A^\mu h^\dagger \,, \tag{2.52}$$

under the local group $\mathrm{SU}(3)_H$. The heavy meson field H_a is transformed as

$$H_a \to H_b h^\dagger_{ba} \,. \tag{2.53}$$

The covariant derivative is give by $D^\mu = \partial^\mu + V^\mu$ with the vector current in Eq. (2.51).

The light vector mesons are introduced as the gauge bosons of the hidden local symmetry. The vector meson field are defined as

$$\rho_\mu = i\frac{g_V}{\sqrt{2}}\hat{\rho}_\mu \,, \tag{2.54}$$

$$\hat{\rho}_\mu = \begin{pmatrix} \dfrac{\rho^0}{\sqrt{2}} + \dfrac{\omega}{\sqrt{2}} & \rho^+ & K^{*+} \\ \rho^- & -\dfrac{\rho^0}{\sqrt{2}} + \dfrac{\omega}{\sqrt{2}} & K^{*0} \\ K^{*-} & \bar{K}^{*0} & \phi \end{pmatrix} \,, \tag{2.55}$$

where $g_V = m_\rho / f\pi$ is the gauge coupling constant of the hidden local symmetry [131]. The field ρ_μ is transformed as the vector current,

$$\rho_\mu \to h\rho_\mu h^\dagger + h\partial_\mu h^\dagger \,. \tag{2.56}$$

The strong interactions of the heavy meson and the light vector meson [118, 132] are given

$$\mathcal{L}_{vHH} = -i\beta \mathrm{Tr}\left[H_b v^\mu (\rho_\mu)_{ba} \bar{H}_a\right] + i\lambda \mathrm{Tr}\left[H_b \sigma^{\mu\nu} F_{\mu\nu}(\rho)_{ba} \bar{H}_a\right] , \tag{2.57}$$

where the field tensor $F_{\mu\nu}(\rho)$ is defined as

$$F_{\mu\nu}(\rho) = \partial_\mu \rho_\nu - \partial_\nu \rho_\mu + [\rho_\mu, \rho_\nu] . \tag{2.58}$$

This Lagrangian provides vPP, vPP^* and vP^*P^* vertices as

$$\mathcal{L}_{vPP} = -\sqrt{2}\beta g_V P_b P_a^\dagger v \cdot \hat{\rho}_{ba} , \tag{2.59}$$

$$\mathcal{L}_{vPP^*} = -2\sqrt{2}\lambda g_V v_\mu \varepsilon^{\mu\nu\alpha\beta} (P_a^\dagger P^*_{b\beta} - P^{*\dagger}_{a\beta} P_b) \partial_\nu (\hat{\rho}_\alpha)_{ba} , \tag{2.60}$$

$$\mathcal{L}_{vP^*P^*} = \sqrt{2}\beta g_V P_b^* P_a^{*\dagger} v \cdot \hat{\rho}_{ba} + i2\sqrt{2}\lambda g_V P^{*\dagger}_{a\mu} P^*_{b\nu} (\partial^\mu (\hat{\rho}^\nu)_{ba} - \partial^\nu (\hat{\rho}^\mu)_{ba}) . \tag{2.61}$$

The coupling constant $\beta = 0.9$ is determined by the vector meson dominance as discussed in Ref. [133]. Therefore, β can be related to the $\gamma\rho$ coupling. The coupling constants $\lambda = 0.59$ GeV^{-1} are obtained by a form factor of a semileptonic decay of a heavy meson [117, 133].

Chapter 3

Exotic baryons formed by heavy meson and nucleon (2-body system)

3.1 Introduction

In this chapter, the possible existence of two-body hadronic molecules formed by a heavy meson and a nucleon is discussed both in charm and bottom sectors. As for the heavy meson, we consider both $P(=\bar{D}, B)$ meson and their antiparticles, $\bar{P}(=D, \bar{B})$ meson[‡] . The heavy meson and the nucleon N would compose of the PN molecule for the exotic channel, and the $\bar{P}N$ molecule for non-exotic channel, drawn in Fig. 3.1.

A unique feature of the $\bar{D}N$ (BN) states is their genuinely exotic flavor structure with the minimal quark content $\bar{Q}qqqq$ [33–41], where $\bar{Q}$ is a heavy antiquark and q's are light quarks. Therefore, the $\bar{D}N$ (BN) states have no lower channels coupled by the strong decay and such molecules give us a new aspect of the pentaquark states with a heavy antiquark. The counterpart, KN molecules, in the strangeness sector doesn't exist due to the repulsion between a K meson and a nucleon [94], while the pentaquark state Θ^+ has been investigated [34, 42–47].

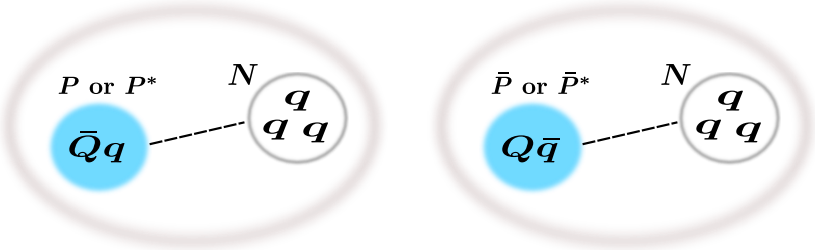

Fig.3.1 PN and $\bar{P}N$ molecules for the two-body systems.

[‡] In this thesis, P $(\bar{P})$ is defined as a meson $\bar{Q}q$ $(Q\bar{q})$. (For clarity, the $\bar{P}$ will sometimes be omitted.)

The DN ($\bar{B}N$) states with the non-exotic flavor structure are intimately related to the ordinary heavy baryons such as Λ_c and Σ_c (Λ_b and Σ_b). Heavy baryons have been studied as Qqq states by the standard quark model [68,69]. Recently, the excited baryon states with a composite structure are discussed. The $\Lambda_c(2595)$ is studied as a deeply quasi-bound state of DN in Ref. [49], which is analogous to the $\Lambda(1405)$ as a quasi-bound state of $\bar{K}N$ [8]. The DN interaction is expected to be stronger than the $\bar{D}N$ interaction because the short-range forces, namely ρ and ω exchanges, for DN produce a strong attraction, while the ρ exchange is attraction but the ω exchange is repulsion for $\bar{D}N$. This can be seen in the light flavor sector. The $N\bar{N}$ and $\bar{K}N$ interactions are known to produce the strong attraction rather than the NN and KN interactions. In the deeply bound systems for DN (and also for $\bar{B}N$), the couplings to the three-quark states are not negligible because the size of such composite states is expected to be small, and constituent hadrons overlap each other. Near the DN ($\bar{B}N$) threshold, however, it is expected that the DN ($\bar{B}N$) molecular components dominate because the spatially size is extended.

In the systems of a heavy meson and a nucleon, the one pion exchange potential (OPEP) is expected to play a dominant role to produce a strong attraction because it is enhanced by the heavy quark spin symmetry. This symmetry manifests in mass degeneracy of heavy pseudoscalar mesons $P = \bar{D}$, B ($\bar{P} = D$, $\bar{B}$) and vector mesons $P^* = \bar{D}^*$, B^* ($\bar{P}^* = D^*$, $\bar{B}^*$) due to the suppression of the spin-dependent forces between heavy quarks and light degrees of freedom in the heavy hadron [99, 100]. Indeed, the mass splitting between a $\bar{D}$ (B) meson and a $\bar{D}^*$ (B^*) meson is small; 140 MeV for $\bar{D}$ and $\bar{D}^*$ mesons and 45 MeV for B and B^* mesons. The small mass splittings in the heavy flavor sectors should be compared with the large mass splittings, ~ 400 MeV for $\bar{K}$ and $\bar{K}^*$ mesons, and ~ 600 MeV for π and ρ mesons, in the light flavor sectors. Because of this, the heavy quark spin symmetry introduces the mixing of PN and P^*N states. Therefore, both P and P^* mesons are considered on the same footing as fundamental degrees of freedom in the dynamics. For convenience, in the following, we introduce a notation $P^{(*)}$ to stand for P or P^*. Thanks to the $PN - P^*N$ mixing, the OPEP between a $P^{(*)}$ meson and a nucleon N is supplied by $PP^*\pi$ and $P^*P^*\pi$ vertices [37, 134–136].

The importance of the OPEP has been discussed in the nuclear physics. The pion was introduced by H. Yukawa to explain the nuclear force [137]. The specific features of the pion are the small mass and the pseudoscalar nature, coming from the fact that it is a Nambu-Goldstone boson. The small mass of the pion provides the long-range force, and the pseudoscalar nature leads to the presence of the tensor force in the OPEP. The tensor force mixing the channels with different orbital angular momenta is a driving force to produce the bound states of atomic nuclei. In the deuteron, the tensor force inducing the ${}^3S_1 - {}^3D_1$ channel coupling generates a strong attraction [95, 96]. For the PN interaction, this mechanism also emerges through the mixing of PN and P^*N channels as shown in Fig. 3.2, and therefore we expect that the OPEP plays an important role in the hadronic molecules including the heavy meson. We note that the OPEP does not exist $PN - PN$ only because the $PP\pi$ vertex is forbidden by the parity conservation. The $PN - P^*N$ mixing becomes important as the mass splitting between P and P^* mesons decreases. Therefore, the OPEP is more essential in the heavy meson systems due to the heavy quark spin

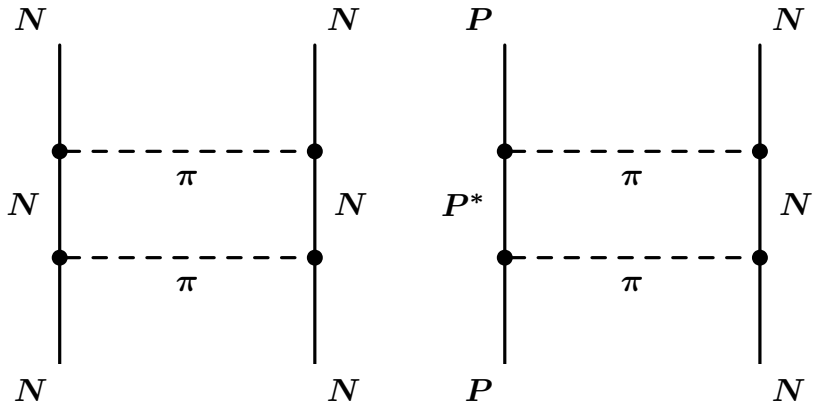

Fig.3.2 OPEP between two nucleons (left) and a heavy meson and a nucleon (right). The tensor force emerges through the $NN(^3S_1) - NN(^3D_1)$ mixing for the deuteron, and the $PN(^2S_{1/2}) - P^*N(^4D_{1/2})$ mixing for the PN state with $J^P = 1/2^-$.

symmetry. In contrast, the mass splitting between K and K^* mesons, and π and ρ mesons are much larger than the heavy flavor sectors, $m_{K^*} - m_K \sim 400$ MeV, and $m_\rho - m_\pi \sim 600$ MeV. Hence, the nature of interactions is expected to be different from the PN states, and KN ($\bar{K}N$) and πN states.

Those $P^{(*)}N$ states can be classified by total angular momentum J, parity P and isospin I. In the present study, we investigate the states with $J^P = 1/2^\pm$, $3/2^\pm$, $5/2^\pm$, $7/2^\pm$ and $9/2^\pm$ for $I = 0$ and 1, as summarized in Table. 3.1. As mentioned above, the channel couplings for PN and P^*N become important in the $P^{(*)}N$ states. Therefore, it is necessary to solve coupled-channel equations for PN and P^*N channels.

3.2 Heavy meson-Nucleon Interactions

3.2.1 Interaction Lagrangians and Form factors

In this section, we construct the one boson exchange potential between a $P^{(*)}$ meson and a nucleon from the effective Lagrangian introduced in the previous chapter. We employ the Lagrangians for a light meson (π, ρ, ω) and heavy mesons, given in Eqs. (2.40)-(2.41) and (2.59)-(2.61), namely

$$\mathcal{L}_{\pi PP^*} = 2\frac{g_\pi}{f_\pi}(P_a^\dagger P^*_{b\mu} + P^{*\dagger}_{a\mu} P_b)\partial^\mu \hat{\pi}_{ba}\,, \tag{3.1}$$

$$\mathcal{L}_{\pi P^*P^*} = 2i\frac{g_\pi}{f_\pi}\varepsilon^{\nu\mu\alpha\beta} v_\mu P^{*\dagger}_{a\beta} P^*_{b\nu}\partial_\alpha \hat{\pi}_{ba}\,. \tag{3.2}$$

for the pion and

$$\mathcal{L}_{vPP} = -\sqrt{2}\beta g_V P_b P_a^\dagger v\cdot\hat{\rho}_{ba}\,, \tag{3.3}$$

$$\mathcal{L}_{vPP^*} = -2\sqrt{2}\lambda g_V v_\mu \varepsilon^{\mu\nu\alpha\beta}(P_a^\dagger P^*_{b\beta} - P^{*\dagger}_{a\beta} P_b)\partial_\nu(\hat{\rho}_\alpha)_{ba}\,, \tag{3.4}$$

$$\mathcal{L}_{vP^*P^*} = \sqrt{2}\beta g_V P_b^* P_a^{*\dagger} v\cdot\hat{\rho}_{ba} + i2\sqrt{2}\lambda g_V P^{*\dagger}_{a\mu} P^*_{b\nu}(\partial^\mu(\hat{\rho}^\nu)_{ba} - \partial^\nu(\hat{\rho}^\mu)_{ba})\,. \tag{3.5}$$

Table.3.1 Various coupled channels for a given quantum number J^P in $P^{(*)}N$ systems. The channels for the J^P state are specified by orbital angular momentum L and total spin S as $^{2S+1}L_J$.

J^P	channels	# of channels
$1/2^-$	$PN(^2S_{1/2})$ $P^*N(^2S_{1/2}, {}^4D_{1/2})$	3
$1/2^+$	$PN(^2P_{1/2})$ $P^*N(^2P_{1/2}, {}^4P_{1/2})$	3
$3/2^-$	$PN(^2D_{3/2})$ $P^*N(^4S_{3/2}, {}^2D_{3/2}, {}^4D_{3/2})$	4
$3/2^+$	$PN(^2P_{3/2})$ $P^*N(^2P_{3/2}, {}^4P_{3/2}, {}^4F_{3/2})$	4
$5/2^-$	$PN(^2D_{5/2})$ P^*N $(^2D_{5/2}, {}^4D_{5/2}, {}^4G_{5/2})$	4
$5/2^+$	$PN(^2F_{5/2})$ P^*N $(^4P_{5/2}, {}^2F_{5/2}, {}^4F_{5/2})$	4
$7/2^-$	$PN(^2G_{7/2})$ P^*N $(^4D_{7/2}, {}^2G_{7/2}, {}^4G_{7/2})$	4
$7/2^+$	$PN(^2F_{7/2})$ P^*N $(^2F_{7/2}, {}^4F_{7/2}, {}^4H_{7/2})$	4
$9/2^-$	$PN(^2G_{9/2})$ P^*N $(^2G_{9/2}, {}^4G_{9/2}, {}^4I_{9/2})$	4
$9/2^+$	$PN(^2H_{9/2})$ P^*N $(^4F_{9/2}, {}^2H_{9/2}, {}^4H_{9/2})$	4

for the vector mesons, where the scrips π and v are for the pion and vector meson (ρ and ω), respectively. For pion vertices, there is no πPP vertex due to parity conservation. The pion and vector meson fields are

$$\hat{\pi} = \begin{pmatrix} \frac{\pi^0}{\sqrt{2}} & \pi^+ \\ \pi^- & -\frac{\pi^0}{\sqrt{2}} \end{pmatrix} = \frac{\vec{\tau}\cdot\vec{\pi}}{\sqrt{2}}\,, \tag{3.6}$$

$$\hat{\rho}_\mu = \begin{pmatrix} \frac{\rho^0}{\sqrt{2}} + \frac{\omega^0}{\sqrt{2}} & \rho^+ \\ \rho^- & -\frac{\rho^0}{\sqrt{2}} + \frac{\omega^0}{\sqrt{2}} \end{pmatrix} = \frac{\vec{\tau}\cdot\vec{\rho}_\mu}{\sqrt{2}}\,. \tag{3.7}$$

Here, $\vec{\tau}$ are isospin matrices represented by Pauli matrices. Spherical components $(\pi^\pm, \pi^0)$ in Eq. (3.6) are related to cartesian components (π_1, π_2, π_3) as

$$\pi^\pm = \frac{\pi_1 \pm i\pi_2}{\sqrt{2}}\,,\ \pi^0 = \pi_3\,. \tag{3.8}$$

From the heavy quark spin symmetry, we use the coupling constants with same value for Eqs. (3.1)-(3.2) for g_π, and for Eqs. (3.3)-(3.5) for β and γ. The couplings are employed both in charm and bottom sectors due to the heavy quark flavor symmetry. The values are summarized in Table 3.2.

Table.3.2 Masses and coupling constants of mesons $\alpha(=\pi,\rho,\omega)$ for $\bar{D}N$ and BN systems [37,134–136]. For DN and $\bar{B}N$, the signs of g_π, β and λ for vertices of π and ω are reversed due to G-parity transformation.

Meson	m_α [MeV]	g_π	β	λ [GeV^{-1}]	$g^2_{\alpha NN}/4\pi$	κ
π	137.27	0.59	—	—	13.6	—
ρ	769.9	—	0.9	0.56	0.84	6.1
ω	781.94	—	0.9	0.56	20.0	0.0

Table.3.3 Cutoff parameter Λ_N and low energy properties of the NN system, namely binding energy E_B, mixing ratio of $^3D_1$ channel P_D, relative distance $\langle r^2\rangle^{1/2}$, scattering length a and effective range r_e. Results for π potential and $\pi\rho\omega$ potential are compared.

Potential	Λ_N [MeV]	E_B [MeV]	P_D [%]	$\langle r^2\rangle^{1/2}$ [fm]	a [fm]	r_e [fm]
π	837	2.22	5.4	3.7	5.27	1.50
$\pi\rho\omega$	846	2.22	5.3	3.7	5.23	1.49

The interaction Lagrangians for nucleons and a light meson are given by Bonn model [138, 139] as

$$\mathcal{L}_{\pi NN} = \sqrt{2} i g_{\pi NN} \bar{N}\gamma_5 \hat{\pi} N = i g_{\pi NN} \bar{N}\gamma_5 \vec{\tau} N \cdot \vec{\pi}\,, \tag{3.9}$$

$$\mathcal{L}_{vNN} = \sqrt{2} g_{vNN} \left[\bar{N}\gamma_\mu \hat{\rho} N + \frac{\kappa}{2m_N} \bar{N}\sigma_{\mu\nu}\partial^\nu \hat{\rho}^\mu N \right], \tag{3.10}$$

where $N = (p,n)^T$ is nucleon field and $m_N = 940$ MeV is the mass of nucleon. The coupling constants are determined by NN scattering data phenomenologically [139] and summarized also in Table 3.2.

To parametrize internal structure of hadrons, we introduce dipole-type form factor

$$F_\alpha(\Lambda,\vec{q}) = \frac{\Lambda_N^2 - m_\alpha^2}{\Lambda_N^2 + |\vec{q}|^2} \frac{\Lambda_P^2 - m_\alpha^2}{\Lambda_P^2 + |\vec{q}|^2} \tag{3.11}$$

with cutoff parameters $\Lambda = \Lambda_N, \Lambda_P$, where m_α and $\vec{q}$ are the mass and three momentum of the incoming meson $\alpha = \pi, \rho, \omega$, respectively. These cutoffs are fixed as follows. First, the cutoff Λ_N for the nucleon vertex is determined to reproduce the properties of the deuteron, the binding energy, scattering length and effective range, when we solve the nucleon-nucleon system for π exchange potential and $\pi\rho\omega$ exchange potentials. The NN potential is also constructed by Eqs. (3.9) and (3.10), and form factor $F(\Lambda_N,\vec{q}) = ((\Lambda_N^2 - m_\alpha^2)/(\Lambda_N^2 + |\vec{q}|^2))^2$. Then, we obtain $\Lambda_N = 837$ MeV for π potential, and $\Lambda_N = 846$ MeV for $\pi\rho\omega$ potential summarized in Table 3.3. We find that these cutoffs can reproduce the low energy properties of the deuteron and NN scattering as shown in Table 3.3.

Second, we fix cutoff parameter Λ_P for the heavy meson vertex. We assume the relation $\Lambda_P/\Lambda_N = r_N/r_P$, where r_N (r_P) is the matter radius of the nucleon (heavy meson). From quark model estimation [37], we use $\Lambda_D = 1.35\Lambda_N$ for $\bar{D}^{(*)}$ ($D^{(*)}$) meson, $\Lambda_B = 1.29\Lambda_N$ for $B^{(*)}$ ($\bar{B}^{(*)}$), where $r_N = 0.58$ fm, $r_D = 0.43$ fm and $r_B = 0.45$ fm.

We would like to give a comment on the meson exchange interaction in our model. In the present study, we doesn't consider the σ exchange potential explicitly to simplify our model calculation, while this plays non-negligible role in the realistic NN potential model. In particular, the σ exchange potential cancels out the contribution of vector meson (ω) exchange potential. However, we assume that the effect of the σ exchange potential is in the small value of the cutoff Λ_N in Table 3.3. In fact the cutoff Λ_N is smaller than in Bonn potential (over 1 GeV) [138,139], and close to the masses of vector mesons, 769.9 MeV for ρ meson and 781.94 MeV for ω meson. Therefore, in our model, the contribution of vector meson exchange potential is suppressed by the small cutoff Λ_N effectively (See Eq.(3.11)). In fact, our NN potential can reproduce the properties of the deuteron without the σ exchange potential as seen in Table 3.3.

3.2.2 Meson exchange potentials between a heavy meson and a nucleon

The meson exchange potentials between a heavy meson and a nucleon are obtained by the second-order Feynman diagrams shown in Fig. 3.3. In the c.m system, the Feynman amplitude for an α meson exchange is calculated as

$$-i\bar{V}_\alpha(p',p) = \Gamma_P^\alpha \bar{u}_N(-p')\Gamma_N^\alpha u_N(-p)\frac{P_\alpha}{q^2 - m_\alpha^2}\,, \tag{3.12}$$

where u_N is the Dirac spinor for the nucleon, p (p') is a four-momentum in the initial (final) state and $\Gamma_i^{(\alpha)}$ is a vertex obtained by interaction Lagrangians and the form factor. P_α is a numerator in the meson propagator; $P_\alpha = i$ for a pseudo-meson and $P_\alpha = -ig_{\mu\nu}$ for a vector meson. q is defined as $q = p' - p$. Dirac spinors are given by

$$u_N(p,s) = \sqrt{\frac{E_p + m_N}{2m_N}} \begin{pmatrix} 1 \\ (\vec{\sigma}\cdot\vec{p})/(E_p + m_N) \end{pmatrix} \chi_s\,, \tag{3.13}$$

$$\begin{aligned}\bar{u}_N(p,s) = u^\dagger(p,s)\gamma^0 &= \sqrt{\frac{E_p + m_N}{2m_N}}\chi_s^\dagger \begin{pmatrix} 1 & \dfrac{\vec{\sigma}\cdot\vec{p}}{E_p + m_N} \end{pmatrix} \begin{pmatrix} 1 & 0 \\ 0 & -1 \end{pmatrix} \\ &= \sqrt{\frac{E_p + m_N}{2m_N}}\chi_s^\dagger \begin{pmatrix} 1 & -\dfrac{\vec{\sigma}\cdot\vec{p}}{E_p + m_N} \end{pmatrix}\,,\end{aligned} \tag{3.14}$$

with $E_p = \sqrt{m_N^2 + \vec{p}^{\,2}}$ and a Pauli spinor χ_s. The Dirac spinors are normalized as $\bar{u}_N(p)u_N(p) = 1$.

The potentials in the coordinate space are obtained from Eq. (3.12) by performing the Fourier transformation. As a consequence, we obtain meson exchange potentials for $PN - PN$, $PN - P^*N$ and $P^*N - P^*N$ scatterings. Here we consider the static approximation $v^\mu = (1, \vec{0})$ in the potentials.

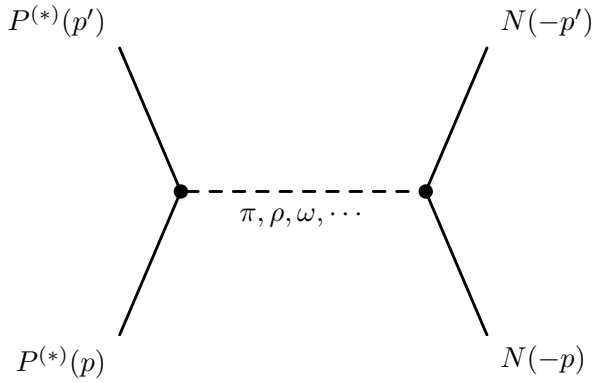

Fig.3.3 Feynman diagrams of one boson exchange potentials. Solid (dashed) line denotes the $P^{(*)}$ mesons and nucleons N (the exchanged bosons).

The one pion exchange potentials (OPEP) are given by $\mathcal{L}_{\pi PP^*}$, $\mathcal{L}_{\pi P^*P^*}$ and $\mathcal{L}_{\pi NN}$ as

$$V^{\pi}_{PN-P^*N}(r) = -\frac{g_\pi g_{\pi NN}}{\sqrt{2} m_N f_\pi} \frac{1}{3} \left[\vec{\varepsilon}^{\,\dagger} \cdot \vec{\sigma} C(r; m_\pi) + S_\varepsilon T(r; m_\pi) \right] \vec{\tau}_P \cdot \vec{\tau}_N, \tag{3.15}$$

$$V^{\pi}_{P^*N-P^*N}(r) = \frac{g_\pi g_{\pi NN}}{\sqrt{2} m_N f_\pi} \frac{1}{3} \left[\vec{S} \cdot \vec{\sigma} C(r; m_\pi) + S_S T(r; m_\pi) \right] \vec{\tau}_P \cdot \vec{\tau}_N, \tag{3.16}$$

where $\vec{S}$ is the spin-one operator of P^*, defined by $S^i_{\lambda'\lambda} = i\varepsilon^{ijk} \varepsilon^{(\lambda')\dagger}_j \varepsilon^{(\lambda)}_k$, and S_ε (S_S) is the tensor operator $S_{\mathcal{O}}(\hat{r}) = 3(\vec{\mathcal{O}} \cdot \hat{r})(\vec{\sigma} \cdot \hat{r}) - \vec{\mathcal{O}} \cdot \vec{\sigma}$ with $\hat{r} = \vec{r}/r$ and $r = |\vec{r}|$ for $\vec{\mathcal{O}} = \vec{\varepsilon}\,(\vec{S}\,)$, where $\vec{r}$ is the relative position vector between $P^{(*)}$ and N. $\vec{\sigma}$ are Pauli matrices acting on nucleon spin. $\vec{\tau}_P$ ($\vec{\tau}_N$) are isospin operators for $P^{(*)}$ (N). The central and tensor forces, $C(r)$ and $T(r)$, are written by

$$C(r; m) = \int \frac{d^3\vec{q}}{(2\pi)^3} \frac{m^2}{\vec{q}^{\,2} + m^2} e^{i\vec{q}\cdot\vec{r}} F(\Lambda, \vec{q}) \tag{3.17}$$

$$= \frac{m^2}{4\pi r} \left[e^{-mr} + \frac{\Lambda_N^2 - m^2}{\Lambda_P^2 - \Lambda_N^2} e^{-\Lambda_P r} + \frac{\Lambda_P^2 - m^2}{\Lambda_N^2 - \Lambda_P^2} e^{-\Lambda_N r} \right], \tag{3.18}$$

$$S_{\mathcal{O}}(\hat{r}) T(r; m)$$

$$= \int \frac{d^3\vec{q}}{(2\pi)^3} \frac{-\vec{q}^{\,2}}{\vec{q}^{\,2} + m^2} S_{\mathcal{O}}(\hat{q}) e^{i\vec{q}\cdot\vec{r}} F(\Lambda, \vec{q}) \tag{3.19}$$

$$= S_{\mathcal{O}}(\hat{r}) \frac{1}{4\pi r^3} \left[(3 + 3mr + m^2 r^2) e^{-mr} + \frac{\Lambda_N^2 - m^2}{\Lambda_P^2 - \Lambda_N^2} (3 + 3\Lambda_P r + \Lambda_P^2 r^2) e^{-\Lambda_P r} \right.$$

$$\left. + \frac{\Lambda_P^2 - m^2}{\Lambda_N^2 - \Lambda_P^2} (3 + 3\Lambda_N r + \Lambda_N^2 r^2) e^{-\Lambda_N r} \right], \tag{3.20}$$

respectively.

The vector meson exchange potentials (ρ and ω) are also obtained by $\mathcal{L}_{vPP}$, $\mathcal{L}_{vPP^*}$,

$\mathcal{L}_{vP^*P^*}$ and $\mathcal{L}_{vNN}$ as

$$V^v_{PN-PN}(r) = \frac{\beta g_V g_{vNN}}{\sqrt{2}m_v^2} C(r;m_v)\vec{\tau}_P\cdot\vec{\tau}_N, \tag{3.21}$$

$$V^v_{PN-P^*N}(r) = \frac{g_V g_{vNN}\lambda(1+\kappa)}{\sqrt{2}m_N}\frac{1}{3}\left[-2\vec{\varepsilon}\cdot\vec{\sigma}C(r;m_v) + S_\varepsilon T(r;m_v)\right]\vec{\tau}_P\cdot\vec{\tau}_N, \tag{3.22}$$

$$\begin{aligned} V^v_{P^*N-P^*N}(r) = {} & \frac{\beta g_V g_{vNN}}{\sqrt{2}m_v^2} C(r;m_v)\vec{\tau}_P\cdot\vec{\tau}_N \\ & + \frac{g_V g_{vNN}\lambda(1+\kappa)}{\sqrt{2}m_N}\frac{1}{3}\left[2\vec{S}\cdot\vec{\sigma}C(r;m_v) - S_S T(r;m_v)\right]\vec{\tau}_P\cdot\vec{\tau}_N. \end{aligned} \tag{3.23}$$

The explicit forms of the meson exchange potentials for each J^P are summarized in Appendix B.2.

3.3 Numerical results of $\bar{D}^{(*)}N$ and $B^{(*)}N$ (Exotic states)

Let us discuss exotic channels for the $PN - P^*N$ system. To obtain bound and resonant states, we solve the coupled-channel Schrödinger equations numerically for PN and P^*N channels. The total Hamiltonian $H_{J^P} = K_{J^P} + V_{J^P}$ for each J^P is given by the kinetic term K_{J^P} summarized in the Appendix B.2 and the potentials V_{J^P} between a $P^{(*)}$ meson and a nucleon, introduced in the previous section. As for a method to solve second order differential equations with the channel-couplings, we apply the renormalized Numerov method developed by B. R. Johnson in Refs. [140–142]. This method is also applied to $\bar{P}N$ systems for the non-exotic channels in Sec.3.4.

Two potentials are employed in our calculations, the π potential and $\pi\rho\omega$ potential, and we discuss the importance of the OPEP in the hadronic molecules.

We present the results for the bound states in Sec. 3.3.1 and the resonances in Sec. 3.3.2. The obtained energies are summarized in Tables 3.4 and 3.8, and also in Fig. 3.8.

3.3.1 Bound states

In the present section, we discuss the bound states for the $P^{(*)}N$ systems. We find bound states in the $(I, J^P) = (0, 1/2^-)$ both for $\bar{D}^{(*)}N$ and $B^{(*)}N$. We emphasize that they are stable against the strong decay, because there is no lower hadronic state. The binding energies E_B and relative distance between constituent hadrons $\langle r^2\rangle^{1/2}$ are summarized in Table. 3.4. We find that the results of π potential is almost same as those of $\pi\rho\omega$ potential. In Table. 3.4, the bound state of $\bar{D}^{(*)}N$ has the small binding energy, about 2 MeV, which is close to $\bar{D}N$ threshold, and large relative distance, over 3 fm. Hence, the $\bar{D}^{(*)}N$ states form a loosely bound state like the

deuteron. For the bottom sector, the $B^{(*)}N$ states have large binding energy, about 20 MeV. The corresponding relative distance, over 1 fm, is slightly large compared to twice of typical hadron size, namely 1 fm.

Table.3.4 Binding energy E_B and relative distance $\langle r^2 \rangle^{1/2}$ for $\bar{D}^{(*)}N$ and $B^{(*)}N$ bound states. Results for π and $\pi\rho\omega$ potentials are compared.

	$\bar{D}^{(*)}N(\pi)$	$\bar{D}^{(*)}N(\pi\rho\omega)$	$B^{(*)}N(\pi)$	$B^{(*)}N(\pi\rho\omega)$
E_B [MeV]	1.6	2.1	19.5	23.0
$\langle r^2 \rangle^{1/2}$ [fm]	3.5	3.2	1.3	1.2

The wave functions of the $\bar{D}^{(*)}N$ and $B^{(*)}N$ are displayed in Fig. 3.4. We depict only the results for the $\pi\rho\omega$ potential because the difference between results for the π and $\pi\rho\omega$ potentials are small. In Fig. 3.4, the wave function of the $\bar{D}N(^2S_{1/2})$ has a long tail which is not negligible even at a distance of 10 fm. Both in the charm and bottom sectors, the $PN(^2S_{1/2})$ channel is most dominant component in the bound states, while the P^*N channels are suppressed due to the excess of mass of about 140 MeV for the charm sector and about 45 MeV for the bottom sector. From the wave functions, we obtain the mixing ratios of $PN(^2S_{1/2})$, $P^*N(^2S_{1/2})$ and $P^*N(^4D_{1/2})$ channels listed in Table 3.5. The mixing ratios of the P^*N channels are very small in comparison with ratio of the $PN(^2S_{1/2})$ channel. However, the $P^*N(^4D_{1/2})$ channel plays an important role to form the bound state as will be shown later.

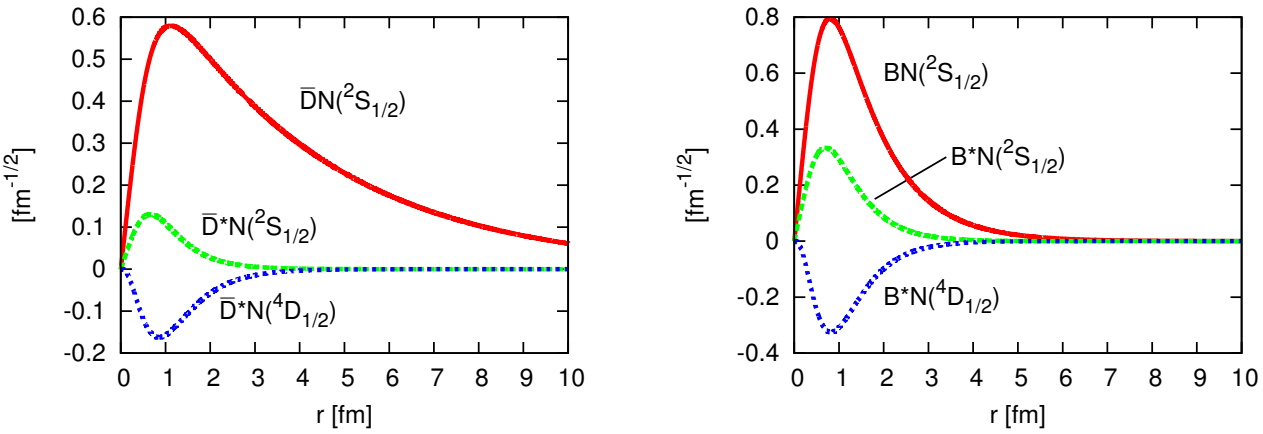

Fig.3.4 Wave functions of the $\bar{D}^{(*)}N$ and $B^{(*)}N$ bound states for the $(I, J^P) = (0, 1/2^-)$ state when the $\pi\rho\omega$ potential is used [39].

To investigate how the bound states are formed, we estimate the energy expectation values of interaction matrix elements. The expectation values of the π, ρ and ω exchange potentials, sandwiched by the obtained wave functions, are shown in Tables. 3.6 and 3.7. We find that the $\langle PN(S)\,|\,V\,|\,P^*N(D)\rangle$ component of the π exchange potential plays a dominant role both in the $\bar{D}^{(*)}N$ and $B^{(*)}N$ states. This component of the OPEP has the tensor force corresponding to the second term in Eq. (3.15) (see

Table.3.5 Mixing ratios of each channel in the $\bar{D}^{(*)}N$ and $B^{(*)}N$ bound states when $\pi\rho\omega$ potential is used.

	$PN(^2S_{1/2})$	$P^*N(^2S_{1/2})$	$P^*N(^4D_{1/2})$
$\bar{D}^{(*)}N$	95.76 %	1.56 %	2.68 %
$B^{(*)}N$	79.02 %	10.82 %	10.16 %

Table.3.6 Energy expectation values of the $\bar{D}N(1/2^-)$ potentials in the bound states. Each component of π, ρ and ω potentials is listed. All values are in units of MeV.

Components	V^π	V^ρ	V^ω
$\langle \bar{D}N(S) \vert V \vert \bar{D}N(S) \rangle$	0.0	-2.7	3.6
$\langle \bar{D}N(S) \vert V \vert \bar{D}^*N(S) \rangle$	-2.4	-5.2	1.0
$\langle \bar{D}N(S) \vert V \vert \bar{D}^*N(D) \rangle$	-35.2	3.4	-0.6
$\langle \bar{D}^*N(S) \vert V \vert \bar{D}^*N(S) \rangle$	0.4	0.7	0.1
$\langle \bar{D}^*N(S) \vert V \vert \bar{D}^*N(D) \rangle$	-5.0	0.6	-0.1
$\langle \bar{D}^*N(D) \vert V \vert \bar{D}^*N(D) \rangle$	3.7	-0.9	0.4
Total	-38.5	-4.1	4.4

Table.3.7 Energy expectation values of the $BN(1/2^-)$ potentials in the bound states. The same convention is used as Table. 3.6.

Component	V^π	V^ρ	V^ω
$\langle BN(S) \vert V \vert BN(S) \rangle$	0	-5.4	7.0
$\langle BN(S) \vert V \vert B^*N(S) \rangle$	-8.2	-16.4	3.1
$\langle BN(S) \vert V \vert B^*N(D) \rangle$	-90.2	8.3	-1.5
$\langle B^*N(S) \vert V \vert B^*N(S) \rangle$	2.0	3.2	0.6
$\langle B^*N(S) \vert V \vert B^*N(D) \rangle$	-22.3	2.1	-0.4×10^{-2}
$\langle B^*N(D) \vert V \vert B^*N(D) \rangle$	13.2	-3.2	1.4
Total	-105.5	-11.4	10.6

also Eq. (B.16)). The tensor force causing the $PN - P^*N$ mixing of different angular momenta by $\Delta L = 2$ generates the strong attraction in the bound states. Although the mixing ratio of the $P^*N(^4D_{1/2})$ channel is very small, the channel-coupling of $PN(^2S_{1/2})$ and $P^*N(^4D_{1/2})$ is essential to form the bound states. This mechanism is similar with the deuteron in which the tensor force causing the $^3S_1 - ^3D_1$ mixing produces a strong attraction [95, 96]. The ratio of the $^3D_1$ channel in the deuteron is also no more than 5 %.

When the results of the $\bar{D}^{(*)}N$ and $B^{(*)}N$ are compared, the $B^{(*)}N$ state is more bound than the $\bar{D}^{(*)}N$. It is understood as follows. The tensor force mixing PN and

P^*N is enhanced , where P and P^* mesons degenerate in the heavy quark sector. Furthermore, the large reduced mass suppresses the kinetic term.

Finally, we find no bound state in the other J^P states and isotriplet states.

3.3.2 Scattering states and Resonances

Let us now move to the scattering state above the PN thresholds. We find several resonances in the isosinglet channel ($I = 0$).

In the present study, we determine the resonance energy and decay width by analyzing the phase shift. When a decay width is relatively smaller than corresponding resonance energy from the threshold, we identify the resonance at the position where the phase shift crosses $\pi/2$. However, it will turn out that the decay widths are not necessarily small. Hence, we define the resonance position $E_{\rm re}$ by an inflection point of the phase shift as discussed in Ref. [143].

3.3.2.1 Negative parity states

First, the results of scattering states with negative parity are shown. In Fig. 3.5, we present the phase shifts δ of $PN(^2S_{1/2})$, $P^*N(^2S_{1/2})$ and $P^*N(^4D_{1/2})$ channels in the $(I, J^P) = (0, 1/2^-)$ when the $\pi\rho\omega$ potential is used. Each phase shift is plotted as a function of the scattering energy E in the center of mass system. The $PN(^2S_{1/2})$ phase shift starts at $\delta = \pi$ because of the presence of the bound state shown in the previous section. Otherwise the energy dependence of all the phase shifts is rather smooth.

We show the total cross sections of $\bar{D}^{(*)}N$ and $B^{(*)}N$ scatterings for the $\pi\rho\omega$ potential in Fig. 3.6. They start from the maximum value at the threshold and decrease monotonically. For shallower bound state (for the $\bar{D}^{(*)}N$ system), the peak value at the threshold is larger, due to the presence of the bound state near the threshold. In the limit the binding energy $E_B \to 0$, the peak diverges as explained by the zero-energy resonance.

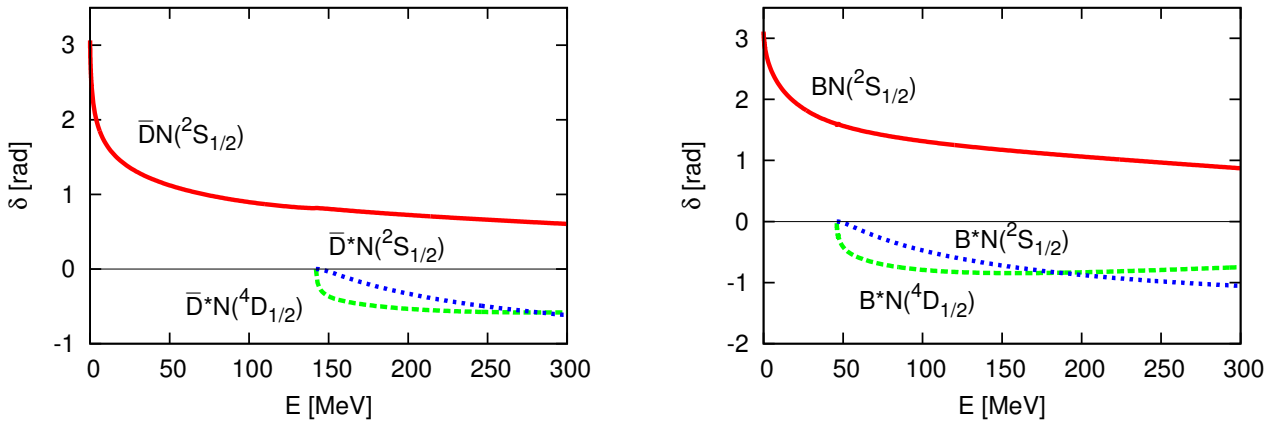

Fig.3.5 Phase shift of the $\bar{D}^{(*)}N$ and $B^{(*)}N$ scattering states for the $(I, J^P) = (0, 1/2^-)$ when $\pi\rho\omega$ potential is used [39].

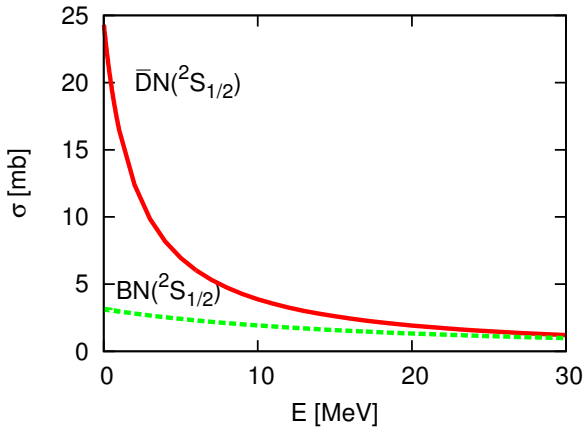

Fig.3.6 Total cross section of the $\bar{D}N(^2S_{1/2})$ and $BN(^2S_{1/2})$ scattering states for $(I, J^P) = (0, 1/2^-)$ when the $\pi\rho\omega$ potential is used [39].

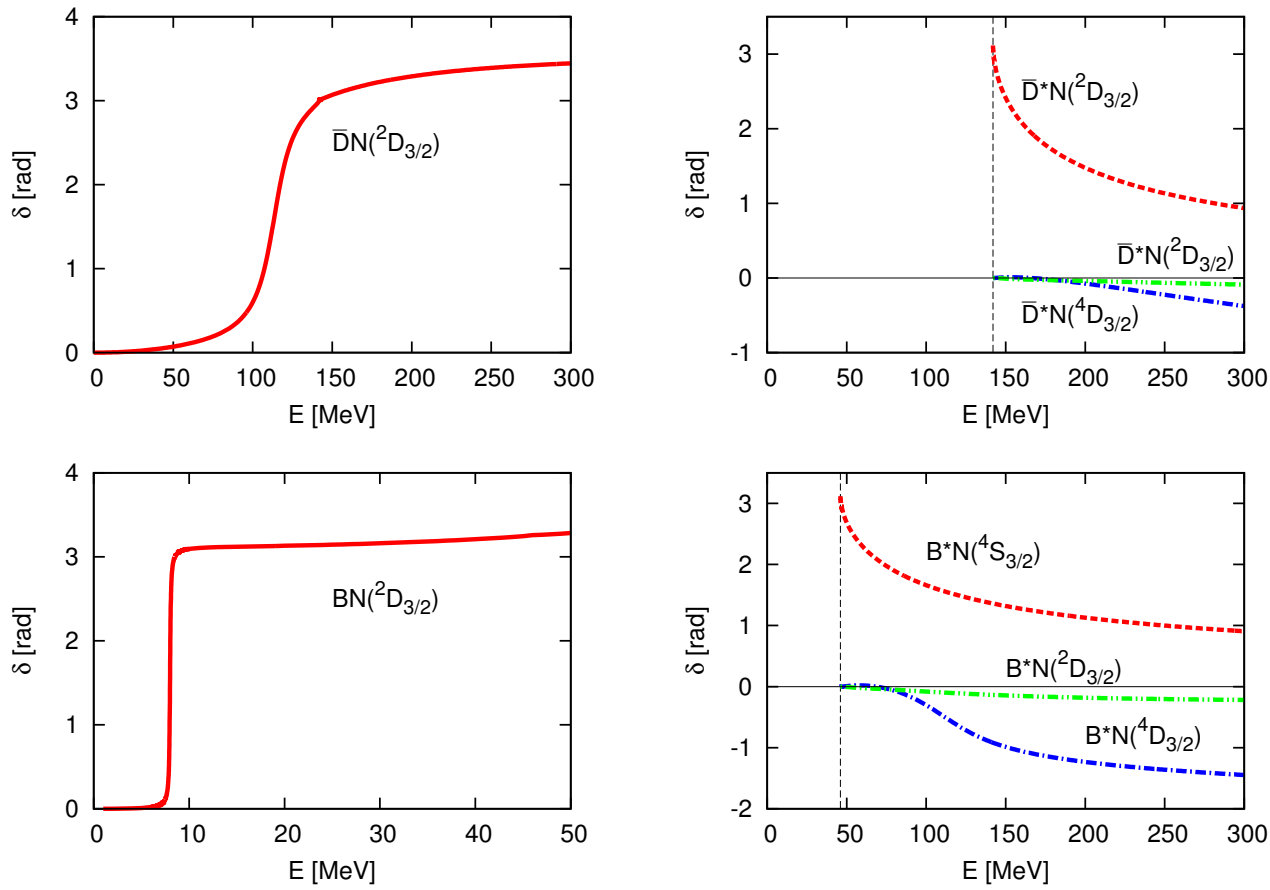

Fig.3.7 Phase shift of the $\bar{D}^{(*)}N$ and $B^{(*)}N$ scattering states for the $(I, J^P) = (0, 3/2^-)$ when $\pi\rho\omega$ potential is used [39]. The $\bar{D}^*N$ and B^*N phase shifts (shown in the right side) start from the $\bar{D}^*N$ and B^*N thresholds, respectively.

Table.3.8 Properties of resonances of $\bar{D}^{(*)}N$ and $B^{(*)}N$ systems for $I = 0$. The energies E are complex as $E_{\rm re} - i\Gamma/2$ where $E_{\rm re}$ is the resonance energy and $\Gamma/2$ is the half-width. The resonance energies are measured from the lowest thresholds (DN and $\bar{B}N$).

J^P	Potential	$\bar{D}^{(*)}N$ E [MeV]	$B^{(*)}N$ E [MeV]
$3/2^-$	π	$113.5 - i9.7$	$8.4 - i8.0 \times 10^{-2}$
	$\pi\rho\omega$	$113.2 - i8.6$	$6.9 - i4.7 \times 10^{-2}$
$1/2^+$	π	$26.1 - i62.6$	$5.8 - i2.9$
	$\pi\rho\omega$	$26.8 - i65.7$	$5.8 - i3.0$
$3/2^+$	π	$148.2 - i5.0$	$32.3 - i14.5$
	$\pi\rho\omega$	$148.2 - i5.0$	$31.8 - i14.4$
$5/2^+$	π	$177.1 - i92.3$	$58.5 - i26.1$
	$\pi\rho\omega$	$176.0 - i87.4$	$58.4 - i24.8$

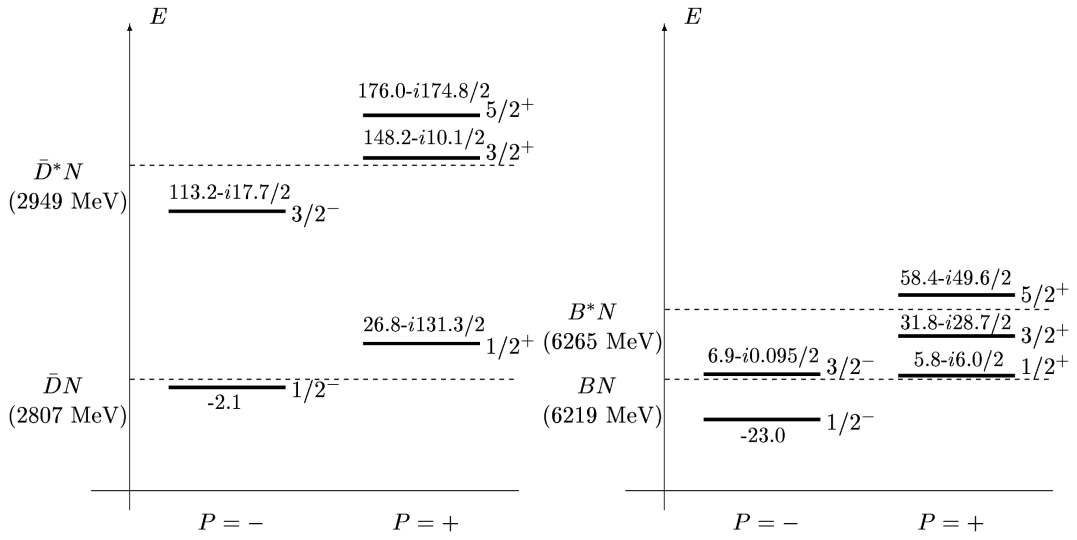

Fig.3.8 Exotic states with negative parity ($P = -$) and positive parity ($P = +$) for $I = 0$. The energies are measured from the lowest thresholds ($\bar{D}N$ and BN). The binding energy is given as a real negative value, and the resonance energy $E_{\rm re}$ and decay width Γ are given as $E_{\rm re} - i\Gamma/2$, in units of MeV. The values are given when the $\pi\rho\omega$ potential is used [40].

In the $(I, J^P) = (0, 3/2^-)$ states, we obtain resonances above the PN thresholds. The phase shifts of PN channels shown in Fig. 3.7 indicate the existence of a resonance at the scattering energy $E_{\rm re} = 113.2$ MeV for $\bar{D}N$ and at $E_{\rm re} = 6.9$ MeV for BN when the $\pi\rho\omega$ potential is used. The corresponding half decay widths are 8.6 MeV for $\bar{D}N$ and 4.7 $\times 10^{-2}$ MeV for BN. The results are also tabulated in Table 3.8 and displayed in Fig. 3.8. The mechanism of the resonance can be understood by looking

at the phase shifts in other channels; in particular, we find that those of $P^*N(^4S_{3/2})$ start from $\delta = \pi$, indicating the presence of a bound state in these channels. Indeed, we checked that, when the $PN(^2D_{3/2})$ channel is ignored and only the $P^*N(^4S_{3/2})$, $P^*N(^4D_{3/2})$ and $P^*N(^2D_{3/2})$ channels are considered, there are bound states at $E_B = 11.5$ MeV for $\bar{D}^*N$ and at $E_B = 21.7$ MeV for B^*N, measured from $\bar{D}^*N$ and B^*N thresholds. Therefore, these resonances are the Feshbach resonances.

We plot the cross section in the $(I, J^P) = (0, 3/2^-)$ states shown in Fig. 3.9. Because there is a resonant state at $E_{re} \sim 113$ MeV in the $\bar{D}N$ scattering and at $E_{re} \sim 7$ MeV in the BN scattering, the cross section becomes maximum at each resonance energy.

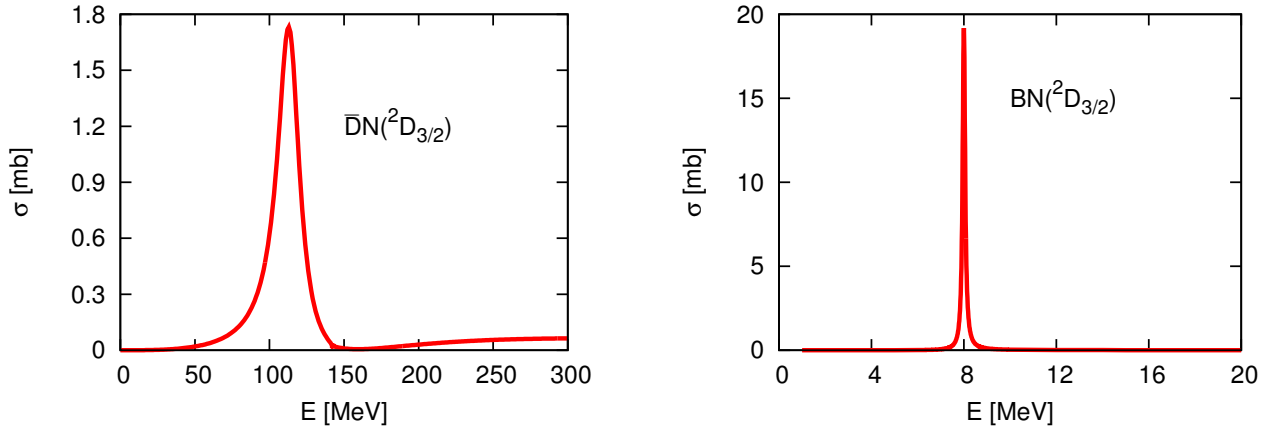

Fig.3.9 Total cross section of the $\bar{D}N$ and BN scattering states for $(I, J^P) = (0, 3/2^-)$ when the $\pi\rho\omega$ potential is used [39].

Finally, we note that there is no resonance in $J^P = 1/2^-$, $5/2^-$, $7/2^-$ and $9/2^-$ for negative parity states.

3.3.2.2 Positive parity states

Now, let us discuss the results of $(I, J^P) = (0, 1/2^+)$, $(0, 3/2^+)$ and $(0, 5/2^+)$. In the $(I, J^P) = (0, 1/2^+)$ channel, we find resonances in both $\bar{D}^{(*)}N$ and $B^{(*)}N$ systems. The phase shifts δ's of $PN(^2P_{1/2})$, $P^*N(^2P_{1/2})$ and $P^*N(^4P_{1/2})$ channels obtained for the $\pi\rho\omega$ potential are shown in Fig. 3.10. The vertical dashed lines in the figures represent the positions of $\bar{D}^*N$ and B^*N thresholds. The sharp increase of the phase shift of the $PN(^2P_{1/2})$ channel indicates the existence of a resonance. A similar behavior is obtained also when the π exchange potential is employed. The resonance energies and half decay widths are summarized in Table 3.8 and in Fig. 3.8. We obtain the resonance energy at 26.8 MeV for $\bar{D}^{(*)}N$ and at 5.8 MeV for $B^{(*)}N$, with the half decay widths 65.7 MeV and 3.0 MeV, respectively, for the $\pi\rho\omega$ potential. The difference between two results by the π potential and the $\pi\rho\omega$ potential is very small and therefore the vector meson exchange interactions play a minor role as seen in the negative parity states. The attractive force forming the resonance is mainly provided by the π exchange potential in the $PN - P^*N$ mixing component. As a consequence, the mixing effect yields the so-called shape resonance in the $PN(^2P_{1/2})$ channel with

the p-wave centrifugal barrier. Finally, the total cross sections for the $\bar{D}^{(*)}N$ and $B^{(*)}N$ scatterings when the $\pi\rho\omega$ potential is used are shown in Figs. 3.11 and 3.12, respectively. The peaks are found at around each resonance energy, 26.8 MeV and 5.8 MeV, for $\bar{D}^{(*)}N$ and $B^{(*)}N$, respectively.

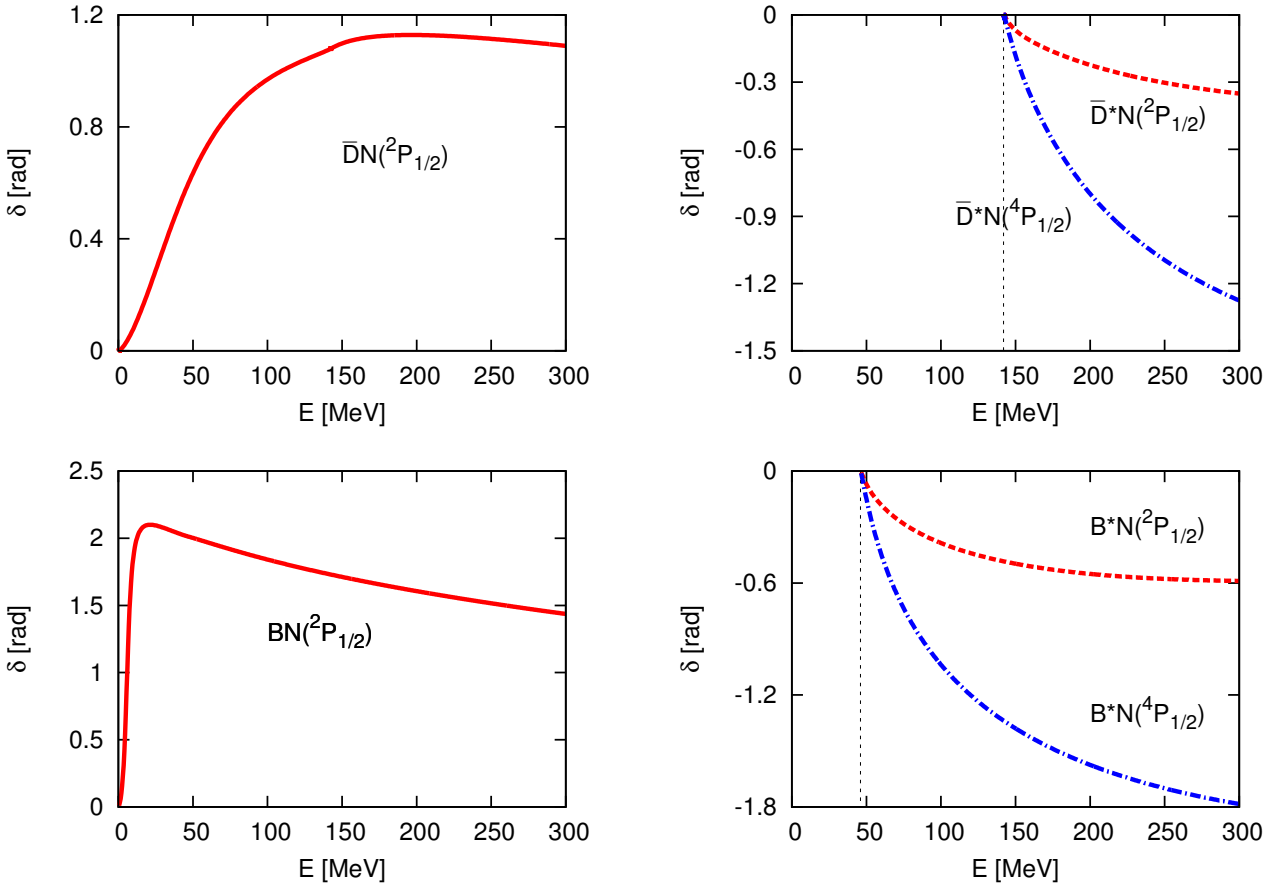

Fig.3.10 Phase shift of the $\bar{D}^{(*)}N$ and $B^{(*)}N$ scattering states for $(I, J^P) = (0, 1/2^+)$ when the $\pi\rho\omega$ potential is used [40].

In the $(I, J^P) = (0, 3/2^+)$ state, we find a resonance for each $\bar{D}^{(*)}N$ and $B^{(*)}N$ state. However, the structures of the resonances are different. For the $\bar{D}^{(*)}N$ state, The phase shifts δ's of $\bar{D}N(^2P_{3/2})$, $\bar{D}^*N(^2P_{3/2})$, $\bar{D}^*N(^4P_{3/2})$ and $\bar{D}^*N(^4F_{3/2})$ are shown in Fig. 3.13. In the phase shift of $\bar{D}N(^2P_{3/2})$, there is a small peak structure at the $\bar{D}^*N$ threshold, which is interpreted as a cusp. Indeed we have checked numerically that the location of the peak is precisely at the $\bar{D}^*N$ threshold. On the other hand, the phase shift of $\bar{D}^*N(^4P_{3/2})$ which rises sharply indicates the presence of a resonance above the $\bar{D}^*N$ threshold in this channel. The resonance energies and decay widths are summarized in Table 3.8 and in Fig. 3.8. When the $\bar{D}N - \bar{D}^*N$ mixing is ignored, there still exists a resonance at the resonance energy 145.5 MeV with the decay width 6.1 MeV, which are close to the original values in the full channel-couplings. Therefore, the obtained resonance is a shape resonance generated mainly

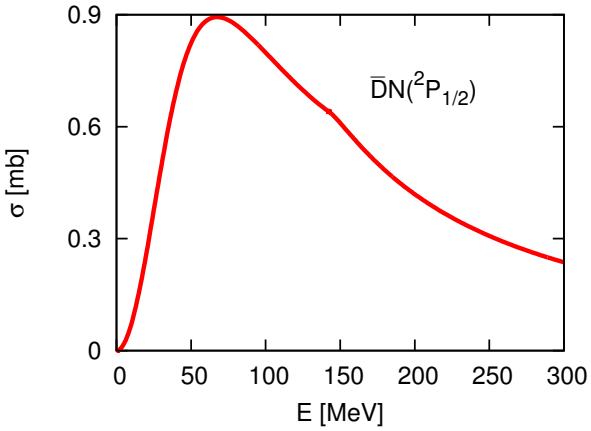

Fig.3.11 Total cross section of the $\bar{D}^{(*)}N$ scattering states for $(I, J^P) = (0, 1/2^+)$ when the $\pi\rho\omega$ potential is used [40].

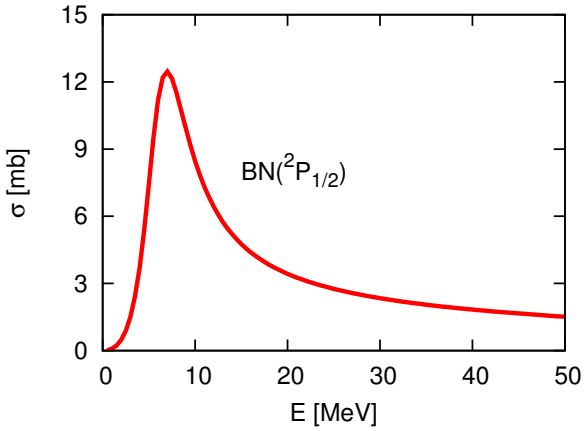

Fig.3.12 Total cross section of the $B^{(*)}N$ scattering states for $(I, J^P) = (0, 1/2^+)$ when the $\pi\rho\omega$ potential is used [40].

by the p-wave centrifugal barrier in the $\bar{D}^*N(^4P_{3/2})$ states. In the resonance, the $\bar{D}N - \bar{D}^*N$ mixing effect is not significant. We show the cross section for $\bar{D}N(^4P_{3/2})$ for the $\pi\rho\omega$ potential in Fig. 3.15, in which the peak appears at the resonance energy.

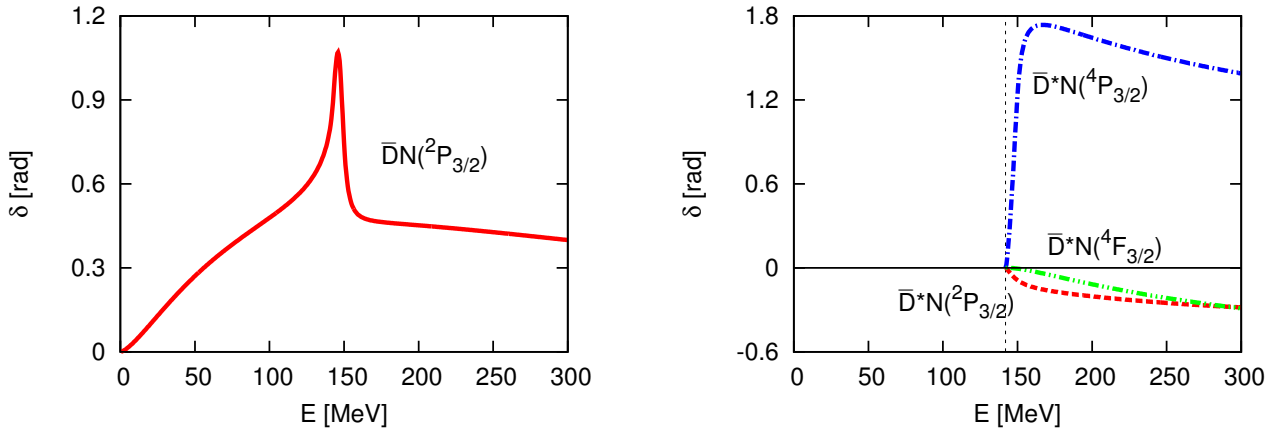

Fig.3.13 Phase shifts of the $\bar{D}^{(*)}N$ scattering states with $(I, J^P) = (0, 3/2^+)$ when the $\pi\rho\omega$ potential is used [40].

For the BN state with $(I, J^P) = (0, 3/2^+)$, the phase shifts δ's of $BN(^2P_{3/2})$, $B^*N(^2P_{3/2})$, $B^*N(^4P_{3/2})$ and $B^*N(^4F_{3/2})$ are plotted in Fig. 3.14. The sharp increase of the phase shift passing through $\pi/2$ in $BN(^2P_{3/2})$ as an indication of a resonance. We also find that the phase shift in $B^*N(^4P_{3/2})$ starts from π. Therefore, we conclude that the resonance in the BN state with $(I, J^P) = (0, 3/2^+)$ is a Feshbach resonance. Indeed, when we switch off the $BN(^2P_{3/2})$ channel, we obtain a bound state of B^*N which energy is close to the original resonance position. The

resonance energy is 31.8 MeV and the decay width is 28.7 MeV as summarized in Table 3.8 and in Fig. 3.8. The resonance locates below the B^*N threshold, while the $\bar{D}^{(*)}N$ resonance in the $(I, J^P) = (0, 3/2^+)$ is above the $\bar{D}^*N$ threshold. The total cross section plotted in Fig. 3.16 also show a peak at around the resonance energy.

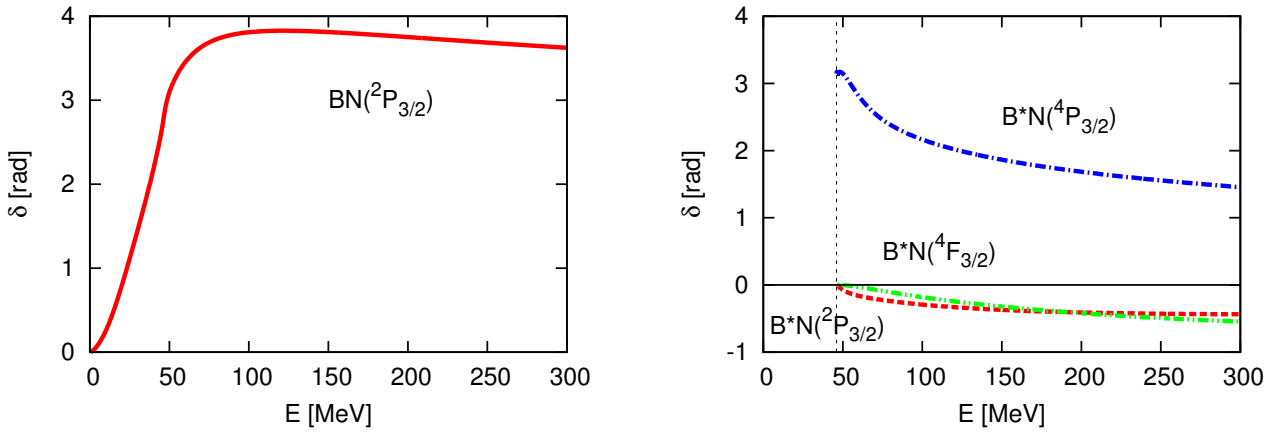

Fig.3.14 Phase shifts of the $B^{(*)}N$ scattering states with $(I, J^P) = (0, 3/2^+)$ when the $\pi\rho\omega$ potential is used [40].

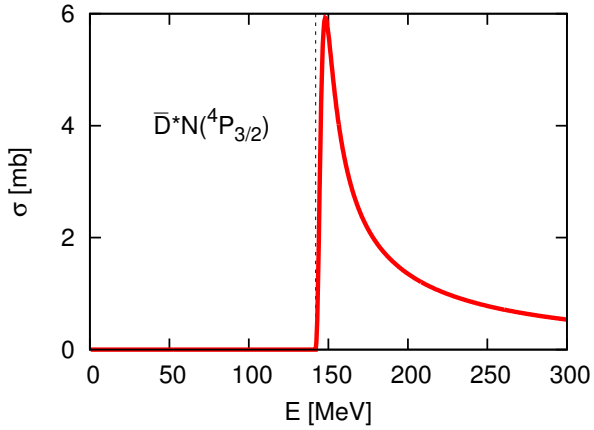

Fig.3.15 Total cross section of the $\bar{D}^*N(^4P_{3/2})$ scattering when the $\pi\rho\omega$ potential is used [40].

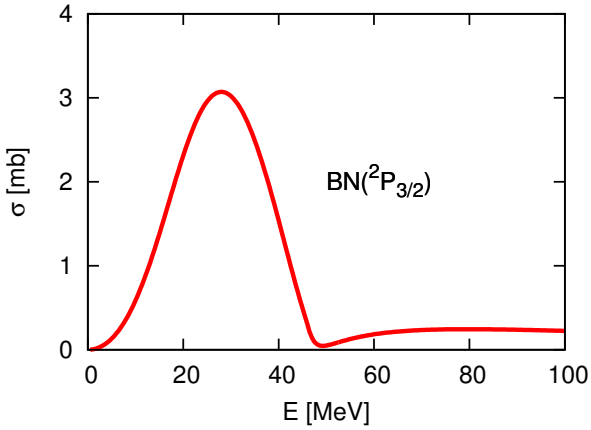

Fig.3.16 Total cross section of the $BN(^2P_{3/2})$ scattering state with $(I, J^P) = (0, 3/2^+)$ when the $\pi\rho\omega$ potential is used [40].

In the $(I, J^P) = (0, 5/2^+)$ state, we find a resonance for each $\bar{D}^{(*)}N$ and $B^{(*)}N$ above the P^*N threshold. The phase shifts δ's of $PN(^2F_{5/2})$, $P^*N(^4P_{5/2})$, $P^*N(^2F_{5/2})$ and $P^*N(^4F_{5/2})$ are shown in Fig. 3.17. Small peak structures in the phase shifts of $\bar{D}N(^2F_{5/2})$ and $BN(^2F_{5/2})$ are interpreted as cusps. Above the P^*N threshold, the phase shifts of $\bar{D}^*N(^4P_{5/2})$ and $B^*N(^4P_{5/2})$ rise up and these structures indicate the presence of resonances. The resonance energies are 176.0

MeV for $\bar{D}^*N$ and 58.4 MeV for B^*N, and the decay widths are 174.8 MeV and 49.6 MeV, respectively. We summarize the results in Table 3.8 and in Fig 3.8. When the $PN - P^*N$ mixing is ignored, the resonant states in the $\bar{D}^*N(^4P_{5/2})$ and $B^*N(^4P_{5/2})$ channels still exist at the resonance energies close to the values from the full channel-couplings. Therefore, these resonant states are shape resonances generated mainly by the p-wave centrifugal barrier in the $P^*N(^4P_{5/2})$ channel. In the resonance, the $PN - P^*N$ mixing effect plays a minor role. Finally, The cross sections for $\bar{D}^*N(^4P_{5/2})$ and $B^*N(^4P_{5/2})$ are plotted in Figs. 3.18 and 3.19, respectively. They also have a peak structure around the resonance energies.

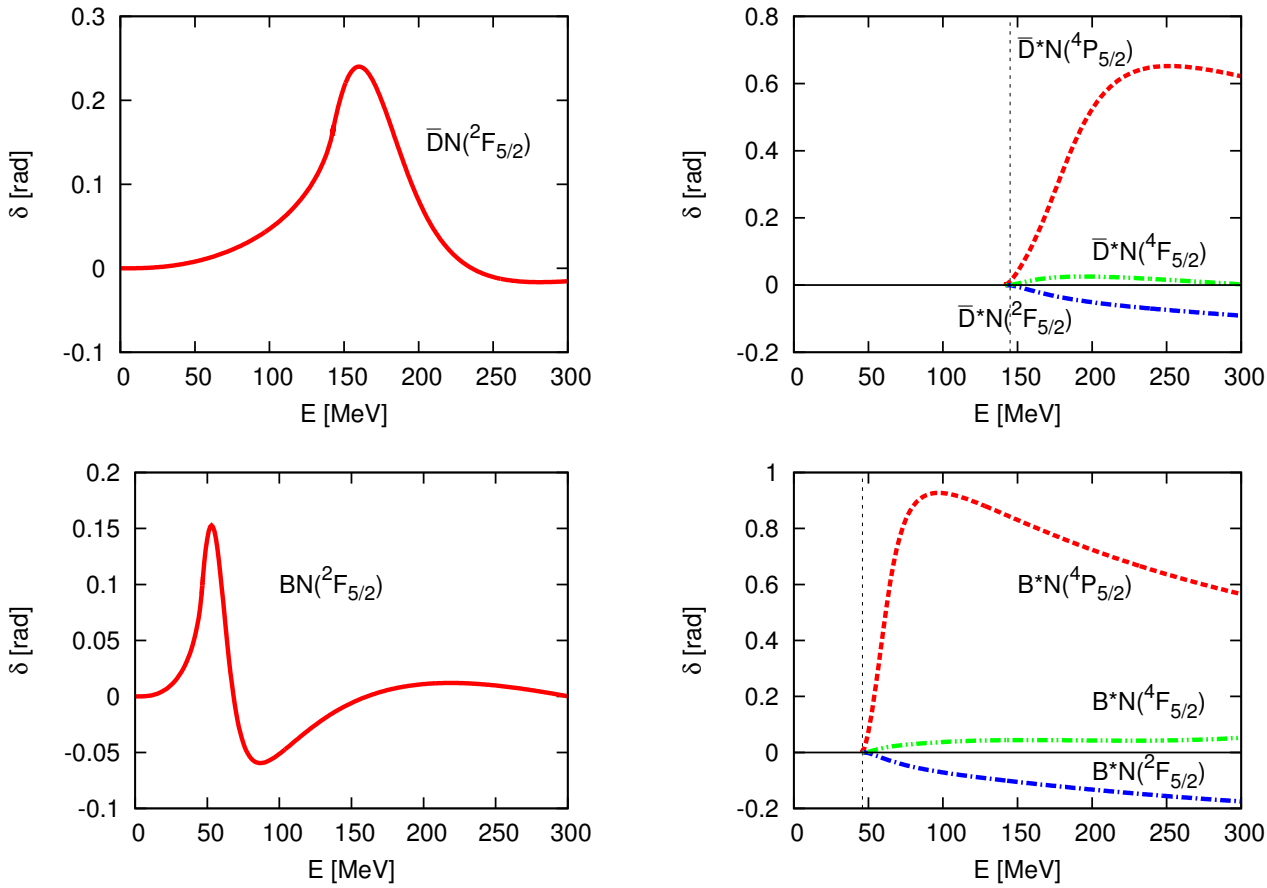

Fig.3.17 Phase shifts of the $\bar{D}^{(*)}N$ and $B^{(*)}N$ scattering states with $(I, J^P) = (0, 5/2^+)$ when the $\pi\rho\omega$ potential is used [40].

3.3.3 Summary and Discussion for $\bar{D}^{(*)}N$ and $B^{(*)}N$

Brief summary for results of $\bar{D}^{(*)}N$ and $B^{(*)}N$ is given in this section. The exotic states, being $\bar{D}^{(*)}N$ and $B^{(*)}N$, have been investigated. They have genuinely exotic flavor structure whose minimal quark content is $\bar{Q}qqqq$. We employ the π, ρ and ω exchange potentials as an interaction between a heavy meson and a nucleon, and the π and $\pi\rho\omega$ potentials are compared. We have found the bound states in the

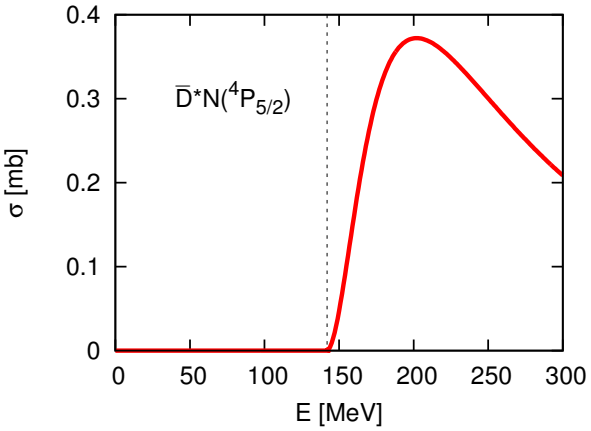

Fig.3.18 Total cross section of the $\bar{D}^*N(^4P_{5/2})$ scattering when the $\pi\rho\omega$ potential is used [40].

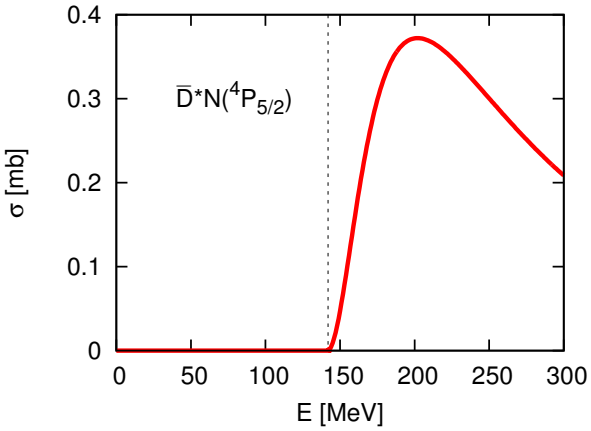

Fig.3.19 Total cross section of the $B^*N(^4P_{5/2})$ scattering when the $\pi\rho\omega$ potential is used [40].

$(I, J^P) = (0, 1/2^-)$ and the resonances in $(I, J^P) = (0, 1/2^+)$, $(0, 3/2^\pm)$ and $(0, 5/2^+)$ both for $\bar{D}^{(*)}N$ and $B^{(*)}N$.

In each (I, J^P) state, we verify that the results of the π potential is similar to those of the $\pi\rho\omega$ potential. It means that both $\bar{D}^{(*)}N$ and $B^{(*)}N$ systems are dominated almost by the long range force due to the π exchange.

The mixing between PN and P^*N channels is enhanced due to the heavy quark spin symmetry and becomes important in the $P^{(*)}N$ states (except for the states above the P^*N threshold). The effect of the mixing which induces the tensor force becomes more significant for the bottom sector where the mass difference between PN and P^*N is smaller. This causes differences in results in the charm and bottom sectors. For the $(I, J^P) = (0, 1/2^-)$, the tensor force in the $PN(^2S_{1/2}) - P^*N(^4D_{1/2})$ mixing component plays an important role in the $P^{(*)}N$ bound states. The $P^{(*)}N$ resonances with $(I, J^P) = (0, 1/2^+)$ are generated with the p-wave centrifugal barrier in the PN channel by the attraction induced from the $PN - P^*N$ mixing. The mixing effect is also significant for the Feshbach resonances in the $P^{(*)}N$ with $(I, J^P) = (0, 3/2^-)$ and the BN with $(I, J^P) = (0, 3/2^+)$. Above the P^*N threshold, however, the $\bar{D}N$ resonance with $(I, J^P) = (0, 3/2^+)$ and the PN resonances with $(I, J^P) = (0, 5/2^+)$ are generated with the p-wave centrifugal barrier in the P^*N channel mainly by the P^*N interaction, in which the $PN - P^*N$ mixing effect plays a minor role. For the resonances in the $P^{(*)}N$ states, the combination of the centrifugal barrier in higher partial wave and the attraction caused by the $PN - P^*N$ mixing yields more variety of resonance structures. The mechanisms of the resonance structure are summarized in Table 3.9.

To compare the result of the negative parity states with the result of the positive parity states, energy levels for the exotic $P^{(*)}N$ states , shown in Fig. 3.8, are useful. We find that the bound states exist in the negative parity states, while no bound state exists in the positive parity states. This is because the lowest state $PN(^2P_{1/2})$ in $J^P = 1/2^+$ has a p-wave orbital angular momentum $L = 1$, while $PN(^2S_{1/2})$ in

$J^P = 1/2^-$ has an s-wave orbital angular momentum $L = 0$. In the same way, we see that the resonance energies of the positive parity states tend to be higher than those of the negative parity states.

Finally, let us discuss the isospin triplet channel. We find no bound and resonant states in the isospin triplet state ($I = 1$), while many states are found in the isospin singlet state ($I = 0$). The reason can be understood by the isospin factor $\vec{\tau}_P \cdot \vec{\tau}_N$ of the meson exchange potentials. The isospin factor for $I = 0$ is $\vec{\tau}_P \cdot \vec{\tau}_N = -3$, while the absolute value of the isospin factor for $I = 1$ is small, $\vec{\tau}_P \cdot \vec{\tau}_N = 1$. Due to the small isospin factor, the attraction from isotriplet meson exchanges becomes weak. In particular, the π exchange potential in which the off-diagonal terms play a crucial role is sensitive to this factor. Therefore, the isospin triplet state cannot obtain the strong attraction from the π exchange potential which dominates in the $P^{(*)}N$ states.

Table.3.9 The mechanism to form the resonances in the $\bar{D}^{(*)}N$ and $B^{(*)}N$ states with $(I, J^P) = (0, 1/2^\pm)$, $(0, 3/2^+)$ and $(0, 5/2^+)$. All the shape resonances in PN (P^*N) with the positive parity are induced by the p-wave centrifugal barrier in the PN (P^*N) channel.

(I, J^P)	$\bar{D}N$ states	BN states
$(0, 1/2^-)$	Feshbach resonance	
$(0, 1/2^+)$	shape resonance in PN	
$(0, 3/2^+)$	shape resonance in P^*N	Feshbach resonance
$(0, 5/2^+)$	shape resonance in P^*N	

3.4 Numerical results of $D^{(*)}N$ and $\bar{B}^{(*)}N$ (Non-Exotic states)

In this section, we consider non-exotic states for the $\bar{P}N - \bar{P}^*N$ systems, where $\bar{P}^{(*)}$ denotes $D^{(*)}$ or $\bar{B}^{(*)}$ meson composed of $Q\bar{q}$. The $\bar{P}^{(*)}$ mesons are the antiparticle of $P^{(*)}$ discussed in Sec. 3.3. The $\bar{P}^{(*)}N$ molecule should couple not only to three quark states (Qqq) but also to other meson-baryon states such as $\pi\Lambda_{\rm h}$, $\pi\Sigma_{\rm h}$ and $\pi\Sigma^*_{\rm h}$, where ${\rm h} = {\rm c}, {\rm b}$. However, it is expected that such couplings are small for $D^{(*)}N$ and $\bar{B}^{(*)}N$ baryons near the thresholds. For the couplings to the three quark states, the wave functions of $\bar{P}^{(*)}N$ molecules are spatially large as compared to the conventional Qqq states. For the couplings to other meson-baryon states, the transitions, e.g. from $\bar{P}N$ to $\pi\Sigma_{\rm h}$, are suppressed by a heavy quark exchange. From those points of view, in the present section, we do not consider the channel couplings to other states such as Qqq and $\pi\Sigma_{\rm h}$ as long as the relative distance between the $\bar{P}$ meson and the nucleon is large. We study the bound and resonant states generated by the $D^{(*)}N$ and $\bar{B}^{(*)}N$ states.

The meson exchange potentials employed in the $\bar{P}^{(*)}N$ states are the same as those in the $P^{(*)}N$ states, except for the signs of coupling constants of π and ω in Table 3.2, which are reversed due to G-parity transformation between $D^{(*)}$ ($\bar{B}^{(*)}$)

and $\bar{D}^{(*)}$ ($B^{(*)}$). To obtain the bound states and resonances, the coupled-channel Schrödinger equations are solved by using the same method for the $P^{(*)}N$ states as discussed in Sec. 3.3. In the non-exotic channel, we also compare results for the π potential with those for the $\pi\rho\omega$ potentials.

First, the results for the isosinglet state ($I = 0$) are presented. We discuss the states with $J^P = 1/2^{\pm}$ and $3/2^-$ in Sec. 3.4.1, and then those with $J^P = 3/2^+$, $5/2^{\pm}$ and $7/2^{\pm}$ in Sec. 3.4.2. In fact, it will turn out that the results in those two categories have different behaviors. The energies of bound and resonant states are summarized in Table 3.10 and also presented in Figs. 3.20 and 3.21. The results are shown for the π and $\pi\rho\omega$ potentials, and the corresponding energy levels are connected by arrows in Figs. 3.20 and 3.21. The numerical values are measured from the DN and $\bar{B}N$ thresholds, respectively.

Second, we present the results for the isotriplet state ($I = 1$) in Sec. 3.4.3. The energies are shown in Table 3.10 and Fig. 3.22.

3.4.1 $J^P = 1/2^{\pm}$ and $3/2^-$ for $I = 0$

For $(I, J^P) = (0, 1/2^-)$, we find bound states in both of $D^{(*)}N$ and $\bar{B}^{(*)}N$. For $D^{(*)}N$, the binding energies are -14.4 MeV for the π potential and -82.5 MeV for the $\pi\rho\omega$ potential. The relative radii are 1.51 fm and 0.86 fm, respectively. As expected, for a larger binding energy, the system becomes smaller. The tensor force from the π exchange which is the main driving force of the DN-D^*N mixing plays an important role to form the bound states. In fact, we have verified that neither bound nor resonant state exists when the tensor force from the π exchange is switched off and the DN-D^*N mixing is small. For $J^P = 1/2^-$, the results in the π and $\pi\rho\omega$ potentials are very different as indicated in Figs. 3.20 and 3.21. Since both the ρ and ω exchanges are attractive for the $D^{(*)}N$ ($\bar{B}^{(*)}N$) system, the vector meson exchanges contribute to form the deeply bound state of the binding energy around 80 MeV. This contrasts with the result for the $\bar{D}^{(*)}N$ and $B^{(*)}N$ systems of truly exotic channels in Sec. 3.3, where the ρ and ω exchanges play a minor role due to the cancellation of these two potentials.

We estimate the mixing ratio of various channels in the bound states as summarized in Table 3.11. We observe that, for $J^P = 1/2^-$ states, the most dominant component is $DN(^2S_{1/2})$ with the fraction 71.8 %. The second dominant component is $D^*N(^4D_{1/2})$ with the fraction 20.4 %. Therefore, the tensor force which mixes the S-wave in $DN(^2S_{1/2})$ and the D-wave in $D^*N(^4D_{1/2})$ is important to provide a strong attraction.

For $\bar{B}^{(*)}N$ of $(I, J^P) = (0, 1/2^-)$, we also obtain bound states. The binding energies are -57.8 MeV for the π potential and -145.9 MeV for the $\pi\rho\omega$ potential, and the relative radii are 0.99 fm and 0.76 fm, respectively. Again the results of the two potentials are very different with the same reason for the $D^{(*)}N$ system. As compared to the $D^{(*)}N$ system, the binding energy in the $\bar{B}^{(*)}N$ system is much larger, because heavier particles suppress kinetic energy. For the mixing ratios, we also find a similar tendency as we discussed for the $D^{(*)}N$ system; 56.1 % for $\bar{B}N(^2S_{1/2})$, 13.3 % for $\bar{B}^*N(^2S_{1/2})$ and 30.6 % for $\bar{B}^*N(^4D_{1/2})$.

Table.3.10 Properties of bound and resonant states of $D^{(*)}N$ and $\bar{B}^{(*)}N$ systems. The energies E are either pure real for bound states or complex for resonant states. The complex energies for resonances are written as $E_{\rm re} - i\Gamma/2$ where $E_{\rm re}$ is the resonance energy and $\Gamma/2$ is the half-width. The binding and resonance energies are measured from the lowest threshold (DN and $\bar{B}N$). Relative distances are shown only for bound states.

$I(J^P)$	Potential	DN		$\bar{B}N$	
		E [MeV]	$\langle r^2\rangle^{1/2}$ [fm]	E [MeV]	$\langle r^2\rangle^{1/2}$ [fm]
$0(1/2^-)$	π	-14.4	1.51	-57.8	0.99
	$\pi\rho\,\omega$	-82.5	0.86	-145.9	0.76
$0(1/2^+)$	π	$1.4 - i0.2$	—	-83.8	0.92
	$\pi\rho\,\omega$	-81.5	0.85	-185.0	0.75
$0(3/2^-)$	π	$63.5 - i7.9$	—	-38.7	0.99
	$\pi\rho\,\omega$	-13.7	0.89	-127.8	0.76
$0(3/2^+)$	π	$23.8 - i118.1$	—	$12.9 - i15.5$	—
	$\pi\rho\,\omega$	$26.0 - i44.2$	—	-2.6	1.81
$0(5/2^-)$	π	$153.6 - i671.9$	—	$63.7 - i177.6$	—
	$\pi\rho\,\omega$	$160.0 - i375.4$	—	$71.3 - i102.8$	—
$0(5/2^+)$	π	$160.8 - i3.1$	—	$46.0 - i1.1$	—
	$\pi\rho\,\omega$	$137.0 - i7.6$	—	$20.0 - i0.2$	—
$0(7/2^-)$	π	$217.7 - i182.4$	—	$85.6 - i74.5$	—
	$\pi\rho\,\omega$	$220.8 - i109.1$	—	$87.5 - i46.7$	
$0(7/2^+)$	π	no	—	no	—
	$\pi\rho\,\omega$	no	—	no	—
$1(1/2^-)$	π	no	—	no	—
	$\pi\rho\,\omega$	$147.2 - i105.5$	—	$50.7 - i75.5$	—

Table.3.11 Mixing ratio of each channel in the bound $D^{(*)}N$ and $\bar{B}^{(*)}N$ states for $J^P = 1/2^\pm$ and $3/2^\pm$ with $I = 0$ when the $\pi\rho\,\omega$ potential is employed.

$1/2^-$	$PN(^2S_{1/2})$	$P^*N(^2S_{1/2})$	$P^*N(^4D_{1/2})$	—
DN	71.8%	7.8%	20.4%	—
$\bar{B}N$	56.1%	13.3%	30.6%	—
$3/2^-$	$PN(^2D_{3/2})$	$P^*N(^4S_{3/2})$	$P^*N(^4D_{3/2})$	$P^*N(^2D_{3/2})$
DN	19.8%	62.8%	14.2%	3.2%
$\bar{B}N$	14.6%	64.7%	16.7%	4.0%
$1/2^+$	$PN(^2P_{1/2})$	$P^*N(^2P_{1/2})$	$P^*N(^4P_{1/2})$	—
DN	38.8%	6.0%	55.2%	—
$\bar{B}N$	28.4%	7.7%	63.9%	—
$3/2^+$	$PN(^2P_{3/2})$	$P^*N(^2P_{3/2})$	$P^*N(^4P_{3/2})$	$P^*N(^4F_{3/2})$
DN	—	—	—	—
$\bar{B}N$	71.2%	6.7%	7.5%	14.6%

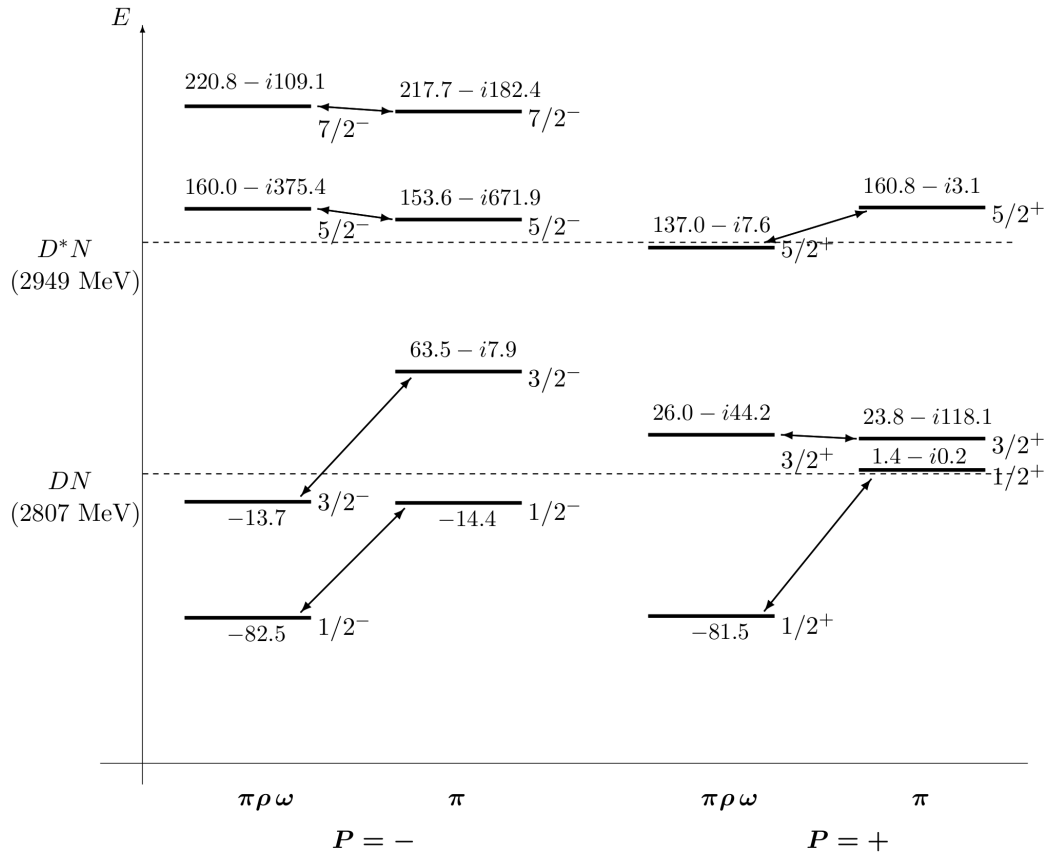

Fig.3.20 Energies of bound and resonant states of $D^{(*)}N$ for $I = 0$ with positive parity ($P = +$) and negative parity ($P = -$), quoted from Ref. [136]. The energies are measured from the DN threshold. The results for π and $\pi\rho\omega$ potentials are shown, where corresponding states are connected by arrows. The binding energies are given as real negative value, and the resonance energies $E_{\rm re}$ and decay widths Γ are given as $E_{\rm re} - i\Gamma/2$.

Let us move to $(I, J^P) = (0, 1/2^+)$ state. For $D^{(*)}N$, we find one resonance near the DN threshold when the π potential is used. The resonance energy is 1.4 MeV and the half decay width is 0.2 MeV as shown in Table 3.10. When the $\pi\rho\omega$ potential is used, however, we find a bound state with a binding energy -81.5 MeV and with a relative radius 0.85 fm. Therefore, we also find large difference between the results for the π and $\pi\rho\omega$ potentials. Interestingly, in the mixing ratio of the bound state shown in Table 3.11, the ratio of $D^*N(^4P_{1/2})$ channel is largest in the DN states for $(I, J^P) = (0, 1/2^+)$, although the mass of D^*N is heavier than the mass of DN. This is because the attraction of tensor force is the strongest for the $D^*N(^4P_{1/2})$ channel, and hence this channel dominates in the state.

For $\bar{B}^{(*)}N$ of $(I, J^P) = (0, 1/2^+)$, we also find bound states for both cases when the π and $\pi\rho\omega$ potentials are used. The binding energies are large, -83.8 MeV for the π potential and -185.0 MeV for the $\pi\rho\omega$ potential, and the relative radii are 0.92 fm and 0.75 fm, respectively. In this case again, $\bar{B}^*N(^4P_{1/2})$ is the most dominant

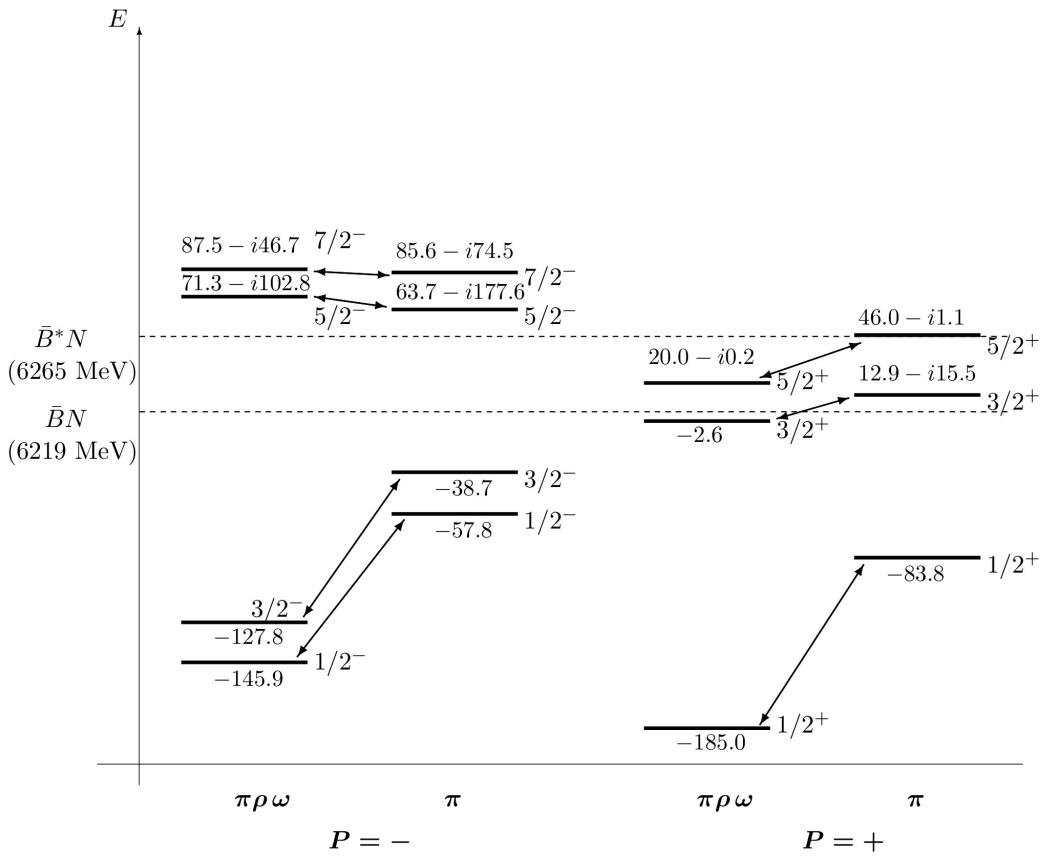

Fig.3.21 Energies of bound and resonant states of $\bar{B}^{(*)}N$ for $I = 0$ with positive parity ($P = +$) and negative parity ($P = -$), quoted from Ref. [136]. The energies are measured from the $\bar{B}N$ threshold. The same convention is used as Fig. 3.20.

component regardless of its heavy mass.

The behavior of the $(I, J^P) = (0, 3/2^-)$ states is also the same as the $(0, 1/2^-)$ and $(0, 1/2^+)$ states. We find a resonant DN state for the π potential with the resonance energy 63.5 MeV and the half decay width 7.9 MeV as shown in Table 3.10. In contrast, for the $\pi\rho\omega$ potential, we find a bound DN state with the binding energy -13.7 MeV and the relative radius 0.89 fm. For the bound state, the mixing ratios are 19.8 % for $DN(^2D_{3/2})$, 62.8 % for $D^*N(^4S_{3/2})$, 14.2 % for $D^*N(^4D_{3/2})$ and 3.2 % for $D^*N(^2D_{3/2})$. Thus, $D^*N(^4S_{3/2})$ is the dominant channel although its mass is heavier than the mass of $DN(^2D_{3/2})$; once again a large attraction due to the tensor force is provided.

For $\bar{B}^{(*)}N$ state of $(I, J^P) = (0, 3/2^-)$, we obtain bound states for both cases the π and $\pi\rho\omega$ potentials are used. We also find the difference between the binding energies for the π and $\pi\rho\omega$ potentials, -38.7 MeV for the π potential and -127.8 MeV for the $\pi\rho\omega$ potential. The mixing ratios displayed in Table 3.11 indicates the dominance of the $\bar{B}^*N(^4S_{3/2})$ channel as seen in the $D^{(*)}N$ state of $(I, J^P) = (0, 3/2^-)$.

3.4.2 $J^P = 3/2^+$, $5/2^\pm$ and $7/2^-$ for $I = 0$

For $(I, J^P) = (0, 3/2^+)$, we find resonant states above the PN threshold. For $D^{(*)}N$, the resonance energies are 23.8 MeV for the π potential and 26.0 MeV for the $\pi\rho\omega$ potential. The half decay widths are 118.1 MeV and 44.2 MeV, respectively. As compared to the cases of $1/2^\pm$ and $3/2^-$, the results of the π and $\pi\rho\omega$ potentials are not very much different, as indicated in Fig. 3.20. Since the wave functions are extended due to larger orbital angular momenta of P-wave ($L = 1$) and F-wave ($L = 3$) for $J^P = 3/2^+$, the long range potential of the π exchange dominates, while the short range potentials from ρ and ω exchanges are suppressed. For $\bar{B}^{(*)}N$, when the π potential is used, we find a resonant state whose resonance energy is 12.9 MeV and half decay width is 15.5 MeV, while when the $\pi\rho\omega$ potential is used, we find a loosely bound state of a binding energy -2.6 MeV and a relative radius 1.81 fm. In the mixing ratios in Table 3.11, we see that the most dominant component is $\bar{B}N(^2P_{3/2})$, 71.2 %, and the second dominant one is $\bar{B}^*N(^4F_{3/2})$, 14.6 %. This indicates that the tensor force in the $\bar{B}N(^2P_{3/2}) - \bar{B}^*N(^4F_{3/2})$ component in Eq. (B.19) plays an important role to form the $\bar{B}^{(*)}N$ bound state.

For $(I, J^P) = (0, 5/2^-)$, we obtain resonant states for both cases when the π and $\pi\rho\omega$ potentials are used. For $D^{(*)}N$, the resonance energies are 153.6 MeV for the π potential and 160.0 MeV for the $\pi\rho\omega$ potential, which are above the D^*N threshold. The corresponding half decay widths are 671.9 MeV and 375.4 MeV, respectively. The difference between the results of the π and $\pi\rho\omega$ potentials is once again small, due to the same reason as before with large angular momenta. For $\bar{B}^{(*)}N$ state, we also find resonant states above the $\bar{B}^*N$ threshold. The resonance positions are 63.7 MeV for the π potential and 71.3 MeV for the $\pi\rho\omega$ potential. The corresponding half decay widths are 177.6 MeV and 102.8 MeV, respectively. We observe from Table 3.10 that the widths of the $5/2^-$ states of both DN and $\bar{B}N$ are very large. The reason is that there is only very weak attraction in these channels. Because of the very large widths of order 1 GeV, it is not easy to interpret physically them as particle states.

For $(I, J^P) = (0, 5/2^+)$, we find resonant states with narrow widths for both cases when the π and $\pi\rho\omega$ potentials are used. For $D^{(*)}N$, when the π potential is used, the resonance energy is 160.8 MeV and the half decay width $\Gamma/2 = 3.1$ MeV. When the $\pi\rho\omega$ potential is used, the resonance energy is 137.0 MeV and the half decay width $\Gamma/2 = 7.6$ MeV. For $\bar{B}^{(*)}N$, we also find resonances whose energies are 46.0 MeV for the π potential and 20.0 MeV for the $\pi\rho\omega$ potential, with the corresponding half decay widths 1.1 MeV and 0.2 MeV, respectively. Again, the results for the π and $\pi\rho\omega$ potentials are similar.

For $(I, J^P) = (0, 7/2^-)$, we obtain resonances above the D^*N and $\bar{B}^*N$ thresholds. For $D^{(*)}N$, there exist resonances at 217.7 MeV for the π potential and at 220.8 MeV for the $\pi\rho\omega$ potential, with half decay widths 182.4 MeV and 109.1 MeV, respectively. For $\bar{B}^{(*)}N$, there also exist resonances whose energies are 85.6 MeV for the π potential and 87.5 MeV for the $\pi\rho\omega$ potential, with half decay widths 74.5 MeV and 46.7 MeV, respectively.

3.4.3 Isospin triplet ($I = 1$)

Let us move to the states of isospin triplet ($I = 1$). We summarize the results for $D^{(*)}N$ and for $\bar{B}^{(*)}N$ in Table 3.10 and show the energy levels in Fig. 3.22. As a result, we find resonant states only for $J^P = 1/2^-$ when the $\pi\rho\omega$ potential is employed. For $D^{(*)}N$, the resonance energy is 147.2 MeV and the half decay width is 105.5 MeV. For $\bar{B}^{(*)}N$ state, we obtain the resonance whose energy is 50.7 MeV and half width 75.5 MeV. The reason that there are not many states in isospin triplet channel can be understood as follows; as compared to the isosinglet channel, the attractive force in the isotriplet channel is weak due to small isospin factor; $\vec{\tau}_P \cdot \vec{\tau}_N = -3$ for isosinglet and $\vec{\tau}_P \cdot \vec{\tau}_N = 1$ for isotriplet.

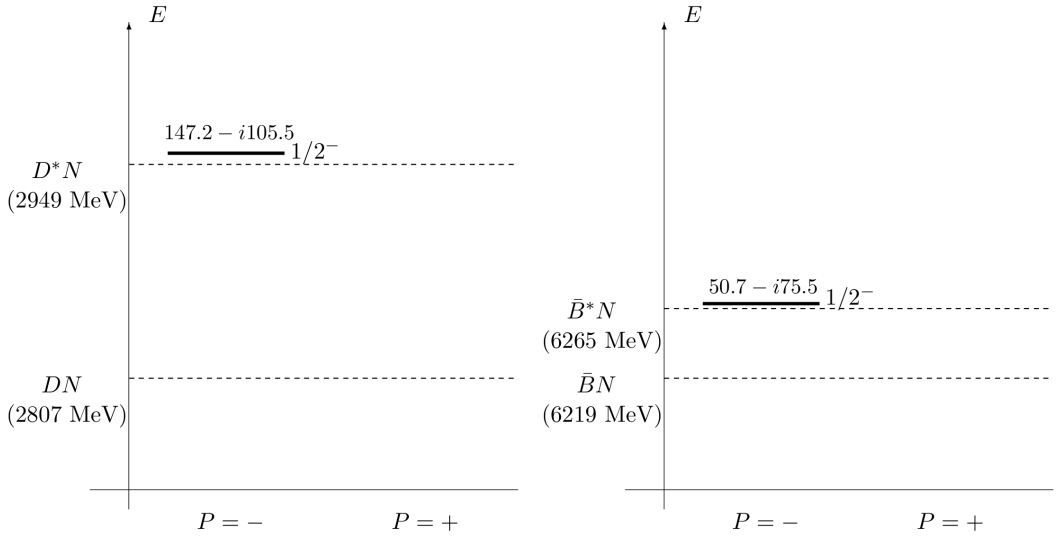

Fig.3.22 Energies of bound and resonant states of $D^{(*)}N$ and $\bar{B}^{(*)}N$ for $I = 1$ when the $\pi\rho\omega$ potential is used [136]. The same convention is used as Fig. 3.20.

3.5 Summary and Discussion for $D^{(*)}N$ and $\bar{B}^{(*)}N$

A brief summary for results of $D^{(*)}N$ and $\bar{B}^{(*)}N$ is given in this section. Non-exotic baryon states with ordinary quantum number have been investigated. The π, ρ and ω exchange potentials between a $\bar{P}$ meson and a nucleon were employed, while we did not consider the channel couplings to other hadronic channels such as $\Lambda_c(\Lambda_b)$ and $\pi\Sigma_c(\pi\Sigma_b)$. By solving coupled channel Schrödinger equations for $\bar{P}N$ and $\bar{P}^*N$ channels, we have found many bound and resonant states with $1/2^\pm$, $3/2^\pm$, $5/2^\pm$ and $7/2^-$ for $I = 0$ and few resonances with $1/2^-$ for $I = 1$. For these states, the tensor force of the π exchange potential plays a significant role to produce them.

The π exchange potential becomes more important in the bottom sector than in the charm sector. The small mass difference between $\bar{B}$ and $\bar{B}^*$ mesons helps to yield

the strong attraction because it induces the strong $\bar{B}N - \bar{B}^*N$ mixing with the tensor force. Furthermore, the $\bar{B}^{(*)}N$ has heavier reduced mass and hence the kinetic term is suppressed. For these reasons, the binding energies of $\bar{B}^{(*)}N$ states are larger than these of $D^{(*)}N$ states.

When we compare the results of the π potential and of the $\pi\rho\omega$ potential, they are quite different for $J^P = 1/2^{\pm}$, $3/2^-$ with $I = 0$, where the ρ and ω exchange potentials become important to produce an attraction. For $D^{(*)}N$ and $\bar{B}^{(*)}N$ states, both ρ and ω exchange potentials are attractive, and hence they increase the binding energy significantly. On the other hand, for $J^P = 3/2^+$, $5/2^{\pm}$ and $7/2^-$, the results for the $\pi\rho\omega$ potential are similar to those for the π potential. For large J states, the π exchange potential plays a dominant role to generate bound and resonant states, while the ρ and ω exchanges play only a minor one. This is attributed to the fact that these states have large orbital angular momenta. If relevant channels include large orbital angular momenta, the wave functions tend to extend spatially, and the long range force, namely the π exchange potential, becomes important while the short range force is suppressed.

In the present study, we discuss the molecular structure formed by the $\bar{P}^{(*)}N$ bound and resonant states. However, the hadronic molecular picture is not applicable to deeply bound states with small radii. For such states, the constituent hadrons, namely the $D^{(*)}$ ($\bar{B}^{(*)}$) meson and the nucleon, overlap each other, and therefore we have to consider short range effects such as an internal structure of hadrons, channel couplings to conventional three quark states, etc. As a naive criterion for the hadronic molecule, we have shown the relative radii of the bound states as discussed in Ref. [24]. If the size of the bound state is larger than twice of typical hadron size (namely 1 fm), the state could be well described by a molecular structure. For resonant states, we identify the states as the hadronic molecule. According to the criterion, for the $\pi\rho\omega$ potential, only the bound state for $J^P = 3/2^+$ of $\bar{B}^{(*)}N$ constructs a hadronic molecule, where the relative radius is 1.81 fm. Contrary to this, the bound states for $J^P = 1/2^{\pm}$ and $3/2^-$ with $I = 0$ which have a small radius and a large binding energy are not described as simple molecules. For such states, we need to consider the short range effects including various channel couplings to do more realistic discussions.

Chapter 4

Exotic dibaryons formed by $P^{(*)}NN$ (3-body system)

4.1 Introduction

In section 3.3, we investigated the exotic $\bar{D}^{(*)}N$ and $B^{(*)}N$ states and saw that the attraction coming from the OPEP was important to yield the bound and resonant states. This attractive force between a heavy meson and a nucleon motivates us to explore the few- and many-body problems in mesic nuclei with a heavy antiquark, namely $\bar{D}$ (B) nuclei. It is naturally expected that the binding energy increases as the baryon number increases. In fact, in the hyperon-nucleon systems in the strangeness sector, several Λ hypernuclei have been found in experiments [71], while the ΛN two-body bound/resonant states are not observed. A unique feature of the $\bar{D}$ (B) nuclei is their genuinely exotic flavor structure. Therefore, their bound states have no lower channels coupled by a strong interaction.

In the many-nucleon systems with heavy mesons as impurity, we can explore rich phenomena which are not seen in the normal nuclei, as follows:

- The heavy meson plays a glue-like role, providing a strong attraction leading to a more shrinking in nucleus as discussed in the hypernuclei [70–72] and the $\bar{K}$ nuclei [73, 74] in the strangeness sector.
- We expect the changes of the properties of the heavy meson, such as mass modifications [77,84,85], which is related to the problems of the chiral symmetry restoration.

Furthermore, we would extract the information about the interaction between a heavy meson and a nucleon. In particular, we can study the few-body force, such as a three-body PNN force, in the mesic nuclei as a few-body system.

There have been several works for the $\bar{D}^{(*)}(B^{(*)})$ mesons in nuclear matter with infinite volume [76–87] and the atomic nuclei with large nucleon number such as ^{12}C, ^{40}Ca and ^{208}Pb [81, 83, 88–91], while few-body $\bar{D}^{(*)}(B^{(*)})$ nuclei have not been studied in the literature so far. However, the OPEP enhanced by the heavy quark spin symmetry appears in the $\bar{D}(B)$ nuclei as seen in the $\bar{D}^{(*)}N(B^{(*)}N)$ states. Therefore, it is expected the existence of bound states and/or resonances of the few-body

$\bar{D}^{(*)}(B^{(*)})$ nuclei.

In this chapter, we discuss the possible existence of exotic dibaryons with a heavy antiquark, being realized three-body systems, $\bar{D}^{(*)}NN$ and $B^{(*)}NN$ as shown in Fig. 4.1. We emphasize that in the strangeness sector, such exotic systems, i.e. K nuclei, do not appear because of the repulsion between a kaon and a nucleon. We introduce the OPEP between a $P^{(*)}(= \bar{D}^{(*)}, B^{(*)})$ meson and a nucleon. In this study, we do not consider the vector meson exchange potential yet. However, we expect that the results for the π exchange potential is valid because the long-range force dominates in the loosely bound states whose size is sufficiently large. Indeed, we saw the dominance of the OPEP in the exotic $P^{(*)}N$ states in the previous chapter.

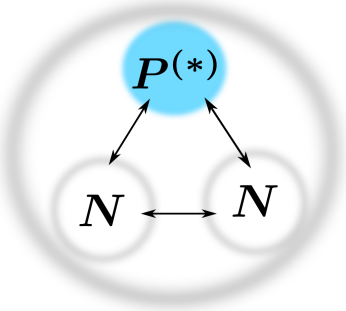

Fig.4.1 Three-body systems of PNN.

This chapter is organized as follows. In Sec. 4.2, we briefly summarize the interactions of $\bar{D}^{(*)}N$ ($B^{(*)}N$) and NN. In Sec. 4.3, we show the method to solve the $\bar{D}^{(*)}NN$ and $B^{(*)}NN$ systems with appropriate three-body wave functions. In Sec. 4.4, the numerical results are shown. we investigate bound and resonant states both of $\bar{D}^{(*)}NN$ and $B^{(*)}NN$ states with quantum numbers $J^P = 0^-$ and 1^-, and $I = 1/2$. In Sec. 4.5, we summarize this chapter and give the discussions.

4.2 Interactions

Let us introduce the interactions of the $P^{(*)}NN$ systems. In this study, We employ only the OPEPs for $PN - P^*N$ and $P^*N - P^*N$, given in Eqs. (3.15) and (3.16). As we have emphasized in the previous section for the $P^{(*)}N$ two-body systems, the OPEP is the basic ingredient to yield the strong attraction, thanks to the heavy quark spin symmetry inducing the mass splitting between a P and P^* mesons.

We could also consider the short-range interaction such as the vector meson exchanges [38, 53, 54, 144] and the quark exchange model [41, 145, 146]. It is discussed that the short-range interaction plays an important role for systems of a pseudscalar meson and a baryon in the strangeness sector, e.g. a KN system [94], where the π exchange causing the $KN - K^*N$ mixing is not significant because of the large mass difference of K and K^* mesons. However, the short-range interaction would not be as important as long-range interaction for loosely bound states, where the spatial distance between constituent hadrons becomes large. In fact, we have found that the dominant force in the two-body $P^{(*)}N$ systems is the OPEP rather than the ρ

and ω exchange potentials in the previous section. This situation is analogous to the deuteron which is the loosely bound state of the proton and neutron [96, 147].

For the nucleon-nucleon interaction, we employ the Argonne v_8' (AV8′) potential which is the realistic NN potential developed by the Argonne group [148]. This potential is written by the π exchange part, and the short- and intermediate-range parts:

$$v_8'(r) = v^\pi(r) + \sum_{P=1,8} v_p'(r)\mathcal{O}^P\,, \tag{4.1}$$

with eight operators,

$$\begin{aligned}\mathcal{O}^{P=1,\cdots,8} =& 1,\ \vec{\sigma}_1\cdot\vec{\sigma}_2,\ \vec{\tau}_1\cdot\vec{\tau}_2,\ \vec{\sigma}_1\cdot\vec{\sigma}_2\,\vec{\tau}_1\cdot\vec{\tau}_2,\\ & S_{12},\ S_{12}\,\vec{\tau}_1\cdot\vec{\tau}_2,\ \vec{L}\cdot\vec{S},\ \vec{L}\cdot\vec{S}\,\vec{\tau}_1\cdot\vec{\tau}_2\,.\end{aligned} \tag{4.2}$$

The functions $v^\pi(r)$ and $v_p'(r)$ are summarized in Appendix B.3.3. The AV8′ potential is simpler than the more elaborated one of the Argonne v_{18} (AV18) potential [149], which is the reason that we employ the former in the present study. The AV8′ is realistic because it reproduces NN phase shifts and deuteron properties. When applied to three or more nucleon systems, however, the AV8′ provides slightly more attraction than the AV18 potential [150,151]. In the $\bar{D}^{(*)}NN$ systems, however, there are only two nucleons with the binding energy similar to that of the deuteron, and therefore, the AV8′ gives essentially the same results as the AV18.

4.3 Hamiltonian and Three-body wave functions

The total Hamiltonian is given by

$$H = T + V_{P^{(*)}N} + V_{NN}, \tag{4.3}$$

where T is the kinetic term, and $V_{P^{(*)}N}$ (V_{NN}) is the interaction potential between a $P^{(*)}$ meson and a nucleon (between two nucleons) as introduced above. We investigate $\bar{D}^{(*)}NN$ and $B^{(*)}NN$ with $J^P = 0^-$ and 1^- and $I = 1/2$ (total angular momentum J, parity P and total isospin I).

The three-body wave function is described as a sum of the rearrange channel amplitudes ($c = 1, 2$) as functions of the Jacobi coordinates shown in Fig. 4.2:

$$\begin{aligned}\Psi_{JM} =& \sum_{c=1}^{2}\sum_{nl_1,Nl_2,L}\sum_{s_{12}S,I_{12}} C^{(c)}_{nl_1,Nl_2,L,s_{12}S,I_{12}I}\mathcal{A}\Big\{\Big[\Big[\phi^{(c)}_{nl_1m_1}(\vec{r}_c)\psi^{(c)}_{Nl_2m_2}(\vec{R}_c)\Big]_L\\ & \times\ \big[[\chi_{s_1}\chi_{s_2}]_{s_{12}}\chi_{s_3}\big]_S\Big]_{JM}\big[[\eta_{I_1}\eta_{I_2}]_{I_{12}}\eta_{I_3}\big]_I\Big\}\,.\end{aligned} \tag{4.4}$$

$\mathcal{A}$ is the anti-symmetrization operator for exchange between two nucleons. l_1 and l_2 stand for the relative orbital angular momenta associated with the coordinates $\vec{r}_c$ and $\vec{R}_c$, respectively. L is the total orbital angular momentum of the three-body system. χ_{s_i} (η_{I_i}) with $i = 1, 2, 3$ is the spin (isospin) function of the particle with the

spin s_i (isospin I_i). s_{12} (I_{12}) is the spin (isospin) of two particles combined by the relative coordinate $\vec{r}_c$, and S is the total spin of the three-body system. The functions $\phi_{nl_1m_1}(\vec{r})$ and $\psi_{Nl_2m_2}(\vec{R})$ are expressed by the Gaussian expansion method [152–154] as

$$\phi_{nl_1m_1}(\vec{r}) = \sqrt{\frac{2}{\Gamma(l_1+3/2)b_n^3}}\left(\frac{r}{b_n}\right)^{l_1}\exp\left(-\frac{r^2}{2b_n^2}\right)Y_{l_1m_1}(\hat{r})\,, \tag{4.5}$$

$$\psi_{Nl_2m_2}(\vec{R}) = \sqrt{\frac{2}{\Gamma(l_2+3/2)B_N^3}}\left(\frac{R}{B_N}\right)^{l_2}\exp\left(-\frac{R^2}{2B_N^2}\right)Y_{l_2m_2}(\hat{R})\,. \tag{4.6}$$

The Gaussian ranges b_n and B_N are given by the form of geometric series as

$$b_n = b_1 a^{n-1}\,, \quad B_N = B_1 A^{N-1}\,. \tag{4.7}$$

For the sum of Eq. (4.4), we consider all possible coupled channels to obtain solutions with sufficiently good accuracy. For instance, we include orbital angular momentum space of $l_1, l_2 \leq 2$. Furthermore, we consider two independent isospin states to form the total isospin $I = 1/2$, the NN subsystems of $I = 0$ and 1 which are combined with the $\bar{D}$ meson of $I = 1/2$ for the total $I = 1/2$.

By diagonalizing the total Hamiltonian by using the three-body bases introduced above, we obtain eigenenergies and coefficient $C^{(c)}_{nl_1,Nl_2,L,s_{12}S,I_tI}$. We also calculate the poles for resonances as complex eigenvalues by using the complex scaling method [155–159].

4.4 Numerical Results of $\bar{D}^{(*)}NN$ and $B^{(*)}NN$

Let us present the results of $\bar{D}^{(*)}NN$ and $B^{(*)}NN$ for $J^P = 0^-$. We obtain bound states both of $\bar{D}^{(*)}NN$ and $B^{(*)}NN$. The energy levels are shown in Fig. 4.3. The bound state of $\bar{D}^{(*)}NN$ with the binding energy -5.2 MeV, locates below the threshold of $\bar{D}N(1/2^-)+N$. Here $\bar{D}N(1/2^-)$ is the bound state of $\bar{D}^{(*)}$ and N with binding energy -1.6 MeV for $J^P = 1/2^-$ and $I = 0$ as discussed in Sec. 3.3 (See also Table 3.4 and Fig. 3.8). Therefore, the $\bar{D}^{(*)}NN$ three-body state is more deeply bound than

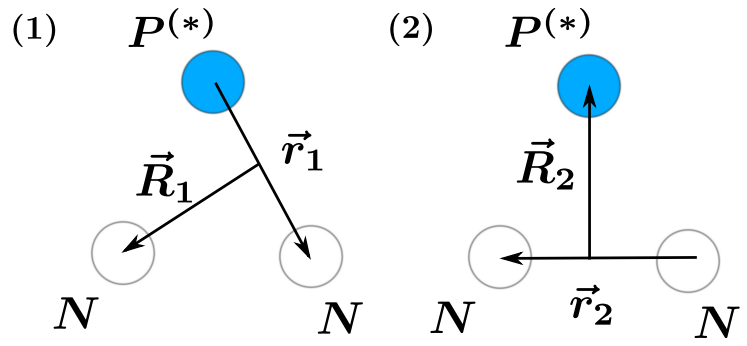

Fig.4.2 Jacobi coordinates ($c = 1, 2$) of the $P^{(*)}NN$ systems.

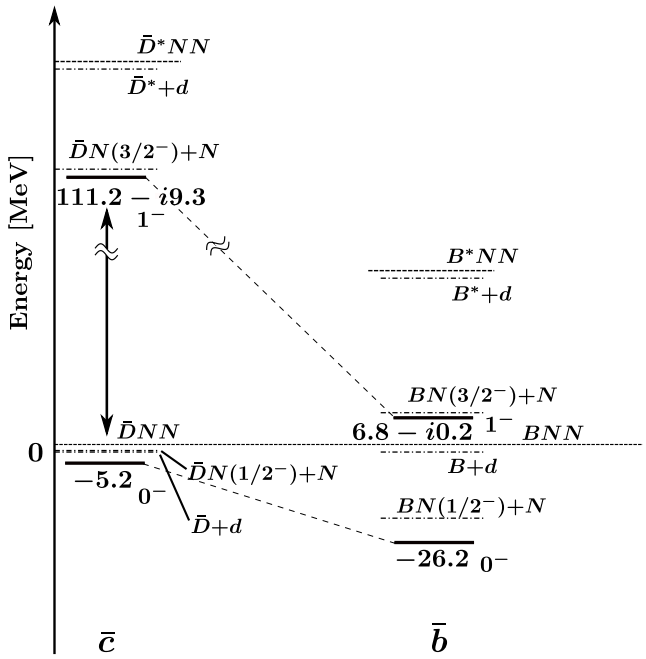

Fig.4.3 Energy levels of $\bar{D}^{(*)}NN$, $B^{(*)}NN$ with $I = 1/2$ and $J^P = 0^-$ and 1^- (solid lines) from Ref. [93]. The complex energies for resonances are given as $E_{re} - i\Gamma/2$, where E_{re} is a resonance energy and $\Gamma/2$ is a half decay width. Thresholds (subthresholds) are denoted by dashed (dashed-dotted) lines.

Table.4.1 Expectation values of central, tensor and LS forces of the $\bar{D}^{(*)}N$ ($B^{(*)}N$) and NN potentials in the bound state of $\bar{D}^{(*)}NN$ ($B^{(*)}NN$). All values are in units of MeV.

$\bar{D}^{(*)}NN$	$\langle V_{\bar{D}N-\bar{D}^*N}\rangle$	$\langle V_{\bar{D}^*N-\bar{D}^*N}\rangle$	$\langle V_{NN}\rangle$
Central	-2.3	-0.1	-9.5
Tensor	-47.1	0.7	-0.2
LS	—	—	-0.03
$B^{(*)}NN$	$\langle V_{BN-B^*N}\rangle$	$\langle V_{B^*N-B^*N}\rangle$	$\langle V_{NN}\rangle$
Central	-6.5	0.3	-11.6
Tensor	-92.0	-2.7	-1.0
LS	—	—	-0.1

the $\bar{D}^{(*)}N$ two-body state, as naturally expected. We also find the $B^{(*)}NN$ state with the binding energy -26.2 MeV. The $B^{(*)}NN$ state is more deeply bound than the $\bar{D}^{(*)}NN$ state, because the mixing effect between PNN and P^*NN is enhanced, when P and P^* mesons become more degenerate.

Let us investigate how the bound states are formed. For this purpose, we analyze various components of interaction matrix elements. In Table 4.1, we summarize the expectation values of the potentials, V_{PN-P^*N}, $V_{P^*N-P^*N}$ and V_{NN}, sandwiched by the obtained wave functions. In $\bar{D}^{(*)}NN$, we find that the tensor force of $V_{\bar{D}N-\bar{D}^*N}$

mixing $\bar{D}NN$ and $\bar{D}^*NN$ is the dominant contribution. In contrast, $V_{\bar{D}^*N-\bar{D}^*N}$ is very small. Thus, the tensor force of $V_{\bar{D}N-\bar{D}^*N}$ is a driving force giving bound states in $\bar{D}^{(*)}NN$. We note that the strong tensor force also provides a dominant attraction in the two-body $\bar{D}^{(*)}N$ systems as discussed in Sec. 3.3. The same result holds also to $B^{(*)}NN$.

For V_{NN}, one may expect that the tensor force causing the ${}^3S_1 - {}^3D_1$ mixing could be the most dominant one, because it is a driving force giving a deuteron d. However, the tensor force in V_{NN} is almost irrelevant in the present systems. In fact, it is shown in Table 4.1 that the tensor force is suppressed, while the central force is rather dominant. This is reasonable because d does not exist in the main component of $\bar{D}NN$ channel with $J^P = 0^-$ due to limited combinations of quantum numbers, which means that the combinations of 0^- ($\bar{D}$) and 1^+ (d) cannot compose the quantum number $J^P = 0^-$. It may exist in the $\bar{D}^*NN$ component, but the amplitude of the $\bar{D}^*NN$ is small due to the excess of mass of about 140 MeV ($\sim m_{\bar{D}^*} - m_{\bar{D}}$). Thus, the NN interaction provides only a weak attraction. Therefore, the tensor force mixing $\bar{D}N$ and $\bar{D}^*N$ gives the most dominant term of attraction in the $\bar{D}^{(*)}NN$ state. The same behavior is also found in the $B^{(*)}NN$ state as shown in Table 4.1.

The quantum number 0^- of the $\bar{D}^{(*)}NN$ state may be investigated in experiments through two particle correlations. The $\bar{D}^{(*)}NN$ state can decay into $K + \pi$ (or $\pi\pi$) + $N + N$ by the weak decay of a $\bar{D}$ meson. The absence of d in the final NN state will be an important signal suggesting 0^-. In contrast, if d might be observed, the quantum number would be 1^-. It will be also the case for $B^{(*)}NN$.

In scattering states, we find resonances for $J^P = 1^-$ and $I = 1/2$ as shown in Fig. 4.3. The resonance energy for $\bar{D}^{(*)}NN$ is 111.2 MeV measured from the threshold of $\bar{D}NN$. The decay width is 18.6 MeV. We note that there are open channels of the $\bar{D}NN$ and $\bar{D} + d$ scattering states below the resonance, and of the $\bar{D}^* + d$ and $\bar{D}N(3/2^-) + N$ scattering states above the resonance. Here $\bar{D}N(3/2^-)$ is a Feshbach resonance of $\bar{D}^{(*)}$ and N with $J^P = 3/2^-$ and $I = 0$, which was found in Sec. 3.3. We obtain a resonance also for $B^{(*)}NN$ with much smaller resonance energy and decay width, 6.8 MeV and 0.4 MeV, respectively. The mechanism of formation of the resonances is interesting. When we ignore the $\bar{D}NN$ channel and consider only the $\bar{D}^*NN$ channel, we obtain a bound state of $\bar{D}^*NN$. Hence, the $\bar{D}^*NN$ channel predominates. Therefore, the obtained resonance is a Feshbach resonance for the three-body system, as in the case of the two-body $\bar{D}N(3/2^-)$ system. These features also hold for $B^{(*)}NN$.

From the above analysis, we see that the many features of the two-body $P^{(*)}N$ system survive in the three-body $P^{(*)}NN$ system, because the $P^{(*)}N$ interaction is the dominant force which determines the main properties of the system rather than the NN interaction.

4.5 Summary and Discussion for $\bar{D}^{(*)}NN$ and $B^{(*)}NN$

Let us summarize this chapter. We have investigated the possible existence of genuinely exotic dibaryons of $\bar{D}^{(*)}NN$ and $B^{(*)}NN$ for charm and bottom sectors. The OPEP introduced by the heavy quark symmetry and chiral symmetry was employed between a heavy meson and a nucleon. As for the NN interaction, the Argonne v_8' potential was used. By solving the coupled channel Schrödinger equations for PNN and P^*NN channels, we have obtained bound states with $J^P = 0^-$ and resonances with $J^P = 1^-$ for $I = 1/2$ both in $\bar{D}^{(*)}NN$ and $B^{(*)}NN$. We found that the resonances was the Feshbach resonances in which the $P^{(*)}NN$ components predominate. These bound and resonant states are located below the subthresholds of $\bar{D}N(1/2^-)+N$ and $\bar{D}N(3/2^-) + N$, respectively. Therefore, the binding and resonance energies of the three-body $P^{(*)}NN$ systems are lower than those of the two-body $P^{(*)}N$ systems.

In these states, the OPEP of the $P^{(*)}N$ potential plays a dominant role to produce a strong attraction. In particular, the role of the tensor force of the OPEP mixing PN and P^*N is essential. On the other hand, the contributions of the potential of $P^*N - P^*N$ components are small due to the excess of the mass.

For the contributions of the NN interaction in the bound states, the attraction from the central force is stronger than that from the tensor force, while the tensor force is the driving force giving the deuteron. However, the $NN(1^+)$ subsystem corresponding to the deuteron is suppressed due to the limited combinations of angular momentum in the bound states with $J^P = 0^-$. In all, the $P^{(*)}N$ interaction dominates rather than the NN interaction in the three-body $P^{(*)}NN$ systems.

In this study, we introduced the OPEP only as the interaction between the heavy meson and the nucleon because the dominance of the long-range force was expected in the loosely bound states as seen in the two-body systems discussed in chapter. 3. However, we could consider the vector and scalar meson exchange potentials as short- and middle-range forces. To obtain the more accurate results, we employ these interaction in the future works.

In addition, we can also consider the few-body forces in the PNN systems. It is known that the predictions using the two-body forces only underestimate the experimental data for the atomic nuclei [160–164]. The few-body forces become important as the particle number increases and therefore this effect is not negligible in the nuclear matter with large nucleon numbers [165]. Moreover, the few-body forces are also discussed in the hypernuclei with the strangeness degree of freedom [166].

The basic idea of the few-body force was proposed by J. Fujita and H. Miyazawa in 1957 [167]. The three-nucleon potential called Fujita-Miyazawa force was described phenomenologically by a 2π exchange among three nucleons with a Δ excitation. This idea has been employed in recent phenomenological models of the three-nucleon force; the Urbana IX three-nucleon potentials [148, 168], the Tucson-Melbourne 2π-exchange three-nucleon potential [169] and Illinois model [150]. The realistic NN potentials combined with these three-nucleon force models are successfully reproduced

the properties of the atomic nuclei. As for the different approaches to discuss the few-body forces, there are several works by using the chiral effective field theory [170–173] and the Lattice QCD simulation [174].

In the PNN systems, the 2π exchange among the three-particles can emerge via the P^* excitation as well as via the Δ excitation. Thanks to the small mass splitting between P and P^* mesons, namely $m_{\bar{D}^*} - m_{\bar{D}} \sim 140$ MeV and $m_{B^*} - m_B \sim 45$ MeV, the three-body forces from $PN - P^*N$ coupling effects are more important than those from $NN - N\Delta$ coupling effects, where the mass difference between N and Δ is about 300 MeV. The three-body force becomes more important as number of particles increases. Therefore, the effects of the $PN - P^*N$ mixing are expected to be unignorable in the $P^{(*)}$ nuclei with large baryon numbers.

Chapter 5

Spin degeneracy of the hadronic molecules

5.1 Introduction

For a hadron containing heavy quarks, the heavy quark symmetry appears due to suppression of the spin-dependent interaction between quarks, caused by the large heavy quark mass. Therefore, the heavy quark spin is decoupled from the light degrees of freedom, called brown muck, in the heavy hadron. Brown muck is defined as everything other than the heavy quark in the hadron [101], e.g. light quarks and gluons. The spin decoupling leads to mass degeneracy of the states [103, 104]. For instance, for hadrons with a single heavy quark, the states with total angular momentum and parity, $(j-1/2)^P$ and $(j+1/2)^P$ are degenerate for $j \neq 0$, where j is the total angular momentum of the brown muck. For $j = 0$, non-degenerate states emerge. In fact, the mass degenerate states are found as the doublet with small mass splitting. For the heavy mesons, the small mass splitting between pseudoscalar and vector mesons are found, such as $m_{D^*} - m_D \sim 140$ MeV and $m_{B^*} - m_B \sim 45$ MeV. This values can be compared with the mass splittings of π and ρ, and K and K^* mesons, namely $m_\rho - m_\pi \sim 600$ MeV, and $m_{K^*} - m_K \sim 400$ MeV.

The degenerate multiplet has been also discussed for the normal heavy baryons such as Λ_c (Λ_b), Σ_c (Σ_b), and these excited states, from the heavy quark effective theory [69,100,101,103,105–108]. We can also see the degeneracy in the heavy baryon states. The mass difference between $\Sigma_c(1/2^+)$ ($\Sigma_b(1/2^+)$) and $\Sigma_c^*(3/2^+)$ ($\Sigma_b^*(3/2^+)$) are small, namely about 65 (20) MeV, and hence they are considered to be doublet states. On the other hand, $\Lambda_c(1/2^+)$ ($\Lambda_b(1/2^+)$) is expected to be a non-degenerate state.

The spin degeneracy is a general feature for heavy hadrons from the heavy quark symmetry. This has been discussed not only for the normal heavy hadrons, but also multi-hadron systems with heavy quarks [104, 109]. For the multi-hadron states, the brown muck has a more complicated structure because it could contain light hadrons. For example, in the systems formed by a heavy meson and a light baryon, the brown muck is a composite system constructed by the light components in the heavy meson and the light baryon. These brown mucks are called spin-complex. It is a useful object

to discuss the multi-hadron systems with heavy quarks such as hadronic molecules and exotic nuclei.

The spin degeneracy is expected to be applied to the exotic PN and PNN systems with a heavy antiquark, discussed in chapters. 3 and 4. We investigate the hadronic molecules in the heavy quark limit.

This chapter is organized as follows. In Sec. 5.2, general discussions about the heavy quark spin symmetry are present briefly. In Sec. 5.3, wave functions and Hamiltonians of the P_QN states are discussed from the point of view of the spin-complex. Here, the $P_Q^{(*)}$ meson is defined as a meson $(\bar{Q}q)_{\mathrm{spin}0(1)}$ with an infinite heavy quark mass. In Sec. 5.4, numerical results of the P_QN and P_QNN states in the heavy quark limit are shown. Finally, we summarize this chapter in Sec. 5.5.

5.2 Heavy quark symmetry and Spin degeneracy

Let us discuss the spin degeneracy from the heavy quark spin symmetry in the heavy quark effective theory (HQET). The HQET was discussed in Sec. 2.2. The effective Lagrangian of HQET is given in Eq. (2.21). We saw that the leading term of the Lagrangian does not depend on a heavy quark mass and spin. Hence, in the heavy quark limit ($m_Q \to \infty$), the HQET Lagrangian manifests spin and flavor symmetries, namely heavy quark flavor and spin symmetry.

The absence of the spin-dependent interactions in the HQET Lagrangian in the heavy quark limit leads to separation of the heavy quark spin s_Q and total angular momentum j of light degrees of freedom, namely brown muck. Then, the total angular momentum of the system can be rewritten as

$$\vec{J} = \vec{L} + \vec{S} = \vec{s}_Q + \vec{j}\,. \tag{5.1}$$

The total angular momentum J is conserved, and the heavy quark spin s_Q is also conserved in the heavy quark limit. Therefore, the total angular momentum j of the brown muck is also a conserved value. We can utilize s_Q and j to classify the heavy hadron states.

Let us consider a hadron with a heavy quark Q or a heavy antiquark $\bar{Q}$. The hadron with single Q ($\bar{Q}$) is written as a superposition of various components with light quarks q, $q\bar{q}$ pairs and gluons g;

$$|H_Q\rangle = |Qq^n\rangle + |Qq^nq\bar{q}\rangle + |Qq^ng\rangle + \cdots, \tag{5.2}$$

$$\left|H_{\bar{Q}}\right\rangle = \left|\bar{Q}q^m\right\rangle + \left|\bar{Q}q^mq\bar{q}\right\rangle + \left|\bar{Q}q^mg\right\rangle + \cdots, \tag{5.3}$$

where $n = 3B-1$ and $m = 3B+1$ with baryon number $B \geq 0$. The light components, $q^n + q^nq\bar{q} + q^ng + \cdots$ ($q^m + q^mq\bar{q} + q^mg + \cdots$), compose the brown muck whose total angular momentum j is conserved. Due to the suppression of the spin-dependent forces, the heavy quark spin $s_Q = 1/2$ is decoupled from the total angular momentum j of the light components.

This spin decoupling yields the degeneracy of the hadron H_Q with total angular momentum and parity, $(j-1/2)^P$, and their excited state H_Q^* with $(j+1/2)^P$ for $j \neq 0$. For the brown muck with $j = 0$, the singlet state H_Q with $1/2^P$ emerges. In

this thesis, the degenerate states and singlet states are called the Heavy quark spin (HQS) doublets and the HQS singlets, respectively.

For exotic hadrons, however, brown muck is composed not only of light quarks and gluons, but also of light hadrons, and therefore the systems have a bit more complicated structure than the normal heavy hadrons. For example, the brown muck of the $\bar{D}N$ molecules is formed by the light degrees of freedom (light quarks and gluons) in the $\bar{D}$ meson, and the nucleon N as a hadronic degree of freedom. The brown muck having such complex structures, is called "light spin-complex" (or "spin-complex" in short) in Refs. [104, 109]. The spin-complex with conserved quantum number $j^{\mathcal{P}}$ is also decoupled from the heavy quark spin in the exotic states. Hence, the HQS doublets for $j \neq 0$ and/or the HQS singlets can also emerge in the multi-hadron systems with a single heavy (anti-)quark. The spin-complex is useful to classify structures of the multi-hadron states such as hadronic molecules and exotic nuclei.

5.3 Hadronic molecules in the heavy quark limit

In this section, we discuss the degenerate states of the hadronic molecules as a concrete example of the multi-hadron systems. The $P_Q N$ and $P_Q NN$ states formed by a heavy meson and nucleons are heavy (di)baryons with a single heavy antiquark, where P_Q is defined as a heavy meson having an infinite heavy quark mass. The spin-complex has composite structures containing a light quark q in the heavy meson, and a nucleon as a hadronic degree of freedom, denoted by $[qN]$ ($[qNN]$) for $P_Q N$ ($P_Q NN$). The internal spin structures of the $P_Q N$ ($P_Q NN$) molecules become clear by introducing the spin-complex $[qN]$ ($[qNN]$).

5.3.1 Wave functions in the spin-complex-basis

Let us consider the wave functions of the $P_Q N$ molecules in point of view of the spin-complex. The wave functions in the $P_Q^{(*)} N$ state with $J^P = 1/2^-$ are written in

$$\left|P_Q N(^2S_{1/2})\right\rangle, \left|P_Q^* N(^2S_{1/2})\right\rangle, \left|P_Q^* N(^4D_{1/2})\right\rangle \tag{5.4}$$

from Table 5.1. The heavy quark spin symmetry manifests that the heavy quark $\bar{Q}$ in the $P_Q^{(*)}$ meson is decoupled from the spin-complex, namely the light degrees of freedom in the $P_Q^{(*)}$ meson and the nucleon N. Therefore, the wave functions expressed by P_Q and N (called particle basis) are expected to be rewritten as those expressed by the heavy antiquark and spin-complex (called spin-complex basis).

In this study, we consider that the P_Q and P_Q^* mesons with the infinite heavy quark mass are composed of $P \sim (\bar{Q}q)_{\text{spin0}}$ and $P^* \sim (\bar{Q}q)_{\text{spin1}}$, respectively. The $P_Q^{(*)} N$ states are described as $\bar{Q}qN$, where the spin-complex is constructed by the constituent light quark q and the nucleon N. Here, we do not consider to include components with more than one light quark, gluons, and hadrons in the $P_Q^{(*)} N$ system, such as $\bar{Q}q\cdots qN$, $\bar{Q}q\cdots qq\bar{q}N$ $\bar{Q}q\cdots qgN$ and $\bar{Q}q,\cdots,qNH\bar{H}$, where H ($\bar{H}$) is a hadron (an

Table.5.1 Various coupled channels in the $P_Q^{(*)}N$ systems with quantum number J^P written in the particle basis (PN) and the spin-complex basis (SC).

J^P	basis	channels			
$1/2^-$	PN	$P_QN(^2S_{1/2})$	$P_Q^*N(^2S_{1/2})$	$P_Q^*N(^4D_{1/2})$	—
	SC	$[Nq]^{0,S}_{(0^+)}\bar{Q}$	$[Nq]^{(1,S)}_{1^+}\bar{Q}$	$[Nq]^{(1,D)}_{1^+}\bar{Q}$	—
$3/2^-$	PN	$P_QN(^2D_{3/2})$	$P_Q^*N(^4S_{3/2})$	$P_Q^*N(^2D_{3/2})$	$P_Q^*N(^4D_{3/2})$
	SC	$[Nq]^{(1,S)}_{1^+}\bar{Q}$	$[Nq]^{(1,D)}_{1^+}\bar{Q}$	$[Nq]^{(0,D)}_{2^+}\bar{Q}$	$[Nq]^{(1,D)}_{2^+}\bar{Q}$
$5/2^-$	PN	$P_QN(^2D_{5/2})$	$P_Q^*N(^2D_{5/2})$	$P_Q^*N(^4D_{5/2})$	$P_Q^*N(^4G_{5/2})$
	SC	$[Nq]^{(0,D)}_{2^+}\bar{Q}$	$[Nq]^{(1,D)}_{2^+}\bar{Q}$	$[Nq]^{(1,D)}_{3^+}\bar{Q}$	$[Nq]^{(1,G)}_{3^+}\bar{Q}$
$7/2^-$	PN	$P_QN(^2G_{7/2})$	$P_Q^*N(^4D_{7/2})$	$P_Q^*N(^2G_{7/2})$	$P_Q^*N(^4G_{7/2})$
	SC	$[Nq]^{(1,D)}_{3^+}\bar{Q}$	$[Nq]^{(1,G)}_{3^+}\bar{Q}$	$[Nq]^{(0,G)}_{4^+}\bar{Q}$	$[Nq]^{(1,G)}_{4^+}\bar{Q}$
$1/2^+$	PN	$P_QN(^2P_{1/2})$	$P_Q^*N(^2P_{1/2})$	$P_Q^*N(^4P_{1/2})$	—
	SC	$[Nq]^{(1,P)}_{0^-}\bar{Q}$	$[Nq]^{(0,P)}_{1^-}\bar{Q}$	$[Nq]^{(1,P)}_{1^-}\bar{Q}$	—
$3/2^+$	PN	$P_QN(^2P_{3/2})$	$P_Q^*N(^2P_{3/2})$	$P_Q^*N(^4P_{3/2})$	$P_Q^*N(^4F_{3/2})$
	SC	$[Nq]^{(0,P)}_{1^-}\bar{Q}$	$[Nq]^{(1,P)}_{1^-}\bar{Q}$	$[Nq]^{(1,P)}_{2^-}\bar{Q}$	$[Nq]^{(1,F)}_{2^-}\bar{Q}$
$5/2^+$	PN	$P_QN(^2F_{5/2})$	$P_Q^*N(^4P_{5/2})$	$P_Q^*N(^2F_{5/2})$	$P_Q^*N(^4F_{5/2})$
	SC	$[Nq]^{(1,P)}_{2^-}\bar{Q}$	$[Nq]^{(1,F)}_{2^-}\bar{Q}$	$[Nq]^{(0,F)}_{3^-}\bar{Q}$	$[Nq]^{(1,F)}_{3^-}\bar{Q}$
$7/2^+$	PN	$P_QN(^2F_{7/2})$	$P_Q^*N(^2F_{7/2})$	$P_Q^*N(^4F_{7/2})$	$P_Q^*N(^4H_{7/2})$
	SC	$[Nq]^{(0,F)}_{3^-}\bar{Q}$	$[Nq]^{(1,F)}_{3^-}\bar{Q}$	$[Nq]^{(1,F)}_{4^-}\bar{Q}$	$[Nq]^{(1,H)}_{4^-}\bar{Q}$

antihadron). We introduce the notation of the spin-complex component,

$$[Nq]^{(s_l,L)}_{j^{\mathcal{P}}} \ , \tag{5.5}$$

in the wave function. s_l is the total spin of N and q. L stands for the relative orbital angular momentum between N and q. j and $\mathcal{P}$ are the total angular momentum and the parity of the spin-complex. Then the wave function of the P_QN states in the spin-complex basis is written as

$$\left|[Nq]^{(s_l,L)}_{j^{\mathcal{P}}}\bar{Q}\right\rangle_{J^P} \ . \tag{5.6}$$

For the $P_Q^{(*)}N$ state with $J^P = 1/2^-$, the wave functions in the particle basis in Eq. (5.4) are using the formulas of the angular momentum recoupling [175, 176] as transformed to those in the spin-complex basis by

$$\begin{pmatrix} \left|P_QN(^2S_{1/2})\right\rangle \\ \left|P_Q^*N(^2S_{1/2})\right\rangle \\ \left|P_Q^*N(^4D_{1/2})\right\rangle \end{pmatrix} = U_{1/2^-} \begin{pmatrix} \left|[Nq]^{(0,S)}_{0^+}\bar{Q}\right\rangle_{1/2^-} \\ \left|[Nq]^{(1,S)}_{1^+}\bar{Q}\right\rangle_{1/2^-} \\ \left|[Nq]^{(1,D)}_{1^+}\bar{Q}\right\rangle_{1/2^-} \end{pmatrix} , \tag{5.7}$$

where the unitary matrix U_{J^P} is given by

$$U_{1/2^-} = \begin{pmatrix} -\frac{1}{2} & \frac{\sqrt{3}}{2} & 0 \\ \frac{\sqrt{3}}{2} & \frac{1}{2} & 0 \\ 0 & 0 & -1 \end{pmatrix} . \tag{5.8}$$

Because the states contain the two spin-complex components with $j = J - 1/2$ and $J + 1/2$ from Eq. (5.1), the wave functions for $J^P = 1/2^-$ in the spin-complex basis have the channels with $j^{\mathcal{P}} = 0^+$ and 1^+. The component with $j^{\mathcal{P}} = 0^+$ corresponds to the HQS singlet, while the component with $j^{\mathcal{P}} = 1^+$ forms the HQS doublet together with the $J^P = 3/2^-$ state.

In a similar way, we obtain the wave functions in the spin-complex basis for other J^P states. For instance, we demonstrate the transformation for $J^P = 3/2^-$ for a negative parity state, and $J^P = 1/2^+$ and $3/2^+$ for a positive parity state. The wave functions for $J^P = 3/2^-$ is transformed to

$$\begin{pmatrix} \left|P_Q N(^2D_{3/2})\right\rangle \\ \left|P_Q^* N(^4S_{3/2})\right\rangle \\ \left|P_Q^* N(^4D_{3/2})\right\rangle \\ \left|P_Q^* N(^2D_{3/2})\right\rangle \end{pmatrix} = U_{3/2^-} \begin{pmatrix} \left|[Nq]^{(1,S)}_{1^+}\bar{Q}\right\rangle_{3/2^-} \\ \left|[Nq]^{(1,D)}_{1^+}\bar{Q}\right\rangle_{3/2^-} \\ \left|[Nq]^{(0,D)}_{2^+}\bar{Q}\right\rangle_{3/2^-} \\ \left|[Nq]^{(1,D)}_{2^+}\bar{Q}\right\rangle_{3/2^-} \end{pmatrix} \tag{5.9}$$

with

$$U_{3/2^-} = \begin{pmatrix} 0 & \frac{\sqrt{6}}{4} & \frac{1}{2} & \frac{\sqrt{6}}{4} \\ 1 & 0 & 0 & 0 \\ 0 & \frac{1}{\sqrt{2}} & 0 & -\frac{1}{\sqrt{2}} \\ 0 & \frac{1}{2\sqrt{2}} & -\frac{\sqrt{3}}{2} & \frac{1}{2\sqrt{2}} \end{pmatrix} \tag{5.10}$$

The state for $J^P = 3/2^-$ includes two spin-complex components with $j^{\mathcal{P}} = 1^+$ and 2^+. In comparison with the state for $J^P = 1/2^-$, both states in the spin-complex basis have $\left|[Nq]^{(1,S)}_{1^+}\bar{Q}\right\rangle_{J^-}$ and $\left|[Nq]^{(1,D)}_{1^+}\bar{Q}\right\rangle_{J^-}$. This result implies the appearance of the spin degeneracy of the states with $J^P = 1/2^-$ and $3/2^-$.

For the positive parity states, we obtain the

$$\begin{pmatrix} \left|P_Q N(^2P_{1/2})\right\rangle \\ \left|P_Q^* N(^2P_{1/2})\right\rangle \\ \left|P_Q^* N(^4P_{1/2})\right\rangle \end{pmatrix} = U_{1/2^+} \begin{pmatrix} \left|[Nq]^{(1,P)}_{0^-}\bar{Q}\right\rangle_{1/2^+} \\ \left|[Nq]^{(0,P)}_{1^-}\bar{Q}\right\rangle_{1/2^+} \\ \left|[Nq]^{(1,P)}_{1^-}\bar{Q}\right\rangle_{1/2^+} \end{pmatrix} \tag{5.11}$$

with

$$U_{1/2^+} = \begin{pmatrix} \frac{1}{2} & \frac{1}{2} & \frac{1}{\sqrt{2}} \\ \frac{1}{2\sqrt{3}} & -\frac{\sqrt{3}}{2} & \frac{1}{\sqrt{6}} \\ \sqrt{\frac{2}{3}} & 0 & -\frac{1}{\sqrt{3}} \end{pmatrix} \tag{5.12}$$

for $1/2^+$, and

$$\begin{pmatrix} \left|P_Q N(^2P_{3/2})\right\rangle \\ \left|P_Q^* N(^2P_{3/2})\right\rangle \\ \left|P_Q^* N(^4P_{3/2})\right\rangle \\ \left|P_Q^* N(^4F_{3/2})\right\rangle \end{pmatrix} = U_{3/2^+} \begin{pmatrix} \left|[Nq]^{(0,P)}_{1^-}\bar{Q}\right\rangle_{3/2^+} \\ \left|[Nq]^{(1,P)}_{1^-}\bar{Q}\right\rangle_{3/2^+} \\ \left|[Nq]^{(1,P)}_{2^-}\bar{Q}\right\rangle_{3/2^+} \\ \left|[Nq]^{(1,F)}_{2^-}\bar{Q}\right\rangle_{3/2^+} \end{pmatrix}, \tag{5.13}$$

with

$$U_{3/2^+} = \begin{pmatrix} -\frac{1}{2} & \frac{1}{2\sqrt{2}} & \frac{\sqrt{10}}{4} & 0 \\ \frac{\sqrt{3}}{2} & \frac{1}{2\sqrt{6}} & \frac{1}{2}\sqrt{\frac{5}{6}} & 0 \\ 0 & \sqrt{\frac{5}{6}} & -\frac{1}{\sqrt{6}} & 0 \\ 0 & 0 & 0 & -1 \end{pmatrix}, \tag{5.14}$$

for $3/2^+$. We obtain that the states with $J^P = 1/2^+$ and $3/2^+$ include the common components with $j^{\mathcal{P}} = 1^-$, namely $\left|[Nq]^{(0,P)}_{1^-}\bar{Q}\right\rangle_{J^+}$ and $\left|[Nq]^{(1,P)}_{1^-}\bar{Q}\right\rangle_{J^+}$.

The wave functions in the spin-complex basis are also summarized in Appendix C.1.

5.3.2 Hamiltonian in the spin-complex basis

The transformation discussed in the wave functions derives the Hamiltonian in the spin-complex basis. In the heavy quark limit, the Hamiltonian in the $J^P = 1/2^-$ and $3/2^-$ states in the particle basis are given from Eqs. (3.16) and (3.16) as

$$H_{1/2^-} = \begin{pmatrix} K_0 & \sqrt{3}V_C^\pi & -\sqrt{6}V_T^\pi \\ \sqrt{3}V_C^\pi & K_0 - 2V_C^\pi & -\sqrt{2}V_T^\pi \\ -\sqrt{6}V_T^\pi & -\sqrt{2}V_T^\pi & K_2 + V_C^\pi - 2V_T^\pi \end{pmatrix}, \tag{5.15}$$

$$H_{3/2^-} = \begin{pmatrix} K_2 & \sqrt{3}V_T^\pi & -\sqrt{3}V_T^\pi & \sqrt{3}V_C^\pi \\ \sqrt{3}V_T^\pi & K_0 + V_C^\pi & 2V_T^\pi & V_T^\pi \\ -\sqrt{3}V_T^\pi & 2V_T^\pi & K_2 + V_C^\pi & -V_T^\pi \\ \sqrt{3}V_C^\pi & V_T^\pi & -V_T^\pi & K_2 - 2V_C^\pi \end{pmatrix}, \tag{5.16}$$

as summarized in Appendix B.2, where K_l is the kinetic term,

$$K_l = -\frac{1}{2\mu}\left(\frac{\partial^2}{\partial r^2} + \frac{2}{r}\frac{\partial}{\partial r} - \frac{l(l+1)}{r^2}\right), \tag{5.17}$$

with the reduced mass $\mu = m_N$, and V_C^π (V_T^π) is the central (tensor) force of the OPEP in Eq. (B.26). Here we suppress the vector meson exchange potentials for simplicity's sake. However, the discussions considering the OPEP only are essentially same as those considering the π, ρ and ω exchanges.

From unitary matrices in Eqs. (5.8) and (5.10), the Hamiltonians in Eqs. (5.15) and (5.16) in the particle basis can be written as the Hamiltonians $H^{\rm SC}_{1/2^-}$ and $H^{\rm SC}_{3/2^-}$ in the spin-complex basis:

$$\begin{aligned} H^{\rm SC}_{1/2^-} &= U^{-1}_{1/2^-} H_{1/2^-} U_{1/2^-} \\ &= \left(\begin{array}{c|cc} K_0 - 3V_C^\pi & 0 & 0 \\ \hline 0 & K_0 + V_C^\pi & -2\sqrt{2}V_T^\pi \\ 0 & -2\sqrt{2}V_T^\pi & K_2 + V_C^\pi - 2V_T^\pi \end{array}\right) \\ &\equiv \left(\begin{array}{c|c} H^{{\rm SC}(0^+)}_{1/2^-} & 0 \\ \hline 0 & H^{{\rm SC}(1^+)}_{1/2^-} \end{array}\right), \end{aligned} \tag{5.18}$$

and

$$\begin{aligned} H^{\rm SC}_{3/2^-} &= U^{-1}_{3/2^-} H_{3/2^-} U_{3/2^-} \\ &= \left(\begin{array}{cc|cc} K_0 + V_C^\pi & 2\sqrt{2}V_T^\pi & 0 & 0 \\ 2\sqrt{2}V_T^\pi & K_2 + V_C^\pi - 2V_T^\pi & 0 & 0 \\ \hline 0 & 0 & K_2 - 3V_C^\pi & 0 \\ 0 & 0 & 0 & K_2 + V_C^\pi + 2V_T^\pi \end{array}\right) \\ &\equiv \left(\begin{array}{c|c} H^{{\rm SC}(1^+)}_{3/2^-} & 0 \\ \hline 0 & H^{{\rm SC}(2^+)}_{3/2^-} \end{array}\right), \end{aligned} \tag{5.19}$$

where the $H^{{\rm SC}(j^{\mathcal{P}})}_{J^P}$ denotes the component for spin-complex with $J^{\mathcal{P}}$ of the Hamiltonian $H^{\rm SC}_{J^P}$. As seen in Eqs. (5.18) and (5.19), the Hamiltonians $H^{\rm SC}_{1/2^-}$ and $H^{\rm SC}_{3/2^-}$ are written as the block-diagonalizing forms, and we obtain the $H^{{\rm SC}(1^+)}_{1/2^-}$ is consistent with the $H^{{\rm SC}(1^+)}_{3/2^-}$ except for the sign of the off-diagonal terms. Therefore, the eigenenergy of the $H^{{\rm SC}(1^+)}_{1/2^-}$ is also equal to the one of the the $H^{{\rm SC}(1^+)}_{3/2^-}$, and they yield spin degenerate states, namely the HQS doublet, of $J^P = 1/2^-$ and $3/2^-$, containing the spin-complex with $j^{\mathcal{P}} = 1^+$. For the $H^{{\rm SC}(2^+)}_{3/2^-}$, we expect the existence of the partner with $j^{\mathcal{P}} = 2^+$ in the $J^P = 5/2^-$ state. In fact, the $H^{\rm SC}_{5/2^-}$ is decomposed to the $H^{{\rm SC}(2^+)}_{5/2^-}$ and $H^{{\rm SC}(3^+)}_{5/2^-}$, and the $H^{{\rm SC}(2^+)}_{5/2^-}$ coincides with the $H^{{\rm SC}(3^+)}_{5/2^-}$ as summarized in Appendix C.2. On the other hand, the $H^{{\rm SC}(0^+)}_{1/2^-}$ in Eq. (5.18) does not have the corresponding partner because this component contains the spin-complex with $J^{\mathcal{P}} = 0^+$. Thus, the $H^{{\rm SC}(0^+)}_{1/2^-}$ forms the HQS single.

For the $J^P = 1/2^+$ and $3/2^+$ states in the heavy quark limit, the Hamiltonian in the particle basis can be written as

$$H_{1/2^+} = \left(\begin{array}{ccc} K_1 & \sqrt{3}V_C^\pi & -\sqrt{6}V_T^\pi \\ \sqrt{3}V_C^\pi & K_1 - 2V_C^\pi & -\sqrt{2}V_T^\pi \\ -\sqrt{6}V_T^\pi & -\sqrt{2}V_T^\pi & K_1 + V_C^\pi - 2V_T^\pi \end{array}\right) \tag{5.20}$$

and

$$H_{3/2^+} = \begin{pmatrix} K_1 & \sqrt{3}V_C^\pi & \sqrt{\frac{3}{5}}V_T^\pi & -3\sqrt{\frac{3}{5}}V_T^\pi \\ \sqrt{3}V_C^\pi & K_1 - 2V_C^\pi & \frac{1}{\sqrt{5}}V_T^\pi & -\sqrt{3}V_T^\pi \\ \sqrt{\frac{3}{5}}V_T^\pi & \frac{1}{\sqrt{5}}V_T^\pi & K_1 + V_C^\pi + \frac{8}{5}V_T^\pi & \frac{6}{5}V_T^\pi \\ -3\sqrt{\frac{3}{5}}V_T^\pi & -\sqrt{3}V_T^\pi & \frac{6}{5}V_T^\pi & K_3 + V_C^\pi - \frac{8}{5}V_T^\pi \end{pmatrix}. \tag{5.21}$$

These Hamiltonians are rewritten by using unitary matrices in Eqs. (5.12) and (5.14):

$$\begin{aligned} H^{\rm SC}_{1/2^+} &= U^{-1}_{1/2^+} H_{1/2^+} U_{1/2^+} \\ &= \left(\begin{array}{c|cc} K_1 + V_C^\pi - 4V_T^\pi & 0 & 0 \\ \hline 0 & K_1 - 3V_C^\pi & 0 \\ 0 & 0 & K_1 + V_C^\pi + 2V_T^\pi \end{array}\right) \\ &\equiv \left(\begin{array}{c|c} H^{{\rm SC}(0^-)}_{1/2^+} & 0 \\ \hline 0 & H^{{\rm SC}(1^-)}_{1/2^+} \end{array}\right) \end{aligned} \tag{5.22}$$

and

$$\begin{aligned} H^{\rm SC}_{3/2^+} &= U^{-1}_{3/2^+} H_{3/2^+} U_{3/2^+} \\ &= \left(\begin{array}{cc|cc} K_1 - 3V_C^\pi & 0 & 0 & 0 \\ 0 & K_1 + V_C^\pi + 2V_T^\pi & 0 & 0 \\ \hline 0 & 0 & K_1 + V_C^\pi - \frac{2}{5}V_T^\pi & \frac{6\sqrt{6}}{5}V_T^\pi \\ 0 & 0 & \frac{6\sqrt{6}}{5}V_T^\pi & K_3 + V_C^\pi - \frac{8}{5}V_T^\pi \end{array}\right) \\ &\equiv \left(\begin{array}{c|c} H^{{\rm SC}(1^-)}_{3/2^+} & 0 \\ \hline 0 & H^{{\rm SC}(2^-)}_{3/2^+} \end{array}\right). \end{aligned} \tag{5.23}$$

As a consequence, we find that the $H^{({\rm SC})(1^-)}_{1/2^+}$ and $H^{({\rm SC})(1^-)}_{3/2^+}$ form the HQS doublet. The $H^{({\rm SC})(0^-)}_{1/2^+}$ belongs to the HQS singlet, and the $H^{({\rm SC})(2^-)}_{3/2^+}$ forms the HQS doublet with the $H^{({\rm SC})(2^-)}_{5/2^+}$.

From the analysis above, we expect that in the PN states, the HQS doublet of $J^P = (j-1/2)^P$ and $(j+1/2)^P$, having the common spin complex with $j^{\mathcal{P}}$ emerges as

$$H^{{\rm SC}(j^{\mathcal{P}})}_{(j-1/2)^P} \approx H^{{\rm SC}(j^{\mathcal{P}})}_{(j+1/2)^P}, \tag{5.24}$$

where $\approx$ stands for equality of the eigenenergies. The HQS singlet appears when the spin-complex takes $j = 0$. We emphasize that the formation of degenerate states or singlet state depends on whether the interaction generates a strong attraction enough to yield bound states and/or resonances.

5.3.3 Fractions of the wave functions

The wave functions of the J^P state have two components with $j = (J-1/2)^{-P}$ and $(J+1/2)^{-P}$ as discussed above. For the $J^P = 1/2^-$ state, there are two components $|0^+\rangle_{1/2^-}$ and $|1^+\rangle_{1/2^-}$ corresponding to the states with $j^{\mathcal{P}} = 0^+$ and 1^+, respectively. The HQS singlet state $|0^+\rangle_{1/2^-}$ is written as

$$\left|0^+\right\rangle_{1/2^-} = \left|[Nq]^{(0,S)}_{0^+}\bar{Q}\right\rangle_{1/2^-} . \tag{5.25}$$

The state with $j^{\mathcal{P}} = 1^+$ is obtained by superpositions of $[Nq]^{(1,S)}_{1^+}$ and $[Nq]^{(1,D)}_{1^+}$, namely

$$\left|1^+\right\rangle_{1/2^-} = \sin\theta \left|[Nq]^{(1,S)}_{1^+}\bar{Q}\right\rangle_{1/2^-} + \cos\theta \left|[Nq]^{(1,D)}_{1^+}\bar{Q}\right\rangle_{1/2^-} . \tag{5.26}$$

These states are mixed by the mixing angle θ. The angle θ is not determined by the heavy quark symmetry, while depends on the dynamics.

For $J^P = 3/2^-$, the states with $j^{\mathcal{P}} = 1^+$ and 2^+ are obtained by

$$\left|1^+\right\rangle_{3/2^-} = \sin\theta \left|[Nq]^{(1,S)}_{1^+}\bar{Q}\right\rangle_{3/2^-} + \cos\theta \left|[Nq]^{(1,D)}_{1^+}\bar{Q}\right\rangle_{3/2^-} , \tag{5.27}$$

$$\left|2^+\right\rangle_{3/2^-} = \sin\theta \left|[Nq]^{(0,D)}_{2^+}\bar{Q}\right\rangle_{3/2^-} + \cos\theta \left|[Nq]^{(0,D)}_{2^+}\bar{Q}\right\rangle_{3/2^-} . \tag{5.28}$$

The states $|0^+\rangle_{1/2^-}$, $|1^+\rangle_{1/2^-}$ and $|1^+\rangle_{3/2^-}$ can be expressed by the wave functions in the particle basis. From Eq. (5.7), the wave functions in the spin-complex basis, $\left|[Nq]^{(0,S)}_{0^+}\bar{Q}\right\rangle_{1/2^-}$, $\left|[Nq]^{(1,S)}_{1^+}\bar{Q}\right\rangle_{1/2^-}$, $\left|[Nq]^{(1,D)}_{1^+}\bar{Q}\right\rangle_{1/2^-}$, for the $J^P = 1/2^-$ state are written as

$$\left|[Nq]^{(0,S)}_{0^+}\bar{Q}\right\rangle_{1/2^-} = -\frac{1}{2}\left|P_Q N(^2S_{1/2})\right\rangle + \frac{\sqrt{3}}{2}\left|P^*_Q N(^2S_{1/2})\right\rangle , \tag{5.29}$$

$$\left|[Nq]^{(1,S)}_{1^+}\bar{Q}\right\rangle_{1/2^-} = \frac{\sqrt{3}}{2}\left|P_Q N(^2S_{1/2})\right\rangle + \frac{1}{2}\left|P^*_Q N(^2S_{1/2})\right\rangle , \tag{5.30}$$

$$\left|[Nq]^{(1,D)}_{1^+}\bar{Q}\right\rangle_{1/2^-} = -\left|P_Q N(^4D_{1/2})\right\rangle . \tag{5.31}$$

In a similar way, the states with $j^{\mathcal{P}} = 1^+$ for the $J^P = 3/2^-$ can be expressed by

$$\left|[Nq]^{(1,S)}_{1^+}\bar{Q}\right\rangle_{3/2^-} = \left|P^*_Q N(^4S_{3/2})\right\rangle , \tag{5.32}$$

$$\left|[Nq]^{(1,D)}_{1^+}\bar{Q}\right\rangle_{3/2^-} = \frac{\sqrt{6}}{4}\left|P_Q N(^2D_{3/2})\right\rangle + \frac{1}{\sqrt{2}}\left|P^*_Q N(^4D_{3/2})\right\rangle + \frac{\sqrt{2}}{4}\left|P^*_Q N(^2D_{3/2})\right\rangle , \tag{5.33}$$

from Eq. (5.9). Therefore, the states $|0^+\rangle_{1/2^-}$, $|1^+\rangle_{1/2^-}$ and $|1^+\rangle_{3/2^-}$ are described by

$$\left|0^+\right\rangle_{1/2^-} = -\frac{1}{2}\left|P_Q N(^2S_{1/2})\right\rangle + \frac{\sqrt{3}}{2}\left|P_Q^* N(^2S_{1/2})\right\rangle \tag{5.34}$$

for the HQS singlet, and

$$\left|1^+\right\rangle_{1/2^-} = \sin\theta\left(\frac{\sqrt{3}}{2}\left|P_Q N(^2S_{1/2})\right\rangle + \frac{1}{2}\left|P_Q^* N(^2S_{1/2})\right\rangle\right) - \cos\theta\left|P_Q^* N(^4D_{1/2})\right\rangle\,, \tag{5.35}$$

$$\begin{aligned}\left|1^+\right\rangle_{3/2^-} =& \sin\theta\left|P_Q^* N(^4S_{3/2})\right\rangle \\ &+ \cos\theta\left(\frac{\sqrt{6}}{4}\left|P_Q N(^2D_{3/2})\right\rangle + \frac{1}{\sqrt{2}}\left|P_Q^* N(^4D_{3/2})\right\rangle + \frac{\sqrt{2}}{4}\left|P_Q^* N(^2D_{3/2})\right\rangle\right),\end{aligned} \tag{5.36}$$

for the HQS doublet.

The results in Eqs. (5.34)-(5.36) are related to the fractions of wave functions in the particle basis. For the HQS singlet state, the fractions are given by Eq. (5.34) as

$$f(P_Q N(^2S_{1/2})) : f(P_Q^* N(^2S_{1/2})) = 1 : 3\,. \tag{5.37}$$

If we obtain the bound state with $J^P = 1/2^-$ corresponding to the HQS singlet by solving the eigenvalue problem, the mixing ratio of the eigenfunctions in the particle basis is expected to be the fractions. For the HQS doublet with $j^{\mathcal{P}} = 1^+$, the fractions of the wave functions are obtained from Eqs. (5.35) and (5.36):

$$f(P_Q N(^2S_{1/2})) : f(P_Q^* N(^2S_{1/2})) = 3 : 1\,, \tag{5.38}$$

for $J^P = 1/2^-$, and

$$f(P_Q N(^2D_{3/2})) : f(P_Q^* N(^4D_{3/2})) : f(P_Q^* N(^2D_{3/2})) = 3 : 4 : 1\,, \tag{5.39}$$

for $J^P = 3/2^-$. Interestingly, these fractions are obtained by the heavy quark symmetry directly, and independent of the dynamics. However, the mixing angle θ is dependent on the dynamics, and hence, for $J^P = 1/2^-$, the ratio of $PN(^2S_{1/2})$ ($P^*N(^2S_{1/2})$) to $P^*N(^4D_{1/2})$ is not determined by the symmetry.

We also obtain the fractions in the positive parity states. The states $|0^-\rangle_{1/2^+}$ and

$|1^-\rangle_{1/2^+,3/2^+}$ are expressed by

$$\left|0^-\right\rangle_{1/2^+} = \frac{1}{2}\left|P_Q N(^2P_{1/2})\right\rangle + \frac{1}{2\sqrt{3}}\left|P_Q^* N(^2P_{1/2})\right\rangle + \sqrt{\frac{2}{3}}\left|P_Q^* N(^4P_{1/2})\right\rangle , \tag{5.40}$$

$$\begin{aligned}\left|1^-\right\rangle_{1/2^+} = &\sin\theta\left(\frac{1}{2}\left|P_Q N(^2P_{1/2})\right\rangle - \frac{\sqrt{3}}{2}\left|P_Q^* N(^2P_{1/2})\right\rangle\right)\\ &+\cos\theta\left(\frac{1}{\sqrt{2}}\left|P_Q N(^2P_{1/2})\right\rangle + \frac{1}{\sqrt{6}}\left|P_Q^* N(^2P_{1/2})\right\rangle - \frac{1}{\sqrt{3}}\left|P_Q^* N(^4P_{1/2})\right\rangle\right) ,\end{aligned} \tag{5.41}$$

$$\begin{aligned}\left|1^-\right\rangle_{3/2^+} = &\sin\theta\left(-\frac{1}{2}\left|P_Q N(^2P_{3/2})\right\rangle + \frac{\sqrt{3}}{2}\left|P_Q^* N(^2P_{3/2})\right\rangle\right)\\ &+\cos\theta\left(\frac{1}{2\sqrt{2}}\left|P_Q N(^2P_{3/2})\right\rangle + \frac{1}{2\sqrt{6}}\left|P_Q^* N(^2P_{3/2})\right\rangle - \sqrt{\frac{5}{6}}\left|P_Q^* N(^4P_{3/2})\right\rangle\right) .\end{aligned} \tag{5.42}$$

For the $|0^-\rangle_{1/2^+}$ state, we obtain

$$f(P_Q N(^2P_{1/2})) : f(P_Q^* N(^2P_{1/2})) : f(P_Q^* N(^4P_{1/2})) = 3 : 1 : 8\,. \tag{5.43}$$

For the $|1^-\rangle_{1/2^+,3/2^+}$ states, the upper and lower components of the Hamiltonian $H^{\mathrm{SC}(1^+)}_{1/2^+,3/2^+}$ in Eqs. (5.22) and (5.23) are not coupled. Hence, for $|1^-\rangle_{1/2^+}$ states, the we obtain two states with fractions

$$f(P_Q N(^2P_{1/2})) : f(P_Q^* N(^2P_{1/2})) = 1 : 3 \tag{5.44}$$

and

$$f(P_Q N(^2P_{1/2})) : f(P_Q^* N(^2P_{1/2})) : f(P_Q^* N(^4P_{1/2})) = 3 : 1 : 2 \tag{5.45}$$

for first and second terms in Eq (5.41), respectively. For $|1^-\rangle_{3/2^+}$ states, we find

$$f(P_Q N(^2P_{3/2})) : f(P_Q^* N(^2P_{3/2})) = 1 : 3 \tag{5.46}$$

and

$$f(P_Q N(^2P_{3/2})) : f(P_Q^* N(^2P_{3/2})) : f(P_Q^* N(^4P_{3/2})) = 3 : 1 : 20 \tag{5.47}$$

for first and second terms in Eq (5.42), respectively.

5.4 Numerical results in the heavy quark limit

5.4.1 Numerical results of P_QN states

Let us show the numerical results of the P_QN states in the heavy quark limit. By solving coupled-channel Schrödinger equations, we study the existence of the spin degeneracy in the $P_Q^{(*)}N$ molecular states. We investigate the states with $J^P = 1/2^\pm$ and $3/2^\pm$ for $I = 0$. As for the interaction between the $P^{(*)}$ meson and the nucleon N, we employ two potentials, the π potential and $\pi\rho\omega$ potential. These results are compared. The meson exchange potentials are given in Eqs. (3.15) and (3.16) for the π exchange, and Eqs. (3.21)-(3.23) for the vector meson exchanges, where we use the cutoff $\Lambda_P = 1.12\Lambda_N$ for the $P_Q^{(*)}$ meson with $\Lambda_N = 837$ MeV (846 MeV) for the π ($\pi\rho\omega$) potential [93].

First, the results of the negative parity states are shown. We obtain the degenerate bound states of $J^P = 1/2^-$ and $3/2^-$ with same binging energy -34.1 MeV for the π potential and -37.4 MeV for the $\pi\rho\omega$ potential, displayed in Table 5.2. The results of the π potential is almost same as those of the $\pi\rho\omega$ potential as seen in the $P^{(*)}N$ states in the chapter 3. The degenerate states are considered as the HQS doublet containing the spin-complex with $j^{\mathcal{P}} = 1^+$. We also find that the equivalent relative distances of the P_QN bound states with $J^P = 1/2^-$ and $3/2^-$, 1.2 fm for the π potential and 1.1 fm for $\pi\rho\omega$ potential.

For the positive parity states with $J^P = 1/2^+$ and $3/2^+$, we also fine the degenerate states with binding energy -11.8 MeV for the π potential and -12.8 MeV for the $\pi\rho\omega$ potential, shown in Table 5.2. The degenerate bound states are considered to belong to the HQS doublet containing the spin-complex with $j^{\mathcal{P}} = 1^-$. The corresponding relative radius is found, 1.6 fm for the π and $\pi\rho\omega$ potentials.

We estimate mixing ratios of the obtained bound states with $J^P = 1/2^\pm$ and $3/2^\pm$, summarized in Table 5.3. In the results, we show the ratios for the π potential and $\pi\rho\omega$ potential. For the $J^P = 1/2^-$ state, we obtain the ratios, 63.6 % (64.0 %) for $P_QN(^2S_{1/2})$, 21.2 % (21.3 %) for $P_Q^*N(^2S_{1/2})$ and 15.2 % (14.7 %) for $P_Q^*N(^4D_{1/2})$ when the π ($\pi\rho\omega$) potential is used. For the results of $P_QN(^2S_{1/2})$ and $P_Q^*N(^2S_{1/2})$, we find that the fractions satisfy the ratio in Eq. (5.38), i.e. $f(P_QN(^2S_{1/2})) : f(P_Q^*N(^2S_{1/2})) = 3 : 1$. This indicates that the degenerate bound states do not

Table.5.2 Binding energy E_B and relative distance $\langle r^2\rangle^{1/2}$ for degenerate bound states with $J^P = 1/2^-, 3/2^-$ ($P = -$) and $J^P = 1/2^+, 3/2^+$ ($P = +$) in the P_QN systems. Results for the π and $\pi\rho\omega$ potentials are compared.

	$P = -$ (π)	$P = -$ ($\pi\rho\omega$)	$P = +$ (π)	$P = +$ ($\pi\rho\omega$)
E_B [MeV]	-34.1	-37.4	-11.8	-12.8
$\langle r^2\rangle^{1/2}$ [fm]	1.2	1.1	1.6	1.6

happen by accident but form as the HQS doublet with $j^{\mathcal{P}} = 1^+$. The difference between results of the π and $\pi\rho\,\omega$ potentials are due to the mixing angle θ which is dependent on the dynamics.

For the $J^P = 3/2^-$ state, we find that the fractions of $P_Q N(^2D_{3/2})$, $P_Q^* N(^2D_{3/2})$ and $P_Q^* N(^2D_{3/2})$ channels consist with the fractions in Eq. (5.39), namely $f(P_Q N(^2D_{3/2})) : f(P_Q^* N(^4D_{3/2}^*)) : f(P_Q^* N(^4D_{3/2})) = 3 : 4 : 1$ Therefore, we emphasize again that the bound states of the $J^P = 1/2^-$ and $3/2^-$ belong to the HQS doublet with $j^{\mathcal{P}} = 1^+$.

We calculate the mixing ratios of the positive parity states, shown in Table 5.3. For $J^P = 1/2^+$, the fractions are obtained as $f(P_Q N(^2P_{1/2})) : f(P_Q^* N(^2P_{1/2})) : f(P_Q^* N(^4P_{1/2})) = 3 : 1 : 2$ which corresponds to Eq. (5.45). We also obtain the fractions for $J^P = 3/2^+$ as $f(P_Q N(^2P_{3/2})) : f(P_Q^* N(^2P_{3/2})) : f(P_Q^* N(^4P_{3/2})) = 3 : 1 : 20$ corresponding to Eq. (5.47). The results indicate that the degenerate states for $J^P = 1/2^+$ and $3/2^+$ belong to the HQS doublet with $j^{\mathcal{P}} = 1^-$.

We note that there is no bound state corresponding to the HQS singlet from the $H_{1/2^-}^{\mathrm{SC}(0^+)}$ and $H_{1/2^+}^{\mathrm{SC}(0^-)}$ components. For these states, the attraction is not enough to form the bound and resonant states. In addition, we find no state for the isotriplet channel.

Table.5.3 Mixing ratio of each channel in the bound states with $J^P = 1/2^\pm$ and $3/2^\pm$ for $I = 0$. The results of the π and $\pi\rho\,\omega$ potentials are compared.

$1/2^-$	$PN(^2S_{1/2})$	$P^*N(^2S_{1/2})$	$P^*N(^4D_{1/2})$	—
π	63.6 %	21.2 %	15.2 %	—
$\pi\rho\,\omega$	64.0 %	21.3 %	14.7 %	—
$3/2^-$	$PN(^2D_{1/2})$	$P^*N(^4S_{1/2})$	$P^*N(^4D_{1/2})$	$P^*N(^2D_{1/2})$
π	5.7 %	84.4 %	7.6 %	1.9 %
$\pi\rho\,\omega$	5.5 %	85.3 %	7.4 %	1.8 %
$1/2^+$	$PN(^2P_{1/2})$	$P^*N(^2P_{1/2})$	$P^*N(^4P_{1/2})$	—
π	50.0 %	16.7 %	33.3 %	—
$\pi\rho\,\omega$	50.0 %	16.7 %	33.3 %	—
$3/2^+$	$PN(^2P_{3/2})$	$P^*N(^2P_{3/2})$	$P^*N(^4P_{3/2})$	$P^*N(^4F_{3/2})$
π	12.5 %	4.2 %	83.3 %	0.0 %
$\pi\rho\,\omega$	12.5 %	4.2 %	83.3 %	0.0 %

Finally, let us compare the results in the heavy quark limit with those in the charm and bottom sectors. Whereas the energy differences between the degenerate bound states with $J^P = 1/2^\pm$ and $3/2^\pm$ are exactly zero, the differences between the states with $J^P = 1/2^\pm$ and $3/2^\pm$ in the charm and bottom sectors are finite due to the breaking of the heavy quark symmetry. For negative parity states, the energy splitting of the bound states with $J^P = 1/2^-$ and the resonances with $J^P = 3/2^-$ is 115.3 MeV for $\bar{D}N$, and 29.9 MeV for BN as seen in Fig. 3.8 Therefore, we see that the energy difference decreases as the heavy quark mass increases. The degrees

of the energy splitting are comparable with the mass splittings of the $P = \bar{D}, B$ and $P^* = \bar{D}^*, B^*$ mesons. For the positive parity states, we also find the same behavior as the negative parity states. The difference between the resonances with $J^P = 1/2^+$ and $3/2^+$ is 121.4 MeV for $\bar{D}N$, and 26.0 MeV for BN.

The breaking of the heavy quark symmetry is also characterized by the mixing ratio of the component with $j = 0$. In the heavy quark limit, the degenerate bound states with the spin-complex with $j = 1$ do not contain the components with $j = 0$ because the angular momentum j of the spin-complex is conserved. For the $\bar{D}N$ and BN states, however, the heavy quark symmetry is broken and therefore the spin-complex components with $j = 0$ would be mixed. By using the wave functions in the spin-complex basis for $J^P = 1/2^-$ in Eq. (5.7), the mixing ratios of the bound states with $J^P = 1/2^-$ for $\bar{D}N$ and BN in Table 3.5 can be transformed into the ratios of the wave functions in the spin-complex basis. As a results, for the $\bar{D}N$ bound state when the $\pi\rho\omega$ potential is used, we obtain the ratios, 83.3 % for $j = 1$ and 16.7 % for $j = 0$, which are summarized in Table 5.4. For the BN states for the $\pi\rho\omega$ potential, we obtain the ratios, 97.3 % for $j = 1$ and 2.7 % for $j = 0$. Comparing the results of $\bar{D}N$ and BN, the ratio of the components with $j = 1$ for BN is almost 100 %, while the mixing ratio of the components with $j = 0$ for the $\bar{D}N$ is not small. Therefore, we expect that the effects of the breaking of heavy quark symmetry is non-negligible for the charmed hadrons.

Table.5.4 Mixing ratios of the states for $(I, J^P) = (0, 1/2^-)$ in the spin-complex basis. The ratios of the spin-complex components with $j = 1$ and $j = 0$ are compared.

	$\bar{D}N$	BN	P_QN
$j = 1$	83.3 %	97.3 %	100 %
$j = 0$	16.7 %	2.7 %	0 %

5.4.2 Numerical results of P_QNN states

Let us present the numerical results of the three-body P_QNN states. The states with $J^P = 0^-$ and 1^- with $I = 1/2$ in the heavy quark limit are investigated. As for the interaction, the OPEP between a heavy meson and a nucleon, and AV8′ potential between two nucleons are employed.

By solving the Schrödinger equations, where P_Q and P_Q^* are exactly degenerate in mass, we find the bound states both for $J^P = 0^-$ and 1^- with the same binding energy -38.5 MeV measured from P_QNN threshold. Those numerical results indicate that degenerate states are realized in the P_QNN systems. This HQS doublet state having $J^P = 0^-$ and 1^- contain the spin-complex component with $j^{\mathcal{P}} = 1/2^+$ and $I = 1/2$. As seen in the analysis of the two-body systems, the energy splitting between the states with $J^P = 0^-$ and 1^- decrease as the mass of the heavy quark increase, namely 116.4 MeV for $\bar{D}NN$, 33.0 MeV for BNN and 0.0 MeV for P_QNN in the heavy quark limit. The energy splittings are expected to be characterized by

the breaking of the heavy quark symmetry, namely the mass of the heavy quark, as discussed in the two-body P_QN states.

In the three-body P_QNN states, we find no singlet state. We saw that the HQS singlet was absent in the two-body P_QN states because of the small attraction in these channels. For the P_QNN states, however, the situation is different. The HQS singlet is corresponding to the eigenstate with the spin-complex with $j = 0$. Whereas the Hamiltonian of the P_QN states with $J^P = 1/2^\pm$ contains these components as seen in Eqs (5.18) and (5.22), the P_QNN states do not have the corresponding one because the spin-complex $[qNN]_{j^\mathcal{P}}$ cannot take $j = 0$. In general, P_Q nuclei with even baryon numbers, e.g. P_QNN, P_QNNNN, $P_QNNNNNN$, $\cdots$, do not contain the spin-complex with $j = 0$, and therefore no HQS singlet state is found.

5.5 Summary and Discussion

We have considered the P_QN and P_QNN systems in the heavy quark limit. The heavy quark symmetry manifests the spin degeneracy with total angular momentum and parity $(j-1/2)^P$ and $(j+1/2)^P$ in heavy hadron states containing a single heavy quark. This is the universal phenomenon which appears not only in normal hadrons, but also in multi-hadron states in the heavy quark limit.

Thanks to the suppression of the spin-dependent force in the heavy quark limit, the spin configurations of these systems are separated into a heavy anitquark spin and remaining light degrees of freedom. The light degrees of freedom, namely the spin-complex, are composed of a light quark q in the heavy meson and nucleons N in the systems. Then, the wave functions of the P_QN states in the particle basis can be transformed into those in the spin-complex basis. We saw that by using the wave functions in the spin-complex basis, the Hamiltonians are rewritten as block-diagonalizing forms with two components for $j = J - 1/2$ and $j = J + 1/2$.

By solving the coupled channel Schrödinger equations numerically, we have found the degenerate bound states both in the P_QN and P_QNN states. In the two-body P_QN states, the doublet states with $J^P = 1/2^-$ and $3/2^-$, and $J^P = 1/2^+$ and $3/2^+$ for $I = 0$ have been obtained. The lowest bound states found for $J^P = 1/2^-$ and $3/2^-$, containing the spin complex with $j^\mathcal{P} = 1^+$ and $I = 0$. The degenerate states with $J^P = 1/2^+$ and $3/2^+$ contained the spin-complex with $j^\mathcal{P} = 1^-$ and $I = 0$. For these bound states, the obtained mixing ratios also indicated they belonged the HQS doublet. On the other hand, we found no HQS singlet because of the small attraction in the corresponding channels.

By comparing the states for $\bar{D}N$, BN and P_QN in the heavy quark limit, we discussed the breaking of the heavy quark symmetry in the charm and bottom sectors. We saw that the energy splittings of the degenerate states increase as the heavy quark mass decreases. For the charm sector, the effects of the breaking of the heavy quark symmetry were expected to be non negligible.

For the P_QNN states, the degenerate bound states have been present in the $J^P = 0^-$ and 1^- states with $I = 1/2$. The doublet contained the spin-complex with $j^\mathcal{P} = 1/2^+$ and $I = 1/2$. We have not obtained a HQS singlet state. For the few-baryon systems with a $\bar{D}$ or B meson, the states with even baryon numbers cannot contain

the spin-complex with $j = 0$ due to the limited combinations of angular momenta. For instance, in the $P_Q NN$ states, the total angular momentum of the spin-complex $[qNN]$ should be half-integer and therefore not be zero.

Chapter 6

Summary

In this thesis, the possible existence of the two-body PN and three-body PNN states for charm and bottom sectors, and in the heavy quark limit has been explored.

In chapter 3, the $\bar{D}N$ and BN molecules for exotic channels, and the DN and $\bar{B}N$ molecules for non-exotic channels have been investigated. As interactions between a heavy meson and a nucleon, the one pion and vector exchange potentials are introduced by the chiral and heavy quark symmetries. In the PN systems, the tensor force of the OPEP mixing the PN and P^*N channels was expected to play an important role to generate a strong attraction as discussed in the deuteron. Therefore, the coupled-channel Schrödinger equations for PN and P^*N with different angular momentum states L and $L \pm 2$ have been solved numerically.

The $\bar{D}N$ and BN states were genuinely exotic states whose minimal quark content was $\bar{Q}qqqq$, called a pentaquark state. Therefore, their bound states were stable against a strong decay. We have obtained the loosely bound states and resonances near the $\bar{D}N$ and $\bar{D}^*N$ (BN and B^*N) thresholds for the isosinglet states. For the $(I, J^P) = (0, 1/2^-)$ channel, the small binding energy and large relative distance of the $\bar{D}N$ state indicate that this forms the loosely bound states. We found that the tensor force of the OPEP was important to yield the bound states. In particular, the $PN - P^*N$ mixing components produced the strongest attraction in the systems. The tensor force was also essential to produce the resonances above the PN threshold. Comparing the results of the π and $\pi\rho\omega$ potentials, we found the OPEP dominance in the PN molecules. Because the ρ exchange is attractive but the ω exchange is repulsive, they are canceled out. In addition, the OPEP as a long-range force becomes dominant in such loosely bound states which are expanded spatially. We obtained that these features also held for the BN states. Comparing the charm and bottom sectors, the BN states were more deeply bound that the $\bar{D}N$ states. This was caused not only by the large reduced mass, but also by the small mass splitting between B and B^* mesons. The tensor force mixing the PN and P^*N channels became important when P and P^* mesons degenerated. Finally, we found no state in the isotriplet channel. The attraction was not enough to form a bound or resonant state due to the small isospin factor $\vec{\tau}_P \cdot \vec{\tau}_N$.

The DN and $\bar{B}N$ states had an ordinary flavor structure. We have investigated the $\bar{P}N$ and $\bar{P}^*N$ channels, but the couplings to three-quark states and other meson-baryon states such as $\pi\Lambda_c$, $\pi\Sigma_c$, and $\pi\Sigma_c^*$ ($\pi\Lambda_b$, $\pi\Sigma_b$, and $\pi\Sigma_b^*$) have not considered

in the calculations. We expected the suppression of the transitions to there states near the $\bar{P}^{(*)}N$ thresholds because the heavy quark exchanges were needed. As a consequence, we have obtained many bound and resonant states. The ω exchange potential became an attractive force due to the G-parity transformation in the non-exotic states, and therefore the attractions from the vector meson exchanges were stronger than those in the exotic states. We have obtained the different behaviors in the states with small and large orbital angular momenta. For the $J^P = 1/2^{\pm}$ and $3/2^-$ for $I = 0$, they formed deeply bound states. In particular, the binding energies of $J^P = 1/2^{\pm}$ states are over 80 MeV for DN, and over 100 MeV for $\bar{B}N$. The large difference between the results of the π and $\pi\rho\,\omega$ potential indicated that the vector meson exchange potentials produced the strong attraction. For these bound states, the relative distances between the $\bar{P}$ meson and the nucleon were small less than 1 fm and hence it was difficult to identify them as hadronic molecules. On the other hand, the states with $J^P = 3/2^+$, $5/2^{\pm}$ and $7/2^-$ emerged near the thresholds. For these states, the difference between the results of the π and $\pi\rho\,\omega$ potentials were small compared to deeply bound states. The OPEP played a dominant role in the states with large orbital angular momenta.

In chapter 4, we have discussed the possible existence of the exotic dibaryons with heavy antiquark, being realized three-body systems, $\bar{D}NN$ and BNN. The PNN states were unique as few-body systems. The counterparts of KNN in the strangeness sector have not found due to the repulsive force between the K meson and the nucleon. In the states, we have considered the OPEP between the heavy meson and the nucleon. As for the NN interaction, the Argonne v_8' has been employed. For $I = 1/2$, we have found the bound states with $J^P = 0^-$ and the Feshbach resonances with $J^P = 1^-$ both in the $\bar{D}NN$ and BNN. The obtained energies of these states were larger than those of the two-body $\bar{D}N$ and BN states. The energy expectation values of the bound states showed that the tensor force of the $PN - P^*N$ mixing components provided the strong attraction. This force dominated in the PNN systems as seen in the two-body PN states. For the nucleon-nucleon interaction, the tensor force which was important in the deuteron played a minor role, while the central force was major. Therefore, the NN subsystem with $J^P = 0^+$ dominated in the bound states. The resonances with $J^P = 1^-$ formed the Feshbach resonances in which the P^*NN channels predominated. We found that the many features of the two-body systems survived in the three-body systems, because the OPEP between the P meson and the nucleon played a dominant force to determine the properties of the bound and resonant states.

In chapter 5, the exotic P_QN and P_QNN states in the heavy quark limit have been discussed. The heavy quark symmetry manifests the spin degeneracy of the states with $(j-1/2)^P$ and $(j+1/2)^P$ with a single heavy (anti-)quark, because of the suppression of the spin-dependent forces. This is a universal phenomena which emerge not only in the normal heavy hadrons, but also in the multi-hadron systems such as hadronic molecules and exotic nuclei. In order to see the spin degenerate states in the P_QN and P_QNN states, we have introduced the spin-complex which was the brown muck containing not only light quarks and gluons in the heavy meson, but also the light hadrons, namely the nucleons. The wave functions of the P_QN states expressed by the particle basis were able to be transformed into those in the spin-complex basis.

The spin-complex was useful object because the states and Hamiltonian were classified by the total angular momentum of the spin-complex, which was the conserved value in the heavy quark limit. For the $P_Q N$ states, we have found the degenerate bound states with $J^P = 1/2^-$ and $3/2^-$, and $J^P = 1/2^+$ and $3/2^+$ in the heavy quark limit, while we have found no singlet state. These results indicated that the bound and resonant states obtained in the charm and bottom sectors had common origins which were degenerate in the heavy quark limit.

By comparing the states for $\bar{D}N$, BN and $P_Q N$ in the heavy quark limit, the breaking of the heavy quark symmetry in the charm and bottom sectors was discussed. Whereas, in the heavy quark limit, the spin complex only with $j = 1$ was contained in the degenerate bound states, the components with $j = 0$ existed in the $\bar{D}N$ and BN. In particular, the mixing ratios of the spin-complex with $j = 0$ was not small in the $\bar{D}N$ bound states and hence the effects of the breaking of the heavy quark symmetry were expected to be non negligible in the charm sector.

The degenerate bound states have been also found in the $P_Q NN$ state. The nature of the three-body systems were similar to behavior of the two-body systems.

Finally, the hadronic molecular states discussed in the thesis, the two-body systems as $\bar{D}N$ (BN) and DN ($\bar{B}N$), and the three-body systems as $\bar{D}NN$ (BNN) can be searched in experiments in hadron colliders. The understanding of production reactions is important issue in the feature. The productions of the exotic hadrons will be studied in relativistic heavy ion collisions in RHIC and LHC [177, 178]. Furthermore, the search for the charmed states would be also carried out in J-PARC and GSI-FAIR.

Appendix A

Notations and Conventions

A.1 Relativistic notation

Space-time four-vector is denoted by x^μ ($\mu = 0, 1, 2, 3$) with time component $x^0 = t$ and space component x^i ($i = 1, 2, 3$). The covvariant vector $x_\mu = (x^0, -x^i)$ is defined from the contravariant vector x^μ as $x_\mu = g_{\mu\nu}x^\mu$, where the metric tensor $g_{\mu\nu}$ is defined by

$$g_{\mu\nu} = g^{\mu\nu} = \begin{pmatrix} 1 & 0 & 0 & 0 \\ 0 & -1 & 0 & 0 \\ 0 & 0 & -1 & 0 \\ 0 & 0 & 0 & -1 \end{pmatrix} . \tag{A.1}$$

The derivative operators are written by

$$\partial_\mu = \frac{\partial}{\partial x^\mu} = \left(\frac{\partial}{\partial t}, \nabla\right), \quad \partial^\mu = \frac{\partial}{\partial x_\mu} = \left(\frac{\partial}{\partial t}, -\nabla\right) . \tag{A.2}$$

A.2 Vector derivatives

A.2.1 Cartesian coordinates

$$d\tau = dxdydz \tag{A.3}$$

$$\nabla A = \frac{\partial A}{\partial x}\hat{x} + \frac{\partial A}{\partial y}\hat{y} + \frac{\partial A}{\partial z}\hat{z} \tag{A.4}$$

$$\nabla \cdot \vec{A} = \frac{\partial A_x}{\partial x} + \frac{\partial A_y}{\partial y} + \frac{\partial A_z}{\partial z} \tag{A.5}$$

$$\nabla \times \vec{A} = \left(\frac{\partial A_z}{\partial y} - \frac{\partial A_y}{\partial z}\right)\hat{x} + \left(\frac{\partial A_x}{\partial z} - \frac{\partial A_z}{\partial x}\right)\hat{y} + \left(\frac{\partial A_y}{\partial x} - \frac{\partial A_x}{\partial y}\right)\hat{z} \tag{A.6}$$

$$\nabla^2 A = \frac{\partial^2 A}{\partial x^2} + \frac{\partial^2 A}{\partial y^2} + \frac{\partial^2 A}{\partial z^2} \tag{A.7}$$

A.2.2 Spherical polar coordinates

$$d\tau = r^2 \sin\theta dr d\theta d\phi \tag{A.8}$$

$$\nabla A = \frac{\partial A}{\partial r}\hat{r} + \frac{1}{r}\frac{\partial A}{\partial \theta}\hat{\theta} + \frac{1}{r\sin\theta}\frac{\partial A}{\partial \phi}\hat{\phi} \tag{A.9}$$

$$\nabla \cdot \vec{A} = \frac{1}{r^2}\frac{\partial}{\partial r}(r^2 A_r) + \frac{1}{r\sin\theta}\frac{\partial}{\partial \theta}(\sin\theta A_\theta) + \frac{1}{r\sin\theta}\frac{\partial A_\phi}{\partial \phi} \tag{A.10}$$

$$\begin{aligned}\nabla \times \vec{A} =& \frac{1}{r\sin\theta}\left[\frac{\partial}{\partial \theta}(\sin\theta A_\phi) - \frac{\partial A_\theta}{\partial \phi}\right]\hat{r} + \frac{1}{r}\left[\frac{1}{\sin\theta}\frac{\partial A_r}{\partial \phi} - \frac{\partial}{\partial r}(rA_\phi)\right]\hat{\theta} \\ &+ \frac{1}{r}\left[\frac{\partial}{\partial r}(rA_\theta) - \frac{\partial A_r}{\partial \theta}\right]\hat{\phi}\end{aligned} \tag{A.11}$$

$$\nabla^2 A = \frac{1}{r^2}\frac{\partial}{\partial r}\left(r^2\frac{\partial A}{\partial r}\right) + \frac{1}{r^2\sin\theta}\frac{\partial}{\partial \theta}\left(\sin\theta\frac{\partial A}{\partial \theta}\right) + \frac{1}{r^2\sin\theta}\frac{\partial^2 A}{\partial \phi^2} \tag{A.12}$$

A.3 Pauli matrices

Pauli matrices, $\vec{\sigma}$, are defined by

$$\sigma_1 = \begin{pmatrix} 0 & 1 \\ 1 & 0 \end{pmatrix},\ \sigma_2 = \begin{pmatrix} 0 & -i \\ i & 0 \end{pmatrix},\ \sigma_3 = \begin{pmatrix} 1 & 0 \\ 0 & -1 \end{pmatrix}. \tag{A.13}$$

$\vec{\sigma}$ provide the rising and lowering operators as

$$\sigma_+ = \frac{1}{2}(\sigma_1 + i\sigma_2) = \begin{pmatrix} 0 & 1 \\ 0 & 0 \end{pmatrix}, \quad \sigma_- = \frac{1}{2}(\sigma_1 - i\sigma_2) = \begin{pmatrix} 0 & 0 \\ 1 & 0 \end{pmatrix}, \tag{A.14}$$

respectively. The Pauli matrices satisfy the formulas,

$$\sigma^i \sigma^j = \delta^{ij} + i\epsilon^{ijk}\sigma^k\,, \tag{A.15}$$

$$(\vec{\sigma}\cdot\vec{a}\,)(\vec{\sigma}\cdot\vec{b}\,) = \vec{a}\cdot\vec{b} + i\vec{\sigma}\cdot(\vec{a}\times\vec{b}\,)\,. \tag{A.16}$$

A.4 Dirac matrices

In the Dirac-Pauli representation, γ matrices are given by

$$\gamma^0 = \begin{pmatrix} 1 & 0 \\ 0 & -1 \end{pmatrix},\ \gamma^i = \begin{pmatrix} 0 & \sigma^i \\ -\sigma^i & 0 \end{pmatrix}, \tag{A.17}$$

where σ are Pauli matrices. The matrices satisfy the anticommutation relations

$$\{\gamma^\mu, \gamma^\nu\} = 2g^{\mu\nu}\,. \tag{A.18}$$

The Hermitian conjugates and squares of γ matrices are summarized as follows.

$$(\gamma^\mu)^\dagger = \gamma^0\gamma^\mu\gamma^0\,, \tag{A.19}$$
$$(\gamma^0)^\dagger = \gamma^0\,, \tag{A.20}$$
$$(\gamma^i)^\dagger = -\gamma^i \quad (i=1,2,3)\,, \tag{A.21}$$
$$(\gamma^0)^2 = 1\,, \tag{A.22}$$
$$(\gamma^i)^2 = -1\,. \tag{A.23}$$

A commutator of γ matrices is often expressed by tensor $\sigma^{\mu\nu}$ as

$$\sigma^{\mu\nu} = \frac{i}{2}[\gamma^\mu,\gamma^\nu] = i\left(\gamma^\mu\gamma^\nu - g^{\mu\nu}\right)\,. \tag{A.24}$$

In this representation, γ_5 matrix is written by

$$\gamma^5 = i\gamma^0\gamma^1\gamma^2\gamma^3 = \begin{pmatrix} 0 & 1 \\ 1 & 0 \end{pmatrix}\,. \tag{A.25}$$

The γ_5 matrix has the properties,

$$(\gamma^5)^\dagger = \gamma^5\,, \tag{A.26}$$
$$(\gamma^5)^2 = 1\,, \tag{A.27}$$
$$\{\gamma^5,\gamma^\mu\} = 0\,. \tag{A.28}$$

Finally, the alternative expression for the γ matrices, namely Weyl (Chiral) representation, are introduced,

$$\gamma^\mu = \begin{pmatrix} 0 & \sigma^\mu \\ \bar{\sigma}^\mu & 0 \end{pmatrix}, \gamma^5 = \begin{pmatrix} -1 & 0 \\ 0 & 1 \end{pmatrix}\,, \tag{A.29}$$

where

$$\sigma^\mu = (1,\boldsymbol{\sigma}), \quad \bar{\sigma}^\mu = (1,-\boldsymbol{\sigma}). \tag{A.30}$$

The γ's also satisfy Eqs. (A.18)-(A.23) and (A.26)-(A.28).

A.5 Traces of γ matrices

Traces of γ matrices in 4-dimensions are summarized as follows:

$$\mathrm{tr}(\text{any odd number of } \gamma\text{'s}) = 0 \tag{A.31}$$
$$\mathrm{tr}(\gamma^\mu\gamma^\nu) = 4g^{\mu\nu} \tag{A.32}$$
$$\mathrm{tr}(\gamma^\mu\gamma^\nu\gamma^\rho\gamma^\sigma) = 4(g^{\mu\nu}g^{\rho\sigma} - g^{\mu\rho}g^{\nu\sigma} + g^{\mu\sigma}g^{\nu\rho}) \tag{A.33}$$
$$\mathrm{tr}(\gamma^5) = 0 \tag{A.34}$$
$$\mathrm{tr}(\gamma^\mu\gamma^\nu\gamma^5) = 0 \tag{A.35}$$
$$\mathrm{tr}(\gamma^\mu\gamma^\nu\gamma^\rho\gamma^\sigma\gamma^5) = -4i\epsilon^{\mu\nu\rho\sigma} \tag{A.36}$$

Appendix B

Meson exchange potentials and Kinetic terms

B.1 Matrix elements of the Heavy meson-Nucleon potentials

In this section, the matrix elements of the Heavy meson-Nucleon potentials are summarized. In the π and vector meson exchange potentials in Eqs. (3.15)-(3.16) and (3.21)-(3.23), there are four operators, $\vec{\varepsilon}\cdot\vec{\sigma}$ and $\vec{S}\cdot\vec{\sigma}$ for the central force, and S_ε and S_S for the tensor force. The matrix elements can be calculated by using the Wigner-Eckart theorem and several formulas for angular momentum.

For two-body systems, the matrix element of $\vec{\varepsilon}\cdot\vec{\sigma}$ for the central force is obtained by

$$\begin{aligned}&\langle [l_1,[s_1,s_2]_s]_J\,|(-\sqrt{3})[0,[\varepsilon,\sigma]_0]_0|\,[l_2,[s_1',s_2']_{s'}]_J\rangle\\&\quad=\delta_{l_1l_2}\delta_{ss'}(-1)^{s_1'+s_2+s}\left\{\begin{array}{ccc}s_1 & s_2 & s\\ s_2' & s_1' & 1\end{array}\right\}\langle s_1||\varepsilon||s_1'\rangle\langle s_2||\sigma||s_2'\rangle\,.\end{aligned}\tag{B.1}$$

For $s_1=1$, $s_1'=0$ and $s_2=s_2'=1/2$, Eq. (B.1) can be reduced to

$$\langle [l_1,[1,1/2]_s]_J\,|(-\sqrt{3})[0,[\varepsilon,\sigma]_0]_0|\,[l_2,[0,1/2]_{s'}]_J\rangle=\delta_{l_1l_2}\delta_{ss'}\delta_{s1/2}\left(-\sqrt{3}\right)\,.\tag{B.2}$$

In the similar way, the matrix element of $\vec{S}\cdot\vec{\sigma}$ is calculated as

$$\begin{aligned}&\langle [l_1,[s_1,s_2]_s]_J\,|(-\sqrt{3})[0,[S,\sigma]_0]_0|\,[l_2,[s_1',s_2']_{s'}]_J\rangle\\&\quad=\delta_{l_1l_2}\delta_{ss'}(-1)^{s_1'+s_2+s}\left\{\begin{array}{ccc}s_1 & s_2 & s\\ s_2' & s_1' & 1\end{array}\right\}\langle s_1||S||s_1'\rangle\langle s_2||\sigma||s_2'\rangle\end{aligned}\tag{B.3}$$

For $s_1=s_1'$ and $s_2=s_2'=1/2$, we obtain

$$\begin{aligned}&\langle [l_1,[1,1/2]_s]_J\,|(-\sqrt{3})[0,[S,\sigma]_0]_0|\,[l_2,[1,1/2]_{s'}]_J\rangle\\&\quad=\delta_{l_1l_2}\delta_{ss'}(-1)^{s+3/2}\cdot 6\left\{\begin{array}{ccc}1 & 1/2 & s\\ 1/2 & 1 & 1\end{array}\right\}\end{aligned}\tag{B.4}$$

Let us move to the matrix elements of the tensor operators in the two-body systems. We use $S_{\mathcal{O}}(\hat{r}) = 3(\vec{\mathcal{O}}\cdot\hat{r})(\vec{\sigma}\cdot\hat{r}) - \vec{\mathcal{O}}\cdot\vec{\sigma} = \sqrt{24\pi}[Y_2(\hat{r}), [\mathcal{O},\sigma]_2]_0$ for $\mathcal{O} = \varepsilon, S$. The matrix element of S_ε is given by

$$\begin{aligned}
&\langle [l_1, [s_1, s_2]_s]_J \,|\sqrt{24\pi}[Y_2, [\varepsilon,\sigma]_2]_0|\, [l_2, [s_1', s_2']_{s'}]_J\rangle \\
&\quad = (-1)^{2l_1+l_2+s+J}\sqrt{30}\sqrt{(2l_1+1)(2s+1)(2s'+1)}\langle s_1||\varepsilon||s_1'\rangle\langle s_2||\sigma||s_2'\rangle \\
&\qquad \times (\, l_1\ 0\ 2\ 0|l_2\ 0\,) \left\{ \begin{array}{ccc} l_1 & s & J \\ s' & l_2 & 2 \end{array} \right\} \left\{ \begin{array}{ccc} s_1 & s_2 & s \\ s_1' & s_2' & s' \\ 1 & 1 & 2 \end{array} \right\} .
\end{aligned} \tag{B.5}$$

For $s_1 = 1$, $s_1' = 0$ and $s_2 = s_2' = 1/2$,

$$\begin{aligned}
&\langle [l_1, [1, 1/2]_s]_J \,|\sqrt{24\pi}[Y_2, [\varepsilon,\sigma]_2]_0|\, [l_2, [0, 1/2]_{s'}]_J\rangle \\
&\quad = \delta_{s'1/2}(-1)^{2l_1+l_2+s+J}6\sqrt{5}\sqrt{(2l_1+1)(2s+1)} \\
&\qquad \times (\, l_1\ 0\ 2\ 0|l_2\ 0\,) \left\{ \begin{array}{ccc} l_1 & s & J \\ s' & l_2 & 2 \end{array} \right\} \left\{ \begin{array}{ccc} 1 & 2 & 1 \\ s & 1/2 & 1/2 \end{array} \right\} .
\end{aligned} \tag{B.6}$$

The matrix elements of S_S is also obtained by

$$\begin{aligned}
&\langle [l_1, [s_1, s_2]_s]_J \,|\sqrt{24\pi}[Y_2, [S,\sigma]_2]_0|\, [l_2, [s_1', s_2']_{s'}]_J\rangle \\
&\quad = (-1)^{2l_1+l_2+s+J}\sqrt{30}\sqrt{(2l_1+1)(2s+1)(2s'+1)}\langle s_1||S||s_1'\rangle\langle s_2||\sigma||s_2'\rangle \\
&\qquad \times (\, l_1\ 0\ 2\ 0|l_2\ 0\,) \left\{ \begin{array}{ccc} l_1 & s & J \\ s' & l_2 & 2 \end{array} \right\} \left\{ \begin{array}{ccc} s_1 & s_2 & s \\ s_1' & s_2' & s' \\ 1 & 1 & 2 \end{array} \right\}
\end{aligned} \tag{B.7}$$

For $s_1 = s_1' = 1$, $s_2 = s_2' = 1/2$, we obtain

$$\begin{aligned}
&\langle [l_1, [1, 1/2]_s]_J \,|\sqrt{24\pi}[Y_2, [S,\sigma]_2]_0|\, [l_2, [1, 1/2]_{s'}]_J\rangle \\
&\quad = (-1)^{2l_1+l_2+s+J}\cdot 6\sqrt{30}\sqrt{(2l_1+1)(2s+1)(2s'+1)} \\
&\qquad \times (\, l_1\ 0\ 2\ 0|l_2\ 0\,) \left\{ \begin{array}{ccc} l_1 & s & J \\ s' & l_2 & 2 \end{array} \right\} \left\{ \begin{array}{ccc} 1 & 1/2 & s \\ 1 & 1/2 & s' \\ 1 & 1 & 2 \end{array} \right\}
\end{aligned} \tag{B.8}$$

Finally, the matrix elements of these operators in the three-body systems are summarized as follows:

$$\begin{aligned}
&\langle [[s_1, s_2]_{s_{12}}, s_3]_s \,|\vec{\varepsilon}\cdot\vec{\sigma}|\, \left[[s_1', s_2']_{s_{12}'}, s_3'\right]_{s'}\rangle \\
&\quad = \delta_{ss'}\delta_{m_s m_{s'}}\delta_{s_{12}s_{12}'}\delta_{s_3 s_3'}(-1)^{2s+3s_{12}+2s_3+1/2} \left\{ \begin{array}{ccc} s_1 & s_1' & 1 \\ s_2' & s_2 & s_{12} \end{array} \right\} \times 3\sqrt{2}\,,
\end{aligned} \tag{B.9}$$

$$\begin{aligned}
&\langle [[s_1, s_2]_{s_{12}}, s_3]_s \,|\vec{S}\cdot\vec{\sigma}|\, \left[[s_1', s_2']_{s_{12}'}, s_3'\right]_{s'}\rangle \\
&\quad = \delta_{ss'}\delta_{m_s m_{s'}}\delta_{s_{12}s_{12}'}\delta_{s_3 s_3'}(-1)^{2s+3s_{12}+2s_3+s_1+s_2} \left\{ \begin{array}{ccc} s_1 & s_1' & 1 \\ s_2' & s_2 & s_{12} \end{array} \right\} \times 6\,,
\end{aligned} \tag{B.10}$$

$$\begin{aligned}
&\langle [[s_1,s_2]_{s_{12}},s_3]_s \,||[\varepsilon,\sigma]_2||\left[[s_1',s_2']_{s_{12}'},s_3'\right]_{s'}\rangle \\
&\quad=\delta_{s_3 s_3'}(-1)^{s'+s_3-1/2}\sqrt{5(2s+1)(2s'+1)(2s_{12}+1)(2s_{12}'+1)} \\
&\qquad\times\left\{\begin{array}{ccc} s_{12} & s & s_3 \\ s' & s_{12}' & 2\end{array}\right\}\left\{\begin{array}{ccc} s_1 & s_2 & s_{12} \\ s_1' & s_2' & s_{12}' \\ 1 & 1 & 2\end{array}\right\}\times 3\sqrt{2}\,,
\end{aligned} \tag{B.11}$$

$$\begin{aligned}
&\langle [[s_1,s_2]_{s_{12}},s_3]_s \,||[S,\sigma]_2||\left[[s_1',s_2']_{s_{12}'},s_3'\right]_{s'}\rangle \\
&\quad=\delta_{s_3 s_3'}(-1)^{s'+s_3+s_{12}}\sqrt{5(2s+1)(2s'+1)(2s_{12}+1)(2s_{12}'+1)} \\
&\qquad\times\left\{\begin{array}{ccc} s_{12} & s & s_3 \\ s' & s_{12}' & 2\end{array}\right\}\left\{\begin{array}{ccc} s_1 & s_2 & s_{12} \\ s_1' & s_2' & s_{12}' \\ 1 & 1 & 2\end{array}\right\}\times 6\,.
\end{aligned} \tag{B.12}$$

B.2 Potentials and Kinetic terms in the systems of a heavy meson and a nucleon

Let us show the explicit forms of the meson exchange potentials for each J^P. The potentials for the coupled channel systems are given in the matrix form of 3×3 for $J^P=1/2^{\pm}$,

$$V_{1/2^\pm}=\begin{pmatrix} V^{11}_{1/2^+} & V^{12}_{1/2^+} & V^{13}_{1/2^+} \\ V^{21}_{1/2^+} & V^{22}_{1/2^+} & V^{23}_{1/2^+} \\ V^{31}_{1/2^+} & V^{32}_{1/2^+} & V^{33}_{1/2^+}\end{pmatrix}, \tag{B.13}$$

(B.14)

and 4×4 for the other J^P states,

$$V_{J^P}=\begin{pmatrix} V^{11}_{J^P} & V^{12}_{J^P} & V^{13}_{J^P} & V^{14}_{J^P} \\ V^{21}_{J^P} & V^{22}_{J^P} & V^{23}_{J^P} & V^{24}_{J^P} \\ V^{31}_{J^P} & V^{32}_{J^P} & V^{33}_{J^P} & V^{34}_{J^P} \\ V^{41}_{J^P} & V^{42}_{J^P} & V^{43}_{J^P} & V^{44}_{J^P}\end{pmatrix}, \tag{B.15}$$

in the basis given in Table 3.1 in the same ordering.

The π exchange potentials $V^{\pi}_{J^P}$ for each J^P are obtained by Eqs. (3.15) and (3.16) as

$$V^{\pi}_{1/2^-}=\begin{pmatrix} 0 & \sqrt{3}V_C^{\pi} & -\sqrt{6}V_T^{\pi} \\ \sqrt{3}V_C^{\pi} & -2V_C^{\pi} & -\sqrt{2}V_T^{\pi} \\ -\sqrt{6}V_T^{\pi} & -\sqrt{2}V_T^{\pi} & V_C^{\pi}-2V_T^{\pi}\end{pmatrix}, \tag{B.16}$$

$$V^{\pi}_{1/2^+}=\begin{pmatrix} 0 & \sqrt{3}V_C^{\pi} & -\sqrt{6}V_T^{\pi} \\ \sqrt{3}V_C^{\pi} & -2V_C^{\pi} & -\sqrt{2}V_T^{\pi} \\ -\sqrt{6}V_T^{\pi} & -\sqrt{2}V_T^{\pi} & V_C^{\pi}-2V_T^{\pi}\end{pmatrix}, \tag{B.17}$$

$$V^{\pi}_{3/2^-} = \begin{pmatrix} 0 & \sqrt{3}V^{\pi}_T & -\sqrt{3}V^{\pi}_T & \sqrt{3}V^{\pi}_C \\ \sqrt{3}V^{\pi}_T & V^{\pi}_C & 2V^{\pi}_T & V^{\pi}_T \\ -\sqrt{3}V^{\pi}_T & 2V^{\pi}_T & V^{\pi}_C & -V^{\pi}_T \\ \sqrt{3}V^{\pi}_C & V^{\pi}_T & -V^{\pi}_T & -2V^{\pi}_C \end{pmatrix}, \tag{B.18}$$

$$V^{\pi}_{3/2^+} = \begin{pmatrix} 0 & \sqrt{3}V^{\pi}_C & \sqrt{\frac{3}{5}}V^{\pi}_T & -3\sqrt{\frac{3}{5}}V^{\pi}_T \\ \sqrt{3}V^{\pi}_C & -2V^{\pi}_C & \frac{1}{\sqrt{5}}V^{\pi}_T & -\sqrt{3}V^{\pi}_T \\ \sqrt{\frac{3}{5}}V^{\pi}_T & \frac{1}{\sqrt{5}}V^{\pi}_T & V^{\pi}_C + \frac{8}{5}V^{\pi}_T & \frac{6}{5}V^{\pi}_T \\ -3\sqrt{\frac{3}{5}}V^{\pi}_T & -\sqrt{3}V^{\pi}_T & \frac{6}{5}V^{\pi}_T & V^{\pi}_C - \frac{8}{5}V^{\pi}_T \end{pmatrix}, \tag{B.19}$$

$$V^{\pi}_{5/2^-} = \begin{pmatrix} 0 & \sqrt{3}V^{\pi}_C & \sqrt{\frac{6}{7}}V^{\pi}_T & -\frac{6}{\sqrt{7}}V^{\pi}_T \\ \sqrt{3}V^{\pi}_C & -2V^{\pi}_C & \sqrt{\frac{2}{7}}V^{\pi}_T & -2\sqrt{\frac{3}{7}}V^{\pi}_T \\ \sqrt{\frac{6}{7}}V^{\pi}_T & \sqrt{\frac{2}{7}}V^{\pi}_T & V^{\pi}_C + \frac{10}{7}V^{\pi}_T & \frac{4}{7}\sqrt{6}V^{\pi}_T \\ -\frac{6}{\sqrt{7}}V^{\pi}_T & -2\sqrt{\frac{3}{7}}V^{\pi}_T & \frac{4}{7}\sqrt{6}V^{\pi}_T & V^{\pi}_C - \frac{10}{7}V^{\pi}_T \end{pmatrix}, \tag{B.20}$$

$$V^{\pi}_{5/2^+} = \begin{pmatrix} 0 & \frac{3}{5}\sqrt{10}V^{\pi}_T & \sqrt{3}V^{\pi}_C & -2\sqrt{\frac{3}{5}}V^{\pi}_T \\ \frac{3}{5}\sqrt{10}V^{\pi}_T & V^{\pi}_C - \frac{2}{5}V^{\pi}_T & \sqrt{\frac{6}{5}}V^{\pi}_T & \frac{4}{5}\sqrt{6}V^{\pi}_T \\ \sqrt{3}V^{\pi}_C & \sqrt{\frac{6}{5}}V^{\pi}_T & -2V^{\pi}_C & -\frac{2}{\sqrt{5}}V^{\pi}_T \\ -2\sqrt{\frac{3}{5}}V^{\pi}_T & \frac{4}{5}\sqrt{6}V^{\pi}_T & -\frac{2}{\sqrt{5}}V^{\pi}_T & V^{\pi}_C + \frac{2}{5}V^{\pi}_T \end{pmatrix}, \tag{B.21}$$

$$V^{\pi}_{7/2^-} = \begin{pmatrix} 0 & 3\sqrt{\frac{3}{7}}V^{\pi}_T & \sqrt{3}V^{\pi}_C & -\sqrt{\frac{15}{7}}V^{\pi}_T \\ 3\sqrt{\frac{3}{7}}V^{\pi}_T & V^{\pi}_C - \frac{4}{7}V^{\pi}_T & \frac{3}{\sqrt{7}}V^{\pi}_T & \frac{6}{7}\sqrt{5}V^{\pi}_T \\ \sqrt{3}V^{\pi}_C & \frac{3}{\sqrt{7}}V^{\pi}_T & -2V^{\pi}_C & -\sqrt{\frac{5}{7}}V^{\pi}_T \\ -\sqrt{\frac{15}{7}}V^{\pi}_T & \frac{6}{7}\sqrt{5}V^{\pi}_T & -\sqrt{\frac{5}{7}}V^{\pi}_T & V^{\pi}_C + \frac{4}{7}V^{\pi}_T \end{pmatrix}, \tag{B.22}$$

$$V^{\pi}_{7/2^+} = \begin{pmatrix} 0 & \sqrt{3}V^{\pi}_C & V^{\pi}_T & -\sqrt{5}V^{\pi}_T \\ \sqrt{3}V^{\pi}_C & -2V^{\pi}_C & \frac{1}{\sqrt{3}}V^{\pi}_T & -\sqrt{\frac{5}{3}}V^{\pi}_T \\ V^{\pi}_T & \frac{1}{\sqrt{3}}V^{\pi}_T & V^{\pi}_C + \frac{4}{3}V^{\pi}_T & \frac{2}{3}\sqrt{5}V^{\pi}_T \\ -\sqrt{5}V^{\pi}_T & -\sqrt{\frac{5}{3}}V^{\pi}_T & \frac{2}{3}\sqrt{5}V^{\pi}_T & V^{\pi}_C - \frac{4}{3}V^{\pi}_T \end{pmatrix}, \tag{B.23}$$

$$V^{\pi}_{9/2^-} = \begin{pmatrix} 0 & \sqrt{3}V^{\pi}_C & 2\sqrt{\frac{3}{11}}V^{\pi}_T & -3\sqrt{\frac{6}{11}}V^{\pi}_T \\ \sqrt{3}V^{\pi}_C & -2V^{\pi}_C & \frac{2}{\sqrt{11}}V^{\pi}_T & -3\sqrt{\frac{2}{11}}V^{\pi}_T \\ 2\sqrt{\frac{3}{11}}V^{\pi}_T & \frac{2}{\sqrt{11}}V^{\pi}_T & V^{\pi}_C + \frac{14}{11}V^{\pi}_T & \frac{12}{11}\sqrt{2}V^{\pi}_T \\ -3\sqrt{\frac{6}{11}}V^{\pi}_T & -3\sqrt{\frac{2}{11}}V^{\pi}_T & \frac{12}{11}\sqrt{2}V^{\pi}_T & V^{\pi}_C - \frac{14}{11}V^{\pi}_T \end{pmatrix}, \tag{B.24}$$

$$V^{\pi}_{9/2^+} = \begin{pmatrix} 0 & 2V^{\pi}_T & \sqrt{3}V^{\pi}_C & -\sqrt{2}V^{\pi}_T \\ 2V^{\pi}_T & 2V^{\pi}_C - \frac{2}{3}V^{\pi}_T & \frac{2}{\sqrt{3}}V^{\pi}_T & \frac{4}{3}\sqrt{2}V^{\pi}_T \\ \sqrt{3}V^{\pi}_C & \frac{2}{\sqrt{3}}V^{\pi}_T & -2V^{\pi}_C & -\sqrt{\frac{2}{3}}V^{\pi}_T \\ -\sqrt{2}V^{\pi}_T & \frac{4}{3}\sqrt{2}V^{\pi}_T & -\sqrt{\frac{2}{3}}V^{\pi}_T & V^{\pi}_C + \frac{2}{3}V^{\pi}_T \end{pmatrix}, \tag{B.25}$$

where

$$V^{\pi}_C = \frac{g_\pi g_{\pi NN}}{\sqrt{2}m_N f_\pi}\frac{1}{3}C(r;m_\pi)\vec{\tau}_P\cdot\vec{\tau}_N, \quad V^{\pi}_T = \frac{g_\pi g_{\pi NN}}{\sqrt{2}m_N f_\pi}\frac{1}{3}T(r;m_\pi)\vec{\tau}_P\cdot\vec{\tau}_N. \tag{B.26}$$

The coupling constants are tabulated in Table 3.2 and the functions $C(r;m)$ and $T(r;m)$ are given by Eqs. (3.17) and (3.20).

The vector meson exchange potentials $V^v_{J^P}$ ($v=\rho,\,\omega$) are also given by Eqs. (3.21)-(3.23),

$$V^{v}_{1/2^-} = \begin{pmatrix} V^{v\,\prime}_C & 2\sqrt{3}V^{v}_C & \sqrt{6}V^{v}_T \\ 2\sqrt{3}V^{v}_C & V^{v\,\prime}_C - 4V^{v}_C & \sqrt{2}V^{v}_T \\ \sqrt{6}V^{v}_T & \sqrt{2}V^{v}_T & V^{v\,\prime}_C + 2V^{v}_C + 2V^{v}_T \end{pmatrix}, \tag{B.27}$$

$$V^{v}_{1/2^+} = \begin{pmatrix} V^{v\,\prime}_C & 2\sqrt{3}V^{v}_C & \sqrt{6}V^{v}_T \\ 2\sqrt{3}V^{v}_C & V^{v\,\prime}_C - 4V^{v}_C & \sqrt{2}V^{v}_T \\ \sqrt{6}V^{v}_T & \sqrt{2}V^{v}_T & V^{v\,\prime}_C + 2V^{v}_C + 2V^{v}_T \end{pmatrix}, \tag{B.28}$$

$$V^v_{3/2^-} = \begin{pmatrix} V_C^{v\,\prime} & -\sqrt{3}V_T^v & \sqrt{3}V_T^v & 2\sqrt{3}V_C^v \\ -\sqrt{3}V_T^v & V_C^{v\,\prime}+2V_C^v & -2V_T^v & -V_T^v \\ \sqrt{3}V_T^v & -2V_T^v & V_C^{v\,\prime}+2V_C^v & V_T^v \\ 2\sqrt{3}V_C^v & -V_T^v & V_T^v & V_C^{v\,\prime}-4V_C^v \end{pmatrix}, \tag{B.29}$$

$$V^v_{3/2^+} = \begin{pmatrix} V_C^{v\,\prime} & 2\sqrt{3}V_C^v & -\sqrt{\frac{3}{5}}V_T^v & 3\sqrt{\frac{3}{5}}V_T^v \\ 2\sqrt{3}V_C^v & V_C^{v\,\prime}-4V_C^v & -\frac{1}{\sqrt{5}}V_T^v & \frac{3}{\sqrt{5}}V_T^v \\ -\sqrt{\frac{3}{5}}V_T^v & -\frac{1}{\sqrt{5}}V_T^v & V_C^{v\,\prime}+2V_C^v-\frac{8}{5}V_T^v & -\frac{6}{5}V_T^v \\ 3\sqrt{\frac{3}{5}}V_T^v & \frac{3}{\sqrt{5}}V_T^v & -\frac{6}{5}V_T^v & V_C^{v\,\prime}+2V_C^v+\frac{8}{5}V_T^v \end{pmatrix}, \tag{B.30}$$

$$V^v_{5/2^-} = \begin{pmatrix} V_C^{v\,\prime} & 2\sqrt{3}V_C^v & -\sqrt{\frac{6}{7}}V_T^v & \frac{6}{\sqrt{7}}V_T^v \\ 2\sqrt{3}V_C^v & V_C^{v\,\prime}-4V_C^v & -\sqrt{\frac{2}{7}}V_T^v & 2\sqrt{\frac{3}{7}}V_T^v \\ -\sqrt{\frac{6}{7}}V_T^v & -\sqrt{\frac{2}{7}}V_T^v & V_C^{v\,\prime}+2V_C^v-\frac{10}{7}V_T^v & -\frac{4}{7}\sqrt{6}V_T^v \\ \frac{6}{\sqrt{7}}V_T^v & 2\sqrt{\frac{3}{7}}V_T^v & -\frac{4}{7}\sqrt{6}V_T^v & V_C^{v\,\prime}+2V_C^v+\frac{10}{7}V_T^v \end{pmatrix}, \tag{B.31}$$

$$V^v_{5/2^+} = \begin{pmatrix} V_C^{v\,\prime} & -\frac{3}{5}\sqrt{10}V_T^v & 2\sqrt{3}V_C^v & 2\sqrt{\frac{3}{5}}V_T^v \\ -\frac{3}{5}\sqrt{10}V_T^v & V_C^{v\,\prime}+2V_C^v+\frac{2}{5}V_T^v & -\sqrt{\frac{6}{5}}V_T^v & -\frac{4}{5}\sqrt{6}V_T^v \\ 2\sqrt{3}V_C^v & -\sqrt{\frac{6}{5}}V_T^v & V_C^{v\,\prime}-4V_C^v & \frac{2}{\sqrt{5}}V_T^v \\ 2\sqrt{\frac{3}{5}}V_T^v & -\frac{4}{5}\sqrt{6}V_T^v & \frac{2}{\sqrt{5}}V_T^v & V_C^{v\,\prime}+2V_C^v-\frac{2}{5}V_T^v \end{pmatrix}, \tag{B.32}$$

$$V^v_{7/2^-} = \begin{pmatrix} V_C^{v\prime} & -3\sqrt{\frac{3}{7}}V_T^v & 2\sqrt{3}V_C^v & \sqrt{\frac{15}{7}}V_T^v \\ -3\sqrt{\frac{3}{7}}V_T^v & V_C^{v\prime}+2V_C^v+\frac{4}{7}V_T^v & -\frac{3}{\sqrt{7}}V_T^v & -\frac{6}{7}\sqrt{5}V_T^v \\ 2\sqrt{3}V_C^v & -\frac{3}{\sqrt{7}}V_T^v & V_C^{v\prime}-4V_C^v & \sqrt{\frac{5}{7}}V_T^v \\ \sqrt{\frac{15}{7}}V_T^v & -\frac{6}{7}\sqrt{5}V_T^v & \sqrt{\frac{5}{7}}V_T^v & V_C^{v\prime}+2V_C^v-\frac{4}{7}V_T^v \end{pmatrix}, \tag{B.33}$$

$$V^v_{7/2^+} = \begin{pmatrix} V_C^{v\prime} & 2\sqrt{3}V_C^v & -V_T^v & \sqrt{5}V_T^v \\ 2\sqrt{3}V_C^v & V_C^{v\prime}-4V_C^v & -\frac{1}{\sqrt{3}}V_T^v & \sqrt{\frac{5}{3}}V_T^v \\ -V_T^v & -\frac{1}{\sqrt{3}}V_T^v & V_C^{v\prime}+2V_C^v-\frac{4}{3}V_T^v & -\frac{2}{3}\sqrt{5}V_T^v \\ \sqrt{5}V_T^v & \sqrt{\frac{5}{3}}V_T^v & -\frac{2}{3}\sqrt{5}V_T^v & V_C^{v\prime}+2V_C^v+\frac{4}{3}V_T^v \end{pmatrix}, \tag{B.34}$$

$$V^v_{9/2^-} = \begin{pmatrix} V_C^{v\prime} & 2\sqrt{3}V_C^v & -2\sqrt{\frac{3}{11}}V_T^v & 3\sqrt{\frac{6}{11}}V_T^v \\ 2\sqrt{3}V_C^v & V_C^{v\prime}-4V_C^v & -\frac{2}{\sqrt{11}}V_T^v & 3\sqrt{\frac{2}{11}}V_T^v \\ -2\sqrt{\frac{3}{11}}V_T^v & -\frac{2}{\sqrt{11}}V_T^v & V_C^{v\prime}+2V_C^v+\frac{14}{11}V_T^v & -\frac{12}{11}\sqrt{2}V_T^v \\ 3\sqrt{\frac{6}{11}}V_T^v & 3\sqrt{\frac{2}{11}}V_T^v & -\frac{12}{11}\sqrt{2}V_T^v & V_C^{v\prime}+2V_C^v-\frac{14}{11}V_T^v \end{pmatrix}, \tag{B.35}$$

$$V^v_{9/2^+} = \begin{pmatrix} V_C^{v\prime} & -2V_T^v & 2\sqrt{3}V_C^v & \sqrt{2}V_T^v \\ -2V_T^v & V_C^{v\prime}+2V_C^v+\frac{2}{3}V_T^v & -\frac{2}{\sqrt{3}}V_T^v & -\frac{4}{3}\sqrt{2}V_T^v \\ 2\sqrt{3}V_C^v & -\frac{2}{\sqrt{3}}V_T^v & V_C^{v\prime}-4V_C^v & \sqrt{\frac{2}{3}}V_T^v \\ \sqrt{2}V_T^v & -\frac{4}{3}\sqrt{2}V_T^v & \sqrt{\frac{2}{3}}V_T^v & V_C^{v\prime}+2V_C^v-\frac{2}{3}V_T^v \end{pmatrix}, \tag{B.36}$$

where $V_C^{v\,\prime}$, V_C^v and V_T^v are defined as

$$V_C^{v\,\prime} = \frac{g_V g_{vNN}\beta}{\sqrt{2}m_v^2} C(r;m_v)\vec{\tau}_P\cdot\vec{\tau}_N\,, \tag{B.37}$$

$$V_C^{v} = \frac{g_V g_{vNN}\lambda(1+\kappa)}{\sqrt{2}m_N}\frac{1}{3} C(r;m_v)\vec{\tau}_P\cdot\vec{\tau}_N\,, \tag{B.38}$$

$$V_T^{v} = \frac{g_V g_{vNN}\lambda(1+\kappa)}{\sqrt{2}m_N}\frac{1}{3} T(r;m_v)\vec{\tau}_P\cdot\vec{\tau}_N\,. \tag{B.39}$$

For instance, the functional forms of potentials for $J^P = 1/2^-$ and $3/2^-$, and $I = 0$ are shown in Fig. B.1-B.3. The dominance of the tensor force of the OPEP is seen clearly in the potentials such as $V^{12}_{1/2^-}$ and $V^{23}_{1/2^-}$.

Finally, the kinetic terms for each J^P are given by

$$K_{1/2^-} = \mathrm{diag}\left(-\frac{1}{2\tilde{m}_P}\triangle_0, -\frac{1}{2\tilde{m}_{P^*}}\triangle_0 + \Delta m_{PP^*}, -\frac{1}{2\tilde{m}_{P^*}}\triangle_2 + \Delta m_{PP^*}\right), \tag{B.40}$$

$$K_{1/2^+} = \mathrm{diag}\left(-\frac{1}{2\tilde{m}_P}\triangle_1, -\frac{1}{2\tilde{m}_{P^*}}\triangle_1 + \Delta m_{PP^*}, -\frac{1}{2\tilde{m}_{P^*}}\triangle_1 + \Delta m_{PP^*}\right), \tag{B.41}$$

$$K_{3/2^-} = \mathrm{diag}\left(-\frac{1}{2\tilde{m}_P}\triangle_2, -\frac{1}{2\tilde{m}_{P^*}}\triangle_0 + \Delta m_{PP^*}, -\frac{1}{2\tilde{m}_{P^*}}\triangle_2 + \Delta m_{PP^*}\,, -\frac{1}{2\tilde{m}_{P^*}}\triangle_2 + \Delta m_{PP^*}\right), \tag{B.42}$$

$$K_{3/2^+} = \mathrm{diag}\left(-\frac{1}{2\tilde{m}_P}\triangle_1, -\frac{1}{2\tilde{m}_{P^*}}\triangle_1 + \Delta m_{PP^*}, -\frac{1}{2\tilde{m}_{P^*}}\triangle_1 + \Delta m_{PP^*}\,, -\frac{1}{2\tilde{m}_{P^*}}\triangle_3 + \Delta m_{PP^*}\right), \tag{B.43}$$

$$K_{5/2^-} = \mathrm{diag}\left(-\frac{1}{2\tilde{m}_P}\triangle_2, -\frac{1}{2\tilde{m}_{P^*}}\triangle_2 + \Delta m_{PP^*}, -\frac{1}{2\tilde{m}_{P^*}}\triangle_2 + \Delta m_{PP^*}\,, -\frac{1}{2\tilde{m}_{P^*}}\triangle_4 + \Delta m_{PP^*}\right), \tag{B.44}$$

$$K_{5/2^+} = \mathrm{diag}\left(-\frac{1}{2\tilde{m}_P}\triangle_3, -\frac{1}{2\tilde{m}_{P^*}}\triangle_1 + \Delta m_{PP^*}, -\frac{1}{2\tilde{m}_{P^*}}\triangle_3 + \Delta m_{PP^*}\,, -\frac{1}{2\tilde{m}_{P^*}}\triangle_3 + \Delta m_{PP^*}\right), \tag{B.45}$$

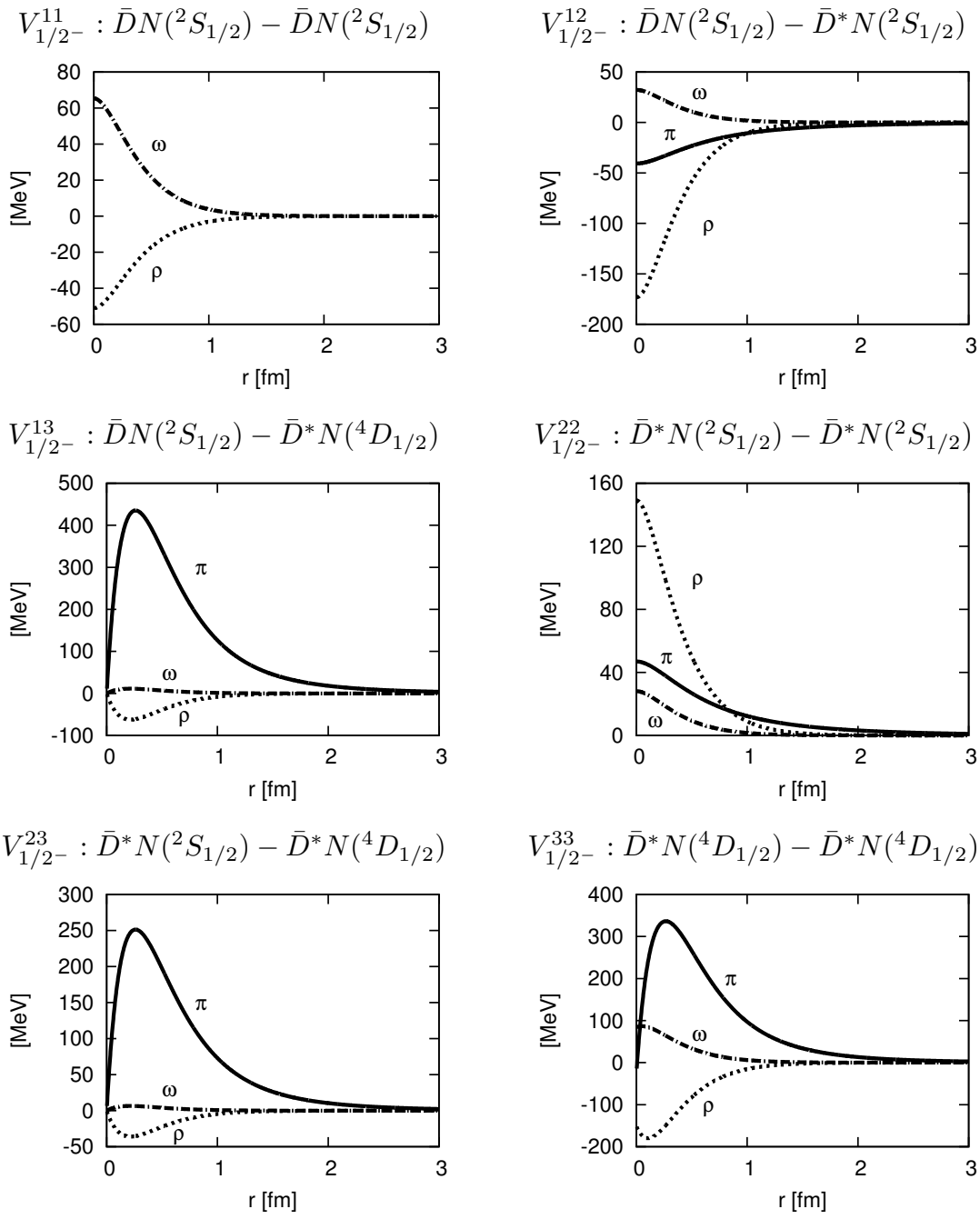

Fig.B.1 Various components of the $\pi\rho\omega$ exchange potential for $(I, J^P) = (0, 1/2^-)$.

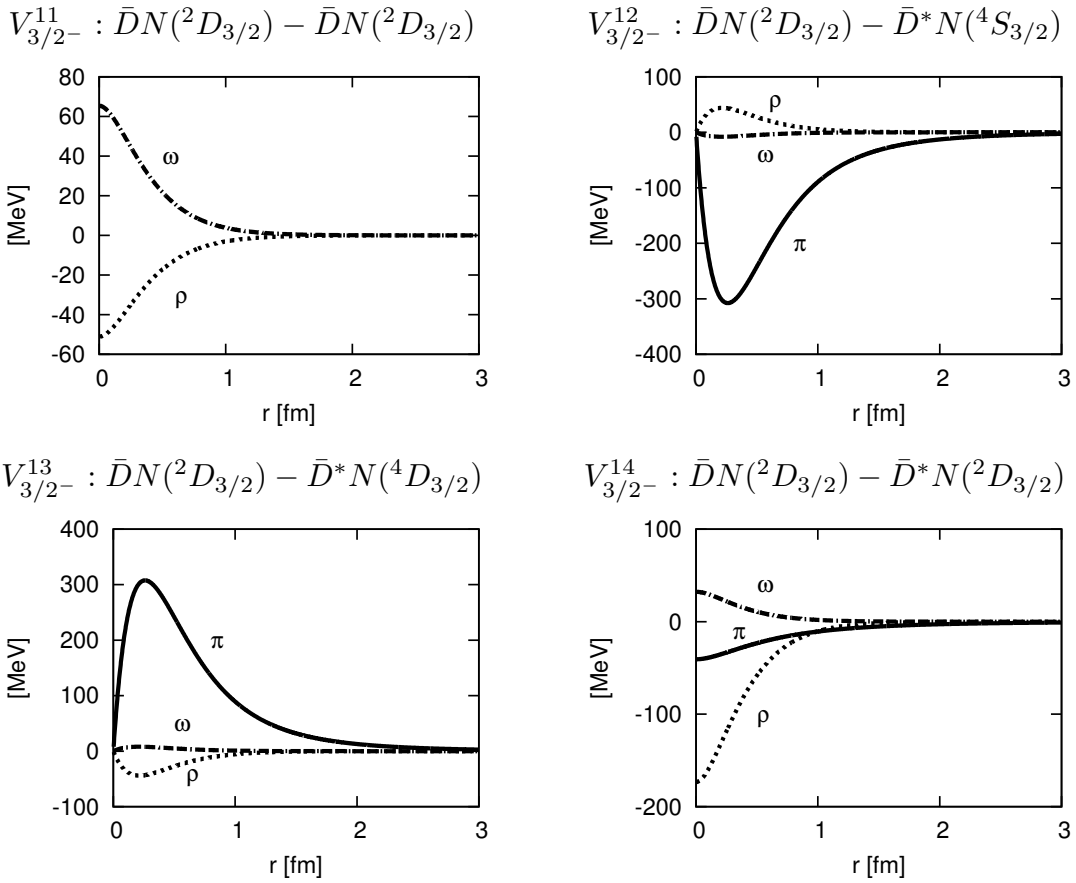

Fig.B.2 Various components of the $\pi\rho\omega$ exchange potential for $(I, J^P) = (0, 3/2^-)$.

$$K_{7/2^-} = \mathrm{diag}\left(-\frac{1}{2\tilde{m}_P}\triangle_4, -\frac{1}{2\tilde{m}_{P^*}}\triangle_2 + \Delta m_{PP^*}, -\frac{1}{2\tilde{m}_{P^*}}\triangle_4 + \Delta m_{PP^*}\ ,\right.$$
$$\left. -\frac{1}{2\tilde{m}_{P^*}}\triangle_4 + \Delta m_{PP^*}\right)\ , \tag{B.46}$$

$$K_{7/2^+} = \mathrm{diag}\left(-\frac{1}{2\tilde{m}_P}\triangle_3, -\frac{1}{2\tilde{m}_{P^*}}\triangle_3 + \Delta m_{PP^*}, -\frac{1}{2\tilde{m}_{P^*}}\triangle_3 + \Delta m_{PP^*}\ ,\right.$$
$$\left. -\frac{1}{2\tilde{m}_{P^*}}\triangle_5 + \Delta m_{PP^*}\right)\ , \tag{B.47}$$

$$K_{9/2^-} = \mathrm{diag}\left(-\frac{1}{2\tilde{m}_P}\triangle_4, -\frac{1}{2\tilde{m}_{P^*}}\triangle_4 + \Delta m_{PP^*}, -\frac{1}{2\tilde{m}_{P^*}}\triangle_4 + \Delta m_{PP^*}\ ,\right.$$
$$\left. -\frac{1}{2\tilde{m}_{P^*}}\triangle_6 + \Delta m_{PP^*}\right)\ , \tag{B.48}$$

$V^{22}_{3/2^-} : \bar{D}^* N(^4S_{3/2}) - \bar{D}^* N(^4S_{3/2})$

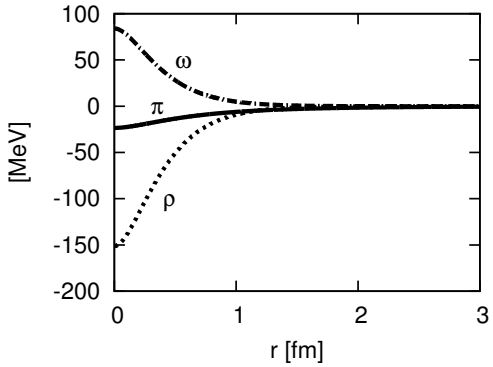

$V^{23}_{3/2^-} : \bar{D}^* N(^4S_{3/2}) - \bar{D}^* N(^4D_{3/2})$

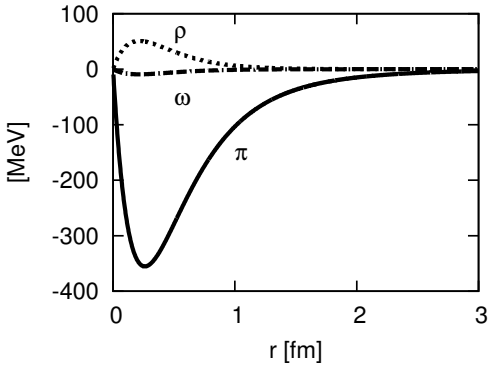

$V^{24}_{3/2^-} : \bar{D}^* N(^4S_{3/2}) - \bar{D}^* N(^2D_{3/2})$

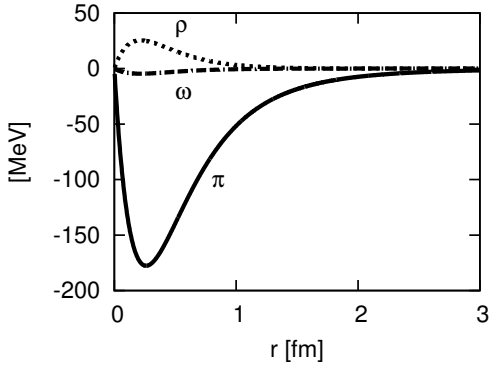

$V^{33}_{3/2^-} : \bar{D}^* N(^4D_{3/2}) - \bar{D}^* N(^4D_{3/2})$

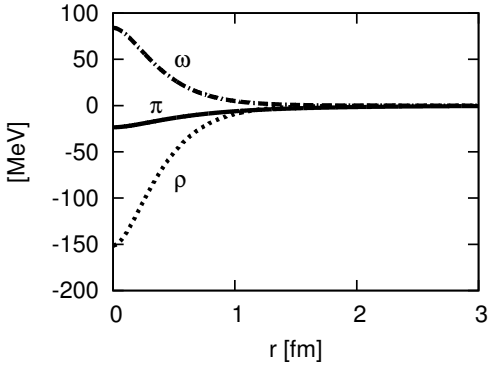

$V^{34}_{3/2^-} : \bar{D}^* N(^4D_{3/2}) - \bar{D}^* N(^2D_{3/2})$

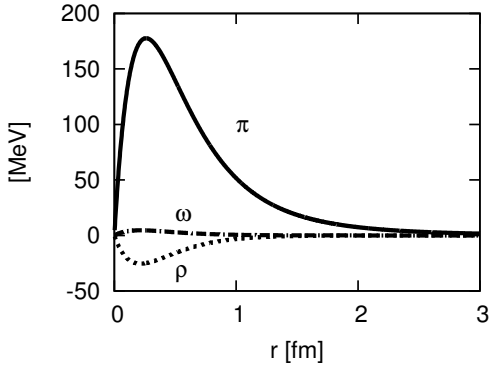

$V^{44}_{3/2^-} : \bar{D}^* N(^2D_{3/2}) - \bar{D}^* N(^2D_{3/2})$

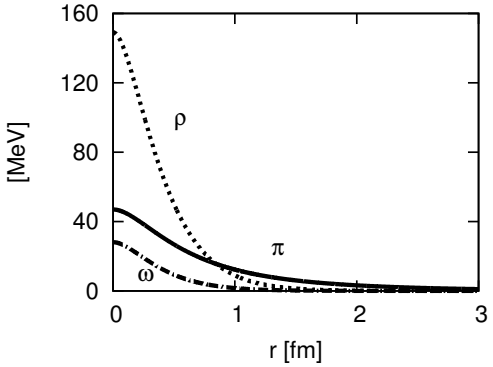

Fig.B.3 Continued from Fig. B.2.

$$K_{9/2^+} = \mathrm{diag}\left(-\frac{1}{2\tilde{m}_P}\triangle_5, -\frac{1}{2\tilde{m}_{P^*}}\triangle_3 + \Delta m_{PP^*}, -\frac{1}{2\tilde{m}_{P^*}}\triangle_5 + \Delta m_{PP^*}\ , \right.$$
$$\left. -\frac{1}{2\tilde{m}_{P^*}}\triangle_5 + \Delta m_{PP^*} \right)\ , \tag{B.49}$$

where $\triangle_l = \partial^2/\partial r^2 + (2/r)\partial/\partial r - l(l+1)/r^2$, $\tilde{m}_{P^{(*)}} = m_N m_{P^{(*)}}/(m_N + m_{P^{(*)}})$, and $\Delta m_{PP^*} = m_{P^*} - m_P$. The total Hamiltonian is then given by $H_{J^P} = K_{J^P} + V_{J^P}$.

B.3 Nucleon-nucleon potentials

The nucleon-nucleon (NN) potential is one of the most basic interaction between two hadrons. The long history of the NN interaction was started from the basic idea by H. Yukawa in 1935 [137]. The pion predicted by Yukawa is the most essential ingredient in the theory of nuclear forces. Based on his Meson Theory, the one boson-exchange models have been developed, constructed from the NN scattering data phenomenologically. Early models of the one boson-exchange potential (OBEP) had been investigated by Hamada-Johnston [179, 180], Reid [181], Bryan-Scott [182–184], Minnesota group [185], etc. In addition, Y. Yamaguchi discussed the non-local NN potential in 1954 [186, 187]. These potentials can describe the properties of the deuteron and the NN phase shifts in low energy region.

In 1990s, high precision potentials were developed. CD-Bonn [188], Argonne v_{18} [149], and Nijmegen potentials (Nijm93, Nijm I, Nijm II and Reid93) [189] are able to reproduce the NN phase shifts with high accuracy, and called the realistic NN potentials. They are utilized widely in the nuclear physics.

From the discovery of the Quantum chromodynamics (QCD), new approaches to describe the NN interactions have been developed. S. Weinberg discussed that one has to write down the general Lagrangian which is consistent with the assuming symmetry, particularly the chiral symmetry of QCD [119]. The idea introduced the effective field theory to the low-energy QCD. In this approach, the pion being the Nambu-Goldstone boson also emerges as the effective degrees of freedom. The NN forces based on the Chiral effective field theory (EFT) were discussed in Refs. [190–194] and reviewed in Refs. [172, 173, 195]. These results reach success to obtain the accurate NN phase shifts.

The NN interactions from QCD have been also studied by the Lattice QCD simulations [196, 197]. This approach succeeds in obtaining the central and tensor forces of the NN interaction, while the calculations have not been done at the physical point yet. However, the behaviors of the obtained potentials are essentially consistent with those of the well-known realistic NN potentials.

The ideas of constructions of the NN interactions are utilized to study many-nucleon forces [148, 150, 167–174], baryon-baryon interaction for the SU(3) flavor-octet baryons [198–203], nucleon-antinucleon forces [204–214], etc.

In this appendix, the several phenomenological potential models are reviewed.

B.3.1 Minnesota potential

The Minnesota potential was developed by the Minnesota group in Ref. [185]. Although this potential has a simple form expressed by a sum of three Gaussian functions and the coulomb term, it can describe the two-nucleon low-energy scattering data, e.g. the scattering lengths and the effective ranges for $^1S_0$ and $^3S_1$ channels, and the properties of the deuteron, triton and α particle. The Minnesota potential is given by

$$V(r) = \left(V_R + \frac{1}{2}(1+P^\sigma)V_t + \frac{1}{2}(1-P^\sigma)V_s \right) \left(\frac{1}{2}u + \frac{1}{2}(2-u)P^r \right) + \frac{1}{2}(1+\tau_{1z})\frac{1}{2}(1+\tau_{2z})\frac{e^2}{r}\,, \tag{B.50}$$

where the potentials V_R, V_t and V_s are

$$V_R = V_{0R}e^{-\kappa_R r^2}, \quad V_t = -V_{0t}e^{-\kappa_t r^2}, \quad V_s = -V_{0s}e^{-\kappa_s r^2}\,. \tag{B.51}$$

The parameters V_0 and κ are summarized in Table B.1. The spin-, isospin- and space-exchange operators are defined by

$$P^\sigma = \frac{1+\vec{\sigma}_1\cdot\vec{\sigma}_2}{2}, \quad P^\tau = \frac{1+\vec{\tau}_1\cdot\vec{\tau}_2}{2}\,, \tag{B.52}$$

$$P^r = -P^\sigma P^\tau = \frac{(1+\vec{\sigma}_1\cdot\vec{\sigma}_2)(1+\vec{\tau}_1\cdot\vec{\tau}_2)}{4}\,. \tag{B.53}$$

The exchange-mixture parameter is chosen as $u = 0.97$. The last term in Eq. (B.50) is the coulomb potential which survives only in the pp system with total isospin $I = 1$ as e^2/r.

For the $^1S_0$, $^3S_1$, $^1P_1$ and $^3P_0$ channels, we obtain

$$(^1S_0): \quad V(r) = V_R + V_s + \frac{1}{2}(1+\tau_{1z})\frac{1}{2}(1+\tau_{2z})\frac{e^2}{r}\,, \tag{B.54}$$

$$(^3S_1): \quad V(r) = V_R + V_t\,, \tag{B.55}$$

$$(^1P_1): \quad V(r) = (V_R + V_s)(u-1)\,, \tag{B.56}$$

$$(^3P_0): \quad V(r) = (V_R + V_s)(u-1) + \frac{1}{2}(1+\tau_{1z})\frac{1}{2}(1+\tau_{2z})\frac{e^2}{r}\,. \tag{B.57}$$

Table.B.1 Parameters of the Minnesota potential, given in Ref. [185]

	V_R	V_t	V_s
V_0 [MeV]	200.0	178.0	91.85
κ [fm^{-2}]	1.487	0.639	0.465

B.3.2 Bonn potential

The Bonn potential is based on the meson exchanges [138, 139, 215]. Masses of the mesons, coupling constants on the Lagrangians, and cutoff parameters on the form factors are determined to fit the world NN data.

The interaction Lagrangians for a meson and nucleons are given by

$$\mathcal{L}^{\rm PS}_{psNN} = -g_{psNN}\bar{N}i\gamma^5 N\phi^{(ps)}\,, \tag{B.58}$$

$$\mathcal{L}^{\rm PV}_{psNN} = \frac{g_{psNN}}{2m_N}\bar{N}\gamma^5\gamma^\mu N\partial_\mu\phi^{(ps)}\,, \tag{B.59}$$

$$\mathcal{L}_{vNN} = g_v\bar{N}\gamma^\mu N\phi^{(v)}_\mu + \frac{f_v}{4m_N}\bar{N}\sigma^{\mu\nu}N\left(\partial_\mu\phi^{(v)}_\nu - \partial_\nu\phi^{(v)}_\mu\right)\,, \tag{B.60}$$

$$\mathcal{L}_{sNN} = g_s\bar{N}N\phi^{(s)}\,, \tag{B.61}$$

for pseudoscalar (ps), vector (v) and scalar (s) mesons, respectively. N (ϕ) is the nucleon (meson) field. The field ϕ is replaced by $\vec{\tau}\cdot\vec{\phi}$ for an isovector meson, where $\vec{\tau}$ are isospin matrices. For pseudoscalar mesons, two couplings can be considered, pseudoscalar coupling $\mathcal{L}^{\rm PS}_{psNN}$ and pseudovector coupling $\mathcal{L}^{\rm PV}_{psNN}$.

The lowest order interactions from Lagrangians in Eqs. (B.58)-(B.61) are given by second-order Feynman diagrams. In the c.m system, the Feynman amplitude for an α meson exchange, depicted in Fig. B.4, is

$$-i\bar{V}_\alpha(p',p) = \bar{u}_1(p')\Gamma^\alpha_1 u_1(p)\bar{u}_2(-p')\Gamma^\alpha_2 u_2(-p)\frac{P_\alpha}{q^2-m^2_\alpha}\,, \tag{B.62}$$

where u_i ($i=1,2$) is the Dirac spinor, p (p') is a four-momentum in the initial (final) state and $\Gamma^{(\alpha)}_i$ is a vertex obtained by interaction Lagrangians. P_α is a numerator in the meson propagator; $P_\alpha = i$ for a (pseudo-)scalar meson and $P_\alpha = -ig_{\mu\nu}$ for a

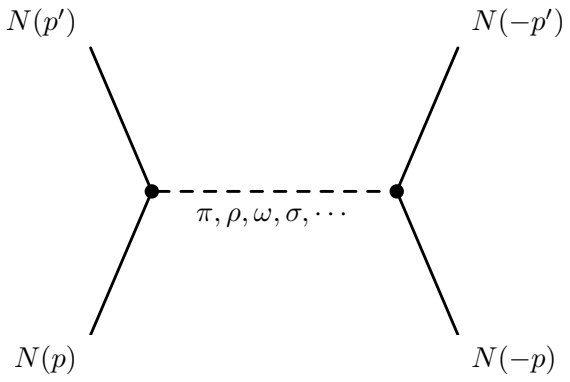

Fig.B.4 Feynman diagrams of one boson exchange potentials. Solid (dashed) line denotes nucleons (exchanged bosons).

vector meson. q is defined as $q = p' - p$. Dirac spinors are given by

$$u(p,s) = \sqrt{\frac{E_p + m_N}{2m_N}} \begin{pmatrix} 1 \\ (\vec{\sigma}\cdot\vec{p})/(E_p + m_N) \end{pmatrix} \chi_s \,, \tag{B.63}$$

$$\begin{aligned} \bar{u}(p,s) = u^\dagger(p,s)\gamma^0 &= \sqrt{\frac{E_p + m_N}{2m_N}} \chi_s^\dagger \begin{pmatrix} 1 & \dfrac{\vec{\sigma}\cdot\vec{p}}{E_p + m_N} \end{pmatrix} \begin{pmatrix} 1 & 0 \\ 0 & -1 \end{pmatrix} \\ &= \sqrt{\frac{E_p + m_N}{2m_N}} \chi_s^\dagger \begin{pmatrix} 1 & -\dfrac{\vec{\sigma}\cdot\vec{p}}{E_p + m_N} \end{pmatrix} , \end{aligned} \tag{B.64}$$

with $E_p = \sqrt{m_N^2 + \vec{p}^{\,2}}$ and a Pauli spinor χ_s. (In the following χ_s is omitted for simplification.) The Dirac spinors are normalized as $\bar{u}(p)u(p) = 1$.

The non-local one boson exchange potential (OBEP) is defined by

$$V_\alpha(p,p') = \sqrt{\frac{m_N}{E_p}} \sqrt{\frac{m_N}{E_{p'}}}\, \bar{V}_\alpha(p,p') F_\alpha^2(p,p';\Lambda) \,. \tag{B.65}$$

In Eq. (B.65), a square root factor $m_N/\sqrt{E_p E_{p'}}$ and form factor $F_\alpha(p,p';\Lambda_\alpha)$ with a cutoff parameter Λ_α are included as customary. In the Bonn potential, the monopole type form factor is employed:

$$F_\alpha(p,p';\Lambda_\alpha) = \frac{\Lambda_\alpha^2 - m_\alpha^2}{\Lambda_\alpha^2 + (\vec{p}\,' - \vec{p})^2} \,. \tag{B.66}$$

(i−1) Pseudoscalar meson exchange potential (Pseudoscalar coupling)
The interaction Lagrangian $\mathcal{L}^{\rm PS}_{psNN}$ in Eq. (B.58) provides the one pseudoscalar meson exchange potential, the Feynman amplitude is

$$\begin{aligned} -i\bar{V}_{ps}^{\rm PS}(p,p') &= g_{psNN}^2 \bar{u}_1(p')\gamma^5 u_1(p) \bar{u}_2(-p')\gamma^5 u_2(-p) \frac{i}{q^2 - m_{ps}^2} \\ &= g_{psNN}^2 \frac{E_{p'} + m_N}{2m_N} \frac{E_p + m_N}{2m_N} \begin{pmatrix} -\dfrac{\vec{\sigma}_1\cdot\vec{p}\,'}{E_{p'} + m_N} & 1 \end{pmatrix} \begin{pmatrix} 1 \\ (\vec{\sigma}_1\cdot\vec{p})/(E_p + m_N) \end{pmatrix} \\ &\quad \times \begin{pmatrix} \dfrac{\vec{\sigma}_2\cdot\vec{p}\,'}{E_{p'} + m_N} & 1 \end{pmatrix} \begin{pmatrix} 1 \\ -(\vec{\sigma}_2\cdot\vec{p})/(E_p + m_N) \end{pmatrix} \frac{i}{q^2 - m_{ps}^2} \\ &= i \left(\frac{g_{psNN}}{2m_N}\right)^2 \frac{(E_{p'} + m_N)(E_p + m_N)}{q^2 - m_{ps}^2} \left(-\frac{\vec{\sigma}_1\cdot\vec{p}\,'}{E_{p'} + m_N} + \frac{\vec{\sigma}_1\cdot\vec{p}}{E_p + m_N} \right) \\ &\quad \times \left(\frac{\vec{\sigma}_2\cdot\vec{p}\,'}{E_{p'} + m_N} - \frac{\vec{\sigma}_2\cdot\vec{p}}{E_p + m_N} \right) . \end{aligned} \tag{B.67}$$

From Eqs. (B.65) and (B.67), the non-local potential is derived by

$$\begin{aligned} V_{ps}^{\rm PS}(p,p') = &- \left(\frac{g_{psNN}}{2m_N}\right)^2 \frac{(E_{p'} + m_N)(E_p + m_N)}{q^2 - m_{ps}^2} \left(-\frac{\vec{\sigma}_1\cdot\vec{p}\,'}{E_{p'} + m_N} + \frac{\vec{\sigma}_1\cdot\vec{p}}{E_p + m_N} \right) \\ &\times \left(\frac{\vec{\sigma}_2\cdot\vec{p}\,'}{E_{p'} + m_N} - \frac{\vec{\sigma}_2\cdot\vec{p}}{E_p + m_N} \right) \frac{m_N}{\sqrt{E_p E_{p'}}} F_{ps}^2(q,q';\Lambda_{ps}) \,. \end{aligned} \tag{B.68}$$

If the static approximation $E_p \sim E_{p'} \sim m_N$ is applied, the local potential is obtained,

$$V_{ps}^{\rm PS}(\vec{q}) = -\left(\frac{g_{psNN}}{2m_N}\right)^2 \frac{\vec{\sigma}_1\cdot\vec{q}\,\vec{\sigma}_2\cdot\vec{q}}{\vec{q}^2+m_{ps}^2} F_{ps}^2(\vec{q};\Lambda_{ps}) \tag{B.69}$$

$$= -\left(\frac{g_{psNN}}{2m_N}\right)^2 \frac{1}{3}\left[\frac{\vec{\sigma}_1\cdot\vec{\sigma}_2\vec{q}^2}{\vec{q}^2+m_{ps}^2} + \frac{S_{12}(\hat{q})\vec{q}^2}{\vec{q}^2+m_{ps}^2}\right] F_{ps}^2(\vec{q};\Lambda_{ps})$$

$$= \left(\frac{g_{psNN}}{2m_N}\right)^2 \frac{1}{3}\left[-\vec{\sigma}_1\cdot\vec{\sigma}_2 + \frac{\vec{\sigma}_1\cdot\vec{\sigma}_2 m_{ps}^2}{\vec{q}^2+m_{ps}^2} - \frac{S_{12}(\hat{q})\vec{q}^2}{\vec{q}^2+m_{ps}^2}\right] F_{ps}^2(\vec{q};\Lambda_{ps})\,, \tag{B.70}$$

where $F_{ps}(\vec{q};\Lambda_{ps}) = (\Lambda_{ps}^2+m_\pi^2)/(\Lambda_{ps}^2-\vec{q}^2)$. S_{12} is the tensor operator defined by $S_{12}(\hat{q}) = 3(\vec{\sigma}_1\cdot\hat{q})(\vec{\sigma}_2\cdot\hat{q}) - \vec{\sigma}_1\cdot\vec{\sigma}_2$ and one uses

$$(\vec{\sigma}_1\cdot\vec{q})(\vec{\sigma}_2\cdot\vec{q}) = \frac{1}{3}\vec{\sigma}_1\cdot\vec{\sigma}_2\,\vec{q}^2 + \frac{1}{3}\left[3(\vec{\sigma}_1\cdot\vec{q})(\vec{\sigma}_2\cdot\vec{q}) - \vec{\sigma}_1\cdot\vec{\sigma}_2\,\vec{q}^2\right]$$

$$= \frac{1}{3}\vec{\sigma}_1\cdot\vec{\sigma}_2\,\vec{q}^2 + \frac{1}{3}S_{12}(\hat{q})\vec{q}^2\,. \tag{B.71}$$

The potential in the coordinate space is given by performing the Fourier transformation [216, 217] as

$$V_{ps}^{\rm PS}(\vec{r}) = \int \frac{d^3q}{(2\pi)^3} V_{ps}^{\rm PS}(\vec{q}) F_{ps}^2(\vec{q};\Lambda_{ps}) e^{i\vec{q}\cdot\vec{r}}\,. \tag{B.72}$$

When the form factor is not considered, Eq. (B.72) is written as

$$V_{ps}^{\rm PS}(\vec{r}) = c_{ps}\int \frac{d^3q}{(2\pi)^3}\left[-\vec{\sigma}_1\cdot\vec{\sigma}_2 + \frac{(\vec{\sigma}_1\cdot\vec{\sigma}_2)m_{ps}^2}{\vec{q}^2+m_{ps}^2} - \frac{S_{12}(\hat{q})\vec{q}^2}{\vec{q}^2+m_{ps}^2}\right] e^{i\vec{q}\cdot\vec{r}}\,, \tag{B.73}$$

where

$$c_{ps} \equiv \left(\frac{g_{psNN}}{2m_N}\right)^2 \frac{1}{3}\,. \tag{B.74}$$

The first term in Eq.(B.73) yields the δ function as

$$-c_{ps}(\vec{\sigma}_1\cdot\vec{\sigma}_2)\int \frac{d^3q}{(2\pi)^3} e^{i\vec{q}\cdot\vec{r}} = -c_{ps}(\vec{\sigma}_1\cdot\vec{\sigma}_2)\delta^{(3)}(\vec{r}) \tag{B.75}$$

The second term in Eq.(B.73) is written as

$$\frac{c_{ps}}{(2\pi)^2 r}\int_{-\infty}^{\infty} dq \left[\frac{(\vec{\sigma}_1\cdot\vec{\sigma}_2)m_{ps}^2}{\vec{q}^2+m_{ps}^2}\right] q\sin qr\,. \tag{B.76}$$

This is obtained by the complex integral

$$\oint_C dz \frac{ze^{izr}}{z^2+m^2}\,. \tag{B.77}$$

The residue of the integrand is

$$a_{-1}(im) = \lim_{z\to\infty}(z-im)\frac{ze^{izr}}{z^2+m^2} = \frac{e^{-mr}}{2}\,. \tag{B.78}$$

Therefore, one obtains

$$\frac{c_{ps}}{(2\pi)^2 r}\int_{-\infty}^{\infty} dq\left[\frac{(\vec{\sigma}_1\cdot\vec{\sigma}_2)m_{ps}^2}{\vec{q}^{\,2}+m_{ps}^2}\right] q\sin qr = (\vec{\sigma}_1\cdot\vec{\sigma}_2)\frac{m_{ps}^2}{4\pi r}c_{ps}e^{-m_{ps}r}\,. \tag{B.79}$$

The third term in Eq.(B.73) is rewritten by using the Rayleigh formula and $S_{12}(\hat{q}) = \sqrt{24\pi}\,[Y_2(\hat{q}),[\sigma_1,\sigma_2]_2]_0$ as

$$\begin{aligned}
&c_{ps}\int\frac{d^3q}{(2\pi)^3}\left[-\frac{S_{12}(\hat{q})\vec{q}^{\,2}}{\vec{q}^{\,2}+m_{ps}^2}\right]e^{i\vec{q}\cdot\vec{r}}\\
&\quad= -c_{ps}\int\frac{d^3q}{(2\pi)^3}\frac{S_{12}(\hat{q})\vec{q}^{\,2}}{\vec{q}^{\,2}+m_{ps}^2}4\pi\sum_l i^l j_l(qr)Y_l^*(\hat{q})\cdot Y_l(\hat{r})\\
&\quad= \frac{c_{ps}}{2\pi^2}S_{12}(\hat{r})\int_0^{\infty}dq\frac{q^4}{q^2+m_{ps}^2}j_2(qr)\\
&\quad= \frac{c_{ps}}{4\pi^2 r^3}S_{12}(\hat{r})\int_{-\infty}^{\infty}dq\frac{\left(3-(qr)^2\right)q\sin qr - 3q^2 r\cos qr}{q^2+m_{ps}^2}\,.
\end{aligned} \tag{B.80}$$

This is calculated by the complex integral as

$$\oint_C dz\left[\frac{\left(3-(zr)^2\right)ze^{izr}}{q^2+m^2} - \frac{3q^2re^{izr}}{q^2+m^2}\right] = 2\pi i\left[\frac{3+m^2r^2}{2} - i\frac{3mr}{2}\right]e^{-mr} \tag{B.81}$$

Therefore, the third term in Eq.(B.73) is obtained as

$$c_{ps}\int\frac{d^3q}{(2\pi)^3}\left[-\frac{S_{12}(\hat{q})\vec{q}^{\,2}}{\vec{q}^{\,2}+m_{ps}^2}\right]e^{i\vec{q}\cdot\vec{r}} = \frac{c_{ps}}{4\pi r^3}S_{12}(\hat{r})\left(3+3m_{ps}r+(m_{ps}r)^2\right)e^{-m_{ps}r}\,. \tag{B.82}$$

Finally, the pseudoscalar meson exchange potential without the form factor in the coordinate space is

$$\begin{aligned}
V_{ps}^{\rm PS}(r) =& \frac{c_{ps}}{4\pi}\left[(\vec{\sigma}_1\cdot\vec{\sigma}_2)\left(m_{ps}^2\frac{e^{-m_{ps}r}}{r} - \delta^{(3)}(\vec{r})\right)\right.\\
&\left. + S_{12}(\hat{r})\left(3+3m_{ps}r+(m_{ps}r)^2\right)\frac{e^{-m_{ps}r}}{r^3}\right]\,.
\end{aligned} \tag{B.83}$$

In a customary way, however, the δ function is omitted because the nucleons are kept apart due to the short-range repulsion.

The potential with the form factor can be calculated in a similar way. The potential in the momentum space is

$$V_{ps}^{\rm PS}(\vec{r}) = c_{ps}\int \frac{d^3q}{(2\pi)^3}\left[-\vec{\sigma}_1\cdot\vec{\sigma}_2 + \frac{(\vec{\sigma}_1\cdot\vec{\sigma}_2)m_{ps}^2}{\vec{q}^{\,2}+m_{ps}^2} - \frac{S_{12}(\hat{q})\vec{q}^{\,2}}{\vec{q}^{\,2}+m_{ps}^2}\right]\left(\frac{\Lambda_{ps}^2-m_{ps}^2}{\Lambda_{ps}^2+\vec{q}^{\,2}}\right)^2 e^{i\vec{q}\cdot\vec{r}}\,. \tag{B.84}$$

The first term in Eq. (B.84) is written as

$$-c_{ps}(\vec{\sigma}_1\cdot\vec{\sigma}_2)\int\frac{d^3q}{(2\pi)^3}\left(\frac{\Lambda_{ps}^2-m_{ps}^2}{\Lambda_{ps}^2+\vec{q}^{\,2}}\right)^2 e^{i\vec{q}\cdot\vec{r}} = -(\vec{\sigma}_1\cdot\vec{\sigma}_2)\frac{c_{ps}}{4\pi}(\Lambda_{ps}^2-m_{ps}^2)^2\frac{e^{-\Lambda_{ps}r}}{2\Lambda_{ps}}\,. \tag{B.85}$$

The second term in Eq. (B.84) is

$$\begin{aligned} &c_{ps}\int\frac{d^3q}{(2\pi)^3}\left[\frac{(\vec{\sigma}_1\cdot\vec{\sigma}_2)m_{ps}^2}{\vec{q}^{\,2}+m_{ps}^2}\right]\left(\frac{\Lambda_{ps}^2-m_{ps}^2}{\Lambda_{ps}^2+\vec{q}^{\,2}}\right)^2 e^{i\vec{q}\cdot\vec{r}} \\ &= c_{ps}(\vec{\sigma}_1\cdot\vec{\sigma}_2)\frac{m_{ps}^2}{4\pi r}\left(e^{-m_{ps}r} - e^{-\Lambda_{ps}r} - \frac{r}{2\Lambda_{ps}}\left(\Lambda_{ps}^2-m_{ps}^2\right)e^{-\Lambda_{ps}r}\right)\,, \end{aligned} \tag{B.86}$$

where one uses

$$\frac{1}{q^2+m^2}\frac{\Lambda^2-m^2}{\Lambda^2+q^2} = \frac{1}{q^2+m^2} - \frac{1}{q^2+\Lambda^2}\,, \tag{B.87}$$

$$\frac{1}{q^2+m^2}\left(\frac{\Lambda^2-m^2}{\Lambda^2+q^2}\right) = \frac{1}{q^2+m^2} - \frac{1}{q^2+\Lambda^2} - \frac{\Lambda^2-m^2}{(q^2+\Lambda^2)^2}\,. \tag{B.88}$$

The third term in Eq. (B.84) is

$$\begin{aligned} &c_{ps}\int\frac{d^3q}{(2\pi)^3}\left[-\frac{S_{12}(\hat{q})\vec{q}^{\,2}}{\vec{q}^{\,2}+m_{ps}^2}\right]\left(\frac{\Lambda_{ps}^2-m_{ps}^2}{\Lambda_{ps}^2+\vec{q}^{\,2}}\right)^2 e^{i\vec{q}\cdot\vec{r}} \\ &= \frac{c_{ps}}{4\pi r^3}S_{12}(\hat{r})\left[\left(3+3m_{ps}r+(m_{ps}r)^2\right)e^{-m_{ps}r} - \left(3+3\Lambda_{ps}r+(\Lambda_{ps}r)^2\right)e^{-\Lambda_{ps}r}\right. \\ &\quad \left. + \frac{m_{ps}^2-\Lambda_{ps}^2}{2}\left(1+\Lambda_{ps}r\right)r^2e^{-\Lambda_{ps}r}\right] \end{aligned} \tag{B.89}$$

Let us summarize the pseudoscalar meson exchange potential in the coordinate space. This is given as

$$V_{ps}^{PS}(r) = \frac{g_{psNN}^2}{4\pi}\frac{1}{12m_N^2}\left[\vec{\sigma}_1\cdot\vec{\sigma}_2\left(m_{ps}^2Y(r)-D(r)\right)+S_{12}(\hat{r})Z(r)\right]\,, \tag{B.90}$$

where

$$D(r) = \begin{cases} 4\pi\delta^{(3)}(\vec{r}) & \text{(without form factor)} \\ \left(\Lambda_{ps}^2-m_{ps}^2\right)^2\dfrac{e^{-\Lambda_{ps}r}}{2\Lambda_{ps}} & \text{(with form factor)} \end{cases}\,, \tag{B.91}$$

$$Y(r) = \begin{cases} \dfrac{e^{-m_{ps}r}}{r} & \text{(without form factor)} \\ \dfrac{e^{-m_{ps}r}}{r} - \dfrac{e^{-\Lambda_{ps}r}}{r} - \dfrac{\left(\Lambda_{ps}^2 - m_{ps}^2\right)}{2\Lambda} e^{-\Lambda_{ps}r} & \text{(with form factor)} \end{cases} , \tag{B.92}$$

$$Z(r) = \begin{cases} \left(3 + 3m_{ps}r + (m_{ps}r)^2\right) \dfrac{e^{-m_{ps}r}}{r^3} & \text{(without form factor)} \\ \left(3 + 3m_{ps}r + (m_{ps}r)^2\right) \dfrac{e^{-m_{ps}r}}{r^3} - \left(3 + 3\Lambda_{ps}r + (\Lambda_{ps}r)^2\right) \dfrac{e^{-\Lambda_{ps}r}}{r^3} \\ + \dfrac{m_{ps}^2 - \Lambda_{ps}^2}{2} \left(1 + \Lambda_{ps}r\right) \dfrac{e^{-\Lambda_{ps}r}}{r} & \text{(with form factor)} \end{cases} \tag{B.93}$$

The potential for isovector mesons is obtained by inserting the isospin factor $\vec{\tau}_1 \cdot \vec{\tau}_2$.

(i−2) Pseudoscalar meson exchange potential (Pseudovector coupling)
The potential for the pseudovector coupling is also yielded in the same manner as the pseudoscalar coupling. When the static approximation is applied, the local potential is provided from Eq. (B.59) as

$$\begin{aligned} \bar{V}_{ps}^{\mathrm{PV}}(q) &= i \times (-1) \left(\frac{g_{psNN}}{2m_N}\right)^2 \bar{u}_1(p')\gamma^5\gamma^\mu u_1(p)\partial_\mu \psi^{(ps)} \bar{u}_2(-p')\gamma^5\gamma^\nu u_2(-p)\partial_\nu \psi^{(ps)} \\ &= \left(\frac{g_{psNN}}{2m_N}\right)^2 \bar{u}_1(p')\gamma^5\gamma^\mu u_1(p) q_\mu \bar{u}_2(-p')\gamma^5\gamma^\nu u_2(-p) q_\nu \frac{1}{q^2 - m_{ps}^2} \,. \end{aligned} \tag{B.94}$$

In Eq. (B.94), the term with $\mu = \nu = 0$ is obtained by

$$\begin{aligned} &\left(\frac{g_{psNN}}{2m_N}\right)^2 \bar{u}_1(p')\gamma^5\gamma^0 u_1(p) q_0 \bar{u}_2(-p')\gamma^5\gamma^0 u_2(-p) q_0 \frac{1}{q^2 - m_{ps}^2} \\ &= \left(\frac{g_{psNN}}{2m_N}\right)^2 \left(\frac{\vec{\sigma}_1 \cdot \vec{p}\,'}{2m_N} + \frac{\vec{\sigma}_1 \cdot \vec{p}}{2m_N}\right) q_0 \left(-\frac{\vec{\sigma}_2 \cdot \vec{p}\,'}{2m_N} - \frac{\vec{\sigma}_2 \cdot \vec{p}}{2m_N}\right) q_0 \frac{i}{q^2 - m_{ps}^2} \\ &\cong 0 \,. \end{aligned} \tag{B.95}$$

The term with $\mu = i$ and $\nu = j$ $(i, j = 1, 2, 3)$ is also calculated by

$$\begin{aligned} &\left(\frac{g_{psNN}}{2m_N}\right)^2 \bar{u}_1(p')\gamma^5\gamma^i u_1(p) q_i \bar{u}_2(-p')\gamma^5\gamma^j u_2(-p) q_j \frac{1}{q^2 - m_{ps}^2} \\ &= \left(\frac{g_{psNN}}{2m_N}\right)^2 \left(-\frac{\vec{\sigma}_1 \cdot \vec{p}\,'}{2m_N}\sigma_1^i \frac{\vec{\sigma}_1 \cdot \vec{p}}{2m_N} - \sigma_1^i\right) q_i \left(-\frac{\vec{\sigma}_2 \cdot \vec{p}\,'}{2m_N}\sigma_2^j \frac{\vec{\sigma}_2 \cdot \vec{p}}{2m_N} - \sigma_2^j\right) q_j \frac{1}{q^2 - m_{ps}^2} \\ &\cong -\left(\frac{g_{psNN}}{2m_N}\right)^2 \frac{\vec{\sigma}_1 \cdot \vec{q}\,\vec{\sigma}_2 \cdot \vec{q}}{\vec{q}^{\,2} + m_{ps}^2} \,. \end{aligned} \tag{B.96}$$

From Eqs. (B.95) and (B.96), therefore, we obtain the local potential for pseudovector coupling;

$$V_{ps}^{\rm PV}(\vec{q}) = -\left(\frac{g_{psNN}}{2m_N}\right)^2 \frac{\vec{\sigma}_1\cdot\vec{q}\,\vec{\sigma}_2\cdot\vec{q}}{\vec{q}^{\,2}+m_{ps}^2}\,F^2(\vec{q};\Lambda_{ps}) \tag{B.97}$$

$$= \left(\frac{g_{psNN}}{2m_N}\right)^2 \frac{1}{3}\left[-\vec{\sigma}_1\cdot\vec{\sigma}_2 + \frac{\vec{\sigma}_1\cdot\vec{\sigma}_2 m_{ps}^2}{\vec{q}^{\,2}+m_{ps}^2} - \frac{S_{12}(\hat{q})\vec{q}^{\,2}}{\vec{q}^{\,2}+m_{ps}^2}\right] F^2(\vec{q};\Lambda_{ps})\,. \tag{B.98}$$

As seen in Eqs. (B.70) and (B.98), pseudoscalar and pseudovector couplings, $\mathcal{L}_{psNN}^{\rm PS}$ and $\mathcal{L}_{psNN}^{\rm PV}$, yield same result on-shell, while chiral symmetry is held when the pseudovector coupling is used. The $V_{ps}^{\rm PV}(r)$ is the same as $V_{ps}^{\rm PS}(r)$ in Eq. (B.90).

(ii) Vector meson exchange potential

The local vector meson exchange potential is obtained by Eq. (B.60),

$$\begin{aligned}
-i\bar{V}_v(q) =& -\left(g_{vNN}\bar{u}_1(p')\gamma^\mu\vec{\tau}_1 u_1(p)\cdot\vec{\phi}_\mu^{(v)} + \frac{f_{vNN}}{2m_N}\bar{u}_1(p')\sigma^{\mu\nu}u_1(p)\vec{\tau}_1\cdot\partial_\mu\vec{\phi}_\nu^{(v)}\right)\\
&\times\left(g_{vNN}\bar{u}_2(-p')\gamma^\alpha\vec{\tau}_2 u_2(-p)\cdot\vec{\phi}_\alpha^{(v)} + \frac{f_{vNN}}{2m_N}\bar{u}_2(-p')\sigma^{\alpha\beta}u_2(-p)\vec{\tau}_2\cdot\partial_\alpha\vec{\phi}_\beta^{(v)}\right)\\
=& -g_{vNN}^2\bar{u}_1(p')\gamma^\mu\vec{\tau}_1 u_1(p)\cdot\vec{\phi}_\mu^{(v)}\bar{u}_2(-p')\gamma^\alpha\vec{\tau}_2 u_2(-p)\cdot\vec{\phi}_\alpha^{(v)}\\
&-\frac{g_{vNN}f_{vNN}}{2m_N}\Big(\bar{u}_1(p')\gamma^\mu\vec{\tau}_1 u_1(p)\cdot\vec{\phi}_\mu^{(v)}\bar{u}_2(-p')\sigma^{\alpha\beta}u_2(-p)\vec{\tau}_2\cdot\partial_\alpha\vec{\phi}_\beta^{(v)}\\
&+\bar{u}_1(p')\sigma^{\mu\nu}u_1(p)\vec{\tau}_1\cdot\partial_\mu\vec{\phi}_\nu^{(v)}\bar{u}_2(-p')\gamma^\alpha\vec{\tau}_2 u_2(-p)\cdot\vec{\phi}_\alpha^{(v)}\Big)\\
&-\left(\frac{f_{vNN}}{2m_N}\right)^2\bar{u}_1(p')\sigma^{\mu\nu}u_1(p)\vec{\tau}_1\cdot\partial_\mu\vec{\phi}_\nu^{(v)}\bar{u}_2(-p')\sigma^{\alpha\beta}u_2(-p)\vec{\tau}_2\cdot\partial_\alpha\vec{\phi}_\beta^{(v)}
\end{aligned} \tag{B.99}$$

First term in Eq. (B.99) is calculated as follows. With $\mu=\alpha=0$, one obtains

$$\begin{aligned}
&-g_{vNN}^2\bar{u}_1(p')\gamma^0 u_1(p)\bar{u}_2(-p')\gamma^0 u_2(-p)\frac{-i}{q^2-m_v^2}\vec{\tau}_1\cdot\vec{\tau}_2\\
&= -g_{vNN}^2\left(1+\frac{\vec{\sigma}_1\cdot\vec{p}\,'\vec{\sigma}_1\cdot\vec{p}}{(2m_N)^2}\right)\left(1+\frac{\vec{\sigma}_2\cdot\vec{p}\,'\vec{\sigma}_2\cdot\vec{p}}{(2m_N)^2}\right)\frac{-i}{q^2-m_v^2}\vec{\tau}_1\cdot\vec{\tau}_2\\
&\cong \frac{-ig_{vNN}^2}{\vec{q}^{\,2}+m_v^2}\left[1+\frac{\vec{\sigma}_1\cdot\vec{p}\,'\vec{\sigma}_1\cdot\vec{p}}{(2m_N)^2}+\frac{\vec{\sigma}_2\cdot\vec{p}\,'\vec{\sigma}_2\cdot\vec{p}}{(2m_N)^2}\right]\vec{\tau}_1\cdot\vec{\tau}_2\\
&= \frac{-ig_{vNN}^2}{\vec{q}^{\,2}+m_v^2}\left[1+\frac{\vec{k}^{\,2}}{2m_N^2}-\frac{\vec{q}^{\,2}}{8m_N^2}+\frac{i}{2m_N^2}\vec{S}\cdot\left(\vec{q}\times\vec{k}\right)\right]\vec{\tau}_1\cdot\vec{\tau}_2\,,
\end{aligned} \tag{B.100}$$

where $\vec{k} = (\vec{p}\,' + \vec{p})/2$ and $\vec{S} = (\vec{\sigma}_1 + \vec{\sigma}_2)/2$, and one uses

$$\begin{cases} \vec{p}\,' = \vec{k} + \vec{q}/2 \\ \vec{p} = \vec{k} - \vec{q}/2 \end{cases} , \tag{B.101}$$

$$\vec{\sigma}\cdot\vec{p}\,'\vec{\sigma}\cdot\vec{p} = \vec{p}\,'\cdot\vec{p} + i\sigma\cdot(\vec{p}\,'\times\vec{p}) = \vec{k}^{\,2} - \vec{q}^{\,2}/4 + i\sigma\cdot\left(\vec{q}\times\vec{k}\right) , \tag{B.102}$$

$$\bar{u}(p')\gamma^0 u(p) = 1 + \frac{\vec{\sigma}\cdot\vec{p}\,'\vec{\sigma}\cdot\vec{p}}{(2m_N)^2} . \tag{B.103}$$

With $\mu = i$ and $\alpha = j$,

$$\begin{aligned} & - g_{vNN}^2 \bar{u}_1(p')\gamma^i u_1(p)\bar{u}_2(-p')\gamma^j u_2(-p)\frac{i\delta_{ij}}{q^2 - m_v^2}\vec{\tau}_1\cdot\vec{\tau}_2 \\ & = \frac{g_{vNN}^2}{(2m_N)^2}\left(2k^i + i\left(\vec{\sigma}_1\times\vec{q}\right)^i\right)\left(2k^i + i\left(\vec{\sigma}_2\times\vec{q}\right)^i\right)\frac{i}{q^2 - m_v^2}\vec{\tau}_1\cdot\vec{\tau}_2 \\ & = \frac{g_{vNN}^2}{(2m_N)^2}\left[4\vec{k}^{\,2} + 2i\vec{k}\cdot\left(\vec{\sigma}_1\times\vec{q}\right)2i\vec{k}\cdot\left(\vec{\sigma}_2\times\vec{q}\right) - \left(\vec{\sigma}_1\times\vec{q}\right)\left(\vec{\sigma}_2\times\vec{q}\right)\right]\frac{i}{q^2 - m_v^2}\vec{\tau}_1\cdot\vec{\tau}_2 \\ & = \frac{-ig_{vNN}^2}{\vec{q}^{\,2} + m_v^2}\left[\frac{\vec{k}^{\,2}}{m_N^2} + \frac{i}{m_N^2}\vec{S}\cdot\left(\vec{q}\times\vec{k}\right) - \frac{1}{4m_N^2}\vec{\sigma}_1\cdot\vec{\sigma}_2\vec{q}^{\,2} + \frac{1}{4m_N^2}\vec{\sigma}_1\cdot\vec{q}\,\vec{\sigma}_2\cdot\vec{q}\right]\vec{\tau}_1\cdot\vec{\tau}_2 , \end{aligned} \tag{B.104}$$

where these formulas are uesd,

$$\sigma^j p^j \sigma^i = p^i + i\varepsilon^{jik}\sigma^k p^j = p^i + i\left(\vec{\sigma}\times\vec{p}\right)_i , \tag{B.105}$$

$$\sigma^i \sigma^j p^j = p^i + i\varepsilon^{ijk}\sigma^k p^j = p^i - i\left(\vec{\sigma}\times\vec{p}\right)_i , \tag{B.106}$$

$$\left(\vec{\sigma}_1\times\vec{q}\right)\cdot\left(\vec{\sigma}_2\times\vec{q}\right) = \vec{\sigma}_1\cdot\vec{\sigma}_2\vec{q}^{\,2} - \vec{\sigma}_1\cdot\vec{q}\,\vec{\sigma}_2\cdot\vec{q}, \tag{B.107}$$

and

$$\bar{u}(p')\gamma^i u(p) = \left(\frac{\vec{\sigma}\cdot\vec{p}\,'}{2m_N}\sigma^i + \sigma^i\frac{\vec{\sigma}\cdot\vec{p}}{2m_N}\right) = \frac{1}{2m_N}\left(2k^i + i\left(\vec{\sigma}\times\vec{q}\right)^i\right) , \tag{B.108}$$

$$\bar{u}(-p')\gamma^i u(-p) = -\frac{1}{2m_N}\left(2k^i + i\left(\vec{\sigma}\times\vec{q}\right)^i\right) . \tag{B.109}$$

From Eqs. (B.100) and (B.104), the first term in Eq. (B.99) is obtained by

$$\begin{aligned} & \frac{-ig_{vNN}^2}{\vec{q}^{\,2} + m_v^2}\left[1 + \frac{3\vec{k}^{\,2}}{2m_N^2} - \frac{\vec{q}^{\,2}}{8m_N^2} + \frac{3i}{2m_N^2}\vec{S}\cdot\left(\vec{q}\times\vec{k}\right) - \frac{1}{4m_N^2}\vec{\sigma}_1\cdot\vec{\sigma}_2\vec{q}^{\,2}\right. \\ & \qquad \left. + \frac{1}{4m_N^2}\vec{\sigma}_1\cdot\vec{q}\,\vec{\sigma}_2\cdot\vec{q}\right]\vec{\tau}_1\cdot\vec{\tau}_2 \\ = & \frac{-ig_{vNN}^2}{\vec{q}^{\,2} + m_v^2}\left[1 + \frac{3\vec{k}^{\,2}}{2m_N^2} - \frac{\vec{q}^{\,2}}{8m_N^2} + \frac{3i}{2m_N^2}\vec{S}\cdot\left(\vec{q}\times\vec{k}\right) - \frac{1}{6m_N^2}\vec{\sigma}_1\cdot\vec{\sigma}_2\vec{q}^{\,2}\right. \\ & \qquad \left. + \frac{1}{12m_N^2}S_{12}(\hat{q})\vec{q}^{\,2}\right]\vec{\tau}_1\cdot\vec{\tau}_2 . \end{aligned} \tag{B.110}$$

Second term in Eq. (B.99) is given in a similar way. When $\mu = \beta = 0$ and $\alpha = i$,

$$\begin{aligned}
&\frac{g_{vNN}f_{vNN}}{2m_N}\left[\left(1+\frac{\vec{\sigma}_1\cdot\vec{p}\,'\vec{\sigma}_1\cdot\vec{p}}{(2m_N)^2}\right)\bar{u}_2(-p')\gamma^0\gamma^i u_2(-p)q_i\right.\\
&\left.+\,\bar{u}_1(p')\gamma^0\gamma^i u_1(p)(-q_i)\left(1+\frac{\vec{\sigma}_2\cdot\vec{p}\,'\vec{\sigma}_2\cdot\vec{p}}{(2m_N)^2}\right)\right]\frac{-i}{q^2-m_v^2}\vec{\tau}_1\cdot\vec{\tau}_2\\
&\cong\frac{ig_{vNN}f_{vNN}}{\vec{q}^{\,2}+m_v^2}\left[\frac{\vec{q}^{\,2}}{2m_N^2}-\frac{i}{m_N^2}\vec{S}\cdot\left(\vec{q}\times\vec{k}\right)\right]\vec{\tau}_1\cdot\vec{\tau}_2\,,
\end{aligned}\tag{B.111}$$

where

$$\bar{u}(p')\gamma^0\gamma^i u(p)=\left(-\frac{\vec{\sigma}\cdot\vec{p}\,'}{2m_N}\sigma^i+\sigma^i\frac{\vec{\sigma}\cdot\vec{p}}{2m_N}\right)=-\frac{1}{2m_N}\left[q^i+2i\left(\vec{\sigma}\times\vec{k}\right)^i\right]\,,\tag{B.112}$$

$$\bar{u}(-p')\gamma^0\gamma^i u(-p)=\frac{1}{2m_N}\left[q^i+2i\left(\vec{\sigma}\times\vec{k}\right)^i\right]\,.\tag{B.113}$$

When $\mu = i$, $\alpha = j$ and $\beta = l$, the second term in Eq. (B.99) is written by

$$\begin{aligned}
&-\frac{g_{vNN}f_{vNN}}{2m_N}\left(\frac{2k^i+i\left(\vec{\sigma_1}\times\vec{q}\right)^i}{2m_N}\varepsilon^{jlk}\sigma^k(-iq_j)-\varepsilon^{jlk}\sigma^k(iq_j)\frac{2k^i+i\left(\vec{\sigma_2}\times\vec{q}\right)^i}{2m_N}\right)\\
&\quad\times\frac{i\delta_{il}}{q^2-m_v^2}\vec{\tau}_1\cdot\vec{\tau}_2\\
&=\frac{g_{vNN}f_{vNN}}{(2m_N)^2}\left(2(\vec{\sigma}_1+\vec{\sigma}_2)\cdot(\vec{q}\times\vec{k}\,)+2i(\vec{\sigma}_1\times\vec{q}\,)\cdot(\vec{\sigma}_2\times\vec{q}\,)\right)\frac{1}{\vec{q}^{\,2}+m_v^2}\vec{\tau}_1\cdot\vec{\tau}_2\\
&=\frac{ig_{vNN}f_{vNN}}{\vec{q}^{\,2}+m_v^2}\left(\frac{-i}{m_N^2}\vec{S}\cdot(\vec{q}\times\vec{k}\,)+\frac{1}{2m_N^2}\left(\vec{\sigma}_1\cdot\vec{\sigma}_2\vec{q}^{\,2}-\vec{\sigma}_1\cdot\vec{q}\,\vec{\sigma}_2\cdot\vec{q}\right)\right)\vec{\tau}_1\cdot\vec{\tau}_2\,,
\end{aligned}\tag{B.114}$$

where one uses

$$\bar{u}(p')\gamma^i\gamma^j u(p)\cong-\sigma^i\sigma^j=-\delta^{jl}-i\varepsilon^{ijk}\sigma^k\,,\tag{B.115}$$

$$\bar{u}(p')\sigma^{ij}u(p)=i\bar{u}(p')\left(\gamma^i\gamma^j+\delta^{ij}\right)u(p)\cong\varepsilon^{ijk}\sigma^k\,.\tag{B.116}$$

From Eqs. (B.111) and (B.114), the second term in Eq. (B.99) is given by

$$\begin{aligned}
&\frac{-i}{\vec{q}^{\,2}+m_v^2}\frac{g_{vNN}f_{vNN}}{2m_N^2}\left[-\vec{q}^{\,2}+4i\vec{S}\cdot\left(\vec{q}\times\vec{k}\right)-\vec{\sigma}_1\cdot\vec{\sigma}_2\vec{q}^{\,2}+\vec{\sigma}_1\cdot\vec{q}\,\vec{\sigma}_2\cdot\vec{q}\right]\vec{\tau}_1\cdot\vec{\tau}_2\\
&=\frac{-i}{\vec{q}^{\,2}+m_v^2}\frac{g_{vNN}f_{vNN}}{2m_N^2}\left[-\vec{q}^{\,2}+4i\vec{S}\cdot\left(\vec{q}\times\vec{k}\right)-\frac{2}{3}\vec{\sigma}_1\cdot\vec{\sigma}_2\vec{q}^{\,2}+\frac{1}{3}S_{12}(\hat{q})\vec{q}^{\,2}\right]\vec{\tau}_1\cdot\vec{\tau}_2\,.
\end{aligned}\tag{B.117}$$

Finally, the third term in Eq. (B.99) is calculated. When $\mu = i$, $\nu = j$, $\alpha = l$ and

$\beta = m$,

$$
\begin{aligned}
&- \left(\frac{f_{vNN}}{2m_N}\right)^2 \bar{u}_1(p')\sigma^{ij}u_1(p)\vec{\tau}_1\cdot\partial_i\vec{\phi}^{(v)}_j\bar{u}_2(-p')\sigma^{lm}u_2(-p)\vec{\tau}_2\cdot\partial_l\vec{\phi}^{(v)}_m \\
&= \frac{i}{\vec{q}^2+m_v^2}\left(\frac{f_{vNN}}{2m_N}\right)^2(\vec{\sigma}_1\times\vec{q})\cdot(\vec{\sigma}_2\times\vec{q})\,\vec{\tau}_1\cdot\vec{\tau}_2 \\
&= \frac{-i}{\vec{q}^2+m_v^2}\left(\frac{f_{vNN}}{2m_N}\right)^2\left[-\vec{\sigma}_1\cdot\vec{\sigma}_2\,\vec{q}^{\,2}+\vec{\sigma}_1\cdot\vec{q}\,\vec{\sigma}_2\cdot\vec{q}\right]\vec{\tau}_1\cdot\vec{\tau}_2 \\
&= \frac{-i}{\vec{q}^2+m_v^2}\left(\frac{f_{vNN}}{2m_N}\right)^2\left[-\frac{2}{3}\vec{\sigma}_1\cdot\vec{\sigma}_2\,\vec{q}^{\,2}+\frac{1}{3}S_{12}(\hat{q})\vec{q}^{\,2}\right]\vec{\tau}_1\cdot\vec{\tau}_2\,. \qquad \text{(B.118)}
\end{aligned}
$$

From Eqs. (B.110), (B.117) and (B.118), the local vector meson exchange potential is obtained as

$$
\begin{aligned}
V_v(\vec{q}) = \Bigg\{ & g_{vNN}^2\left[1+\frac{3\vec{k}^{\,2}}{2m_N^2}-\frac{\vec{q}^{\,2}}{8m_N^2}+\frac{3i}{2m_N^2}\vec{S}\cdot\left(\vec{q}\times\vec{k}\right)-\frac{1}{6m_N^2}\vec{\sigma}_1\cdot\vec{\sigma}_2\vec{q}^{\,2}+\frac{1}{4m_N^2}S_{12}(\hat{q})\vec{q}^{\,2}\right] \\
& + \frac{g_{vNN}f_{vNN}}{2m_N^2}\left[-\vec{q}^{\,2}+4i\vec{S}\cdot\left(\vec{q}\times\vec{k}\right)-\frac{2}{3}\vec{\sigma}_1\cdot\vec{\sigma}_2\vec{q}^{\,2}+\frac{1}{3}S_{12}(\hat{q})\vec{q}^{\,2}\right] \\
& \left(\frac{f_{vNN}}{2m_N}\right)^2\left[-\frac{2}{3}\vec{\sigma}_1\cdot\vec{\sigma}_2\vec{q}^{\,2}+\frac{1}{3}S_{12}(\hat{q})\vec{q}^{\,2}\right]\Bigg\}\frac{-i}{\vec{q}^{\,2}+m_v^2}\vec{\tau}_1\cdot\vec{\tau}_2 \qquad \text{(B.119)}
\end{aligned}
$$

The potential in the coordinate space is given by the Fourier transformation as seen in the pseudoscalar meson exchange potential. One obtains

$$
\begin{aligned}
V_v(r) = & \frac{g_{vNN}^2}{4\pi}\frac{1}{2m_N^2}\left[-\left(1+\frac{1}{3}\vec{\sigma}_1\cdot\vec{\sigma}_2\right)D(r)+\left(2m_N^2+m_v^2+\frac{1}{3}m_v^2\vec{\sigma}_1\cdot\vec{\sigma}_2\right)Y(r)\right. \\
& \left.-3\vec{L}\cdot\vec{S}Z_1(r)-\frac{3}{2}\left(\nabla^2Y(r)+Y(r)\nabla^2\right)-\frac{1}{6}S_{12}(\hat{r})Z(r)\right] \\
& + \frac{g_{vNN}f_{vNN}}{4\pi}\frac{1}{2m_N^2}\left[-\left(1+\frac{2}{3}\vec{\sigma}_1\cdot\vec{\sigma}_2\right)D(r)+\left(m_v^2+\frac{2}{3}m_v^2\vec{\sigma}_1\cdot\vec{\sigma}_2\right)Y(r)\right. \\
& \left.-4\vec{L}\cdot\vec{S}Z_1(r)-\frac{1}{3}S_{12}(\hat{r})Z(r)\right] \\
& + \frac{f_{vNN}^2}{4\pi}\frac{1}{4m_N^2}\left[-\frac{2}{3}\vec{\sigma}_1\cdot\vec{\sigma}_2D(r)+\frac{2}{3}m_v^2\vec{\sigma}_1\cdot\vec{\sigma}_2Y(r)-\frac{1}{3}S_{12}(\hat{r})Z(r)\right], \qquad \text{(B.120)}
\end{aligned}
$$

where

$$
Z_1(r) = \begin{cases} (1+m_vr)\dfrac{e^{-m_vr}}{r^3} & \text{(without form factor)} \\ (1+m_vr)\dfrac{e^{-m_vr}}{r^3}-\left(1+\Lambda_vr+\dfrac{\Lambda_v^2-m_v^2}{2}r^2\right)e^{-\Lambda_vr} & \text{(with form factor)} \end{cases}. \qquad \text{(B.121)}
$$

(iii) Scalar meson exchange potential
The amplitude of local scalar meson exchange potential is calculated by Eq. (B.61),

$$\begin{aligned} -i\bar{V}(\vec{q}) &= -g_s^2 \bar{u}_1(p') u_1(p) \bar{u}_2(-p') u_2(-p) \frac{i}{q^2 - m_s^2} \\ &\cong -g_s^2 \left(1 - \frac{\vec{\sigma}_1 \cdot \vec{p}' \vec{\sigma}_2 \cdot \vec{p}}{(2m_N)^2} - \frac{\vec{\sigma}_2 \cdot \vec{p}' \vec{\sigma}_2 \cdot \vec{p}}{(2m_N)^2} \right) \frac{i}{q^2 - m_s^2} \\ &= \frac{i g_s^2}{\vec{q}^{\,2} + m_s^2} \left[1 - \frac{\vec{k}^{\,2}}{2m_N^2} + \frac{\vec{q}^{\,2}}{8m_N^2} - \frac{i}{2m_N^2} \vec{S} \cdot \left(\vec{q} \times \vec{k} \right) \right] . \end{aligned} \tag{B.122}$$

Therefore, the local scalar meson exchange potential is

$$V_s(\vec{q}) = -\frac{g_s^2}{\vec{q}^{\,2} + m_s^2} \left[1 - \frac{\vec{k}^{\,2}}{2m_N^2} + \frac{\vec{q}^{\,2}}{8m_N^2} - \frac{i}{2m_N^2} \vec{S} \cdot \left(\vec{q} \times \vec{k} \right) \right] . \tag{B.123}$$

The potential in the coordinate space is

$$\begin{aligned} V_s(r) = -\frac{g_s^2}{4\pi} \Bigg[& \left(1 - \frac{1}{4} \left(\frac{m_s}{m_N} \right)^2 \right) Y(r) + \frac{1}{4m_N^2} \left(\nabla^2 Y(r) + Y(r) \nabla^2 \right) \\ & + \frac{1}{2m_N^2} \vec{L} \cdot \vec{S} Z_1(r) \Bigg] \end{aligned} \tag{B.124}$$

B.3.3 Agronne Potential

In this section, the Argonne v_{18} and v_8' potentials are reviewed. The Argonne v_{18} potential (AV18) is high-quality nucleon-nucleon potential developed by the Argonne group in 1995 [149]. This potential is constructed by one pion exchange part and short range force with 18 operators; 14 charge independent operators, additional three charge dependent and one charge asymmetry operators. The AV18 includes 40 parameters which was fitted to the Nijmegen NN scattering data for pp and np in the range $0 - 350$ MeV.

The Argonne v_8' potential (AV8′) is fairly realistic NN potential which is the simplified version of AV18. The AV8′ is formed by a sum of 8 operators and hence it can avoid to have large static errors rather than AV18. However, the AV8′ is a little more attractive than the AV18 as discussed in Refs. [148, 151].

For nuclear systems with nucleon numbers more than three, the AV8′ is more attractive than the AV18, while the AV8′ is able to reproduce the deuteron properties. The difference between the AV8′ and AV18 is about 0.15 MeV for triton (^{3}H) and about 1 MeV for ^{4}He [148, 150].

B.3.3.1 Argonne v_{18} potential (AV18)

The AV18 contains (i) one pion exchange potential, (ii) a charge independent part as discussed in the Argonne v_{14} potential [188], and (iii) a charge independence breaking

part which involves three charge dependent and one charge asymmetry operators [149]. In this section, one pion exchange and charge independent parts are shown, while the charge independence breaking part is skipped.

(i) One pion exchange potential
The pion exchange potential terms having a charge dependence structure are given by

$$v^{\pi}(pp) = f_{pp}^2 v_{\pi}(m_{\pi^0}) \,, \tag{B.125}$$

$$v^{\pi}(np) = f_{pp} f_{nn} v_{\pi}(m_{\pi^0}) + (-1)^{T+1} 2 f_c^2 v_{\pi}(m_{\pi^\pm}) \,, \tag{B.126}$$

$$v^{\pi}(nn) = f_{nn}^2 v_{\pi}(m_{\pi^0}) \,, \tag{B.127}$$

where T is the total isospin and

$$v_{\pi}(m) = \left(\frac{m}{m_{\pi^\pm}}\right)^2 \frac{m}{3} \left[\vec{\sigma}_1 \cdot \vec{\sigma}_2 Y_m(r) + S_{12} T_m(r)\right] \,. \tag{B.128}$$

The Yukawa function Y_m and tensor function T_m are written by

$$Y_m(r) = \frac{e^{-mr}}{mr} \left(1 - e^{-cr^2}\right) \,, \tag{B.129}$$

$$T_m(r) = \left(1 + \frac{3}{mr} + \frac{3}{(mr)^3} +\right) \frac{e^{-mr}}{mr} \left(1 - e^{-cr^2}\right)^2 \tag{B.130}$$

with smooth Gaussian cutoffs that make them vanish at $r = 0$, The cutoff parameter is taken to $c = 2.1$ fm^{-2}. The $\left(1 - e^{-cr^2}\right)^2$ in the T_m provides the effect of ρ meson exchange which is not included explicitly in the model [188]. The coupling constant f is chosen to be charge independent; $f = f_{pp} = -f_{nn}$ with the recommended value $f^2 = 0.075$ in the Nijmegen potential (Nijm93) [189]. This is in good agreement with the πNN coupling constant obtained by the Goldberger-Treiman relation [218–220] which is derived from the low energy theorem associated with the spontaneous breaking of chiral symmetry.

(ii) The charge independent part
The charge independent short- and intermediate-range parts are formed by central, L^2, tensor, spin-orbit (LS) and quadratic spin-orbit ($(LS)^2$) parts as labeled by $i = c$, $l2$, t, ls, $ls2$, respectively. The potentials in different total spin S and total isospin T states are given by

$$\begin{aligned} v_{ST}^{R}(NN) =& v_{ST,NN}^{c}(r) + v_{ST,NN}^{l2}(r) L^2 + v_{ST,NN}^{t}(r) S_{12} \\ &+ v_{ST,NN}^{ls}(r) \vec{L} \cdot \vec{S} + v_{ST,NN}^{ls}(r) (\vec{L} \cdot \vec{S})^2 \,, \end{aligned} \tag{B.131}$$

where

$$v_{ST,NN}^{i}(r) = I_{ST,NN}^{i} T_{\mu}^2(r) + \left[P_{ST,NN}^{i} + \mu r Q_{ST,NN}^{i} + (\mu r)^2 R_{ST,NN}^{i}\right] W(r) \,. \tag{B.132}$$

The parameters $I^i_{ST,NN}$, $P^i_{ST,NN}$, $Q^i_{ST,NN}$ and $R^i_{ST,NN}$ are determined by NN scattering data given in Ref. [188]. The Woods-Saxon function $W(r)$ produced the short range core is given as

$$W(r) = \left[1 + e^{(r-r_0)/a}\right]^{-1} \tag{B.133}$$

with $r_0 = 0.5$ fm and $a = 0.2$ fm.

These potentials in Eq. (B.131) can be projected as 14 operators:

$$v_{ij} = \sum_{p=1,14} v_p(r_{ij}) \mathcal{O}^P_{ij}\,, \tag{B.134}$$

where the operators $\mathcal{O}^{p=1,14}$ are expressed by

$$\begin{aligned}\mathcal{O}^{p=1,14}_{ij} =& 1,\ \vec{\tau}_i\cdot\vec{\tau}_j,\ \vec{\sigma}_i\cdot\vec{\sigma}_j,\ (\vec{\sigma}_i\cdot\vec{\sigma}_j)(\vec{\tau}_i\cdot\vec{\tau}_j),\ S_{ij},\ S_{ij}(\vec{\tau}_i\cdot\vec{\tau}_j),\ \vec{L}\cdot\vec{S},\ \vec{L}\cdot\vec{S}\vec{\tau}_i\cdot\vec{\tau}_j,\\ & L^2,\ L^2(\vec{\tau}_i\cdot\vec{\tau}_j),\ L^2(\vec{\sigma}_i\cdot\vec{\sigma}_j),\ L^2(\vec{\sigma}_i\cdot\vec{\sigma}_j)(\vec{\tau}_i\cdot\vec{\tau}_j),\ (\vec{L}\cdot\vec{S})^2,\ (\vec{L}\cdot\vec{S})^2(\vec{\tau}_i\cdot\vec{\tau}_j)\end{aligned} \tag{B.135}$$

which are denoted by c, τ, σ, $\sigma\tau$, t, $t\tau$, ls, $ls\tau$, $l2$, $l2\tau$, $l2\sigma$, $l2\sigma\tau$, $ls2$ and $ls2\tau$, respectively.

Let us consider to construct the potentials of c, τ, σ and $\sigma\tau$ parts from the potential $v^c_{ST,NN}$ in Eq. (B.131). The charge independent potential v^c_{ST} is introduced as

$$v^c_{S1} = \frac{1}{3}\left(v^c_{S1,pp} + v^c_{S1,nn} + v^c_{S1,np}\right), \quad v^c_{S0} = v^c_{S0,np}\,. \tag{B.136}$$

By using the relation

$$\begin{aligned}v^c_{ST} =& v_c + [2T(T+1) - 3]v_\tau + [2S(S+1) - 3]v_\sigma \\ & + [2S(S+1) - 3][2T(T+1) - 3]v_{\sigma\tau}\,,\end{aligned} \tag{B.137}$$

v_c, v_τ, v_σ and $v_{\sigma\tau}$ potentials are calculated as

$$v_c = \frac{1}{16}\left(9v^c_{11} + 3v^c_{10} + 3v^c_{01} + v^c_{00}\right)\,, \tag{B.138}$$

$$v_\tau = \frac{1}{16}\left(3v^c_{11} - 3v^c_{10} + v^c_{01} - v^c_{00}\right)\,, \tag{B.139}$$

$$v_\sigma = \frac{1}{16}\left(3v^c_{11} + v^c_{10} - 3v^c_{01} - v^c_{00}\right)\,, \tag{B.140}$$

$$v_{\sigma\tau} = \frac{1}{16}\left(v^c_{11} - v^c_{10} - v^c_{01} + v^c_{00}\right)\,. \tag{B.141}$$

In a similar way, the potentials v_{l2}, $v_{l2\tau}$, $v_{l2\sigma}$ and $v_{l2\sigma\tau}$ can be obtained by the the

L^2 part in Eq. (B.131):

$$v_{l2} = \frac{1}{16}\left(9v_{11}^{l2} + 3v_{10}^{l2} + 3v_{01}^{l2} + v_{00}^{l2}\right) , \tag{B.142}$$

$$v_{l2\tau} = \frac{1}{16}\left(3v_{11}^{l2} - 3v_{10}^{l2} + v_{01}^{l2} - v_{00}^{l2}\right) , \tag{B.143}$$

$$v_{l2\sigma} = \frac{1}{16}\left(3v_{11}^{l2} + v_{10}^{l2} - 3v_{01}^{l2} - v_{00}^{l2}\right) , \tag{B.144}$$

$$v_{l2\sigma\tau} = \frac{1}{16}\left(v_{11}^{l2} - v_{10}^{l2} - v_{01}^{l2} + v_{00}^{l2}\right) , \tag{B.145}$$

where

$$v_{S1}^{l2} = \frac{1}{3}\left(v_{S1,pp}^{l2} + v_{S1,nn}^{l2} + v_{S1,np}^{l2}\right) , \quad v_{S0}^{l2} = v_{S0,np}^{l2} . \tag{B.146}$$

The remaining S_{ij}, $\vec{L}\cdot\vec{S}$ and $(\vec{L}\cdot\vec{S})^2$ terms in Eq. (B.131) are rewritten as

$$v_x = \frac{1}{4}\left(3v_{11}^{x} + v_{10}^{x}\right) , \tag{B.147}$$

$$v_{x\tau} = \frac{1}{4}\left(v_{11}^{x} - v_{10}^{x}\right) , \quad (x = t,\, ls,\, ls2) \tag{B.148}$$

by the projection

$$v_{1T}^{x} = v_x + [2T(T+1) - 3]v_{x\tau} . \tag{B.149}$$

B.3.3.2 Argonne v_8' potential

The Argonne v_8' potential has more simply form than the Argonne v_{18} potential. This potential is written by a sum of the π exchange term given in Eqs. (B.125)-(B.127) and remaining terms having 8 operators:

$$v_8'(r) = v^{\pi}(r) + \sum_{P=1,8} v_P'(r)\mathcal{O}^P , \tag{B.150}$$

where

$$\mathcal{O}^{P=1,8} = [1, \vec{\sigma}_1\cdot\vec{\sigma}_2, S_{12}, \vec{L}\cdot\vec{S}] \otimes [1, \vec{\tau}_1\cdot\vec{\tau}_2] , \tag{B.151}$$

which are denoted by c, τ, σ, $\sigma\tau$, t, $t\tau$, ls and $ls\tau$. The function $v_P'(r)$ is determined such that it is equal to the AV18 in the all S- and P- waves, and ${}^3D_1$, namely ${}^1S_0$, ${}^3S_1$, ${}^3D_1$, ${}^1P_1$, ${}^3P_0$, ${}^3P_1$ and ${}^3P_2$ channels, and the ${}^3S_1 - {}^3D_1$ mixing term. Then we

obtain the eight equations:

$$({}^1S_0): \quad v'_c + v'_\tau - 3v'_\sigma - 3v'_{\sigma\tau} = v_c + v_\tau - 3v_\sigma - 3v_{\sigma\tau} \tag{B.152}$$

$$({}^3S_1): \quad v'_c - 3v'_\tau + v'_\sigma - 3v'_{\sigma\tau} = v_c - 3v_\tau + v_\sigma - 3v_{\sigma\tau}\,, \tag{B.153}$$

$$({}^3S_1 - {}^3D_1): \quad v'_t - 3v'_{t\tau} = v_t - 3v_{t\tau}\,, \tag{B.154}$$

$$\begin{aligned}({}^3D_1): \quad & v'_c - 3v'_\tau + v'_\sigma - 3v'_{\sigma\tau} - 2v'_t + 6v'_{t\tau} - 3v'_{ls} + 9v'_{ls\tau}\,, \\ & = v_c - 3v_\tau + v_\sigma - 3v_{\sigma\tau} - 2v_t + 6v_{t\tau} - 3v_{ls} + 9v_{ls\tau} \\ & \quad + 6v_{l2} - 18v_{l2\tau} + 6v_{l2\sigma} - 18v_{l2\sigma\tau} + 9v_{ls2} - 27v_{ls2\tau}\,,\end{aligned} \tag{B.155}$$

$$\begin{aligned}({}^1P_1): \quad & v'_c - 3v'_\tau - 3v'_\sigma + 9v'_{\sigma\tau} \\ & = v_c - 3v_\tau - 3v_\sigma + 9v_{\sigma\tau} + 2v_{l2} - 6v_{l2\tau} - 6v_{l2\sigma} + 18v_{l2\sigma\tau}\,,\end{aligned} \tag{B.156}$$

$$\begin{aligned}({}^3P_0): \quad & v'_c + v'_\tau + v'_\sigma + v'_{\sigma\tau} - 4v'_t - 4v'_{t\tau} - 2v'_{ls} - 2v'_{ls\tau} \\ & = v_c + v_\tau + v_\sigma + v_{\sigma\tau} - 4v_t - 4v_{t\tau} - 2v_{ls} - 2v_{ls\tau} \\ & \quad + 2v_{l2} + 2v_{l2\tau} + 2v_{l2\sigma} + 2v_{l2\sigma\tau} + 4v_{ls2} + 4v_{ls2\tau}\,,\end{aligned} \tag{B.157}$$

$$\begin{aligned}({}^3P_1): \quad & v'_c + v'_\tau + v'_\sigma + v'_{\sigma\tau} + 2v'_t + 2v'_{t\tau} - v'_{ls} - v'_{ls\tau} \\ & = v_c + v_\tau + v_\sigma + v_{\sigma\tau} + 2v_t + 2v_{t\tau} - v_{ls} - v_{ls\tau} \\ & \quad + 2v_{l2} + 2v_{l2\tau} + 2v_{l2\sigma} + 2v_{l2\sigma\tau} + v_{ls2} + v_{ls2\tau}\,,\end{aligned} \tag{B.158}$$

$$\begin{aligned}({}^3P_2): \quad & v'_c + v'_\tau + v'_\sigma + v'_{\sigma\tau} - \frac{2}{5}v'_t - \frac{2}{5}v'_{t\tau} + v'_{ls} + v'_{ls\tau} \\ & = v_c + v_\tau + v_\sigma + v_{\sigma\tau} - \frac{2}{5}v_t - \frac{2}{5}v_{t\tau} + v_{ls} + v_{ls\tau} \\ & \quad + 2v_{l2} + 2v_{l2\tau} + 2v_{l2\sigma} + 2v_{l2\sigma\tau} + v_{ls2} + v_{ls2\tau}\,.\end{aligned} \tag{B.159}$$

By solving the simultaneous equations, we obtain the function $v'_P(r)$ as

$$v'_c = v_c + \frac{5}{4}v_{l2} + \frac{3}{4}v_{l2\tau} + \frac{3}{4}v_{l2\sigma} + \frac{9}{4}v_{l2\sigma\tau} + \frac{3}{4}v_{ls2} + \frac{3}{4}v_{ls2\tau}\,, \tag{B.160}$$

$$v'_\tau = v_\tau + \frac{1}{4}v_{l2} + \frac{3}{4}v_{l2\tau} + \frac{3}{4}v_{l2\sigma} - \frac{3}{4}v_{l2\sigma\tau} + \frac{1}{4}v_{ls2} + \frac{1}{4}v_{ls2\tau}\,, \tag{B.161}$$

$$v'_\sigma = v_\sigma + \frac{1}{4}v_{l2} + \frac{3}{4}v_{l2\tau} + \frac{3}{4}v_{l2\sigma} - \frac{3}{4}v_{l2\sigma\tau} + \frac{1}{4}v_{ls2} + \frac{1}{4}v_{ls2\tau}\,, \tag{B.162}$$

$$v'_{\sigma\tau} = v_{\sigma\tau} + \frac{1}{4}v_{l2} - \frac{1}{4}v_{l2\tau} - \frac{1}{4}v_{l2\sigma} + \frac{5}{4}v_{l2\sigma\tau} + \frac{1}{12}v_{ls2} + \frac{1}{12}v_{ls2\tau}\,, \tag{B.163}$$

$$v'_t = v_t - \frac{5}{16}v_{ls2} - \frac{5}{16}v_{ls2\tau} \tag{B.164}$$

$$v'_{t\tau} = v_{t\tau} - \frac{5}{48}v_{ls2} - \frac{5}{48}v_{ls2\tau} \tag{B.165}$$

$$v'_{ls} = v_{ls} - \frac{1}{2}v_{l2} + \frac{3}{2}v_{l2\tau} - \frac{1}{2}v_{l2\sigma} + \frac{3}{2}v_{l2\sigma\tau} - \frac{9}{8}v_{ls2} + \frac{15}{8}v_{ls2\tau}\,, \tag{B.166}$$

$$v'_{ls\tau} = v_{ls\tau} + \frac{1}{2}v_{l2} - \frac{3}{2}v_{l2\tau} + \frac{1}{2}v_{l2\sigma} - \frac{3}{2}v_{l2\sigma\tau} + \frac{5}{8}v_{ls2} - \frac{19}{8}v_{ls2\tau}\,. \tag{B.167}$$

Appendix C

Transformation into the spin-complex basis

C.1 Wave functions of the $P_Q N$ states

The wave functions in the particle basis can be transformed into those in the spin-complex as

$$\begin{pmatrix} \left|PN(^2S_{1/2})\right\rangle \\ \left|P^*N(^2S_{1/2})\right\rangle \\ \left|P^*N(^4D_{1/2})\right\rangle \end{pmatrix} = U_{1/2^-} \begin{pmatrix} \left|[Nq]^{(0,S)}_{0^+}\bar{Q}\right\rangle_{1/2^-} \\ \left|[Nq]^{(1,S)}_{1^+}\bar{Q}\right\rangle_{1/2^-} \\ \left|[Nq]^{(1,D)}_{1^+}\bar{Q}\right\rangle_{1/2^-} \end{pmatrix}, \tag{C.1}$$

$$U_{1/2^-} = \begin{pmatrix} -\frac{1}{2} & \frac{\sqrt{3}}{2} & 0 \\ \frac{\sqrt{3}}{2} & \frac{1}{2} & 0 \\ 0 & 0 & -1 \end{pmatrix}, \tag{C.2}$$

$$\begin{pmatrix} \left|PN(^2D_{3/2})\right\rangle \\ \left|P^*N(^4S_{3/2})\right\rangle \\ \left|P^*N(^4D_{3/2})\right\rangle \\ \left|P^*N(^2D_{3/2})\right\rangle \end{pmatrix} = U_{3/2^-} \begin{pmatrix} \left|[Nq]^{(1,S)}_{1^+}\bar{Q}\right\rangle_{3/2^-} \\ \left|[Nq]^{(1,D)}_{1^+}\bar{Q}\right\rangle_{3/2^-} \\ \left|[Nq]^{(0,D)}_{2^+}\bar{Q}\right\rangle_{3/2^-} \\ \left|[Nq]^{(1,D)}_{2^+}\bar{Q}\right\rangle_{3/2^-} \end{pmatrix}, \tag{C.3}$$

$$U_{3/2^-} = \begin{pmatrix} 0 & \frac{\sqrt{6}}{4} & \frac{1}{2} & \frac{\sqrt{6}}{4} \\ 1 & 0 & 0 & 0 \\ 0 & \frac{1}{\sqrt{2}} & 0 & -\frac{1}{\sqrt{2}} \\ 0 & \frac{1}{2\sqrt{2}} & -\frac{\sqrt{3}}{2} & \frac{1}{2\sqrt{2}} \end{pmatrix}, \tag{C.4}$$

$$\begin{pmatrix} \left|PN(^2D_{5/2})\right\rangle \\ \left|P^*N(^2D_{5/2})\right\rangle \\ \left|P^*N(^4D_{5/2})\right\rangle \\ \left|P^*N(^4G_{5/2})\right\rangle \end{pmatrix} = U_{5/2^-} \begin{pmatrix} \left|[Nq]^{(0,D)}_{2^+}\bar{Q}\right\rangle_{5/2^-} \\ \left|[Nq]^{(1,D)}_{2^+}\bar{Q}\right\rangle_{5/2^-} \\ \left|[Nq]^{(1,D)}_{3^+}\bar{Q}\right\rangle_{5/2^-} \\ \left|[Nq]^{(1,G)}_{3^+}\bar{Q}\right\rangle_{5/2^-} \end{pmatrix}, \tag{C.5}$$

$$U_{5/2^-} = \begin{pmatrix} -\frac{1}{2} & \frac{1}{\sqrt{6}} & \frac{1}{2}\sqrt{\frac{7}{3}} & 0 \\ \frac{\sqrt{3}}{2} & \frac{1}{3\sqrt{2}} & \frac{\sqrt{7}}{6} & 0 \\ 0 & \frac{\sqrt{7}}{3} & -\frac{\sqrt{2}}{3} & 0 \\ 0 & 0 & 0 & -1 \end{pmatrix}, \tag{C.6}$$

$$\begin{pmatrix} \left|PN(^2G_{7/2})\right\rangle \\ \left|P^*N(^4D_{7/2})\right\rangle \\ \left|P^*N(^2G_{7/2})\right\rangle \\ \left|P^*N(^4G_{7/2})\right\rangle \end{pmatrix} = U_{7/2^-} \begin{pmatrix} \left|[Nq]^{(1,D)}_{3^+}\bar{Q}\right\rangle_{7/2^-} \\ \left|[Nq]^{(1,G)}_{3^+}\bar{Q}\right\rangle_{7/2^-} \\ \left|[Nq]^{(0,G)}_{4^+}\bar{Q}\right\rangle_{7/2^-} \\ \left|[Nq]^{(1,G)}_{4^+}\bar{Q}\right\rangle_{7/2^-} \end{pmatrix}, \tag{C.7}$$

$$U_{7/2^-} = \begin{pmatrix} 0 & \frac{\sqrt{7}}{4} & \frac{1}{2} & \frac{\sqrt{5}}{4} \\ 1 & 0 & 0 & 0 \\ 0 & \frac{1}{4}\sqrt{\frac{7}{3}} & -\frac{\sqrt{3}}{2} & \frac{1}{4}\sqrt{\frac{5}{3}} \\ 0 & \frac{1}{2}\sqrt{\frac{5}{3}} & 0 & -\frac{1}{2}\sqrt{\frac{7}{3}} \end{pmatrix}, \tag{C.8}$$

$$\begin{pmatrix} \left|PN(^2P_{1/2})\right\rangle \\ \left|P^*N(^2P_{1/2})\right\rangle \\ \left|P^*N(^4P_{1/2})\right\rangle \end{pmatrix} = U_{1/2^+} \begin{pmatrix} \left|[Nq]^{(1,P)}_{0^-}\bar{Q}\right\rangle_{1/2^+} \\ \left|[Nq]^{(0,P)}_{1^-}\bar{Q}\right\rangle_{1/2^+} \\ \left|[Nq]^{(1,P)}_{1^-}\bar{Q}\right\rangle_{1/2^+} \end{pmatrix}, \tag{C.9}$$

$$U_{1/2^+} = \begin{pmatrix} \frac{1}{2} & \frac{1}{2} & \frac{1}{\sqrt{2}} \\ \frac{1}{2\sqrt{3}} & -\frac{\sqrt{3}}{2} & \frac{1}{\sqrt{6}} \\ \sqrt{\frac{2}{3}} & 0 & -\frac{1}{\sqrt{3}} \end{pmatrix}, \tag{C.10}$$

$$\begin{pmatrix} \left|PN(^2P_{3/2})\right\rangle \\ \left|P^*N(^2P_{3/2})\right\rangle \\ \left|P^*N(^4P_{3/2})\right\rangle \\ \left|P^*N(^4F_{3/2})\right\rangle \end{pmatrix} = U_{3/2^+} \begin{pmatrix} \left|[Nq]^{(0,P)}_{1^-}\bar{Q}\right\rangle_{3/2^+} \\ \left|[Nq]^{(1,P)}_{1^-}\bar{Q}\right\rangle_{3/2^+} \\ \left|[Nq]^{(1,P)}_{2^-}\bar{Q}\right\rangle_{3/2^+} \\ \left|[Nq]^{(1,F)}_{2^-}\bar{Q}\right\rangle_{3/2^+} \end{pmatrix}, \tag{C.11}$$

$$U_{3/2^+} = \begin{pmatrix} -\frac{1}{2} & \frac{1}{2\sqrt{2}} & \frac{\sqrt{10}}{4} & 0 \\ \frac{\sqrt{3}}{2} & \frac{1}{2\sqrt{6}} & \frac{1}{2}\sqrt{\frac{5}{6}} & 0 \\ 0 & \sqrt{\frac{5}{6}} & -\frac{1}{\sqrt{6}} & 0 \\ 0 & 0 & 0 & -1 \end{pmatrix}, \tag{C.12}$$

$$\begin{pmatrix} \left|PN(^2F_{5/2})\right\rangle \\ \left|P^*N(^4P_{5/2})\right\rangle \\ \left|P^*N(^2F_{5/2})\right\rangle \\ \left|P^*N(^4F_{5/2})\right\rangle \end{pmatrix} = U_{5/2^+} \begin{pmatrix} \left|[Nq]^{(1,P)}_{2^-}\bar{Q}\right\rangle_{5/2^+} \\ \left|[Nq]^{(1,F)}_{2^-}\bar{Q}\right\rangle_{5/2^+} \\ \left|[Nq]^{(0,F)}_{3^-}\bar{Q}\right\rangle_{5/2^+} \\ \left|[Nq]^{(1,F)}_{3^-}\bar{Q}\right\rangle_{5/2^+} \end{pmatrix}, \tag{C.13}$$

$$U_{5/2^+} = \begin{pmatrix} 0 & \frac{1}{2}\sqrt{\frac{5}{3}} & \frac{1}{2} & \frac{1}{\sqrt{3}} \\ 1 & 0 & 0 & 0 \\ 0 & \frac{\sqrt{5}}{6} & -\frac{\sqrt{3}}{2} & \frac{1}{3} \\ 0 & \frac{2}{3} & 0 & -\frac{\sqrt{5}}{3} \end{pmatrix}, \tag{C.14}$$

and

$$\begin{pmatrix} \left|PN(^2F_{7/2})\right\rangle \\ \left|P^*N(^2F_{7/2})\right\rangle \\ \left|P^*N(^4F_{7/2})\right\rangle \\ \left|P^*N(^4H_{7/2})\right\rangle \end{pmatrix} = U_{7/2^+} \begin{pmatrix} \left|[Nq]^{(0,F)}_{3^-}\bar{Q}\right\rangle_{7/2^+} \\ \left|[Nq]^{(1,F)}_{3^-}\bar{Q}\right\rangle_{7/2^+} \\ \left|[Nq]^{(1,F)}_{4^-}\bar{Q}\right\rangle_{7/2^+} \\ \left|[Nq]^{(1,H)}_{4^-}\bar{Q}\right\rangle_{7/2^+} \end{pmatrix}, \tag{C.15}$$

$$U_{7/2^+} = \begin{pmatrix} -\frac{1}{2} & \frac{\sqrt{3}}{4} & \frac{3}{4} & 0 \\ \frac{\sqrt{3}}{2} & \frac{1}{4} & \frac{\sqrt{3}}{4} & 0 \\ 0 & \frac{\sqrt{3}}{2} & -\frac{1}{2} & 0 \\ 0 & 0 & 0 & -1 \end{pmatrix}. \tag{C.16}$$

The $U^{-1}_{J^P}$ is given by $U^t_{J^P}$.

C.2 Hamiltonian of the $P_Q N$ states

In the heavy quark limit, the Hamiltonians of the $P_Q N$ states in the spin-complex basis are given as follows. For the negative parity states, the Hamiltonians are

$$\begin{aligned} H^{\rm SC}_{1/2^-} &= U^{-1}_{1/2^-} H_{1/2^-} U_{1/2^-} \\ &= \left(\begin{array}{c|cc} K_0+C'-3C & 0 & 0 \\ \hline 0 & K_0+C'+C & -2\sqrt{2}T \\ 0 & -2\sqrt{2}T & K_2+C'+C-2T \end{array}\right) \\ &\equiv \left(\begin{array}{c|c} H^{\rm SC(0^+)}_{1/2^-} & 0 \\ \hline 0 & H^{\rm SC(1^+)}_{1/2^-} \end{array}\right), \end{aligned} \tag{C.17}$$

$$\begin{aligned} H^{\rm SC}_{3/2^-} &= U^{-1}_{3/2^-} H_{3/2^-} U_{3/2^-} \\ &= \left(\begin{array}{cc|cc} K_0+C'+C & 2\sqrt{2}T & 0 & 0 \\ 2\sqrt{2}T & K_2+C'+C-2T & 0 & 0 \\ \hline 0 & 0 & K_2+C'-3C & 0 \\ 0 & 0 & 0 & K_2+C+2T \end{array}\right) \\ &\equiv \left(\begin{array}{c|c} H^{\rm SC(1^+)}_{3/2^-} & 0 \\ \hline 0 & H^{\rm SC(2^+)}_{3/2^-} \end{array}\right), \end{aligned} \tag{C.18}$$

$$\begin{aligned} H^{\rm SC}_{5/2^-} &= U^{-1}_{5/2^-} H_{5/2^-} U_{5/2^-} \\ &= \left(\begin{array}{cc|cc} K_2+C'-3C & 0 & 0 & 0 \\ 0 & K_2+C'+C+2T & 0 & 0 \\ \hline 0 & 0 & K_2+C'+C-\frac{4}{7}T & \frac{12}{7}\sqrt{3}T \\ 0 & 0 & \frac{12}{7}\sqrt{3}T & K_4+C'+C-\frac{10}{7}T \end{array}\right) \\ &\equiv \left(\begin{array}{c|c} H^{\rm SC(2^+)}_{5/2^-} & 0 \\ \hline 0 & H^{\rm SC(3^+)}_{5/2^-} \end{array}\right), \end{aligned} \tag{C.19}$$

$$\begin{aligned} H^{\rm SC}_{7/2^-} &= U^{-1}_{7/2^-} H_{7/2^-} U_{7/2^-} \\ &= \left(\begin{array}{cc|cc} K_2+C'+C-\frac{4}{7}T & \frac{12}{7}\sqrt{3}T & 0 & 0 \\ \frac{12}{7}\sqrt{3}T & K_4+C'+C-\frac{10}{7}T & 0 & 0 \\ \hline 0 & 0 & K_4+C'-3C & 0 \\ 0 & 0 & 0 & K_4+C'+C+2T \end{array}\right) \\ &\equiv \left(\begin{array}{c|c} H^{\rm SC(3^+)}_{7/2^-} & 0 \\ \hline 0 & H^{\rm SC(4^+)}_{7/2^-} \end{array}\right). \end{aligned} \tag{C.20}$$

The kinetic term K_l is defined as

$$K_l = -\frac{1}{\mu}\left(\frac{\partial^2}{\partial r^2} + \frac{2}{r}\frac{\partial}{\partial r} - \frac{l(l+1)}{r^2}\right), \tag{C.21}$$

with the reduced mass $\mu = m_N$. The potentials C', C and T are written by

$$C' = V_C^{\rho\prime} + V_C^{\omega\prime}, \tag{C.22}$$
$$C = V_C^{\pi} + 2(V_C^{\rho} + V_C^{\omega}), \tag{C.23}$$
$$T = V_T^{\pi} - (V_T^{\rho} + V_T^{\omega}), \tag{C.24}$$

where V_C^{π}, V_T^{π}, $V_C^{v\prime}$, V_C^{v} and V_T^{v} ($v = \rho, \omega$) are given in Eqs. (B.26) and (B.37)-(B.39). We obtain that the $H^{\mathrm{SC}(0^+)}_{1/2^-}$ belongs to the HQS singlet. The HQS doublet states with $j^{\mathcal{P}} = 1^+, 2^+, 3^+$ are expected to emerge as

$$H^{\mathrm{SC}(1^+)}_{1/2^-} \approx H^{\mathrm{SC}(1^+)}_{3/2^-}, \tag{C.25}$$
$$H^{\mathrm{SC}(2^+)}_{3/2^-} \approx H^{\mathrm{SC}(2^+)}_{5/2^-}, \tag{C.26}$$
$$H^{\mathrm{SC}(3^+)}_{5/2^-} \approx H^{\mathrm{SC}(3^+)}_{7/2^-}. \tag{C.27}$$

For positive parity states, the Hamiltonians in the spin-complex basis in the heavy quark limit are given as

$$\begin{aligned} H^{\mathrm{SC}}_{1/2^+} &= U^{-1}_{1/2^+} H_{1/2^+} U_{1/2^+} \\ &= \left(\begin{array}{c|cc} K_1 + C' + C - 4T & 0 & 0 \\ \hline 0 & K_1 + C' - 3C & 0 \\ 0 & 0 & K_1 + C' + C + 2T \end{array}\right) \\ &\equiv \left(\begin{array}{c|c} H^{\mathrm{SC}(0^-)}_{1/2^+} & 0 \\ \hline 0 & H^{\mathrm{SC}(1^-)}_{1/2^+} \end{array}\right), \end{aligned} \tag{C.28}$$

$$\begin{aligned} H^{\mathrm{SC}}_{3/2^+} &= U^{-1}_{3/2^+} H_{3/2^+} U_{3/2^+} \\ &= \left(\begin{array}{cc|cc} K_1 + C' - 3C & 0 & 0 & 0 \\ 0 & K_1 + C' + C + 2T & 0 & 0 \\ \hline 0 & 0 & K_1 + C' + C - \frac{2}{5}T & \frac{6}{5}\sqrt{6}T \\ 0 & 0 & \frac{6}{5}\sqrt{6}T & K_3 + C' + C - \frac{8}{5}T \end{array}\right) \\ &\equiv \left(\begin{array}{c|c} H^{\mathrm{SC}(1^-)}_{3/2^+} & 0 \\ \hline 0 & H^{\mathrm{SC}(2^-)}_{3/2^+} \end{array}\right), \end{aligned} \tag{C.29}$$

$$
\begin{aligned}
H^{\mathrm{SC}}_{5/2^+} &= U^{-1}_{5/2^+} H_{7/2^+} U_{5/2^+} \\
&\left(\begin{array}{cc|cc}
K_1 + C' + C - \frac{2}{5}T & \frac{6}{5}\sqrt{6}T0 & 0 & \\
\frac{6}{5}\sqrt{6}T & K_3 + C' + C - \frac{8}{5}T0 & 0 & \\
\hline
0 & 0 & K_3 + C' - 3C & 0 \\
0 & 0 & 0 & K_3 + C' + C + 2T
\end{array}\right) \\
&\equiv \left(\begin{array}{c|c}
H^{\mathrm{SC}(2^-)}_{5/2^+} & 0 \\
\hline
0 & H^{\mathrm{SC}(3^-)}_{5/2^+}
\end{array}\right), \qquad \text{(C.30)}
\end{aligned}
$$

$$
\begin{aligned}
H^{\mathrm{SC}}_{7/2^+} &= U^{-1}_{7/2^+} H_{7/2^+} U_{7/2^+} \\
&= \left(\begin{array}{cc|cc}
K_3 + C' - 3C & 0 & 0 & 0 \\
0 & K_3 + C' + C + 2T & 0 & 0 \\
\hline
0 & 0 & K_3 + C' + C - \frac{2}{3}T & \frac{4}{3}\sqrt{5}T \\
0 & 0 & \frac{4}{3}\sqrt{5}T & K_5 + C' + C - \frac{4}{3}T
\end{array}\right) \\
&\equiv \left(\begin{array}{c|c}
H^{\mathrm{SC}(3^-)}_{7/2^+} & 0 \\
\hline
0 & H^{\mathrm{SC}(4^-)}_{7/2^+}
\end{array}\right). \qquad \text{(C.31)}
\end{aligned}
$$

As analysis above, the eigen state of the $H^{\mathrm{SC}(0^-)}_{1/2^+}$ component is the HQS singlet state, while the HQS doublet states with $j^{\mathcal{P}} = 1^-, 2^-, 3^-$ are formed as

$$H^{\mathrm{SC}(1^-)}_{1/2^+} \approx H^{\mathrm{SC}(1^-)}_{3/2^+}, \qquad \text{(C.32)}$$

$$H^{\mathrm{SC}(2^-)}_{3/2^+} \approx H^{\mathrm{SC}(2^-)}_{5/2^+}, \qquad \text{(C.33)}$$

$$H^{\mathrm{SC}(3^-)}_{5/2^+} \approx H^{\mathrm{SC}(3^-)}_{7/2^+}. \qquad \text{(C.34)}$$

Appendix D

Few-body problems and Gaussian expansion method

D.1 Variational Method

The variational method is one of the dominant tool to solve the quantum few-body problems. Let us consider the eigenfunction

$$Hu_k = E_k u_k \,, \tag{D.1}$$

where integer k (≥ 0) is a set of several quantum numbers. The state with $k = 0$ corresponds to the grand state in the system. When an arbitrary function ψ can be expanded in terms of u_k,

$$\psi = \sum_k C_k u_k \,, \tag{D.2}$$

the energy expectation value of H is obtained by

$$\langle H \rangle = \frac{\langle \psi \,|\, H \,|\, \psi \rangle}{\langle \psi \,|\, \psi \rangle} = \frac{\sum_k E_k |C_k|^2}{\sum_k |C_k|^2} \tag{D.3}$$

Since the energy E_k is greater than or equal to the grand states E_0,

$$\langle H \rangle = \frac{\sum_k E_k |C_k|^2}{\sum_k |C_k|^2} \geq \frac{E_0 \sum_k |C_k|^2}{\sum_k |C_k|^2} = E_0 \,. \tag{D.4}$$

Therefore, the energy of the grand state E_0 satisfies

$$E_0 \leq \frac{\langle \psi \,|\, H \,|\, \psi \rangle}{\langle \psi \,|\, \psi \rangle} \quad \text{(Ritz Theorem)} \,. \tag{D.5}$$

D.2 Matrix diagonalization

To obtain the eigenenergies in the few-body problems we often perform diagonalization of the matrix equation

$$\mathbf{HC} = E\mathbf{NC}\,, \tag{D.6}$$

where,

$$H_{ij} = \langle \phi_i | -\frac{\hbar^2}{2m} \triangle + V \, | \phi_j \rangle \,, \tag{D.7}$$

$$N_{ij} = \langle \phi_i \, | \phi_j \rangle \,, \tag{D.8}$$

$$\phi(\vec{r}) = \sum_{i=1}^{n} c_i \phi_i(\vec{r}). \tag{D.9}$$

Because the $\phi(\vec{r})$ is a non-orthogonal function, we diagonalize both $\mathbf{H}$ and $\mathbf{N}$ due to the norm $N_{ij} \neq \delta_{ij}$. The norm $\mathbf{N}$ is diagonalized by unitary matrix $\mathbf{y}$ as

$$\mathbf{Ny} = \mu\mathbf{y}, \tag{D.10}$$

where μ is the eigenvalue. Then, we define the diagonal matrix B;

$$B = \begin{pmatrix} 1/\sqrt{\mu_1} & & \\ & \ddots & \\ & & 1/\sqrt{\mu_N} \end{pmatrix}, B^{-1} = \begin{pmatrix} \sqrt{\mu_1} & & \\ & \ddots & \\ & & \sqrt{\mu_N} \end{pmatrix} \tag{D.11}$$

From Eqs.(D.10) and (D.11), Eq.(D.6) can be written by

$$\begin{aligned} &\left(\mathbf{y}^{-1}\mathbf{Hy}\mathbf{y}^{-1} - E\mathbf{y}^{-1}\mathbf{N}\mathbf{y}\mathbf{y}^{-1}\right)\mathbf{C} = 0 \\ &\rightarrow \left(B\mathbf{y}^{-1}\mathbf{Hy}BB^{-1}\mathbf{y}^{-1} - EB\mu\mathbf{y}^{-1}\right)\mathbf{C} = 0 \\ &\rightarrow \left(B\mathbf{y}^{-1}\mathbf{Hy}BB^{-1}\mathbf{y}^{-1} - EB^{-1}\mathbf{y}^{-1}\right)\mathbf{C} = 0\,. \end{aligned} \tag{D.12}$$

Therefore, by diagonalizing the matrix $B\mathbf{y}^{-1}\mathbf{Hy}B$, we obtain the eigenenergy E and the eigenvector $B^{-1}\mathbf{y}^{-1}\mathbf{C}$. The coefficient $\mathbf{C}$ is also gained from the eigenvector as $\mathbf{y}BB^{-1}\mathbf{y}^{-1}\mathbf{C} = \mathbf{C}$.

D.3 Two-body systems

D.3.1 Gaussian expansion method

When diagonalizing the matrix equation in Eq (D.6) is performed, the wave function expanded in terms of gaussian functions is useful. A set of the gaussian basis can describe both short-range and long-range regions of wave functions accurately. Moreover, the gaussian makes the calculation of matrix elements easy because the gaussian integrations can be solved analytically.

In the Gaussian expansion method [154], a wave function of the spatial part in the two-body systems is expressed by

$$\psi_{lm}(\vec{r}) = \sum_i C_i \phi_{ilm}(\vec{r}) \,, \tag{D.13}$$

$$\phi_{ilm}(\vec{r}) = \sqrt{\frac{2}{\Gamma(l+3/2)b_i^3}} \left(\frac{r}{b_i}\right)^l \exp(-\frac{r^2}{2b_i^2}) Y_{lm}(\theta,\phi) \,. \tag{D.14}$$

From Eq.(D.14), the matrix elements are obtained as follows. Here, we consider only a radial part for simplicity. The radial part of the wave function is expressed by

$$rR_{il}(r) = \sqrt{\frac{2}{\Gamma(l+3/2)b_i^3}} \left(\frac{r^{l+1}}{b_i^l}\right) \exp(-\frac{r^2}{2b_i^2}) \,. \tag{D.15}$$

(i) Norm

Let us show the matrix element of the norm in the two-body systems. It is easily obtained by

$$\langle rR_{il_1} | rR_{jl_2} \rangle = \int_0^\infty dr \frac{2}{\sqrt{\Gamma(l_1+3/2)\Gamma(l_2+3/2)}} \frac{r^{l_1+l_2+2}}{b_i^{l_1+3/2} b_j^{l_2+3/2}} \exp\left(-\frac{r^2}{2}\frac{b_i^2+b_j^2}{b_i^2 b_j^2}\right) \,. \tag{D.16}$$

Since $l_1 + l_2$ is even number, we define $n = (l_1+l_2)/2+1$ and then Eq (D.16) is written by,

$$\begin{aligned}
\langle rR_{il_1} | rR_{jl_2} \rangle &= \frac{2}{\sqrt{\Gamma(l_1+3/2)\Gamma(l_2+3/2)}} \frac{1}{b_i^{l_1+3/2} b_j^{l_2+3/2}} \int_0^\infty dr r^{2n} \exp\left(-\frac{r^2}{2}\frac{b_i^2+b_j^2}{b_i^2 b_j^2}\right) \\
&= \frac{1}{\sqrt{\Gamma(l_1+3/2)\Gamma(l_2+3/2)}} \frac{1}{b_i^{l_1+3/2} b_j^{l_2+3/2}} \Gamma(n+\frac{1}{2}) \left(\frac{2b_i^2 b_j^2}{b_i^2+b_j^2}\right)^{\frac{2n+1}{2}} \\
&= \frac{\Gamma((l_1+l_2)/2+3/2)}{\sqrt{\Gamma(l_1+3/2)\Gamma(l_2+3/2)}} \left(\frac{b_i}{b_j}\right)^{\frac{l_2-l_1}{2}} \left(\frac{2b_i b_j}{b_i^2+b_j^2}\right)^{\frac{l_1+l_2+3}{2}} \,.
\end{aligned} \tag{D.17}$$

For $l = l_1 = l_2$, Eq. (D.17) is simplified by

$$\langle rR_{il} | rR_{jl} \rangle = \left(\frac{2b_i b_j}{b_i^2+b_j^2}\right)^{l+3/2} \,. \tag{D.18}$$

(ii) Kinetic term

The matrix element of kinetic energy is obtained by

$$\langle rR_{il}| \triangle |rR_{jl}\rangle = \langle rR_{il}|\frac{\partial^2}{\partial r^2} - \frac{l(l+1)}{r^2}|rR_{jl}\rangle \ . \tag{D.19}$$

By using

$$\frac{\partial^2}{\partial r^2} rR_{il} = \sqrt{\frac{2}{\Gamma(l+3/2)}}\left(\frac{1}{b_i^{l+3/2}}\right)\left[l(l+1)r^{l-1} - (2l+3)\frac{r^{l+1}}{b_i^2} + \frac{r^{l+3}}{b_i^4}\right]\exp\left(-\frac{r^2}{2b_i^2}\right) , \tag{D.20}$$

the first term of Eq.(D.19) is given by

$$\begin{aligned}
&\langle rR_{il}|\frac{\partial^2}{\partial r^2}|rR_{jl}\rangle \\
&= \frac{2}{\Gamma(l+3/2)}\frac{1}{(b_ib_j)^{l+3/2}} \\
&\quad\times\int_0^\infty dr\left[l(l+1)r^{2l} - (2l+3)\frac{r^{2(l+1)}}{b_i^2} + \frac{r^{2(l+2)}}{b_i^4}\right]\exp\left(-\frac{r^2}{2}\frac{b_i^2+b_j^2}{b_i^2b_j^2}\right) .
\end{aligned} \tag{D.21}$$

In Eq.(D.21), the first term cancels out the centrifugal barrier term in Eq.(D.19). The integrations of the second and third terms of Eq.(D.21) are calculated by using the Gaussian integrals;

$$\begin{aligned}
&\frac{2}{\Gamma(l+3/2)}\frac{1}{(b_ib_j)^{l+3/2}}\int_0^\infty dr\left[-(2l+3)\frac{r^{2(l+1)}}{b_i^2} + \frac{r^{2(l+2)}}{b_i^4}\right]\exp\left(-\frac{r^2}{2}\frac{b_i^2+b_j^2}{b_i^2b_j^2}\right) \\
&= \frac{2}{\Gamma(l+3/2)}\frac{1}{(b_ib_j)^{l+3/2}}\frac{\sqrt{\pi}}{2}\frac{\{2(l+1)\}!}{2^{2(l+1)}(l+1)!}(2l+3)\left(\frac{2b_i^2b_j^2}{b_i^2+b_j^2}\right)^{l+3/2} \\
&\quad\times\left[-\frac{1}{b_j^2} + \frac{1}{2b_j^4}\frac{2b_i^2b_j^2}{b_i^2+b_j^2}\right] \\
&= \frac{2l+3}{(b_ib_j)^{l+3/2}}\left(\frac{2b_i^2b_j^2}{b_i^2+b_j^2}\right)^{l+3/2}\times\frac{-1}{b_i^2+b_j^2} \\
&= -\frac{2l+3}{b_i^2+b_j^2}\left(\frac{2b_ib_j}{b_i^2+b_j^2}\right)^{l+3/2} \ .
\end{aligned} \tag{D.22}$$

Hence, we obtain the matrix element of the kinetic energy in the two-body systems as

$$\langle rR_{il}| \triangle |rR_{jl}\rangle = -\frac{2l+3}{b_i^2+b_j^2}\left(\frac{2b_ib_j}{b_i^2+b_j^2}\right)^{l+3/2} \ . \tag{D.23}$$

(iii) Potentials

In the section, the matrix elements of several potentials are shown. For a gaussian potential, the matrix element can be obtained in the same way as seen in norm.

$$\begin{aligned}&\langle rR_{il_1}|e^{-\alpha r^2}|rR_{jl_2}\rangle \\ &= \frac{\Gamma((l_1+l_2)/2+3/2)}{\sqrt{\Gamma(l_1+3/2)\Gamma(l_2+3/2)}}\left(\frac{b_i}{b_j}\right)^{(l_2-l_1)/2}\left(\frac{b_i^2+b_j^2}{2b_ib_j}+b_ib_j\alpha\right)^{-(l_1+l_2+3)/2}.\end{aligned} \tag{D.24}$$

For $l=l_1=l_2$, Eq. D.24 can be written simply as

$$\langle rR_{il}|e^{-\alpha r^2}|rR_{jl}\rangle = \left(\frac{b_i^2+b_j^2}{2b_ib_j}+b_ib_j\alpha\right)^{-(l+3/2)}. \tag{D.25}$$

A matrix element of a Coulomb potential $(1/r)$ is given by

$$\begin{aligned}&\langle rR_{il_1}|\frac{1}{r}|rR_{jl_2}\rangle \\ &= \frac{\Gamma((l_1+l_2)/2+1)}{\sqrt{\Gamma(l_1+3/2)\Gamma(l_2+3/2)}}\left(\frac{b_i}{b_j}\right)^{(l_2-l_1)/2}\frac{1}{\sqrt{b_ib_j}}\left(\frac{2b_ib_j}{b_i^2+b_j^2}\right)^{(l_1+l_2)/2+1},\end{aligned} \tag{D.26}$$

$$= \frac{\Gamma(l+1)}{\Gamma(l+3/2)}\frac{1}{\sqrt{b_ib_j}}\left(\frac{2b_ib_j}{b_i^2+b_j^2}\right)^{l+1} \quad (l=l_1=l_2). \tag{D.27}$$

For a potential which is proportional to r^m (m is integer.),

$$\begin{aligned}&\langle rR_{il_1}|r^m|rR_{jl_2}\rangle \\ &= \frac{\Gamma((l_1+l_2+m+3)/2)}{\sqrt{\Gamma(l_1+3/2)\Gamma(l_2+3/2)}}\left(\frac{b_i}{b_j}\right)^{(l_2-l_1)/2}(b_ib_j)^{m/2}\left(\frac{2b_ib_j}{b_i^2+b_j^2}\right)^{(l_1+l_2+m+3)/2},\end{aligned} \tag{D.28}$$

$$= \frac{\Gamma(l+(m+3)/2)}{\Gamma(l+3/2)}(b_ib_j)^{m/2}\left(\frac{2b_ib_j}{b_i^2+b_j^2}\right)^{l+(m+3)/2} \quad (l=l_1=l_2). \tag{D.29}$$

When we choose $m=2$ in Eqs.(D.28) and (D.31), the matrix element of the harmonic

oscillator potential is obtained,

$$\begin{aligned}&\langle rR_{il_1}|r^2|rR_{jl_2}\rangle \\ &= \frac{\Gamma((l_1+l_2+5)/2)}{\sqrt{\Gamma(l_1+3/2)\Gamma(l_2+3/2)}}\left(\frac{b_i}{b_j}\right)^{(l_2-l_1)/2} b_i b_j \left(\frac{2b_ib_j}{b_i^2+b_j^2}\right)^{(l_1+l_2+5)/2}, \end{aligned} \tag{D.30}$$

$$= \frac{\Gamma(l+5/2)}{\Gamma(l+3/2)} b_i b_j \left(\frac{2b_ib_j}{b_i^2+b_j^2}\right)^{l+5/2} \qquad (l=l_1=l_2)\,. \tag{D.31}$$

D.4 Three-body problem

D.4.1 Jacobi coordinate

The Jacobi coordinates in the three-body systems for the particles N_1, N_2 and N_3 are given in Fig. D.1.

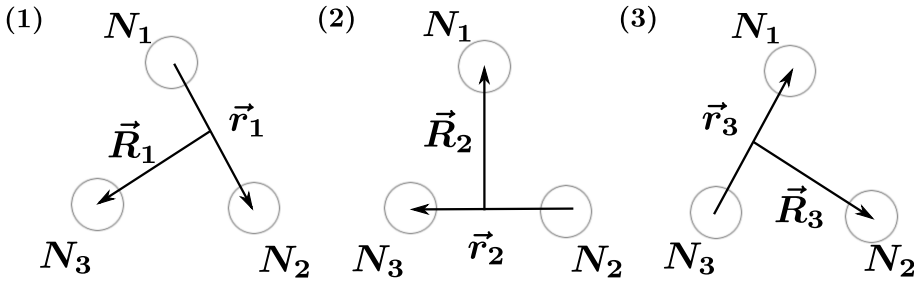

Fig.D.1 Jacobi coordinates in the three-body system

The coordinates (1), (2) and (3) are written by the single-particle coordinates x_i and the mass m_i as follows.

(1)

$$\begin{cases} \vec{r}_1 = \vec{x}_2 - \vec{x}_1 \\ \vec{R}_1 = \vec{x}_3 - \dfrac{m_1\vec{x}_1 + m_2\vec{x}_2}{m_1+m_2} \\ \vec{G}_1 = \vec{G} = \dfrac{m_1\vec{x}_1 + m_2\vec{x}_2 + m_3\vec{x}_3}{m_1+m_2+m_3} \end{cases} \tag{D.32}$$

$$\begin{pmatrix} \vec{r}_1 \\ \vec{R}_1 \\ \vec{G}_1 \end{pmatrix} = \begin{pmatrix} -1 & 1 & 0 \\ -\frac{m_1}{m_{12}} & -\frac{m_2}{m_{12}} & 1 \\ \frac{m_1}{m_{123}} & \frac{m_2}{m_{123}} & \frac{m_3}{m_{123}} \end{pmatrix} \begin{pmatrix} \vec{x}_1 \\ \vec{x}_2 \\ \vec{x}_3 \end{pmatrix} \equiv U_1 \begin{pmatrix} \vec{x}_1 \\ \vec{x}_2 \\ \vec{x}_3 \end{pmatrix} \tag{D.33}$$

$$\rightarrow \begin{pmatrix} \vec{x}_1 \\ \vec{x}_2 \\ \vec{x}_3 \end{pmatrix} = \begin{pmatrix} -\frac{m_2}{m_{12}} & -\frac{m_3}{m_{123}} & 1 \\ \frac{m_1}{m_{12}} & -\frac{m_3}{m_{123}} & 1 \\ 0 & \frac{m_{12}}{m_{123}} & 1 \end{pmatrix} \begin{pmatrix} \vec{r}_1 \\ \vec{R}_1 \\ \vec{G}_1 \end{pmatrix} = U_1^{-1} \begin{pmatrix} \vec{r}_1 \\ \vec{R}_1 \\ \vec{G}_1 \end{pmatrix} \tag{D.34}$$

where $m_{12\cdots i} = m_1 + m_2 + \cdots + m_i$.

(2)

$$\begin{cases} \vec{r}_2 = \vec{x}_3 - \vec{x}_2 \\ \vec{R}_2 = \vec{x}_1 - \dfrac{m_2\vec{x}_2 + m_3\vec{x}_3}{m_2 + m_3} \\ \vec{G}_2 = \vec{G} = \dfrac{m_1\vec{x}_1 + m_2\vec{x}_2 + m_3\vec{x}_3}{m_1 + m_2 + m_3} \end{cases} \tag{D.35}$$

$$\begin{pmatrix} \vec{r}_2 \\ \vec{R}_2 \\ \vec{G}_2 \end{pmatrix} = \begin{pmatrix} -1 & 1 & 0 \\ -\frac{m_2}{m_{23}} & -\frac{m_3}{m_{23}} & 1 \\ \frac{m_2}{m_{123}} & \frac{m_3}{m_{123}} & \frac{m_1}{m_{123}} \end{pmatrix} \begin{pmatrix} \vec{x}_1 \\ \vec{x}_2 \\ \vec{x}_3 \end{pmatrix} \equiv U_2 \begin{pmatrix} \vec{x}_1 \\ \vec{x}_2 \\ \vec{x}_3 \end{pmatrix} \tag{D.36}$$

$$\rightarrow \begin{pmatrix} \vec{x}_1 \\ \vec{x}_2 \\ \vec{x}_3 \end{pmatrix} = \begin{pmatrix} 0 & \frac{m_{23}}{m_{123}} & 1 \\ -\frac{m_3}{m_{23}} & -\frac{m_1}{m_{123}} & 1 \\ \frac{m_2}{m_{23}} & -\frac{m_1}{m_{123}} & 1 \end{pmatrix} \begin{pmatrix} \vec{r}_2 \\ \vec{R}_2 \\ \vec{G}_2 \end{pmatrix} = U_2^{-1} \begin{pmatrix} \vec{r}_2 \\ \vec{R}_2 \\ \vec{G}_2 \end{pmatrix} \tag{D.37}$$

(3)

$$\begin{cases} \vec{r}_3 = \vec{x}_1 - \vec{x}_3 \\ \vec{R}_3 = \vec{x}_2 - \dfrac{m_1\vec{x}_1 + m_3\vec{x}_3}{m_1 + m_3} \\ \vec{G}_3 = \vec{G} = \dfrac{m_1\vec{x}_1 + m_2\vec{x}_2 + m_3\vec{x}_3}{m_1 + m_2 + m_3} \end{cases} \tag{D.38}$$

$$\begin{pmatrix} \vec{r}_3 \\ \vec{R}_3 \\ \vec{G}_3 \end{pmatrix} = \begin{pmatrix} -1 & 1 & 0 \\ -\frac{m_3}{m_{13}} & -\frac{m_1}{m_{13}} & 1 \\ \frac{m_3}{m_{123}} & \frac{m_1}{m_{123}} & \frac{m_2}{m_{123}} \end{pmatrix} \begin{pmatrix} \vec{x}_1 \\ \vec{x}_2 \\ \vec{x}_3 \end{pmatrix} \equiv U_3 \begin{pmatrix} \vec{x}_1 \\ \vec{x}_2 \\ \vec{x}_3 \end{pmatrix} \tag{D.39}$$

$$\rightarrow \begin{pmatrix} \vec{x}_1 \\ \vec{x}_2 \\ \vec{x}_3 \end{pmatrix} = \begin{pmatrix} \frac{m_3}{m_{13}} & -\frac{m_2}{m_{123}} & 1 \\ 0 & \frac{m_{13}}{m_{123}} & 1 \\ -\frac{m_1}{m_{13}} & -\frac{m_2}{m_{123}} & 1 \end{pmatrix} \begin{pmatrix} \vec{r}_1 \\ \vec{R}_1 \\ \vec{G}_1 \end{pmatrix} = U_3^{-1} \begin{pmatrix} \vec{r}_1 \\ \vec{R}_1 \\ \vec{G}_1 \end{pmatrix} \tag{D.40}$$

The coordinates transformations form (r, R) to (r', R') are related to the matrix U_i,

$$\begin{pmatrix} \vec{r}_i \\ \vec{R}_i \\ \vec{G}_i \end{pmatrix} = U_i \begin{pmatrix} \vec{x}_1 \\ \vec{x}_2 \\ \vec{x}_3 \end{pmatrix} = U_i U_j^{-1} \begin{pmatrix} \vec{r}_j\,' \\ \vec{R}_j\,' \\ \vec{G}_j\,' \end{pmatrix} . \tag{D.41}$$

For instance, the transformation from (r_1, R_1) to (r_2, R_2) is obtained by

$$\begin{aligned}
\begin{pmatrix} \vec{r}_1 \\ \vec{R}_1 \\ \vec{G}_1 \end{pmatrix} &= U_1 \begin{pmatrix} \vec{x}_1 \\ \vec{x}_2 \\ \vec{x}_3 \end{pmatrix} = U_1 U_2^{-1} \begin{pmatrix} \vec{r}_2 \\ \vec{R}_2 \\ \vec{G}_2 \end{pmatrix} \\
&= \begin{pmatrix} -1 & 1 & 0 \\ -\frac{m_1}{m_{12}} & -\frac{m_2}{m_{12}} & 1 \\ \frac{m_1}{m_{123}} & \frac{m_2}{m_{123}} & \frac{m_3}{m_{123}} \end{pmatrix} \begin{pmatrix} 0 & \frac{m_{23}}{m_{123}} & 1 \\ -\frac{m_3}{m_{23}} & -\frac{m_1}{m_{123}} & 1 \\ \frac{m_2}{m_{23}} & -\frac{m_1}{m_{123}} & 1 \end{pmatrix} \begin{pmatrix} \vec{r}_2 \\ \vec{R}_2 \\ \vec{G}_2 \end{pmatrix} \\
&= \begin{pmatrix} -\frac{m_3}{m_{23}} & -1 & 0 \\ \frac{m_2 m_{123}}{m_{23} m_{12}} & -\frac{m_1}{m_{12}} & 0 \\ 0 & 0 & 1 \end{pmatrix} \begin{pmatrix} \vec{r}_2 \\ \vec{R}_2 \\ \vec{G}_2 \end{pmatrix} . \qquad \text{(D.42)}
\end{aligned}$$

Therefore,

$$\begin{cases} \vec{r}_1 = -\dfrac{m_3}{m_{23}} \vec{r}_2 - \vec{R}_2 \\ \vec{R}_1 = -\dfrac{m_2 m_{123}}{m_{12} m_{23}} \vec{r}_2 - \dfrac{m_1}{m_{12}} \vec{R}_2 \\ \vec{G}_1 = \vec{G}_2 \end{cases} . \qquad \text{(D.43)}$$

D.4.2 Coordinate transformation $(\boldsymbol{r}, \boldsymbol{R} \to \boldsymbol{r'}, \boldsymbol{R'})$ of wave function

$$\phi(\vec{r}, \vec{R}) = N \exp\left(-\frac{1}{2} a_1 r^2 - \frac{1}{2} a_2 R^2\right) \left[\mathcal{Y}_{l_1}(\vec{r}) \otimes \mathcal{Y}_{l_2}(\vec{R})\right]_{LM} \qquad \text{(D.44)}$$

$$N = \sqrt{\frac{2 a_1^{l_1 + 3/2}}{\Gamma(l_1 + 3/2)}} \sqrt{\frac{2 a_1^{l_2 + 3/2}}{\Gamma(l_2 + 3/2)}} \qquad \text{(D.45)}$$

Transformation

$$\begin{cases} \vec{r} = a_{11} \vec{r}' + a_{12} \vec{R}' \\ \vec{R} = a_{21} \vec{r}' + a_{22} \vec{R}' \end{cases} \qquad \text{(D.46)}$$

$$\begin{aligned}
&-\frac{1}{2} a_1 r^2 - \frac{1}{2} a_2 R^2 \\
&= \frac{1}{2} \left[(a_1 a_{11}^2 + a_2 a_{21}^2) r'^2 + (a_1 a_{12}^2 + a_2 a_{22}^2) R'^2 + 2(a_1 a_{11} a_{12} + a_2 a_{21} a_{22}) \vec{r}' \cdot \vec{R}'\right] \qquad \text{(D.47)}
\end{aligned}$$

$$
\begin{aligned}
&\Big[\mathcal{Y}_{l_1}(\vec{r})\otimes\mathcal{Y}_{l_2}(\vec{R})\Big]_{LM}\\
&\quad=\sum_{l_1'=0}^{l_1}\sqrt{\frac{4\pi(2l_1+1)!}{(2l_1'+1)!(2l_1-2l_1'+1)!}}\sum_{l_2'=0}^{l_2}\sqrt{\frac{4\pi(2l_2+1)!}{(2l_2'+1)!(2l_2-2l_2'+1)!}}\\
&\qquad\times\left[\Big[\mathcal{Y}_{l_1'}(\vec{r}\,')\otimes\mathcal{Y}_{l_1-l_1'}(\vec{R}')\Big]_{l_1m_1}\otimes\Big[\mathcal{Y}_{l_2'}(\vec{r}\,')\otimes\mathcal{Y}_{l_2-l_2'}(\vec{R}')\Big]_{l_2m_2}\right]_{LM}\\
&\quad=\sum_{l_1'=0}^{l_1}\sum_{l_2'=0}^{l_2}\sqrt{\frac{4\pi(2l_1+1)!}{(2l_1'+1)!(2l_1-2l_1'+1)!}}\sqrt{\frac{4\pi(2l_2+1)!}{(2l_2'+1)!(2l_2-2l_2'+1)!}}\\
&\qquad\times(a_{11}r')^{l_1'}(a_{12}R')^{l_1-l_1'}(a_{21}r')^{l_2'}(a_{22}R')^{l_2-l_2'}\\
&\qquad\times\left[\Big[Y_{l_1'}(\hat{r}')\otimes Y_{l_1-l_1'}(\hat{R}')\Big]_{l_1m_1}\otimes\Big[Y_{l_2'}(\hat{r}')\otimes Y_{l_2-l_2'}(\hat{R}')\Big]_{l_2m_2}\right]_{LM}
\end{aligned}
\tag{D.48}
$$

where

$$
\mathcal{Y}_{LM}(\vec{x}_1+\vec{x}_2)=\sum_{l=0}^{L}\sqrt{\frac{4\pi(2L+1)!}{(2l+1)!(2L-2l+1)!}}\,[\mathcal{Y}_l(\vec{x}_1)\otimes\mathcal{Y}_{L-l}(\vec{x}_2)]_{LM}
\tag{D.49}
$$

and

$$
\begin{aligned}
&\left[\Big[Y_{l_1'}(\hat{r}')\otimes Y_{l_1-l_1'}(\hat{R}')\Big]_{l_1m_1}\otimes\Big[Y_{l_2'}(\hat{r}')\otimes Y_{l_2-l_2'}(\hat{R}')\Big]_{l_2m_2}\right]_{LM}\\
&\quad=\sum_{Q_1Q_2}\sqrt{\frac{(2l_1'+1)(2(l_1-l_1')+1)(2l_1+1)(2l_2'+1)(2(l_2-l_2')+1)(2l_2+1)}{(4\pi)^2}}\\
&\qquad\times(\,l_1'\;0\;l_2'\;0|Q_1\;0\,)(\,l_1-l_1'\;0\;l_2-l_2'\;0|Q_2\;0\,)\begin{Bmatrix} l_1' & l_2' & Q_1\\ l_1-l_1' & l_2-l_2' & Q_2\\ l_1 & l_2 & L\end{Bmatrix}\\
&\qquad\times\Big[Y_{Q_1}(\hat{r}')\otimes Y_{Q_2}(\hat{R}')\Big]_{LM}\,.
\end{aligned}
\tag{D.50}
$$

Therefore, the coordinate transformation from (r,R) to (r',R') is obtained as

$$
\begin{aligned}
&\Big[\mathcal{Y}_{l_1}(\vec{r})\otimes\mathcal{Y}_{l_2}(\vec{R})\Big]_{LM}\\
&\quad=(2l_1+1)(2l_2+1)\sum_{l_1'l_2'Q_1Q_2}\sqrt{{}_{2l_1}C_{2l_1'}\,{}_{2l_2}C_{2l_2'}}\,(\,l_1'\;0\;l_2'\;0|Q_1\;0\,)(\,l_1-l_1'\;0\;l_2-l_2'\;0|Q_2\;0\,)\\
&\qquad\times(a_{11})^{l_1'}(a_{12})^{l_1-l_1'}(a_{21})^{l_2'}(a_{22})^{l_2-l_2'}(r')^{l_1'+l_2'}(R')^{l_1+l_2-(l_1'+l_2')}\\
&\qquad\times\begin{Bmatrix} l_1' & l_2' & Q_1\\ l_1-l_1' & l_2-l_2' & Q_2\\ l_1 & l_2 & L\end{Bmatrix}\Big[Y_{Q_1}(\hat{r}')\otimes Y_{Q_2}(\hat{R}')\Big]_{LM}\,.
\end{aligned}
\tag{D.51}
$$

D.4.3 Norm

$$N_{ij} = \langle \phi_i | \phi_j \rangle \tag{D.52}$$

If the Jacobi coordinate of $\phi_i(r', R')$ is different from that of $\phi_j(r, R)$, we should carry out the coordinate transformation $\phi_i(r', R') \to \phi_i(r, R)$.

$$\begin{aligned} N_{ij} = & \int d^3r \int d^3R\, r^{\nu_1} R^{\nu_2} \exp\left(-\beta_1 r^2 - \beta_2 R^2 + \gamma\, \vec{r} \cdot \vec{R}\right) \\ & \times \left[Y_{l_1}(\hat{r}) \otimes Y_{l_2}(\hat{R}) \right]_{LM} \left[Y_{l_3}(\hat{r}) \otimes Y_{l_4}(\hat{R}) \right]_{L'M'} \end{aligned} \tag{D.53}$$

From Rayleigh formula

$$\exp\left(i\vec{r} \cdot \vec{R}\right) = 4\pi \sum_{\lambda=0}^{\infty} i^{\lambda} j_{\lambda}(kr) Y_{\lambda}^{*}(\hat{r}) \cdot Y_{\lambda}(\hat{R})\,, \tag{D.54}$$

$$\exp\left(\gamma\, \vec{r} \cdot \vec{R}\right) = 4\pi \sum_{\lambda=0}^{\infty} i^{\lambda} j_{\lambda}(-i\gamma r R) Y_{\lambda}^{*}(\hat{r}) \cdot Y_{\lambda}(\hat{R}) \tag{D.55}$$

$$= 4\pi \sqrt{\frac{\pi}{2\gamma r R}} \sum_{\lambda=0}^{\infty} I_{\lambda+1/2}(\gamma r R) Y_{\lambda}^{*}(\hat{r}) \cdot Y_{\lambda}(\hat{R}) \tag{D.56}$$

where j_l is the spherical bessel function, and $I_{l+1/2}$ is the modified spherical bessel function of the first kind.

$$\begin{aligned} N_{ij} = & \int_0^{\infty} dr \int_0^{\infty} dR r^{\nu_1+2} R^{\nu_2+2} \exp\left(-\beta_1 r^2 - \beta_2 R^2\right) 4\pi \sqrt{\frac{\pi}{2\gamma r R}} \sum_{l=0}^{\infty} I_{l+1/2}(\gamma r R) \\ & \times \left\langle \left[Y_{l_1}(\hat{r}) \otimes Y_{l_2}(\hat{R}) \right]_{LM} \middle| Y_{\lambda}^{*}(\hat{r}) \cdot Y_{\lambda}(\hat{R}) \middle| \left[Y_{l_3}(\hat{r}) \otimes Y_{l_4}(\hat{R}) \right]_{L'M'} \right\rangle \end{aligned} \tag{D.57}$$

The angular part is calculated as

$$\begin{aligned} & \left\langle \left[Y_{l_1}(\hat{r}) \otimes Y_{l_2}(\hat{R}) \right]_{LM} \middle| Y_{\lambda}^{*}(\hat{r}) \cdot Y_{\lambda}(\hat{R}) \middle| \left[Y_{l_3}(\hat{r}) \otimes Y_{l_4}(\hat{R}) \right]_{L'M'} \right\rangle \\ & = \delta_{LL'} \delta_{MM'} (-1)^{L'+l_3+l_2} \begin{Bmatrix} l_1 & l_2 & L \\ l_4 & l_3 & \lambda \end{Bmatrix} \langle l_1 || Y_{\lambda}(\hat{r}) || l_3 \rangle \langle l_2 || Y_{\lambda}(\hat{R}) || l_4 \rangle \end{aligned} \tag{D.58}$$

$$\begin{aligned} & = \delta_{LL'} \delta_{MM'} \frac{(-1)^{L'+l_3+l_2}}{4\pi} \begin{Bmatrix} l_1 & l_2 & L \\ l_4 & l_3 & \lambda \end{Bmatrix} \\ & \quad \times (2\lambda+1) \sqrt{(2l_3+1)(2l_4+1)}\, (\, l_3\ 0\ \lambda\ 0 | l_1\ 0\,)(\, l_4\ 0\ \lambda\ 0 | l_2\ 0\,)\,. \end{aligned} \tag{D.59}$$

For The spatial part, first, one integrates over R:

$$\begin{aligned}
&\sum_\lambda \sqrt{\frac{\pi}{2\gamma}} \int_0^\infty dr \int_0^\infty dR\, r^{\nu_1+3/2} R^{\nu_2+3/2} e^{-\beta_1 r^2} e^{-\beta_2 R^2} I_{\lambda+1/2}(\gamma r R) \\
&\quad = \sum_\lambda \sqrt{\pi} \int_0^\infty dr\, r^{\nu_1+\lambda+2} e^{-\beta_1 r^2} \frac{\Gamma\left(\frac{\nu_2+\lambda+3}{2}\right)\gamma^\lambda}{2^{\lambda+2}\Gamma\left(\lambda+3/2\right)\sqrt{\beta_2^{\nu_2+\lambda+3}}} \\
&\qquad \times {}_1F_1\left(\frac{\nu_2+\lambda+3}{2}; \lambda+\frac{3}{2}; \frac{(\gamma r)^2}{4\beta_2}\right)
\end{aligned} \tag{D.60}$$

Since the confluent hypergeometric function ${}_1F_1$ is written as

$$\begin{aligned}
{}_1F_1\left(\frac{\nu_2+\lambda+3}{2}; \lambda+\frac{3}{2}; \frac{(\gamma r)^2}{4\beta_2}\right) &= \exp\left(\frac{(\gamma r^2)}{4\beta_2}\right) {}_1F_1\left(\frac{\lambda-\nu_1}{2}; \lambda+\frac{3}{2}; -\frac{(\gamma r^2)}{4\beta_2}\right) \\
&= \exp\left(\frac{(\gamma r^2)}{4\beta_2}\right) \sum_{n=0}^\infty \frac{((\lambda-\nu_2)/2)_n}{(\lambda+3/2)_n} \frac{1}{n!} \left(-\frac{(\gamma r^2)}{4\beta_2}\right)^n
\end{aligned} \tag{D.61}$$

where $(\alpha)_n \equiv \alpha(\alpha+1)\cdots(\alpha+n-1)$, the gaussian integral is applied to the integral over r.

$$\begin{aligned}
\text{(D.60)} &= \sum_\lambda \sqrt{\pi} \frac{\Gamma\left(\frac{\nu_2+\lambda+3}{2}\right)\gamma^\lambda}{2^{\lambda+2}\Gamma\left(\lambda+3/2\right)\sqrt{\beta_2^{\nu_2+\lambda+3}}} \sum_{n=0}^\infty \frac{((\lambda-\nu_2)/2)_n}{(\lambda+3/2)_n} \frac{1}{n!} \left(-\frac{\gamma}{4\beta_2}\right)^n \\
&\quad \times \int_0^\infty dr\, r^{\nu_1+\lambda+2n+2} \exp\left(-\beta_1 r^2 + \frac{\gamma^2 r^2}{4\beta_2}\right) \\
&= \sum_{\lambda,n} \frac{\sqrt{\pi}}{2^3} \frac{(-1)^n}{n!} \frac{\Gamma\left(\frac{\nu_2+\lambda+3}{2}\right)\Gamma\left(\frac{\nu_1+\lambda+2n+3}{2}\right)}{\Gamma(\lambda+3/2)} \frac{((\lambda-\nu_2)/2)_n}{(\lambda+3/2)_n} \\
&\quad \times \left(\frac{\gamma}{\sqrt{2\beta_1' 2\beta_2}}\right)^{\lambda+2n} \frac{1}{(\beta_1')^{\frac{\nu_1+3}{2}} \beta_2^{\frac{\nu_2+3}{2}}}
\end{aligned} \tag{D.62}$$

where $\beta_1' \equiv \beta_1 - \gamma^2/4\beta_2$. Then, Γ functions in (D.62) is rewritten as

$$(\lambda+3/2)_n \Gamma(\lambda+3/2) = \Gamma(\lambda+n+3/2)\,, \tag{D.63}$$

$$\Gamma(\lambda+n+3/2) = \frac{(2(\lambda+n)+1)!!}{2^{\lambda+n+1}}\sqrt{\pi}\,, \tag{D.64}$$

$$\Gamma((\nu_1+\lambda+2n+3)/2) = \frac{(\nu_1+\lambda+2n+1)!!}{2^{(\nu_1+\lambda+2n)/2+1}}\sqrt{\pi}\,, \tag{D.65}$$

$$\Gamma((\nu_2+\lambda+3)/2) = \frac{(\nu_2+\lambda+1)!!}{2^{(\nu_2+\lambda)/2+1}}\sqrt{\pi}\,, \tag{D.66}$$

and one obtain

$$
\begin{aligned}
(\text{D.62}) =& \sum_{\lambda,n} \frac{\pi}{2} \frac{(-1)^n}{n!} \frac{(\nu_2+\lambda+1)!!(\nu_1+\lambda+2n+1)!!}{(2(\lambda+n)+1)!!} \left(\frac{\lambda-\nu_2}{2}\right)_n \\
& \times \left(\frac{\gamma}{\sqrt{2\beta_1' 2\beta_2}}\right)^{\lambda+2n} \frac{1}{(2\beta_1')^{(\nu_1+3)/2}(2\beta_2)^{(\nu_2+3)/2}} \qquad (\text{D.67}) \\
=& \sum_{\lambda,n} \frac{\pi}{2} \frac{1}{n!} \frac{(\nu_2+\lambda+1)!!(\nu_1+\lambda+2n+1)!!}{(2(\lambda+n)+1)!!} \frac{((\nu_2-\lambda)/2)!}{((\nu_2-\lambda)/2-n)!} \\
& \times \left(\frac{\gamma}{\sqrt{2\beta_1' 2\beta_2}}\right)^{\lambda+2n} \frac{1}{(2\beta_1')^{(\nu_1+3)/2}(2\beta_2)^{(\nu_2+3)/2}} \,. \qquad (\text{D.68})
\end{aligned}
$$

From the spatial part (D.68) and the angular part (D.59), the norm is described as

$$
\begin{aligned}
N_{ij} =& \sum_{\lambda,n} \frac{\pi}{2} \frac{1}{n!} \frac{(\nu_2+\lambda+1)!!(\nu_1+\lambda+2n+1)!!}{(2(\lambda+n)+1)!!} \frac{((\nu_2-\lambda)/2)!}{((\nu_2-\lambda)/2-n)!} \\
& \times \left(\frac{\gamma}{\sqrt{2\beta_1' 2\beta_2}}\right)^{\lambda+2n} \frac{1}{(2\beta_1')^{(\nu_1+3)/2}(2\beta_2)^{(\nu_2+3)/2}} \\
& \times \delta_{LL'}\delta_{MM'} \frac{(-1)^{L'+l_3+l_2}}{4\pi} \left\{ \begin{array}{ccc} l_1 & l_2 & L \\ l_4 & l_3 & \lambda \end{array} \right\} \\
& \times (2\lambda+1)\sqrt{(2l_3+1)(2l_4+1)}\,(\,l_3\ 0\ \lambda\ 0|l_1\ 0\,)(\,l_4\ 0\ \lambda\ 0|l_2\ 0\,)\,. \qquad (\text{D.69})
\end{aligned}
$$

The summation of λ is restricted by the Clebsch-Gordan coefficients as $|l_1 - l_3| \leq \lambda \leq l_1 + l_3$ and $|l_2 - l_4| \leq \lambda \leq l_2 + l_4$.

D.4.4 Kinetic term

The kinetic term is calculated as

$$
\begin{aligned}
\nabla^2 r^l \exp\left(-\frac{1}{2}ar^2\right) Y_l(\hat{r}) &= \left(\frac{\partial^2}{\partial r^2} - \frac{l(l+1)}{r^2}\right) r^{l+1} \exp\left(-\frac{1}{2}ar^2\right) Y_l(\hat{r}) \\
&= \left[a^2r^2 - a(2l+3)\right] r^{l+1} \exp\left(-\frac{1}{2}ar^2\right) Y_l(\hat{r})\,. \qquad (\text{D.70})
\end{aligned}
$$

Therefore, it is calculated in the same manner as the norm.

Appendix E

Least squares method

The least squares method is useful when one expresses an obtained function, having a complicated shape generally, as a sum of well-known functions. In this appendix, let us show that the obtained function $v(r)$ given by n set of $(r_i, v(r_i))$ $(i = 1, 2, \cdots, n)$ fits in a sum of the Gaussian functions $V(r)$ as

$$V(r) = \alpha_1 e^{-\beta_1 r^2} + \alpha_2 e^{-\beta_2 r^2} + \cdots + \alpha_m e^{-\beta_m r^2} \,. \tag{E.1}$$

The parameter β_i $(m = 1, 2, \cdots, m)$ in Eq. (E.1) is given by geometric series as

$$\beta_i = \frac{1}{2b_i^2}, \quad b_i = b_1 \gamma^{i-1} \,, \tag{E.2}$$

where b_1 and γ are the initial value and the geometric ratio, respectively. The coefficients α_i are determined to minimize the sum of square of difference between $v(r_i)$ and $V(r_i)$:

$$S = \sum_{i=1}^{n} \left(v(r_i) - V(r_i) \right)^2 \,. \tag{E.3}$$

Since the function S is a quadratic function of α_j $(1 \leq j \leq m)$,

$$\frac{\partial S}{\partial \alpha_j} = -2 \sum_{i=1}^{n} \left(v(r_i) - V(r_i) \right) e^{-\beta_j r_i^2} = 0 \tag{E.4}$$

$$\rightarrow \sum_{i=1}^{n} \left[v(r_i) - \left(\alpha_1 e^{-\beta_1 r_i^2} + \cdots + \alpha_j e^{-\beta_j r_i^2} + \cdots \alpha_m e^{-\beta_m r_i^2} \right) \right] e^{-\beta_j r_i^2} = 0$$

$$\rightarrow \alpha_1 \sum_{i=1}^{n} e^{-(\beta_1 + \beta_j) r_i^2} + \cdots \alpha_j \sum_{i=1}^{n} e^{-2\beta_j r_i^2} + \cdots + \alpha_m \sum_{i=1}^{n} e^{-(\beta_j + \beta_m) r_i^2} \tag{E.5}$$

$$= \sum_{i=1}^{n} v(r_i) e^{-b_i r_i^2} \,. \tag{E.6}$$

For $\alpha_1 \cdots \alpha_m$, one obtains the simultaneous linear equations of α_i,

$$\begin{pmatrix} \sum_{i=1}^{n} e^{-2\beta_1 r_i^2} & \sum_{i=1}^{n} e^{-(\beta_2+\beta_1) r_i^2} & \dots & \sum_{i=1}^{n} e^{-(\beta_m+\beta_1) r_i^2} \\ \sum_{i=1}^{n} e^{-(\beta_1+\beta_2) r_i^2} & \sum_{i=1}^{n} e^{-2\beta_2 r_i^2} & \dots & \sum_{i=1}^{n} e^{-(\beta_m+\beta_2) r_i^2} \\ \vdots & \vdots & \ddots & \vdots \\ \sum_{i=1}^{n} e^{-(\beta_1+\beta_m) r_i^2} & \sum_{i=1}^{n} e^{-(\beta_2+\beta_m) r_i^2} & \dots & \sum_{i=1}^{n} e^{-2\beta_m r_i^2} \end{pmatrix} \begin{pmatrix} \alpha_1 \\ \alpha_2 \\ \vdots \\ \alpha_m \end{pmatrix}$$

$$= \begin{pmatrix} \sum_{i=1}^{n} v(r_i) e^{-\beta_1 r_i^2} \\ \sum_{i=1}^{n} v(r_i) e^{-\beta_2 r_i^2} \\ \vdots \\ \sum_{i=1}^{n} v(r_i) e^{-\beta_m r_i^2} \end{pmatrix} . \tag{E.7}$$

By solving this equations, the coefficients α_i are obtained, and hence the function $v(r)$ is transformed into a sum of the Gaussian functions.

Appendix F

Special Function

F.1 Gamma Function

Definition

$$\Gamma(z) = \int_0^\infty e^{-t} t^{z-1} dt. \tag{F.1}$$

For $n = 0, 1, 2, \cdots$,

$$\Gamma(-n) = \pm\infty \tag{F.2}$$

$$\Gamma(n+1) = n! \tag{F.3}$$

$$\Gamma\left(n + \frac{1}{2}\right) = \frac{(2n)!}{2^{2n} n!}\sqrt{\pi} \tag{F.4}$$

$$\Gamma\left(-n + \frac{1}{2}\right) = \frac{(-4)^n n!}{(2n)!}\sqrt{\pi} \tag{F.5}$$

Recurrence formula

$$\Gamma(n+1) = n\Gamma(n) \tag{F.6}$$

$$\Gamma\left((n+1) + \frac{1}{2}\right) = \left(n + \frac{1}{2}\right)\Gamma\left(n + \frac{1}{2}\right) \tag{F.7}$$

$$\Gamma\left(-(n+1) + \frac{1}{2}\right) = \frac{-2}{2n+1}\Gamma\left(-n + \frac{1}{2}\right) \tag{F.8}$$

F.2 Spherical Bessel Function

Definition

$$j_n(z) = z^n \left(-\frac{1}{z}\frac{d}{dz}\right)^n \frac{\sin z}{z} \tag{F.9}$$

$$j_0(z) = \frac{\sin z}{z} \tag{F.10}$$

$$j_1(z) = \frac{\sin z - z\cos z}{z^2} \tag{F.11}$$

$$j_2(z) = \frac{(3-z^2)\sin z - 3z\cos z}{z^3} \tag{F.12}$$

$$j_3(z) = \frac{(15-6z^2)\sin z - z(15-z^2)\cos z}{z^4} \tag{F.13}$$

$$j_4(z) = \frac{(105-45z^2+z^4)\sin z - z(105-10z^2)\cos z}{z^5} \tag{F.14}$$

$$j_5(z) = \frac{(945-420z^2+15z^4)\sin z - z(945-105z^2+z^4)\cos z}{z^6} \tag{F.15}$$

Recurrence formula

$$j_{n-1}(z) + j_{n+1}(z) = \frac{2n+1}{z} j_n(z) \tag{F.16}$$

F.3 Neumann Function

Definition

$$n_n(z) = -z^n \left(-\frac{1}{z}\frac{d}{dz}\right)^n \frac{\cos z}{z} \tag{F.17}$$

$$n_0(z) = -\frac{\cos z}{z} \tag{F.18}$$

$$n_1(z) = -\frac{\cos z + z\sin z}{z^2} \tag{F.19}$$

$$n_2(z) = -\frac{(3-z^2)\cos z + 3z\sin z}{z^3} \tag{F.20}$$

$$n_3(z) = -\frac{(15-6z^2)\cos z + z(15-z^2)\sin z}{z^4} \tag{F.21}$$

$$n_4(z) = -\frac{(105-45z^2+z^4)\cos z + z(105-10z^2)\sin z}{z^5} \tag{F.22}$$

$$n_5(z) = -\frac{(945-420z^2+15z^4)\cos z + z(945-105z^2+z^4)\sin z}{z^6} \tag{F.23}$$

Recurrence formula

$$n_{n-1}(z) + n_{n+1}(z) = \frac{2n+1}{z} n_n(z) \tag{F.24}$$

F.4 Modified Spherical Bessel Function (First Kind)

Definition

$$I_{n+1/2}(z) = \frac{1}{\sqrt{2\pi z}} \left[e^z \sum_{r=0}^{n} \frac{(-1)^r (n+r)!}{r!(n-r)!(2z)^r} + (-1)^{n+1} e^{-z} \sum_{r=0}^{n} \frac{(n+r)!}{r!(n-r)!(2z)^r} \right] \tag{F.25}$$

$$I_{-n-1/2}(z) = \frac{1}{\sqrt{2\pi z}} \left[e^z \sum_{r=0}^{n} \frac{(-1)^r (n+r)!}{r!(n-r)!(2z)^r} + (-1)^{n} e^{-z} \sum_{r=0}^{n} \frac{(n+r)!}{r!(n-r)!(2z)^r} \right] \tag{F.26}$$

$$I_{1/2}(z) = \sqrt{\frac{2}{\pi z}} \sinh z \tag{F.27}$$

$$I_{3/2}(z) = \sqrt{\frac{2}{\pi z}} \left(\cosh z - \frac{1}{z} \sinh z \right) \tag{F.28}$$

$$I_{5/2}(z) = \sqrt{\frac{2}{\pi z}} \left[\left(1 + \frac{3}{z^2} \right) \sinh z - \frac{3}{z} \cosh z \right] \tag{F.29}$$

$$I_{7/2}(z) = \sqrt{\frac{2}{\pi z}} \left[- \left(\frac{6}{z} + \frac{15}{z^3} \right) \sinh z + \left(1 + \frac{15}{z^2} \right) \cosh z \right] \tag{F.30}$$

$$I_{9/2}(z) = \sqrt{\frac{2}{\pi z}} \left[\left(1 + \frac{45}{z^2} + \frac{105}{z^4} \right) \sinh z - \left(\frac{10}{z} + \frac{105}{z^3} \right) \cosh z \right] \tag{F.31}$$

$$I_{11/2}(z) = \sqrt{\frac{2}{\pi z}} \left[- \left(\frac{15}{z} + \frac{420}{z^3} + \frac{945}{z^5} \right) \sinh z + \left(1 + \frac{105}{z^2} + \frac{945}{z^4} \right) \cosh z \right] \tag{F.32}$$

Another representation

$$i_l(z) = \sqrt{\frac{\pi}{2z}} I_{l+1/2}(z) = (-i)^l j_l(iz) \tag{F.33}$$

Recurrence formula

$$I_{\nu-1}(z) - I_{\nu+1}(z) = \frac{2\nu}{z} I_\nu(z) \tag{F.34}$$

F.5 Modified Spherical Bessel Function (Third Kind)

Definition

$$K_{n+1/2}(z) = K_{-n-1/2}(z) = \sqrt{\frac{\pi}{2z}} e^{-z} \sum_{r=0}^{n} \frac{(n+r)!}{r!(n-r)!(2z)^r} \tag{F.35}$$

$$K_{1/2}(z) = \sqrt{\frac{\pi}{2z}} e^{-z} \tag{F.36}$$

$$K_{3/2}(z) = \sqrt{\frac{\pi}{2z}} \left(1 + \frac{1}{z}\right) e^{-z} \tag{F.37}$$

$$K_{5/2}(z) = \sqrt{\frac{\pi}{2z}} \left(1 + \frac{3}{z} + \frac{3}{z^2}\right) e^{-z} \tag{F.38}$$

$$K_{7/2}(z) = \sqrt{\frac{\pi}{2z}} \left(1 + \frac{6}{z} + \frac{15}{z^2} + \frac{15}{z^3}\right) e^{-z} \tag{F.39}$$

$$K_{9/2}(z) = \sqrt{\frac{\pi}{2z}} \left(1 + \frac{10}{z} + \frac{45}{z^2} + \frac{105}{z^3} + \frac{105}{z^4}\right) e^{-z} \tag{F.40}$$

$$K_{11/2}(z) = \sqrt{\frac{\pi}{2z}} \left(1 + \frac{15}{z} + \frac{105}{z^2} + \frac{420}{z^3} + \frac{945}{z^4} + \frac{945}{z^5}\right) e^{-z} \tag{F.41}$$

Recurrence formula

$$K_{\nu-1}(z) - K_{\nu+1}(z) = -\frac{2\nu}{z} K_\nu(z) \tag{F.42}$$

F.6 Legendre function

Definition

$$P_l(x) = \frac{1}{2^l l!} \frac{d^l}{dx^l} (x^2-1)^l = {}_2F_1(-l, l+1, 1; \frac{1-x}{2}) \quad (l = 0, 1, 2, \cdots) \tag{F.43}$$

$P_l(x)$ is a solution of differential equation

$$((1-x^2)\frac{d^2}{dx^2} - 2x\frac{d}{dx} + l(l+1))P_l(x) = 0\,. \tag{F.44}$$

Orthogonality relation

$$\frac{2l+1}{2}\int_{-1}^{1} dx P_l(x)P_{l'}(x) = \delta_{ll'} \tag{F.45}$$

Recurrence formula

$$lP_l(x) = (2l-1)xP_{l-1}(x) - (l-1)P_{l-2}(x) \tag{F.46}$$

F.7 Spherical Harmonics

Definition

$$Y_{lm}(\theta,\phi) = \sqrt{\frac{2l+1}{4\pi}\frac{(l-m)!}{(l+m)!}}(-1)^m P_l^m(\cos\theta)e^{im\phi} \tag{F.47}$$

$$Y_{lm}(0,\phi) = Y_{lm}(0,0) = \sqrt{\frac{2l+1}{4\pi}}\delta_{m0} \tag{F.48}$$

Solid spherical harmonics $\mathcal{Y}_{LM}(\vec{r})$ is often used.

$$\mathcal{Y}_{LM}(\vec{r}) = r^L Y_{LM}(\hat{r}) \tag{F.49}$$

Orthogonality relation

$$\int_0^\pi d\theta \sin\theta \int_0^{2\pi} d\phi\ Y^*_{l'm'}(\theta,\phi)Y_{lm}(\theta,\phi) = \delta_{ll'}\delta_{mm'} \tag{F.50}$$

Useful formulas

$$(Y_l(\hat{r}_1)\cdot Y_l(\hat{r}_2)) = \sum_{m=-l}^{l} Y^*_{lm}(\hat{r}_1)\cdot Y_{lm}(\hat{r}_2) = (-1)^l\sqrt{2l+1}\,[(Y_l(\hat{r}_1)\otimes Y_l(\hat{r}_2))]_{00} \tag{F.51}$$

$$[Y_l(\hat{r})\otimes Y_{l'}(\hat{r})]_{LM} = C(ll';L)Y_{LM}(\hat{r}), \tag{F.52}$$

where

$$C(ll';L) = \sqrt{\frac{(2l+1)(2l'+1)}{4\pi(2L+1)}}(\,l\ 0\ l'\ 0|L\ 0\,) \tag{F.53}$$

$$\Big[\big[Y_{l_1'}(\hat{r}_1)\otimes Y_{l_2'}(\hat{r}_2)\big]_{L'M'}\otimes\big[Y_{l_1''}(\hat{r}_1)\otimes Y_{l_2''}(\hat{r}_2)\big]_{L''M''}\Big]_{LM}$$
$$=\sum_{l_1 l_2}\sqrt{\frac{(2l_1'+1)(2l_2'+1)(2L'+1)(2l_1''+1)(2l_2''+1)(2L''+1)}{(4\pi)^2}}$$
$$\times(\,l_1'\;0\;l_1''\;0|l_1\;0\,)(\,l_2'\;0\;l_2''\;0|l_2\;0\,)\begin{Bmatrix} l_1' & l_1'' & l_1\\ l_2' & l_2'' & l_2\\ L' & L'' & L\end{Bmatrix}[Y_{l_1}(\hat{r}_1)\otimes Y_{l_2}(\hat{r}_2)]_{LM} \tag{F.54}$$

$$\mathcal{Y}_{LM}(\vec{x}_1+\vec{x}_2)=\sum_{l=0}^{L}\sqrt{\frac{4\pi(2L+1)!}{(2l+1)!(2L-2l+1)!}}\,[\mathcal{Y}_l(\vec{x}_1)\otimes\mathcal{Y}_{L-l}(\vec{x}_2)]_{LM} \tag{F.55}$$

F.8 Confluent Hypergeometric Function

Definition

$${}_1F_1(\alpha;\gamma;z)=\sum_{n=0}^{\infty}\frac{\alpha(\alpha+1)\cdots(\alpha+n-1)}{\gamma(\gamma+1)\cdots(\gamma+n-1)}\frac{z^n}{n!}\equiv\sum_{n=0}^{\infty}\frac{(\alpha)_n}{(\gamma)_n}\frac{z^n}{n!} \tag{F.56}$$
$$=1+\sum_{n=1}^{\infty}\frac{(\alpha)_n}{(\gamma)_n}\frac{z^n}{n!} \tag{F.57}$$
$${}_1F_1(\alpha;\gamma;z)=e^z\,{}_1F_1(\gamma-\alpha;\gamma;-z)\quad(\gamma\text{ is not negative value}) \tag{F.58}$$
$$=e^z\sum_{n=0}^{\infty}\frac{(\gamma-\alpha)_n}{(\gamma)_n}\frac{(-z)^n}{n!} \tag{F.59}$$
$$(\alpha)_n\Gamma(\alpha)=\Gamma(\alpha+n) \tag{F.60}$$

F.9 Error Function

Definition

$$\mathrm{erf}(x)=\frac{2}{\sqrt{\pi}}\int_0^x e^{-t^2}dt=\frac{2}{\sqrt{\pi}}e^{-x^2}\sum_{n=0}^{\infty}\frac{2^n}{1\cdot3\cdots(2n+1)}x^{2n+1} \tag{F.61}$$
$$\mathrm{erfc}(x)=1-\mathrm{erf}(x)=\frac{e^{-x^2}}{\sqrt{\pi}x}\left(1+\sum_{n=1}^{\infty}\frac{1\cdot3\cdots(2n-1)}{(-2x^2)^n}\right) \tag{F.62}$$

$$i^n\text{erfc}(x) = \frac{2}{\sqrt{\pi}} \int_x^\infty \frac{(t-x)^n}{n!} e^{-t^2} dt \tag{F.63}$$

$$= \sum_{n=0}^{\infty} \frac{(-1)^k x^k}{2^{n-k} k! \Gamma\left(1 + (n-k)/2\right)} \tag{F.64}$$

Appendix G

Integrals and useful formulas

G.1 Gaussian Integrals

$$\int_0^\infty e^{-ax^2}dx = \frac{1}{2}\sqrt{\frac{\pi}{a}} \tag{G.1}$$

$$\int_0^\infty x^2 e^{-ax^2}dx = \frac{1}{2}\cdot\frac{1}{2}\sqrt{\frac{\pi}{a^3}} \tag{G.2}$$

$$\int_0^\infty x^4 e^{-ax^2}dx = \frac{1}{2}\cdot\frac{1}{2}\frac{3}{2}\sqrt{\frac{\pi}{a^5}} \tag{G.3}$$

$$\int_0^\infty x^{2n} e^{-ax^2}dx = \frac{1}{2}\cdot\frac{1}{2}\frac{3}{2}\cdots\frac{2n-1}{2}\sqrt{\frac{\pi}{a^{2n+1}}} = \frac{1}{2}\cdot\frac{(2n)!}{2^{2n}n!}\sqrt{\frac{\pi}{a^{2n+1}}} \tag{G.4}$$

$$= \frac{1}{2}\cdot\Gamma(n+\frac{1}{2})\sqrt{\frac{1}{a^{2n+1}}} \tag{G.5}$$

$$\int_0^\infty x^{2n+1} e^{-ax^2}dx = \frac{1}{2}\cdot n!\frac{1}{a^{n+1}} = \frac{1}{2}\cdot\Gamma(n+1)\frac{1}{a^{n+1}} \tag{G.6}$$

$$\int_{-\infty}^\infty e^{-ax^2+bx+c}dx = \exp\left(\frac{b^2}{4a}+c\right)\sqrt{\frac{\pi}{a}} \tag{G.7}$$

$$\int_{-\infty}^\infty e^{ic\{(x-a)^2+(b-x)^2\}}dx = \exp\left(\frac{ic(a-b)^2}{2}\right)\sqrt{\frac{i\pi}{2c}} \tag{G.8}$$

$$\int_{-\infty}^\infty e^{ic\{(x_1-a)^2+(x_2-x_1)^2+\cdots+(b-x_n)^2\}}dx_1\cdots dx_n = \exp\left(\frac{ic(a-b)^2}{n+1}\right)\sqrt{\frac{i^n\pi^n}{(n+1)c^n}} \tag{G.9}$$

G.2 Useful Integrals

$$\int \frac{dx}{\sqrt{a^2-x^2}} = \arcsin\frac{x}{a} \tag{G.10}$$

$$\int \frac{dx}{\sqrt{x^2+a^2}} = \ln\left(x+\sqrt{x^2+a^2}\right) \tag{G.11}$$

$$\int \frac{dx}{x^2+a^2} = \frac{1}{a}\arctan\frac{x}{a} \tag{G.12}$$

$$\int \frac{dx}{(x^2+a^2)^{3/2}} = \frac{1}{a^2}\frac{x}{\sqrt{x^2+a^2}} \tag{G.13}$$

$$\int \frac{xdx}{(x^2+a^2)^{3/2}} = -\frac{1}{\sqrt{x^2+a^2}} \tag{G.14}$$

$$\int_0^\infty e^{-ax^2}x^\mu I_\nu(bx)dx = \frac{\Gamma(\frac{\mu+\nu+1}{2})b^\nu}{2^{\nu+1}a^{\frac{\mu+\nu+1}{2}}\Gamma(\nu+1)}\,{}_1F_1\left(\frac{\mu+\nu+1}{2};\nu+1;\frac{b^2}{4a}\right) \tag{G.15}$$

G.3 Dirac delta function

$$\delta^{(3)}(\vec{r}) = \int \frac{d^3k}{(2\pi)^3}e^{i\vec{k}\cdot\vec{r}} \tag{G.16}$$

$$\int_{\text{all space}} f(\vec{r})\delta^{(3)}(\vec{r}-\vec{a})d^3r = f(\vec{a}) \tag{G.17}$$

$$\nabla\cdot\left(\frac{\hat{r}}{r^2}\right) = 4\pi\delta^{(3)}(\vec{r}) \tag{G.18}$$

$$\nabla^2\frac{1}{r} = -4\pi\delta^{(3)}(\vec{r}) \tag{G.19}$$

$$\nabla^2\frac{e^{-mr}}{r} = m^2\frac{e^{-mr}}{r} - 4\pi e^{-mr}\delta^{(3)}(\vec{r}) \tag{G.20}$$

$$\int_{-\infty}^\infty \delta(cx)f(x)dx = \frac{f(0)}{|c|} \tag{G.21}$$

When the function $g(x)$ has roots a_1, a_2, $\cdots$, a_n,

$$\delta(g(x)) = \sum_{i=1}^n \frac{\delta(x-a_i)}{|\partial g/\partial x|_{x=a_i}} \tag{G.22}$$

G.4 Rayleigh Formula

$$e^{i\vec{k}\cdot\vec{r}} = \sum_{l=0}^{\infty}(2l+1)i^l j_l(kr)P_l(\cos\theta) \tag{G.23}$$

$$= 4\pi\sum_{l=0}^{\infty} i^l j_l(kr)\boldsymbol{Y}_l^*(\Omega_1)\cdot\boldsymbol{Y}_l(\Omega_2) \tag{G.24}$$

G.5 Vector identities

Cross product with ϵ^{ijk}

$$(\vec{A}\times\vec{B})_i = \epsilon_{ijk}A_jB_k \tag{G.25}$$

Triple Products

$$\vec{A}\cdot(\vec{B}\times\vec{C}) = \vec{B}\cdot(\vec{C}\times\vec{A}) = \vec{C}\cdot(\vec{A}\times\vec{B}) \tag{G.26}$$

$$\vec{A}\times(\vec{B}\times\vec{C}) = \vec{B}(\vec{A}\cdot\vec{C}) - \vec{C}(\vec{A}\cdot\vec{B}) \tag{G.27}$$

G.6 Double factorial

$$(2n+1)!! = (2n+1)\cdot(2n-1)\cdots 3\cdot 1 = \frac{(2n+1)!}{2^n n!} \tag{G.28}$$

$$(2n)!! = 2n\cdot(2n-2)\cdots 4\cdot 2 = 2^n n! \tag{G.29}$$

G.7 Clebsch-Gordan Coefficients

The Clebsch-Gordan Coefficients $(\, j_1\ m_1\ j_2\ m_2|j\ m\,)$ satisfies

$$|j_1 - j_2| \le j \le j_1 + j_2 \quad \text{(the triangular conditions)}\,, \tag{G.30}$$

and

$$m_1 + m_2 = m\,. \tag{G.31}$$

G.7.1 Explicit forms of the Clebsch-Gordan Coefficients

$$
\begin{aligned}
&(\,a\ \alpha\ b\ \beta|c\ \gamma\,) \\
&\quad = \delta_{\gamma,\alpha+\beta}\Delta(abc)\left[(a+\alpha)!(a-\alpha)!(b+\beta)!(b-\beta)!(c+\gamma)!(c-\gamma)!(2c+1)\right]^{1/2} \\
&\qquad \times \sum_z \frac{(-1)^z}{z!(a+b-c-z)!(a-\alpha-z)!(b+\beta-z)!(c-b+\alpha+z)!(c-a-\beta+z)!},
\end{aligned}
\tag{G.32}
$$

where

$$
\Delta(abc) = \left[\frac{(a+b-c)!(a-b+c)!(-a+b+c)!}{(a+b+c+1)!}\right]^{1/2}. \tag{G.33}
$$

Because factorial of negative values diverges, the summation of z becomes restricted. The minimum of z is 0, $b-b-\alpha$ or $a+\beta-c$ and the maximum of z is $a+b-c$, $a-\alpha$ or $b+\beta$.

G.7.2 Special values

$$
(a\,0\,b\,0|c\,0) = \begin{cases} 0, & \text{if } a+b+c = 2g+1, \\ \frac{(-1)^{g-c}\sqrt{2c+1}\,g!}{(g-a)!(g-b)!(g-c)!}\left[\frac{(2g-2a)!(2g-2b)!(2g-2c)!}{(2g+1)!}\right]^{1/2}, & \text{if } a+b+c = 2g, \end{cases} \tag{G.34}
$$

where g is positive integer.

$$
(a\,\alpha\,b\,\beta|0\,0) = (-1)^{a-\alpha}\frac{\delta_{ab}\delta_{\alpha,-\beta}}{\sqrt{2a+1}} \tag{G.35}
$$

$$
(a\,\alpha\,0\,0|c\,\gamma) = \delta_{ac}\delta_{\alpha\gamma} \tag{G.36}
$$

$$
(a\,\alpha\,b\,\beta|a+b\,\alpha+\beta) = \sqrt{\frac{(2a)!(2b)!(a+b+\alpha+\beta)!(a+b-\alpha-\beta)!}{(2a+2b)!(a+\alpha)!(a-\alpha)!(b+\beta)!(b-\beta)!}} \tag{G.37}
$$

G.7.3 Symmetry properties

$$
\begin{aligned}
(a\,\alpha\,b\,\beta|c\,\gamma) &= (-1)^{a+b-c}(b\,\beta\,a\,\alpha|c\,\gamma) = (-1)^{a-\alpha}\frac{\hat{c}}{\hat{b}}(a\,\alpha\,c\,-\gamma|b\,-\beta) \\
&= (-1)^{a-\alpha}\frac{\hat{c}}{\hat{b}}(c\,\gamma\,a\,-\alpha|b\,-\beta) = (-1)^{b+\beta}\frac{\hat{c}}{\hat{a}}(c\,-\gamma\,b\,\beta|a\,-\alpha) \\
&= (-1)^{b+\beta}\frac{\hat{c}}{\hat{a}}(b\,-\beta\,c\,\gamma|a\,\alpha) = (-1)^{a+b-c}(a\,-\alpha\,b\,-\beta|c\,-\gamma)
\end{aligned}
\tag{G.38}
$$

G.7.4 Two Particle with Arbitrary Spin

$$|[j_1, j_2]_{jm}\rangle = \sum_{m1\, m2} (j_1\, m_1\, j_2\, m_2|j\, m)|j_1\, m_1\rangle|j_2\, m_2\rangle \tag{G.39}$$

$$|j_1\, m_1\rangle|j_2\, m_2\rangle = \sum_{j} (j_1\, m_1\, j_2\, m_2|j\, m)||[j_1, j_2]_{jm}\rangle \tag{G.40}$$

$$|\,[[j_1 j_2]_{J_{12}}, j_3]_{JM}\rangle = \sum_{J_{23}} U(j_1 j_2 J j_3; J_{12} J_{23})|[j_1, [j_2, j_3]_{J_{23}}]_{JM}\rangle \tag{G.41}$$

$$|\,[[j_1 j_2]_{J_{12}}, j_3]_{JM}\rangle = (-1)^{j_1+j_2-J_{12}}|\,[[j_2 j_1]_{J_{12}}, j_3]_{JM}\rangle \tag{G.42}$$

G.7.5 Unitary Racah coefficient

A unitary Racah coefficient is given by the overlap of two basis states as

$$U(j_1 j_2 J j_3; J_{12} J_{23}) = \langle [j_1, [j_2, j_3]_{J_{23}}]_{JM}\,|\,[[j_1, j_2]_{J_{12}}, j_3]_{JM}\rangle \tag{G.43}$$

$$= (-1)^{j_1+j_2+J+j_3}\sqrt{(2J_{12}+1)(2J_{23}+1)}\begin{Bmatrix} j_1 & j_2 & J_{12} \\ j_3 & J & J_{23} \end{Bmatrix} \tag{G.44}$$

$$= \sum_{m_1 m_2 m_3 M_{12} M_{23}} (\, j_1\; m_1\; j_2\; m_2|J_{12}\; M_{12}\,)(\, J_{12}\; M_{12}\; j_3\; m_3|J\; M\,) \times (\, j_2\; m_2\; j_3\; m_3|J_{23}\; M_{23}\,)(\, j_1\; m_1\; J_{23}\; M_{23}|J\; M\,)\,. \tag{G.45}$$

When J_{12} or J_{23} is equal to zero,

$$U(j_1, j_2, j_1, j_2; J_{12} 0) = U(j_1 j_1 j_2 j_2; 0 J_{12}) = (-1)^{j_1+j_2-J_{12}}\sqrt{\frac{2J_{12}+1}{(2j_1+1)(2j_2+1)}} \tag{G.46}$$

G.8 Angular momentum recoupling

$$|j_1 j_2(J_{12}), j_3; JM\rangle = \sum_{J_{23}} U(j_1 j_2 J j_3; J_{12} J_{23})\, |j_1, j_2 j_3(J_{23}); JM\rangle \tag{G.47}$$

$$|j_1, j_2 j_3(J_{23}); JM\rangle = \sum_{J_{12}} U(j_1 j_2 J j_3; J_{12} J_{23})\, |j_1 j_2(J_{12}), j_3; JM\rangle \tag{G.48}$$

$$|j_1 j_2(J_{12}), j_3; JM\rangle = (-1)^{j_1+j_2-J_{12}}\, |j_2 j_1(J_{12}), j_3; JM\rangle \tag{G.49}$$

$$= (-1)^{j_1+j_2-J_{12}} \sum_{J_{13}} U(j_2 j_1 J j_3; J_{12} J_{13})\, |j_2, j_1 j_3(J_{13}); JM\rangle \tag{G.50}$$

$$= \sum_{J_{13}} (-1)^{j_1+J-J_{12}-J_{13}} U(j_2 j_1 J j_3; J_{12} J_{13})\, |j_1 j_3(J_{13}), j_2; JM\rangle \tag{G.51}$$

G.9 6j Symbol

G.9.1 Relation between the Clebsch-Gordan coefficient and 6j symbol

$$\begin{aligned} \sum_{m_1,m_2,m_3,m_{12},m_{23}} & (\, j_{12}\ m_{12}\ j_3\ m_3 | j\ m\,)(\, j_1\ m_1\ j_2\ m_2 | j_{12}\ m_{12}\,) \\ & \times (\, j_1\ m_1\ j_{23}\ m_{23} | j'\ m'\,)(\, j_2\ m_2\ j_3\ m_3 | j_{23}\ m_{23}\,) \\ = \delta_{jj'}\delta_{mm'}(-1)^{j_1+j_2+j_3+j} & \sqrt{(2j_{12}+1)(2j_{23}+1)} \begin{Bmatrix} j_1 & j_2 & j_{12} \\ j_3 & j & j_{23} \end{Bmatrix} \end{aligned} \tag{G.52}$$

The 6j symbol satisfies

$$\begin{aligned} &|j_1 - j_2| \le j_{12} \le j_1 + j_2\,, \qquad |j_2 - j_3| \le j_{23} \le j_2 + j_3\,, \\ &|j_{12} - j_3| \le j \le j_{12} + j_3\,, \qquad |j_1 - j_{23}| \le j \le j_1 + j_{23}\,. \end{aligned} \tag{G.53}$$

G.9.2 Explicit forms of 6j symbols

$$\begin{Bmatrix} a & b & c \\ d & e & f \end{Bmatrix} = \Delta(abc)\Delta(cde)\Delta(aef)\Delta(bdf) \sum_z \frac{(-1)^z (z+1)!}{\mathcal{F}(abcdef; z)}\,, \tag{G.54}$$

where

$$\begin{aligned} \mathcal{F}(abcdef; z) =& (z-a-b-c)!(z-c-d-e)!(z-a-e-f)!(z-b-d-f)! \\ & \times (a+b+d+e-z)!(a+c+d+f-z)!(b+c+e+f-z)!\,. \end{aligned} \tag{G.55}$$

G.9.3 Symmetry properties of the $6j$ symbols

The $6j$ symbol is invariant under any permutation of its columns or under interchange of the upper and lower arguments in each of any two columns.

$$\begin{aligned}\left\{\begin{array}{ccc} j_{11} & j_{12} & j_{13} \\ j_{21} & j_{22} & j_{23} \end{array}\right\} &= \left\{\begin{array}{ccc} j_{11} & j_{13} & j_{12} \\ j_{21} & j_{23} & j_{22} \end{array}\right\} = \left\{\begin{array}{ccc} j_{12} & j_{11} & j_{13} \\ j_{22} & j_{21} & j_{23} \end{array}\right\} \\ &= \left\{\begin{array}{ccc} j_{12} & j_{13} & j_{11} \\ j_{22} & j_{23} & j_{21} \end{array}\right\} = \left\{\begin{array}{ccc} j_{13} & j_{11} & j_{12} \\ j_{23} & j_{21} & j_{22} \end{array}\right\} \\ &= \left\{\begin{array}{ccc} j_{21} & j_{22} & j_{13} \\ j_{11} & j_{12} & j_{23} \end{array}\right\} = \left\{\begin{array}{ccc} j_{11} & j_{22} & j_{23} \\ j_{21} & j_{12} & j_{13} \end{array}\right\}\end{aligned} \tag{G.56}$$

G.9.4 One of arguments is equal to zero

$$\left\{\begin{array}{ccc} 0 & b & c \\ d & e & f \end{array}\right\} = (-1)^{b+e+d}\frac{\delta_{bc}\delta_{ef}}{\sqrt{(2b+1)(2e+1)}}, \tag{G.57}$$

$$\left\{\begin{array}{ccc} a & b & c \\ 0 & e & f \end{array}\right\} = (-1)^{a+b+e}\frac{\delta_{bf}\delta_{ce}}{\sqrt{(2b+1)(2c+1)}}, \tag{G.58}$$

$$\left\{\begin{array}{ccc} a & 0 & c \\ d & e & f \end{array}\right\} = (-1)^{a+d+e}\frac{\delta_{ac}\delta_{df}}{\sqrt{(2a+1)(2d+1)}}, \tag{G.59}$$

$$\left\{\begin{array}{ccc} a & b & c \\ d & 0 & f \end{array}\right\} = (-1)^{a+b+d}\frac{\delta_{af}\delta_{cd}}{\sqrt{(2a+1)(2c+1)}}, \tag{G.60}$$

$$\left\{\begin{array}{ccc} a & b & 0 \\ d & e & f \end{array}\right\} = (-1)^{a+e+f}\frac{\delta_{ab}\delta_{de}}{\sqrt{(2a+1)(2d+1)}}, \tag{G.61}$$

$$\left\{\begin{array}{ccc} a & b & c \\ d & e & 0 \end{array}\right\} = (-1)^{a+b+c}\frac{\delta_{ae}\delta_{bd}}{\sqrt{(2a+1)(2b+1)}}. \tag{G.62}$$

G.9.5 One of arguments is equal to the sum of two others

$$\left\{\begin{array}{ccc} a & b & a+b \\ a & b & a+b \end{array}\right\} = (-1)^{2a+2b}\frac{(2a)!(2b)!}{(2a+2b+1)!}, \tag{G.63}$$

$$\left\{\begin{array}{ccc} a & b & a+b \\ a & b & f \end{array}\right\} = (-1)^{2a+2b}\frac{(2a)!(2b)!}{(a+b-f)!(a+b+f+1)!}, \tag{G.64}$$

$$\left\{\begin{array}{ccc} a & b & a+b \\ b & a & f \end{array}\right\} = (-1)^{2a+2b}\frac{(2a)!(2b)!}{\sqrt{(2a-f)!(2a+f+a)!(2b-f)!(2b+f+1)!}}, \tag{G.65}$$

$$\left\{\begin{array}{ccc} a & b & a+b \\ a & b & a+b-1 \end{array}\right\} = (-1)^{2a+2b}\frac{(2a)!(2b)!}{(2a+2b)!}, \tag{G.66}$$

$$\left\{\begin{array}{ccc} a & b & a+b \\ a & b & a-b \end{array}\right\} = (-1)^{2a+2b}\frac{1}{2a+1}. \tag{G.67}$$

G.10 $9j$ Symbol

G.10.1 Relation between the Clebsh-Gordan coefficients and $9j$ symbols

$$\begin{aligned}\sum_{m_i m_{ik}} &(j_1\ m_1\ j_2\ m_2|j_{12}\ m_{12}\,)(\,j_3\ m_3\ j_4\ m_4|j_{34}\ m_{34}\,)(\,j_{12}\ m_{12}\ j_{34}\ m_{34}|j\ m\,)\\ &\times(\,j_1\ m_1\ j_3\ m_3|j_{13}\ m_{13}\,)(\,j_2\ m_2\ j_4\ m_4|j_{24}\ m_{24}\,)(\,j_{13}\ m_{13}\ j_{24}\ m_{24}|j'\ m'\,)\\ &= \delta_{jj'}\delta_{mm'}\hat{J}_{12}\hat{J}_{13}\hat{J}_{24}\hat{J}_{34}\begin{Bmatrix} j_1 & j_2 & j_{12}\\ j_3 & j_4 & j_{34}\\ j_{13} & j_{24} & j\end{Bmatrix}\end{aligned} \tag{G.68}$$

The $9j$ symbol satisfies

$$\begin{aligned}&|j_1-j_2|\le j_{12}\le j_1+j_2\,,\quad |j_3-j_4|\le j_{34}\le j_3+j_4\,,\quad |j_{13}-j_{24}|\le j\le j_{13}+j_{24}\,,\\ &|j_1-j_3|\le j_{13}\le j_1+j_3\,,\quad |j_2-j_4|\le j_{24}\le j_2+j_4\,,\quad |j_{12}-j_{34}|\le j\le j_{12}+j_{34}\,.\end{aligned} \tag{G.69}$$

G.10.2 Explicit forms of $9j$ symbols

$$\begin{aligned}\begin{Bmatrix} a & b & c\\ d & e & f\\ g & h & i\end{Bmatrix} &= \frac{\Delta(abc)\Delta(def)\Delta(beh)\Delta(ghj)}{\Delta(adg)\Delta(cfj)}\,\frac{(a+d-g)!(c+f-j)!(g+h+j+1)!}{(a+d+g+1)!}\\ &\times\frac{1}{(a-b+c)!(-a+b+c)!(d-e+f)!(-d+e+f)!(b-e+h)!(-b+e+h)!}\\ &\times\sum_{xyzt}(-1)^{a-c+e-g+j+x+y+z+t}\,\frac{(2a-x)!(2b-y)!(2d-z)!(2e-t)!}{x!y!z!t!}\\ &\times\frac{(-a+b+c+x)!(-b+e+h+y)!(-d+e+f+z)!}{(a+b-c-x)!(b+e-h-y)!(d+e-f-z)!}\\ &\times\frac{(b-e+g-j+t)!}{(b+e-g+j-t)!(a+d-g-x-z)!(e-b+h+y-t)!(-d+e+f+z-t)!}\\ &\times\frac{(-a-e+f+g+x+t)!(c-d+e+j+z-t)!}{(b-e+g-j-y+t)!(-a+c-e+g-j+x+t)!}\\ &\times\frac{1}{(-a+c-d+f+g+j+1+x+z)!}\end{aligned} \tag{G.70}$$

G.10.3 Relation between $9j$ symbols and $6j$ symbols

$9j$ symbols can be expressed by $6j$ symbols:

$$\left\{ \begin{array}{ccc} a & b & c \\ d & e & f \\ g & h & i \end{array} \right\} = \sum_z (-1)^{2z}(2z+1) \left\{ \begin{array}{ccc} a & b & c \\ f & j & z \end{array} \right\} \left\{ \begin{array}{ccc} d & e & f \\ b & z & h \end{array} \right\} \left\{ \begin{array}{ccc} g & h & j \\ z & a & d \end{array} \right\} . \tag{G.71}$$

The summation of z is restricted by the conditions of $6j$ symbols.

G.10.4 Symmetry properties of the $9j$ symbols

$$\left\{ \begin{array}{ccc} j_{11} & j_{12} & j_{13} \\ j_{21} & j_{22} & j_{23} \\ j_{31} & j_{32} & j_{33} \end{array} \right\} = \epsilon \left\{ \begin{array}{ccc} j_{1i} & j_{1k} & j_{1l} \\ j_{2i} & j_{2k} & j_{2l} \\ j_{3i} & j_{3k} & j_{3l} \end{array} \right\}, \tag{G.72}$$

$$\left\{ \begin{array}{ccc} j_{11} & j_{12} & j_{13} \\ j_{21} & j_{22} & j_{23} \\ j_{31} & j_{32} & j_{33} \end{array} \right\} = \epsilon \left\{ \begin{array}{ccc} j_{i1} & j_{i2} & j_{i3} \\ j_{k1} & j_{k2} & j_{k3} \\ j_{l1} & j_{l2} & j_{l3} \end{array} \right\}, \tag{G.73}$$

$$\left\{ \begin{array}{ccc} j_{11} & j_{12} & j_{13} \\ j_{21} & j_{22} & j_{23} \\ j_{31} & j_{32} & j_{33} \end{array} \right\} = \left\{ \begin{array}{ccc} j_{11} & j_{21} & j_{31} \\ j_{12} & j_{22} & j_{32} \\ j_{13} & j_{23} & j_{33} \end{array} \right\} \tag{G.74}$$

where

$$\epsilon = \left\{ \begin{array}{cl} 1 & \text{for cyclic permutation} \\ (-1)^R & \text{for non-cyclic permutation} \end{array} \right. , \tag{G.75}$$

$$R = \sum_{i,k=1}^{3} j_{ik} \tag{G.76}$$

Even permutations of columns or rows;

$$\begin{aligned} \left\{ \begin{array}{ccc} j_{11} & j_{12} & j_{13} \\ j_{21} & j_{22} & j_{23} \\ j_{31} & j_{32} & j_{33} \end{array} \right\} &= \left\{ \begin{array}{ccc} j_{21} & j_{22} & j_{23} \\ j_{31} & j_{32} & j_{33} \\ j_{11} & j_{12} & j_{13} \end{array} \right\} = \left\{ \begin{array}{ccc} j_{31} & j_{32} & j_{33} \\ j_{11} & j_{12} & j_{13} \\ j_{21} & j_{22} & j_{23} \end{array} \right\} \\ &= \left\{ \begin{array}{ccc} j_{12} & j_{13} & j_{11} \\ j_{22} & j_{23} & j_{21} \\ j_{32} & j_{33} & j_{31} \end{array} \right\} = \left\{ \begin{array}{ccc} j_{13} & j_{11} & j_{12} \\ j_{23} & j_{21} & j_{22} \\ j_{33} & j_{31} & j_{32} \end{array} \right\} \end{aligned} \tag{G.77}$$

G.10.5 One of the arguments is equal to zero

$$\left\{ \begin{array}{ccc} a & b & c \\ d & e & f \\ g & h & 0 \end{array} \right\} = \delta_{cf}\delta_{gh} \frac{(-1)^{b+c+d+g}}{\sqrt{(2c+1)(2g+1)}} \left\{ \begin{array}{ccc} a & b & c \\ e & d & g \end{array} \right\} \tag{G.78}$$

$$\left\{ \begin{array}{ccc} a & b & c \\ d & e & f \\ 0 & 0 & 0 \end{array} \right\} = \frac{\delta_{ad}\delta_{be}\delta_{cf}}{\sqrt{(2a+1)(2b+1)(2c+1)}} \tag{G.79}$$

G.11 Wigner-Eckart theorem

$$\langle J'M' | O_{\kappa\mu} | JM \rangle = \frac{(\, J\ M\ \kappa\ \mu | J'\ M'\,)}{\sqrt{2J'+1}} \langle J' \| O_\kappa \| J \rangle \tag{G.80}$$

The matrix element for the orbital angular momentum and spin coupled with wave function is reduced by

$$\begin{aligned} &\left\langle \Psi_{(L'S')JM} \middle| V(|\vec{r}_i - \vec{r}_i|)\,(O_\kappa(\text{space}) \cdot O_\kappa(\text{spin})) \middle| \Psi_{(LS)JM} \right\rangle \\ &= (-1)^\kappa \frac{U(L\kappa JS'; L'S)}{\sqrt{(2L'+1)(2S+1)}} \langle L' \| V(|\vec{r}_i - \vec{r}_i|) O_\kappa(\text{space}) \| L \rangle \langle S' \| O_\kappa(\text{spin}) \| S \rangle \end{aligned} \tag{G.81}$$

$$\begin{aligned} &= (-1)^{L+2\kappa+J+S'} \left\{ \begin{array}{ccc} L & \kappa & L' \\ S' & J & S \end{array} \right\} \\ &\quad \times \langle L' \| V(|\vec{r}_i - \vec{r}_i|) O_\kappa(\text{space}) \| L \rangle \langle S' \| O_\kappa(\text{spin}) \| S \rangle \end{aligned} \tag{G.82}$$

G.12 Reduced matrix element

$$\langle [j_1 j_2]^J || [k_1 k_2]^k || [j_1' j_2']^{J'} \rangle = \hat{J}\hat{k}\hat{J}' \left\{ \begin{array}{ccc} j_1 & j_2 & J \\ j_1' & j_2' & J' \\ k_1 & k_2 & k \end{array} \right\} \langle j_1 || k_1 || j_1' \rangle \langle j_2 || k_2 || j_2' \rangle \tag{G.83}$$

$$\begin{aligned} &\langle jm | \left[P_a, Q_b \right]_{c\gamma} | j'm' \rangle \\ &\quad = \frac{(\, j'\ m'\ c\ \gamma | j\ m\,)}{\sqrt{2j+1}} \langle jm || \left[P_a, Q_b \right]_{c\gamma} || j'm' \rangle \end{aligned} \tag{G.84}$$

$$\quad = \frac{(\, j'\ m'\ c\ \gamma | j\ m\,)}{\sqrt{2j+1}} (-1)^{j+j'-c} \sqrt{2c+1} \sum_J \left\{ \begin{array}{ccc} a & b & c \\ j' & j & J \end{array} \right\} \langle j || P_a || J \rangle \langle J || Q_b || j' \rangle \tag{G.85}$$

$$\langle [j_1,j_2]_j |\, O_{\alpha a}(1)\, |[j_1',j_2']_{j'}\rangle$$
$$= \delta_{j_2 j_2'}(-1)^{j'+j_1+j_2'-\alpha}\sqrt{2j+1}\,(\,j'\;m'\;\alpha\;a|j\;m\,)\left\{\begin{array}{ccc} j_1' & j_2' & j' \\ j & \alpha & j_1 \end{array}\right\}\langle j_1||\, O_\alpha(1)\,||j_1'\rangle \tag{G.86}$$

$$\langle [j_1,j_2]_j \,||O_\alpha(1)||\, [j_1',j_2']_{j'}\rangle$$
$$= \delta_{j_2 j_2'}(-1)^{j'+j_1+j_2'+\alpha}\sqrt{(2j+1)(2j'+1)}\left\{\begin{array}{ccc} j_1 & j & j_2 \\ j' & j_1' & \alpha \end{array}\right\}\langle j_1||O_\alpha(1)||j_1'\rangle \tag{G.87}$$

$$\langle [j_1,j_2]_j \,||O_\alpha(2)||\, [j_1',j_2']_{j'}\rangle$$
$$= \delta_{j_1 j_1'}(-1)^{j+j_1+j_2'+\alpha}\sqrt{(2j+1)(2j'+1)}\left\{\begin{array}{ccc} j_2 & j & j_1 \\ j' & j_2' & \alpha \end{array}\right\}\langle j_2||O_\alpha(2)||j_2'\rangle \tag{G.88}$$

G.13 Tensor products

$$[O_{k_1}, O_{k_2}]_{km} = \sum_{m_1 m_2} (\,k_1\;m_1\;k_2\;m_2|k\;m\,)O_{k_1 m_1}O_{k_2 m_2} \tag{G.89}$$

$$\vec{A}\cdot\vec{B} = -\sqrt{3}[A,B]_{00} \tag{G.90}$$

$$(\vec{A}\times\vec{B})_\mu = -i\sqrt{2}[A,B]_{1\mu} \tag{G.91}$$

G.14 Matrix Elements of Basic Tensor Operator

G.14.1 Unit operator $\hat{\boldsymbol{I}}$

$$\langle\lambda'|\hat{\boldsymbol{I}}|\lambda\rangle = \langle\lambda|\lambda'\rangle = \delta_{\lambda\lambda'} \tag{G.92}$$

$$\langle l||\hat{\boldsymbol{I}}||l\rangle = \sqrt{2l+1} \tag{G.93}$$

$$\langle l's'J||\hat{\boldsymbol{I}}||lsJ\rangle = \sqrt{2J+1}\delta_{ll'}\delta_{ss'} \tag{G.94}$$

G.14.2 Spherical harmonics Y_k

$$\langle l||Y_k||l'\rangle = (-1)^{2l-k}\sqrt{\frac{(2l+1)(2k+1)}{4\pi}}(\,l\;0\;k\;0|l'\;0\,) \tag{G.95}$$

$$= (-1)^{2l}\sqrt{\frac{(2l'+1)(2k+1)}{4\pi}}(\,l'\;0\;k\;0|l\;0\,) \tag{G.96}$$

$$= (-1)^{l'}\sqrt{\frac{(2l+1)(2l'+1)}{4\pi}}(\,l\;0\;l'\;0|k\;0\,) \tag{G.97}$$

$$\begin{aligned}
&\Big\langle [Y_{l_1}(\hat{r})\otimes Y_{l_2}(\hat{R})]_L \Big\| [Y_{k_1}(\hat{r})\otimes Y_{k_2}(\hat{R})]_K \Big\| [Y_{l_1'}(\hat{r})\otimes Y_{l_2'}(\hat{R})]_{L'} \Big\rangle \\
&\quad = (-1)^{l_1'+l_2'}\sqrt{(2K+1)(2L+1)(2L'+1)(2k_1+1)(2k_2+1)} \\
&\qquad \times C(l_1l_1';k_1)C(l_2l_2';k_2)\begin{Bmatrix} l_1 & l_2 & L \\ l_1' & l_2' & L' \\ k_1 & k_2 & K \end{Bmatrix} \qquad \text{(G.98)} \\
&\quad = \frac{(-1)^{l_1'+l_2'}}{4\pi}\sqrt{(2K+1)(2L+1)(2L'+1)(2l_1+1)(2l_2+1)(2l_1'+1)(2l_2'+1)} \\
&\qquad \times (\,l_1\;0\;l_1'\;0|k_1\;0\,)(\,l_2\;0\;l_2'\;0|k_2\;0\,)\begin{Bmatrix} l_1 & l_2 & L \\ l_1' & l_2' & L' \\ k_1 & k_2 & K \end{Bmatrix} \qquad \text{(G.99)}
\end{aligned}$$

Bibliography

[1] E. S. Swanson, Phys. Rept. **429**, 243 (2006), arXiv:hep-ph/0601110.
[2] M. B. Voloshin, Prog. Part. Nucl. Phys. **61**, 455 (2008), arXiv:0711.4556.
[3] S. Godfrey and S. L. Olsen, Ann.Rev.Nucl.Part.Sci. **58**, 51 (2008), arXiv:0801.3867.
[4] N. Brambilla *et al.*, Eur. Phys. J. **C71**, 1534 (2011), arXiv:1010.5827.
[5] J.-M. Richard, (2012), arXiv:1205.4326.
[6] J. A. Oller and E. Oset, Nucl. Phys. **A620**, 438 (1997), arXiv:hep-ph/9702314, [Erratum-ibid.A652:407,1999].
[7] E. Oset and A. Ramos, Nucl. Phys. **A635**, 99 (1998), arXiv:nucl-th/9711022.
[8] T. Hyodo and D. Jido, Prog. Part. Nucl. Phys. **67**, 55 (2012), arXiv:1104.4474.
[9] Belle Collaboration, S.-K. Choi *et al.*, Phys. Rev. Lett. **91**, 262001 (2003).
[10] CDF Collaboration, D. Acosta *et al.*, Phys.Rev.Lett. **93**, 072001 (2004), arXiv:hep-ex/0312021.
[11] D0 Collaboration, V. Abazov *et al.*, Phys.Rev.Lett. **93**, 162002 (2004), arXiv:hep-ex/0405004.
[12] BaBar Collaboration, B. Aubert *et al.*, Phys.Rev. **D71**, 071103 (2005), arXiv:hep-ex/0406022.
[13] LHCb Collaboration, R. Aaij *et al.*, Phys. Rev. Lett. **110**, 222001 (2013).
[14] BESIII Collaboration, M. Ablikim *et al.*, Phys. Rev. Lett. **110**, 252001 (2013), 1303.5949.
[15] Belle Collaboration, Z. Liu *et al.*, Phys.Rev.Lett. **110**, 252002 (2013), arXiv:1304.0121.
[16] T. Xiao, S. Dobbs, A. Tomaradze, and K. K. Seth, Phys.Lett. **B727**, 366 (2013), arXiv:1304.3036.
[17] Belle Collaboration, A. Bondar *et al.*, Phys. Rev. Lett. **108**, 122001 (2012).
[18] M. Voloshin and L. Okun, JETP Lett. **23**, 333 (1976).
[19] A. De Rújula, H. Georgi, and S. L. Glashow, Phys. Rev. Lett. **38**, 317 (1977).
[20] N. A. Tornqvist, Z. Phys. **C61**, 525 (1994), arXiv:hep-ph/9310247.
[21] M. T. AlFiky, F. Gabbiani, and A. A. Petrov, Phys. Lett. **B640**, 238 (2006), arXiv:hep-ph/0506141.
[22] I. W. Lee, A. Faessler, T. Gutsche, and V. E. Lyubovitskij, Phys. Rev. D **80**, 094005 (2009).
[23] Z.-F. Sun, J. He, X. Liu, Z.-G. Luo, and S.-L. Zhu, Phys. Rev. D **84**, 054002 (2011).
[24] S. Ohkoda, Y. Yamaguchi, S. Yasui, K. Sudoh, and A. Hosaka, Phys. Rev. D **86**, 014004 (2012), arXiv:1111.2921.
[25] M. Cleven *et al.*, Phys. Rev. D **87**, 074006 (2013).

[26] S. Ohkoda, Y. Yamaguchi, S. Yasui, K. Sudoh, and A. Hosaka, Phys. Rev. D **86**, 034019 (2012), arXiv:1202.0760.
[27] D. Gamermann, E. Oset, D. Strottman, and M. J. V. Vacas, Phys. Rev. D **76**, 074016 (2007).
[28] R. Molina, T. Branz, and E. Oset, Phys.Rev. **D82**, 014010 (2010), arXiv:1005.0335.
[29] M. Voloshin, Phys.Rev. **D87**, 091501 (2013), arXiv:1304.0380.
[30] C.-Y. Cui, Y.-L. Liu, W.-B. Chen, and M.-Q. Huang, (2013), arXiv:1304.1850.
[31] S. H. Lee and S. Yasui, Eur.Phys.J. **C64**, 283 (2009), arXiv:0901.2977.
[32] Y. Ikeda *et al.*, Phys.Lett. **B729**, 85 (2014), arXiv:1311.6214.
[33] M. Shmatikov, Phys.Lett. **B349**, 411 (1995), arXiv:hep-ph/9501259.
[34] R. Jaffe and F. Wilczek, Phys. Rev. Lett. **91**, 232003 (2003).
[35] M. Karliner and H. J. Lipkin, (2003), arXiv:hep-ph/0307343.
[36] T. D. Cohen, P. M. Hohler, and R. F. Lebed, Phys. Rev. D **72**, 074010 (2005).
[37] S. Yasui and K. Sudoh, Phys. Rev. **D80**, 034008 (2009).
[38] D. Gamermann, C. García-Recio, J. Nieves, L. L. Salcedo, and L. Tolos, Phys. Rev. D **81**, 094016 (2010).
[39] Y. Yamaguchi, S. Ohkoda, S. Yasui, and A. Hosaka, Phys. Rev. D **84**, 014032 (2011).
[40] Y. Yamaguchi, S. Ohkoda, S. Yasui, and A. Hosaka, Phys. Rev. D **85**, 054003 (2012).
[41] T. F. Caramés and A. Valcarce, Phys. Rev. D **85**, 094017 (2012).
[42] D. Diakonov, V. Petrov, and M. V. Polyakov, Z. Phys. **A359**, 305 (1997), arXiv:hep-ph/9703373.
[43] T. Nakano *et al.*, Phys. Rev. Lett. **91**, 012002 (2003).
[44] DIANA Collaboration, V. Barmin *et al.*, Phys.Atom.Nucl. **66**, 1715 (2003), arXiv:hep-ex/0304040.
[45] CLAS Collaboration, S. Stepanyan *et al.*, Phys.Rev.Lett. **91**, 252001 (2003), arXiv:hep-ex/0307018.
[46] A. Hosaka, Phys. Lett. **B571**, 55 (2003), arXiv:hep-ph/0307232.
[47] R. L. Jaffe and A. Jain, Phys. Rev. D **71**, 034012 (2005).
[48] H1 Collaboration, A. Aktas *et al.*, Phys.Lett. **B588**, 17 (2004), arXiv:hep-ex/0403017.
[49] T. Mizutani and A. Ramos, Phys. Rev. C **74**, 065201 (2006).
[50] C. Garcia-Recio *et al.*, Phys.Rev. **D79**, 054004 (2009), arXiv:0807.2969.
[51] O. Romanets *et al.*, Phys. Rev. D **85**, 114032 (2012).
[52] C. Garcia-Recio, J. Nieves, O. Romanets, L. Salcedo, and L. Tolos, Phys.Rev. **D87**, 034032 (2013), arXiv:1210.4755.
[53] J. Hofmann and M. Lutz, Nucl.Phys. **A763**, 90 (2005), arXiv:hep-ph/0507071.
[54] J. Hofmann and M. Lutz, Nucl.Phys. **A776**, 17 (2006), arXiv:hep-ph/0601249.
[55] J. Haidenbauer, G. Krein, U.-G. Meissner, and L. Tolos, (2010), arXiv:1008.3794.
[56] J. He and X. Liu, Phys. Rev. D **82**, 114029 (2010).
[57] J.-R. Zhang, Phys.Rev. **D87**, 076008 (2013), arXiv:1211.2277.
[58] J.-R. Zhang, (2012), arXiv:1212.5325.
[59] X.-G. He, X.-Q. Li, X. Liu, and X.-Q. Zeng, Eur.Phys.J. **C51**, 883 (2007),

arXiv:hep-ph/0606015.
[60] Y. Dong, A. Faessler, T. Gutsche, and V. E. Lyubovitskij, Phys. Rev. D **81**, 014006 (2010).
[61] Y. Dong, A. Faessler, T. Gutsche, and V. E. Lyubovitskij, Phys. Rev. D **81**, 074011 (2010).
[62] Y. Dong, A. Faessler, T. Gutsche, S. Kumano, and V. E. Lyubovitskij, Phys. Rev. D **82**, 034035 (2010).
[63] Y. Dong, A. Faessler, T. Gutsche, S. Kumano, and V. E. Lyubovitskij, Phys. Rev. D **83**, 094005 (2011).
[64] J.-J. Wu, R. Molina, E. Oset, and B. S. Zou, Phys. Rev. Lett. **105**, 232001 (2010).
[65] J.-J. Wu, R. Molina, E. Oset, and B. S. Zou, Phys. Rev. C **84**, 015202 (2011).
[66] J.-J. Wu and B. Zou, Phys.Lett. **B709**, 70 (2012), arXiv:1011.5743.
[67] E. Klempt and J.-M. Richard, Rev.Mod.Phys. **82**, 1095 (2010), arXiv:0901.2055.
[68] L. A. Copley, N. Isgur, and G. Karl, Phys. Rev. D **20**, 768 (1979).
[69] W. Roberts and M. Pervin, Int.J.Mod.Phys. **A23**, 2817 (2008), arXiv:0711.2492.
[70] T. Motoba, H. Bando, and K. Ikeda, Prog.Theor.Phys. **70**, 189 (1983).
[71] O. Hashimoto and H. Tamura, Prog.Part.Nucl.Phys. **57**, 564 (2006).
[72] H. Tamura, Eur. Phys. J. **A13**, 181 (2002).
[73] T. Yamazaki, A. Dote, and Y. Akaishi, Phys.Lett. **B587**, 167 (2004), arXiv:nucl-th/0310085.
[74] A. Doté, T. Hyodo, and W. Weise, Phys. Rev. C **79**, 014003 (2009).
[75] R. S. Hayano and T. Hatsuda, Rev. Mod. Phys. **82**, 2949 (2010).
[76] K. Tsushima and F. Khanna, Phys.Lett. **B552**, 138 (2003), arXiv:nucl-th/0207036.
[77] A. Mishra, E. L. Bratkovskaya, J. Schaffer-Bielich, S. Schramm, and H. Stöcker, Phys. Rev. C **69**, 015202 (2004).
[78] M. Lutz and C. Korpa, Phys.Lett. **B633**, 43 (2006), arXiv:nucl-th/0510006.
[79] L. Tolós, A. Ramos, and T. Mizutani, Phys. Rev. C **77**, 015207 (2008).
[80] A. Mishra and A. Mazumdar, Phys. Rev. C **79**, 024908 (2009).
[81] A. Kumar and A. Mishra, Phys. Rev. C **81**, 065204 (2010).
[82] C. E. Jiménez-Tejero, A. Ramos, L. Tolós, and I. Vidaña, Phys. Rev. C **84**, 015208 (2011).
[83] A. Kumar and A. Mishra, Eur.Phys.J. **A47**, 164 (2011), arXiv:1102.4792.
[84] A. Hayashigaki, Phys.Lett. **B487**, 96 (2000), arXiv:nucl-th/0001051.
[85] B. Friman, S. H. Lee, and T. Song, Phys.Lett. **B548**, 153 (2002), arXiv:nucl-th/0207006.
[86] T. Hilger, R. Thomas, and B. Kampfer, Phys.Rev. **C79**, 025202 (2009), arXiv:0809.4996.
[87] S. Yasui and K. Sudoh, Phys. Rev. C **88**, 015201 (2013).
[88] A. Sibirtsev, K. Tsushima, and A. W. Thomas, Eur. Phys. J. **A6**, 351 (1999), arXiv:nucl-th/9904016.
[89] K. Tsushima, D. H. Lu, A. W. Thomas, K. Saito, and R. H. Landau, Phys. Rev. C **59**, 2824 (1999).
[90] C. García-Recio, J. Nieves, L. L. Salcedo, and L. Tolos, Phys. Rev. C **85**, 025203 (2012).

[91] S. Yasui and K. Sudoh, Phys. Rev. C **87**, 015202 (2013).
[92] M. Bayar *et al.*, Phys. Rev. C **86**, 044004 (2012).
[93] Y. Yamaguchi, S. Yasui, and A. Hosaka, (2013), arXiv:1309.4324.
[94] R. Buettgen, K. Holinde, A. Mueller-Groeling, J. Speth, and P. Wyborny, Nucl. Phys. **A506**, 586 (1990).
[95] M. A. Preston and R. K. Bhaduri, *Structure Of The Nucleus* (Westview Press, 1993).
[96] K. Ikeda, T. Myo, K. Kato, and H. Toki, Lect.Notes Phys. **818**, 165 (2010), arXiv:1007.2474.
[97] Y. Nambu and G. Jona-Lasinio, Phys. Rev. **122**, 345 (1961).
[98] Y. Nambu and G. Jona-Lasinio, Phys. Rev. **124**, 246 (1961).
[99] N. Isgur and M. B. Wise, Phys. Lett. **B232**, 113 (1989).
[100] N. Isgur and M. B. Wise, Phys. Rev. Lett. **66**, 1130 (1991).
[101] J. Flynn and N. Isgur, J.Phys. **G18**, 1627 (1992), arXiv:hep-ph/9207223.
[102] M. Neubert, Physics Reports **245**, 259 (1994).
[103] A. V. Manohar and M. B. Wise, *Heavy Quark Physics (Cambridge Monographs on Particle Physics, Nuclear Physics and Cosmology)*, 1 ed. (Cambridge University Press, 2007).
[104] S. Yasui *et al.*, Phys.Lett. **B727**, 185 (2013), arXiv:1304.5293.
[105] J. L. Rosner, Comments Nucl.Part.Phys. **16**, 109 (1986).
[106] E. J. Eichten, C. T. Hill, and C. Quigg, Phys.Rev.Lett. **71**, 4116 (1993), arXiv:hep-ph/9308337.
[107] W. A. Bardeen, E. J. Eichten, and C. T. Hill, Phys. Rev. D **68**, 054024 (2003).
[108] T. Matsuki, T. Morii, and K. Sudoh, Prog.Theor.Phys. **117**, 1077 (2007), arXiv:hep-ph/0605019.
[109] Y. Yamaguchi, S. Ohkoda, A. Hosaka, T. Hyodo, and S. Yasui, in preparation .
[110] E. Eichten and B. R. Hill, Phys.Lett. **B234**, 511 (1990).
[111] H. Georgi, Phys.Lett. **B240**, 447 (1990).
[112] T. Mannel, W. Roberts, and Z. Ryzak, Nucl.Phys. **B368**, 204 (1992).
[113] M. B. Wise, Phys. Rev. D **45**, R2188 (1992).
[114] G. Burdman and J. F. Donoghue, Phys.Lett. **B280**, 287 (1992).
[115] T.-M. Yan *et al.*, Phys. Rev. D **46**, 1148 (1992).
[116] A. F. Falk and M. E. Luke, Phys.Lett. **B292**, 119 (1992), arXiv:hep-ph/9206241.
[117] R. Casalbuoni *et al.*, Phys. Lett. **B299**, 139 (1993), arXiv:hep-ph/9211248.
[118] R. Casalbuoni *et al.*, Phys. Rept. **281**, 145 (1997), arXiv:hep-ph/9605342.
[119] S. Weinberg, Physica **A96**, 327 (1979).
[120] J. Gasser and H. Leutwyler, Annals Phys. **158**, 142 (1984).
[121] J. Gasser and H. Leutwyler, Nucl.Phys. **B250**, 465 (1985).
[122] A. Pich, Rept.Prog.Phys. **58**, 563 (1995), arXiv:hep-ph/9502366.
[123] S. Scherer, Adv.Nucl.Phys. **27**, 277 (2003), arXiv:hep-ph/0210398.
[124] Particle Data Group, J. Beringer *et al.*, Phys. Rev. D **86**, 010001 (2012).
[125] A. Abada *et al.*, Phys. Rev. D **66**, 074504 (2002).
[126] M. E. Luke and A. V. Manohar, Phys.Lett. **B286**, 348 (1992), arXiv:hep-ph/9205228.
[127] N. Kitazawa and T. Kurimoto, Phys.Lett. **B323**, 65 (1994), arXiv:hep-ph/9312225.

[128] H.-Y. Cheng *et al.*, Phys.Rev. **D49**, 2490 (1994), arXiv:hep-ph/9308283.
[129] C. G. Boyd and B. Grinstein, Nucl.Phys. **B442**, 205 (1995), arXiv:hep-ph/9402340.
[130] S. Yasui and K. Sudoh, Phys.Rev. **C89**, 015201 (2014), arXiv:1308.0098.
[131] M. Bando, T. Kugo, and K. Yamawaki, Phys. Rept. **164**, 217 (1988).
[132] R. Casalbuoni *et al.*, Phys. Lett. **B292**, 371 (1992), arXiv:hep-ph/9209248.
[133] C. Isola, M. Ladisa, G. Nardulli, and P. Santorelli, Phys. Rev. D **68**, 114001 (2003).
[134] Y. Yamaguchi, S. Ohkoda, S. Yasui, and A. Hosaka, (2011), arXiv:1105.0734.
[135] Y. Yamaguchi, S. Ohkoda, S. Yasui, and A. Hosaka, (2011), arXiv:1111.2691.
[136] Y. Yamaguchi, S. Ohkoda, S. Yasui, and A. Hosaka, Phys. Rev. D **87**, 074019 (2013).
[137] H. Yukawa, Proc.Phys.Math.Soc.Jap. **17**, 48 (1935).
[138] R. Machleidt, K. Holinde, and C. Elster, Physics Reports **149**, 1 (1987).
[139] R. Machleidt, Phys. Rev. C **63**, 024001 (2001).
[140] B. R. Johnson, Journal of Chemical Physics **67**, 4086 (1977).
[141] B. R. Johnson, Journal of Chemical Physics **69**, 4678 (1978).
[142] B. R. Johnson, Journal of Computational Physics **13**, 445 (1973).
[143] K. Arai and A. T. Kruppa, Phys. Rev. C **60**, 064315 (1999).
[144] J. Haidenbauer, G. Krein, U.-G. Meissner, and A. Sibirtsev, Eur. Phys. J. **A33**, 107 (2007), arXiv:0704.3668.
[145] C. Fontoura, G. Krein, and V. Vizcarra, EPJ Web Conf. **3**, 03027 (2010).
[146] C. Fontoura, G. Krein, and V. Vizcarra, (2012), arXiv:1208.4058.
[147] T. Ericson and W. Weise, *Pions and Nuclei* (Clarendon Press, 1988).
[148] B. S. Pudliner, V. R. Pandharipande, J. Carlson, S. C. Pieper, and R. B. Wiringa, Phys. Rev. C **56**, 1720 (1997).
[149] R. B. Wiringa, V. G. J. Stoks, and R. Schiavilla, Phys. Rev. C **51**, 38 (1995).
[150] S. C. Pieper, V. Pandharipande, R. B. Wiringa, and J. Carlson, Phys.Rev. **C64**, 014001 (2001), arXiv:nucl-th/0102004.
[151] R. B. Wiringa and S. C. Pieper, Phys.Rev.Lett. **89**, 182501 (2002), arXiv:nucl-th/0207050.
[152] M. Kamimura, Phys. Rev. A **38**, 621 (1988).
[153] H. Kameyama, M. Kamimura, and Y. Fukushima, Phys. Rev. C **40**, 974 (1989).
[154] E. Hiyama, Y. Kino, and M. Kamimura, Prog. Part. Nucl. Phys. **51**, 223 (2003).
[155] J. Aguilar and J. M. Combes, Communications in Mathematical Physics **22**, 269 (1971).
[156] E. Balslev and J. M. Combes, Communications in Mathematical Physics **22**, 280 (1971).
[157] B. Simon, Communications in Mathematical Physics **27**, 1 (1972).
[158] Y. Ho, Physics Reports **99**, 1 (1983).
[159] S. Aoyama, T. Myo, K. Kato, and K. Ikeda, Prog. Theor. Phys. **116**, 1 (2006).
[160] H. Witala, W. Gloeckle, D. Huber, J. Golak, and H. Kamada, Phys.Rev.Lett. **81**, 1183 (1998), arXiv:nucl-th/9801018.
[161] K. Sekiguchi *et al.*, Phys.Rev. **C65**, 034003 (2002).
[162] K. Hatanaka *et al.*, Phys.Rev. **C66**, 044002 (2002).
[163] Y. Maeda *et al.*, Phys.Rev. **C76**, 014004 (2007).

[164] K. Sagara, Few Body Syst. **48**, 59 (2010).
[165] A. Akmal, V. Pandharipande, and D. Ravenhall, Phys.Rev. **C58**, 1804 (1998), arXiv:nucl-th/9804027.
[166] D. Lonardoni, S. Gandolfi, and F. Pederiva, Phys. Rev. C **87**, 041303 (2013).
[167] J. Fujita and H. Miyazawa, Prog.Theor.Phys. **17**, 360 (1957).
[168] J. Carlson, V. Pandharipande, and R. B. Wiringa, Nucl.Phys. **A401**, 59 (1983).
[169] S. Coon and H. Han, Few Body Syst. **30**, 131 (2001), arXiv:nucl-th/0101003.
[170] S. Weinberg, Phys.Lett. **B295**, 114 (1992), arXiv:hep-ph/9209257.
[171] U. van Kolck, Phys.Rev. **C49**, 2932 (1994).
[172] E. Epelbaum, Prog.Part.Nucl.Phys. **57**, 654 (2006), arXiv:nucl-th/0509032.
[173] R. Machleidt and D. Entem, Phys.Rept. **503**, 1 (2011), arXiv:1105.2919.
[174] HAL QCD Collaboration, T. Doi *et al.*, Prog.Theor.Phys. **127**, 723 (2012), arXiv:1106.2276.
[175] Y. Suzuki and K. Varga, *Stochastic Variational Approach to Quantum-Mechanical Few- Body Problems (Lecture Notes in Physics Monographs)*, 1st ed. softcover of orig. ed. 1998 ed. (Springer-Verlag, 2010).
[176] D. A. Varshalovich and A. N. Moskalev, *Quantum Theory of Angular Momentum* (World Scientific Publishing Company, 1988).
[177] ExHIC Collaboration, S. Cho *et al.*, Phys. Rev. Lett. **106**, 212001 (2011).
[178] ExHIC Collaboration, S. Cho *et al.*, Phys. Rev. C **84**, 064910 (2011), arXiv:1107.1302.
[179] T. Hamada, Progress of Theoretical Physics **24**, 126 (1960).
[180] T. Hamada and I. D. Johnston, Nucl. Phys. **34**, 382 (1962).
[181] J. Roderick V. Reid, Annals of Physics **50**, 411 (1968).
[182] R. A. Bryan and B. L. Scott, Phys.Rev. **135**, B434 (1964).
[183] R. Bryan and B. L. Scott, Phys.Rev. **164**, 1215 (1967).
[184] R. Bryan and B. Scott, Phys.Rev. **177**, 1435 (1969).
[185] D. Thompson, M. Lemere, and Y. Tang, Nucl.Phys. **A286**, 53 (1977).
[186] Y. Yamaguchi, Phys. Rev. **95**, 1628 (1954).
[187] Y. Yamaguchi and Y. Yamaguchi, Phys. Rev. **95**, 1635 (1954).
[188] R. B. Wiringa, R. A. Smith, and T. L. Ainsworth, Phys. Rev. C **29**, 1207 (1984).
[189] V. G. J. Stoks, R. A. M. Klomp, C. P. F. Terheggen, and J. J. de Swart, Phys. Rev. C **49**, 2950 (1994).
[190] S. Weinberg, Nucl.Phys. **B363**, 3 (1991).
[191] C. Ordonez, L. Ray, and U. van Kolck, Phys.Rev.Lett. **72**, 1982 (1994).
[192] N. Kaiser, R. Brockmann, and W. Weise, Nucl.Phys. **A625**, 758 (1997), arXiv:nucl-th/9706045.
[193] D. R. Entem and R. Machleidt, Phys. Rev. C **68**, 041001 (2003).
[194] E. Epelbaum, W. Glockle, and U.-G. Meissner, Nucl.Phys. **A747**, 362 (2005), arXiv:nucl-th/0405048.
[195] P. F. Bedaque and U. van Kolck, Ann.Rev.Nucl.Part.Sci. **52**, 339 (2002), arXiv:nucl-th/0203055.
[196] N. Ishii, S. Aoki, and T. Hatsuda, Phys. Rev. Lett. **99**, 022001 (2007).
[197] HAL QCD Collaboration, S. Aoki *et al.*, PTEP **2012**, 01A105 (2012), arXiv:1206.5088.

[198] HAL QCD Collaboration, T. Inoue *et al.*, Phys. Rev. Lett. **106**, 162002 (2011).
[199] HAL QCD Collaboration, T. Inoue *et al.*, Nucl.Phys. **A881**, 28 (2012), arXiv:1112.5926.
[200] NPLQCD Collaboration, S. R. Beane *et al.*, Phys. Rev. Lett. **106**, 162001 (2011).
[201] NPLQCD Collaboration, S. R. Beane *et al.*, Phys. Rev. D **85**, 054511 (2012).
[202] T. A. Rijken, M. Nagels, and Y. Yamamoto, Prog.Theor.Phys.Suppl. **185**, 14 (2010).
[203] J. Haidenbauer *et al.*, Nucl.Phys. **A915**, 24 (2013), arXiv:1304.5339.
[204] R. PHILLIPS, Rev.Mod.Phys. **39**, 681 (1967).
[205] R. Bryan and R. Phillips, Nucl.Phys. **B5**, 201 (1968).
[206] J. Richard, M. Lacombe, and R. Vinh Mau, Phys.Lett. **B64**, 121 (1976).
[207] C. Dover and J. Richard, Phys.Rev. **D17**, 1770 (1978).
[208] W. Buck, C. Dover, and J. Richard, Annals Phys. **121**, 47 (1979).
[209] C. Dover and J. Richard, Annals Phys. **121**, 70 (1979).
[210] C. Dover, J. Richard, and M. Zabek, Annals Phys. **130**, 70 (1980).
[211] V. Mull and K. Holinde, Phys. Rev. C **51**, 2360 (1995).
[212] E. Klempt, F. Bradamante, A. Martin, and J. Richard, Phys.Rept. **368**, 119 (2002).
[213] E. Klempt, C. Batty, and J.-M. Richard, Phys.Rept. **413**, 197 (2005), arXiv:hep-ex/0501020.
[214] X.-W. Kang, J. Haidenbauer, and U.-G. Meissner, (2013), arXiv:1311.1658.
[215] R. Machleidt, Adv.Nucl.Phys. **19**, 189 (1989).
[216] R. Machleidt, The meson theory of nuclear forces and nuclear matter, in *RELATIVISTIC DYNAMICS AND QUARK-NUCLEAR PHYSICS*, John Wiley & Sons Inc, 1986.
[217] S. Moszkowski, Nuclear forces, nuclear matter and finite nuclei, in *Physique nucleaire; nuclear physics*, Gordon and Breach Science Publishers, 1968.
[218] M. Goldberger and S. Treiman, Phys.Rev. **110**, 1178 (1958).
[219] A. Hosaka and H. Toki, *Quarks, Baryons and Chiral Symmetry* (World Scientific Publishing Company, 2001).
[220] T.-P. Cheng and L.-F. Li, *Gauge Theory of elementary particle physics* (Oxford University Press, USA, 1988).